EFFECT OF TUBE DIAMETER ON CRITICAL HEAT FLUX IN VERTICAL STEAM-WATER FLOW

by

Wai-Chuen Wong

A dissertation submitted to the School of Graduate Studies and Research in Mechanical and Aerospace Engineering of the University of Ottawa in partial fulfilment of the requirements for the degree of Master of Applied Science in Mechanical Engineering

Mechanical and Aerospace Engineering
University of Ottawa, Ottawa, Ontario, Canada K1N 6N5

January 8, 1997

ISBN 0-612-20028-0

Name Wai-Chuen WONG

Dissertation Abstracts International and *Masters Abstracts International* are arranged by broad, general subject categories. Please select the one subject which most nearly describes the content of your dissertation or thesis. Enter the corresponding four-digit code in the spaces provided.

NUCLEAR
SUBJECT TERM

0552
SUBJECT CODE

UMI

Subject Categories

THE HUMANITIES AND SOCIAL SCIENCES

COMMUNICATIONS AND THE ARTS
Architecture 0729
Art History 0377
Cinema 0900
Dance 0378
Fine Arts 0357
Information Science 0723
Journalism 0391
Library Science 0399
Mass Communications 0708
Music 0413
Speech Communication 0459
Theater 0465

EDUCATION
General 0515
Administration 0514
Adult and Continuing 0516
Agricultural 0517
Art 0273
Bilingual and Multicultural 0282
Business 0688
Community College 0275
Curriculum and Instruction 0727
Early Childhood 0518
Elementary 0524
Finance 0277
Guidance and Counseling 0519
Health 0680
Higher 0745
History of 0520
Home Economics 0278
Industrial 0521
Language and Literature 0279
Mathematics 0280
Music 0522
Philosophy of 0998
Physical 0523
Psychology 0525
Reading 0535
Religious 0527
Sciences 0714
Secondary 0533
Social Sciences 0534
Sociology of 0340
Special 0529
Teacher Training 0530
Technology 0710
Tests and Measurements 0288
Vocational 0747

LANGUAGE, LITERATURE AND LINGUISTICS
Language
General 0679
Ancient 0289
Linguistics 0290
Modern 0291
Literature
General 0401
Classical 0294
Comparative 0295
Medieval 0297
Modern 0298
African 0316
American 0591
Asian 0305
Canadian (English) 0352
Canadian (French) 0355
English 0593
Germanic 0311
Latin American 0312
Middle Eastern 0315
Romance 0313
Slavic and East European 0314

PHILOSOPHY, RELIGION AND THEOLOGY
Philosophy 0422
Religion
General 0318
Biblical Studies 0321
Clergy 0319
History of 0320
Philosophy of 0322
Theology 0469

SOCIAL SCIENCES
American Studies 0323
Anthropology
Archaeology 0324
Cultural 0326
Physical 0327
Business Administration
General 0310
Accounting 0272
Banking 0770
Management 0454
Marketing 0338
Canadian Studies 0385
Economics
General 0501
Agricultural 0503
Commerce-Business 0505
Finance 0508
History 0509
Labor 0510
Theory 0511
Folklore 0358
Geography 0366
Gerontology 0351
History
General 0578
Ancient 0579
Medieval 0581
Modern 0582
Black 0328
African 0331
Asia, Australia and Oceania 0332
Canadian 0334
European 0335
Latin American 0336
Middle Eastern 0333
United States 0337
History of Science 0585
Law 0398
Political Science
General 0615
International Law and Relations 0616
Public Administration 0617
Recreation 0814
Social Work 0452
Sociology
General 0626
Criminology and Penology 0627
Demography 0938
Ethnic and Racial Studies 0631
Individual and Family Studies 0628
Industrial and Labor Relations 0629
Public and Social Welfare 0630
Social Structure and Development 0700
Theory and Methods 0344
Transportation 0709
Urban and Regional Planning 0999
Women's Studies 0453

THE SCIENCES AND ENGINEERING

BIOLOGICAL SCIENCES
Agriculture
General 0473
Agronomy 0285
Animal Culture and Nutrition 0475
Animal Pathology 0476
Food Science and Technology 0359
Forestry and Wildlife 0478
Plant Culture 0479
Plant Pathology 0480
Plant Physiology 0817
Range Management 0777
Wood Technology 0746
Biology
General 0306
Anatomy 0287
Biostatistics 0308
Botany 0309
Cell 0379
Ecology 0329
Entomology 0353
Genetics 0369
Limnology 0793
Microbiology 0410
Molecular 0307
Neuroscience 0317
Oceanography 0416
Physiology 0433
Radiation 0821
Veterinary Science 0778
Zoology 0472
Biophysics
General 0786
Medical 0760

EARTH SCIENCES
Biogeochemistry 0425
Geochemistry 0996
Geodesy 0370
Geology 0372
Geophysics 0373
Hydrology 0388
Mineralogy 0411
Paleobotany 0345
Paleoecology 0426
Paleontology 0418
Paleozoology 0985
Palynology 0427
Physical Geography 0368
Physical Oceanography 0415

HEALTH AND ENVIRONMENTAL SCIENCES
Environmental Sciences 0768
Health Sciences
General 0566
Audiology 0300
Chemotherapy 0992
Dentistry 0567
Education 0350
Hospital Management 0769
Human Development 0758
Immunology 0982
Medicine and Surgery 0564
Mental Health 0347
Nursing 0569
Nutrition 0570
Obstetrics and Gynecology 0380
Occupational Health and Therapy 0354
Ophthalmology 0381
Pathology 0571
Pharmacology 0419
Pharmacy 0572
Physical Therapy 0382
Public Health 0573
Radiology 0574
Recreation 0575
Speech Pathology 0460
Toxicology 0383
Home Economics 0386

PHYSICAL SCIENCES
Pure Sciences
Chemistry
General 0485
Agricultural 0749
Analytical 0486
Biochemistry 0487
Inorganic 0488
Nuclear 0738
Organic 0490
Pharmaceutical 0491
Physical 0494
Polymer 0495
Radiation 0754
Mathematics 0405
Physics
General 0605
Acoustics 0986
Astronomy and Astrophysics 0606
Atmospheric Science 0608
Atomic 0748
Electronics and Electricity 0607
Elementary Particles and High Energy 0798
Fluid and Plasma 0759
Molecular 0609
Nuclear 0610
Optics 0752
Radiation 0756
Solid State 0611
Statistics 0463

Applied Sciences
Applied Mechanics 0346
Computer Science 0984

Engineering
General 0537
Aerospace 0538
Agricultural 0539
Automotive 0540
Biomedical 0541
Chemical 0542
Civil 0543
Electronics and Electrical 0544
Heat and Thermodynamics 0348
Hydraulic 0545
Industrial 0546
Marine 0547
Materials Science 0794
Mechanical 0548
Metallurgy 0743
Mining 0551
Nuclear 0552
Packaging 0549
Petroleum 0765
Sanitary and Municipal 0554
System Science 0790
Geotechnology 0428
Operations Research 0796
Plastics Technology 0795
Textile Technology 0994

PSYCHOLOGY
General 0621
Behavioral 0384
Clinical 0622
Developmental 0620
Experimental 0623
Industrial 0624
Personality 0625
Physiological 0989
Psychobiology 0349
Psychometrics 0632
Social 0451

Abstract

The effect of tube diameter on critical heat flux (CHF) has been examined by (1) analyzing existing experimental data, (2) reviewing existing correlations and semi-analytical models, and (3) obtaining CHF measurements in two vertical tubes of different diameters. Based on constant local flow conditions, the parametric trend of available CHF data shows generally a decreasing CHF with increasing tube diameter. Due to the large data scatter (inherent uncertainty within different sets of data), a definite conclusion cannot be drawn. The observations indicated that the tube-diameter effect on CHF is a complex phenomenon and is affected by pressure, mass flux and thermodynamic quality as well as tube diameter itself.

Most existing correlations employ a simple correction factor to account for the tube-diameter effect. The correction factor is expressed as a function of the tube diameter to a power "n", which has a range from -0.5 to 0.1. Due to the limited amount of data employed in optimizing the coefficient, the correction factor is generally valid for a restricted range of flow conditions. In view of the complexity of this effect, relatively more complex forms of correction factors have been proposed recently. These correction factors do not improve the prediction accuracy, compared to the use of a simple factor. In addition, they introduced discontinuity at certain transition regions.

The available semi-analytical models commonly account for the effect of tube diameter on CHF implicitly through various closure relationships (such as entrainment rate, deposition rate, interfacial shear stress, etc.). These relationships were often correlated from low-pressure data, and hence limited their range of application. In all, the relation between CHF and tube diameter displayed in most models can be approximated as proportional to the tube diameter to a power of -0.5.

An improved correction factor has been derived to account for the effect of tube diameter on CHF. It is also presented in terms of the tube diameter to a power "n", consistent with existing

recommendations. Rather than a constant value, the coefficient is expressed as a function of mass flux and thermodynamic quality to include other compounded effects. Compared against 18 000 data points from the AECL CHF data bank, the average prediction error is -4% and the root-mean-square (rms) error is 39% based on a constant dryout-quality analysis. Excluding those questionable 2 000 data points with prediction error outside the ±50% ranges, the average error is reduced to 0.28% while the rms error becomes 17.4%.

Measurements of CHF have been obtained with high-pressure steam-water flow inside two vertical tubes (inside-diameter values of 5.45 mm and 8.94 mm). They covered a wide range of flow conditions and were used to validate the improved correction factor for the tube-diameter effect. The improved correction factor predicted the experimental data well, around 6% average error and 9.5% rms error for a total of 76 data points, and therefore validated its applications outside the development data base.

Acknowledgements

I would like to express my sincere appreciation to Dr. D.C. Groeneveld and Dr. S.C. Cheng for their guidance, encouragement and patience throughout the course of this study. Their valuable ideas and constructive criticisms have certainly made this work much more interesting.

I am also thankful to Dr. L.K.H. Leung for his valuable comments and assistance throughout my work, plus the setting up and the supervising of the experiment.

Table of Contents

APPENDICES

NOMENCLATURE

Symbol	Definition	Unit
A	Flow area	m^2
B_o	Boiling number (= q/(h G))	-
C_p	Specific heat capacity	$J.kg^{-1}.K^{-1}$
D	Deposition rate	-
d	Tube diameter	m
E	Entrainment rate	-
f	Friction factor	-
G	Mass flux	$kg.m^{-2}.s^{-1}$
g	Acceleration due to gravity (= 9.806)	$m.s^{-2}$
h	Heat-transfer coefficient	$W.m^{-2}.K^{-1}$
H	Enthalpy	$J.kg^{-1}$
H_{fg}	Latent heat of vaporization	$J.kg^{-1}$
j	Superficial velocity	$m.s^{-1}$
k	Thermal conductivity	$W.m^{-1}.K^{-1}$
L	Length	m
Nu	Nusselt number (= h d / k)	-
n	Exponent in the diameter correction factor	-
p	Pressure	kPa, MPa, bar
Pr	Prandtl number (= μ C_p / k)	-
q	Heat flux	$W.m^{-2}$
q_c	Critical heat flux	$W.m^{-2}$
Re	Reynolds number (= G d / μ)	-
St	Stanton number (= q / (G C_p (T_{sat} - T_l)))	-
t	Time	second
T	Temperature	°C, K

u	Velocity	$m.s^{-1}$
U	Axial velocity	$m.s^{-1}$
v	Specific volume	$m^3.kg^{-1}$
W	Mass flow rate	$kg.s^{-1}$
We	Weber number ($= G^2 d / (\rho\ \sigma)$)	-
x	Quality	-
y	Radial distance from the tube wall	m
z	Axial distance	m

Greek	Definition	Unit
α	Void fraction	-
ΔP	Pressure drop	kPa, MPa
δ	Liquid-film thickness	m
δ_l	Laminar sublayer thickness	m
ϵ	Absolute roughness height	m
ι	Mixing length	m
κ	Prandtl single-phase constant (=0.4)	-
μ	Dynamic viscosity	$kg.m^{-1}.s^{-1}$
ρ	Density	$kg.m^{-3}$
σ	Surface tension	$N.m^{-1}$
τ	Shear stress	Pa

Subscript	Definition
B	Bubble
b	Bulk fluid condition
c	Critical condition (or core condition in annular flow)
D	Deposition

dd	Droplet drag
e	Equilibrium
E	Entrainment
f	Saturated-liquid condition
g	Gas
i	Two-phase interface
L	Laminar
l	Liquid
le	Liquid entrainment
lf	Liquid film
m	Microlayer
in	Inlet
inj	Injection
sat	At saturation
stream	Main core flow of liquid
sub	Subcooled
T	Turbulent
tp	Two-phase
v	Vapour
vc	Vapour core
w	Near-wall condition

Abbreviation	Definition
CHF	Critical heat flux
DNB	Departure from nucleate boiling
rms	Root-mean-square

LIST OF TABLES

LIST OF FIGURES

Figure Caption Page

1. INTRODUCTION

1.1 BACKGROUND

Flow boiling is commonly encountered in heat-transfer equipment used in chemical and power-generating processes (e.g., boilers, heat exchangers, steam generators, nuclear reactors, etc.). The conditions of flow boiling involve the vaporization of liquid on the heated surface while heat is being removed in the process. Due to the large amount of heat required to evaporate the liquid from the high latent heat of vaporization, flow boiling provides a better heat-transfer rate than most other heat-transfer modes. However, with increasing heating power supplied to the heated surface, a condition is reached where a continuous liquid contact at the heated surface can no longer be maintained, and a vapour film will start to form at the surface. Due to the poor heat-transfer characteristics of vapour, a rapid increase in surface temperature may occur. This phenomenon is identified as the "critical heat flux" (CHF). It is essential to accurately predict the occurrence of dryout (or the critical heat flux) in order to avoid the resulting sharp temperature excursion which can severely damage the heated surface and hence the equipment.

The dryout phenomenon has been studied extensively over the past five decades, resulting in a proliferation of correlations and prediction methods. Groeneveld and Snoek (1986) estimated that over 500 correlations were available for tube flow, which signifies the diversity of the methods in predicting CHF. Despite the vast amount of information, most correlations are valid only for a limited range of flow conditions. However, an alternative is the CHF look-up table of Groeneveld et al. (1996), which is applicable to most practical engineering analyses.

Besides the limitations on flow conditions, empirical correlations also are often restricted to a specific geometry (such as tubes, annuli, rod-bundles, etc.) and certain channel size (such as diameter of tube) for which the experimental data were obtained. Most experiments were performed on a round tube of only one size. For generality, modification factors are required to extend these correlations to other geometries or different channel sizes. A number of empirical modification factors have been derived to represent the trend of the bulk of the data base, although covering only a limited range of flow conditions. The validity of these factors is generally not substantiated for conditions outside the data base.

The objectives of this study are (1) to examine the tube-diameter effect on CHF based on the AECL data bank (one of the largest in the world), and (2) to improve existing prediction methods for the diameter effect by extending their range of applications.

1.2 BOILING HEAT TRANSFER

Boiling heat transfer is a process where evaporation of liquid takes place. It is categorized into pool boiling for natural convection and flow boiling for forced convective flow. However, the present study focuses mainly on those encountered in flow boiling. A brief description of the heat-transfer regimes in tube flow is presented in this chapter. Details of the heat-transfer regimes and mechanisms have been described in Collier (1972), and Hewitt and Hall-Taylor (1970).

Figure 1.1 illustrates the heat-transfer regimes associated with vertical upward flow in a heated tube. With a single-phase liquid introduced at a temperature below the saturation point (i.e., subcooled flow) and a sufficiently high surface heat flux, the heat-transfer regime changes from single-phase forced convection to subcooled liquid, subcooled nucleate boiling, saturated nucleate boiling (or forced convective evaporation at high flows), film boiling, vapour-phase forced convection, to superheated vapour. Strictly speaking, the single-phase liquid flow at the inlet and the single-phase vapour flow at the outlet are not classified as flow boiling, since no evaporation takes place in the process.

Figure 1.1 shows only the transition of heat-transfer regimes for an inlet flow with constant flow conditions. Comparison of the local heat-transfer rate cannot be made at various points along the tube as the local conditions are continuously varying; e.g., the local pressure decreases from point to point due to pressure drop, and the local enthalpy (or quality) changes due to heating along the tube.

The variation of the heat-transfer rate with wall superheat can be examined through the boiling curve, Figure 1.2, which shows the transition of heat-transfer regimes for a constant flow condition (i.e., same pressure, mass flux and thermodynamic quality). The transition point between single-phase liquid flow and nucleate boiling is the onset of nucleate boiling point, between nucleate boiling (or forced convective evaporation) and transition boiling is the critical heat flux point, and between transition boiling and film boiling is the minimum film-boiling point. For a heat-flux controlled system (e.g., an electric heater), the surface temperature increases sharply from nucleate boiling to film boiling once the heat flux exceeds the critical heat flux point. In this case, transition boiling is not present. For a surface-temperature controlled system (e.g., heat exchanger), the heat flux varies from nucleate boiling to film boiling and passes through transition boiling as the surface temperature increases.

1.2.1 Subcooled Nucleate Boiling

Subcooled nucleate boiling is the heat-transfer regime where boiling occurs in the vicinity of the heated surface, while the bulk of the fluid remains below the saturation point. At this regime, the wall temperature is constant and slightly exceeds the liquid saturation temperature, whereas the mean bulk fluid temperature increases towards saturation. The difference between the mean fluid temperature to the saturation temperature is defined as the "degree of subcooling" or simply "subcooling". Vapour bubbles are generated and grow at the "nucleation" sites formed on the inside surface of the tube where temperature is higher than saturation. When the vapour bubbles become large, the combination of the drag force by the liquid and the buoyancy force on the bubbles overcomes the surface-tension force maintained by the near-wall liquid, and lifts the bubbles from the surface. The high subcooling in the liquid core causes the vapour bubbles to condense immediately (or within a short distance) once they leave the surface. As the bubbles condense, the bulk fluid temperature increases accordingly.

1.2.2 Saturated Nucleate Boiling and Forced Convective Evaporation

Saturated nucleate boiling occurs where the bulk fluid temperature has reached saturation. In the near-wall region, the formation of bubbles intensifies and leads to rapid migration of bubbles toward the liquid core. The corresponding flow pattern is referred to as the bubbly flow. Due to the high heat-transfer rate, the increase in surface temperature is relatively small compared to other heat-transfer regimes for a similar increase in heat flux. At low flow conditions, these bubbles coalesce and form vapour slugs. With increasing flow rate, the liquid that bridges the slug may collapse and the vapour travels primarily in the core with a large amount of liquid droplets (or entrainment). The remaining liquid travels in the form of a liquid film along the heated surface. Due to the high liquid-film velocity and heat-transfer rate, nucleation is suppressed at the surface and heat is carried away from the wall by forced convection through a turbulent liquid film to the vapour core at the liquid-vapour interface, where evaporation takes place. This flow regime is often referred to as annular flow, and the corresponding heat-transfer mode is called forced convective evaporation.

1.2.3 Transition Boiling

Transition boiling is an unstable region where intermittent dryout and rewet of the heated surface occur continuously. It has not been studied extensively due to the unstable nature of the flow, and hence will not be further discussed. Furthermore, this heat-transfer regime is not found in a heat-flux controlled system. Groeneveld and Snoek (1986) summarized the heat-transfer prediction methods for transition boiling.

1.2.4 Film Boiling

Film boiling, characterized by a vapour film covering the heated surface, is often associated with a high surface temperature where rewetting is not possible. Due to the low conductivity and heat capacity of the vapour, the heat-transfer rate in film boiling is much lower than in nucleate boiling. Depending on the total flow rate and quality, there are two flow patterns associated with film boiling: inverted annular film boiling and dispersed flow film boiling. Inverted annular film boiling occurs at conditions of low flow rate and low quality. It is usually associated with high surface temperature due to the low convective heat-transfer rate. Dispersed flow film boiling occurs at conditions of high flow rate and high quality. It is associated with moderately high surface temperature due to the relatively high convective heat-transfer rate, compared to inverted annular film boiling.

1.2.5 Transition Points

In general, the variation in heat-transfer characteristics is gradual at both the onset of nucleate-boiling point and the minimum film-boiling point. Near these points, the surface temperature increases smoothly with increasing heat flux, and vice versa. This is primarily caused by the gradual transition of conditions at the surface/liquid interface. At the point of critical heat flux, however, there is a discontinuity in the heat-transfer rate. The surface which is previously cooled efficiently by a convective evaporation or nucleate boiling, is suddenly exposed to vapour which has a poor thermal conductivity and capacity. The disruption causes a sharp increase in surface temperature, which may severely damage the heated surface. This phenomenon has been the focal point of much research for the past five decades partly due to safety issues. On the other hand, there is also a discontinuity at the minimum film-boiling point when heat flux is being reduced for a heat flux controlled system. The discontinuities produce the effects of hysteresis.

1.3 ORGANIZATION OF THESIS

Chapter 1 of this thesis has provided a brief introduction to critical heat flux and the description of various boiling heat-transfer modes and transition points.

Chapter 2 describes various mechanisms for the occurrence of critical heat flux at various flow conditions. It examines effects of various flow parameters on critical heat flux and documents several recommended prediction methods for critical heat flux in tubes with flow boiling. As indicated in Section 1.1, there are over 500 prediction methods (in both correlations and semi-analytical models) available for critical heat flux, and it is not the intention of this study to provide a detailed review. Groeneveld and Snoek (1986) summarized many correlations for various applications.

Chapter 3 focuses on a literature survey of relevant information on the tube-diameter effect on critical heat flux. Available experimental data and prediction methods have been examined, and their respective trend of tube-diameter effect are presented.

Chapter 4 examines, in detail, the tube-diameter effect on CHF as exhibited in data of the AECL data bank, which consists of more than 30 000 CHF data points. Two approaches have been selected in the present analysis: the diameter effect was determined with the overall trend displayed in all data, or based on trends exhibited in data of any individual source. Based upon the findings and by focusing on the trend of the diameter effect, a correction factor for diameter effect on CHF has been derived with data in the data bank. A comparison is shown between CHF predictions based on the CHF look-up table and the updated correction factor and data in the AECL data bank.

Chapter 5 presents a simple analytical study based on two models developed for different CHF phenomena: bubbly flow in subcooled boiling and annular flow in saturated boiling. The tube-diameter effect on CHF as predicted by these models is examined.

Chapter 6 describes an experiment conducted at the Chalk River Laboratories to obtain validation data for the updated correction factor for tube-diameter effect. The experimental set-up and procedure for the tests are described.

The conclusions of the present study are presented in Chapter 7 together with a few final remarks.

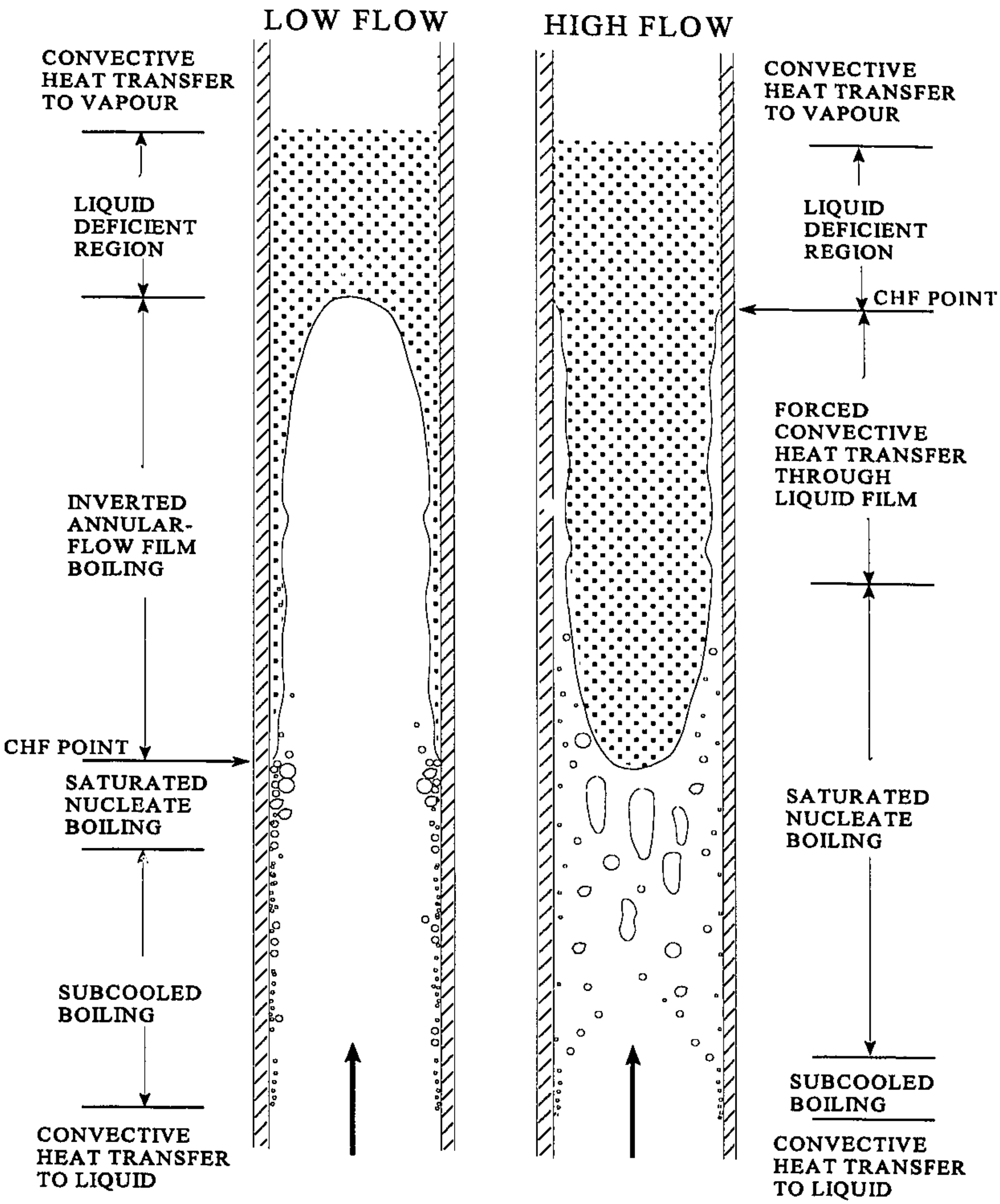

Figure 1.1: Heat-Transfer Regimes for Vertical Upward Flow in Uniformly Heated Tubes.

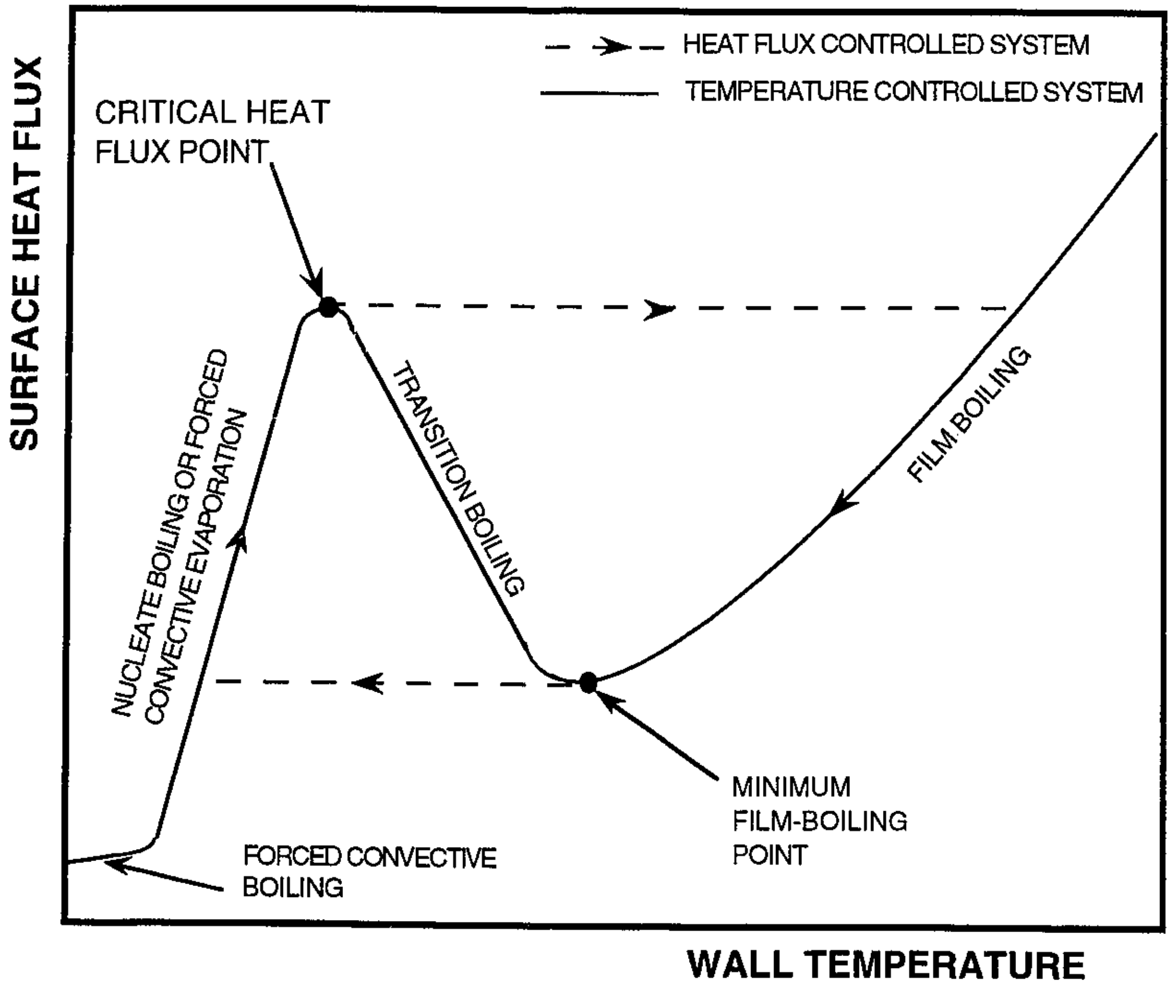

Figure 1.2: Boiling Curve

2. CRITICAL HEAT FLUX FOR UPWARD FLOW IN VERTICAL TUBES

The Critical heat flux (CHF) point depends strongly on flow conditions and can be categorized into two types: departure from nucleate boiling (DNB) and dryout. Departure from nucleate boiling, evolves from nucleation of vapour bubble at the heated surface, is encountered primarily at high heat flux and low quality (mainly at subcooled) conditions. Due to the high surface heat flux, the surface temperature rises sharply at conditions beyond the critical heat flux, and as a result the heated surface can be damaged and hence this phenomenon has also been called burnout. Dryout is encountered at relatively low heat flux and high-quality conditions. The rise in surface temperature is moderate at the critical heat flux point, where the liquid film at the tube wall is completely evaporated. These two types of critical heat flux arise from different mechanisms, which are described below.

2.1 CRITICAL HEAT FLUX MECHANISMS

2.1.1 Departure From Nucleate Boiling

Departure from nucleate boiling occurs at low-quality flows. For a subcooled water flow, a high heat flux is needed to initiate boiling at the heated surface where vapour bubbles form. These vapour bubbles grow at the surface and condense once they detach from the wall into the core of subcooled flow. At heat fluxes below the CHF point, a thin liquid film is maintained between the bubble and the surface. Evaporation continues and the liquid film is replenished by the bulk fluid through a capillary action. When a sufficiently high surface heat flux is applied, the density of bubbles increases in the vicinity of the heated surface. The temperature rises near the heated surface, and when the liquid wedges (or "microlayer") between the bubbles and the heated surface is disrupted, burnout occurs. This is often called the bubble-crowding scenario, and occurs when the bulk fluid remains at subcooled conditions. In another case, at a thermodynamic quality near zero, the size of vapour bubbles increases, causing the neighboring bubbles to coalesce with others, forming long bubble slugs. As the size of the slugs increases, the replenishment of liquid film becomes less efficient and a dry spot is initiated. Due to the high heat flux and inefficient heat-transfer characteristics of vapour, the surface temperature at the dry spot increases rapidly. The dry spot spreads rapidly within the vapour slug, due to conduction and evaporation, and causes a sharp temperature rise of the heated surface. The scenario leading to this type of DNB is referred to as vapour blanketing.

2.1.2 Dryout

Dryout occurs mainly at high-quality conditions ($x_c > \sim 5\%$). For saturated liquid flow, bubbles can migrate freely into the core. With an increase in bubble density, bubbles coalesce to form vapour slug at low flows and vapour churn at high flows. As the amount and velocity of vapour in the core increases, the bridges of liquid crossing over the slugs and churns can be broken to become liquid droplets entrained into the now more continuous flow of vapour in the core. A film of liquid is left and remains between the vapour core and the heated surface. For a thick liquid film, waves are formed at its liquid-vapour interface. With increasing vapour velocity, the crests of the waves are torn off and the liquid is entrained into the vapour core as droplets. At high vapour quality, the liquid film becomes so thin that wave formation is not possible. Under these conditions, the entrainment process terminates and the depletion of liquid film continues through evaporation. When the remaining liquid film is completely vaporized, the heated surface is cooled only by the vapour phase. This is referred to as dryout, signifying the drying out of the liquid film. Due to the high vapour velocity and the high liquid content, the heat transfer coefficient is relatively high and the vapour acts like a heat sink; the rise in temperature is relatively moderate.

The removal of liquid from the film is compensated to some extent by the redeposit of droplets from the core back to the liquid film. Concentration of the droplet density in the core plays an important role in the amount of droplet redeposit rate. This is particularly significant for thin film conditions where entrainment is not possible. The deposition mechanism usually plays a significant role before dryout occurs.

2.2 EFFECT OF FLOW PARAMETERS ON CRITICAL HEAT FLUX

Flow conditions strongly affect the critical heat flux. Previous analyses have used approaches based on either the inlet flow parameters or the local flow parameters as references. The inlet flow parameters include pressure, mass flux (or mass flow rate) and fluid temperature at the entrance of the test section. These parameters are measurable quantities in experiments, and were selected as independent parameters. The inlet flow parameters approach is affected strongly by the geometric parameters, such as tube diameter and tube length, and hence is limited to specific channel geometries only. The local flow parameters include pressure, mass flux and enthalpy (or quality) at the location of CHF. They have to be calculated with conservation equations based on measured inlet flow parameters. In some cases, both the local pressure and mass flow rate (used to calculate the mass flux) can be measured. The local enthalpy, however, must be calculated through a heat balance. Based on local flow conditions, CHF has been shown to be independent of tube length, except for a dryout location close to the start of the heated length (entrance length effect due possibly to the development of the thermal boundary layer). The tube diameter, on the other hand, remains as a crucial parameter and is the subject of the present study.

In this section, the effects of various flow parameters on critical heat flux have been briefly described. Detailed discussions can be found in Collier (1972), Hewitt and Hall-Taylor (1970).

2.2.1 Effect of Pressure on Critical Heat Flux

With increasing pressure, CHF generally increases at low pressure conditions but decreases at high pressure conditions. Collier (1972) suggested that the turning point (i.e., when the increasing trend changes to a decreasing trend) depends on the flow conditions. It occurs generally at pressures between 3 and 5 MPa in steam-water flow. Figure 2.1 illustrates the variation of critical heat flux with respect to pressure at a constant inlet quality and for this example at zero quality.

2.2.2 Effect of Mass Flow Rate (or Mass Flux) on Critical Heat Flux

Based on constant inlet flow conditions, the critical heat flux increases with increasing mass flux. This trend is illustrated in Figure 2.2. The effect of mass flow rate (or mass flux) on CHF for constant local flow conditions is much more complex than for constant inlet flow conditions. This is caused by a strong dependence on local flow patterns. At low-quality (or subcooled) conditions, CHF increases with increasing mass flux due to an increase in the forced convective heat-transfer rate and the turbulence level. The former reduces the bubble formation rate, while the latter enhances the bubble migration rate to the core and reduces the density of bubbles at the heated surface. At medium quality conditions (about 5-45%), however, CHF varies considerably with mass flux. With increasing mass flux, it increases in the low mass-flux region, decreases at medium mass fluxes, and increases at high mass fluxes. A mechanism similar to the one observed in low quality flow brings an increasing trend of CHF at low and high mass fluxes. The decreasing trend at medium mass fluxes is primarily caused by an increase in entrainment rate for the annular flow regime, which leads to an increase in depletion rate of the liquid film, with increasing mass flux. Figure 2.3 illustrates the effect of mass flux on critical heat flux for various local conditions.

2.2.3 Effect of Inlet Fluid Enthalpy (or Temperature) on Critical Heat Flux

The effect of inlet fluid temperature on CHF is often presented in terms of inlet subcooling, which is the difference between saturated liquid enthalpy and inlet liquid enthalpy (i.e., $\Delta H_{in} = H_f - H_{in}$). It is shown in Figure 2.4 for various mass fluxes. In general, CHF increases with increasing inlet subcooling, and a linear relationship is often observed.

2.2.4 Effect of Local Quality on Critical Heat Flux

Local quality is calculated with a heat balance based on the inlet flow conditions, and is defined as:

$$x = \frac{1}{H_{fg}} \left(\frac{Power}{W} - H_f + H_{in} \right) \tag{2.1}$$

where H_{in} is the inlet fluid enthalpy in $J \cdot kg^{-1}$ (based on inlet pressure and fluid temperature), Power is the total applied heat in watts up to the point of interest, W is the mass flow rate in $kg \cdot s^{-1}$, and H_f and H_{fg} are the saturated liquid enthalpy and the latent heat of vaporization in $J \cdot kg^{-1}$ (based on local pressure at the point of interest). Due to the influence of other independent parameters, such as pressure and mass flow rate on local quality, a complex trend of CHF is often observed. In general, CHF decreases with increasing quality for a uniformly heated tube with vertical upward flow, as illustrated in Figure 2.5.

2.2.5 Effect of Heated Length on Critical Heat Flux

The effect of heated length on critical heat flux was shown to be significant at constant inlet flow conditions. As Figure 2.6 shows, CHF decreases with increasing heated length for the same inlet subcooling. In terms of the local dryout parameters, however, the effect of heated length on CHF diminishes in tubes with long heated lengths. For short tubes, CHF increases with decreasing heated length. Figure 2.7 illustrates the variation of CHF for tubes of various heated length values at constant local dryout qualities.

2.3 PREDICTION METHODS FOR CRITICAL HEAT FLUX

The complexity of the CHF mechanism has resulted in a very large number of CHF prediction methods, which can be generally categorized into empirical correlations, semi-analytical models, and look-up tables. Most of them, however, are in the form of empirical correlations.

2.3.1 Empirical Correlations

Empirical correlations were usually developed from data sets of a narrow range of conditions, based on either the inlet-flow parameters or the local-flow parameters. They are often based on some predetermined forms of equation (corresponding to the trend of data, in most cases), which may provide unrealistic predictions (e.g., negative CHF) outside the range of data base. Therefore, it is essential to apply correlations within their range of validity.

The inlet-flow-conditions type of correlations are limited to a specific geometry and hence are usually not recommended, except for ad-hoc applications. However, good prediction accuracy has been reported with correlations of this type. Most of them are based on the assumption that CHF is linearly proportional to the inlet subcooling. While this trend has been observed over a limited range of inlet subcooling, it cannot be substantiated for use over wider ranges. The Bowring (1972) correlation is one that was derived based on inlet-flow conditions.

The local-flow-conditions type of correlations are generally more suitable for tubes of long heated length. They express CHF in terms of pressure, mass flux, local quality, and tube diameter. There are two ways to derive a correlation based on local conditions. The first way is simply to transform an inlet-flow-conditions type of correlation into a local-flow-conditions type via the heat-balance equation. It has the advantage of maintaining the same sets of correlation constants and coefficients for both correlations, but the transformed correlation is less accurate than the inlet-flow-conditions type of correlation. The second way is to use a predetermined form of the local-flow-conditions correlation and correlate the constants and coefficients with the data base. This usually provides a better fit of the data, but may produce predictions different from those of the inlet-flow-conditions correlation. Both the Doroschuk et al. (1975) and the Biasi et al. (1967) correlations were derived using the second method, and they predicted closely with their respective data bases.

2.3.1.1 The Macbeth Correlations

Macbeth (1963) employed the local-flow-conditions hypothesis to develop two empirical correlations from experimental data, to predict CHF for high- and low-flow conditions. The high- and low-flow regimes are defined by functions of system pressure and the ratio of tube diameter to heated length. The correlations relate to pressure, mass flux, tube diameter, latent heat of vaporization, and local quality. The CHF in the low-flow region is expressed as (in British units)

$$\frac{q_c}{10^6} = 0.00633\, H_{fg}\, d^{-0.1} \left(\frac{G}{10^6} \right)^{0.51} (1 - x_c) \tag{2.2}$$

where G is the mass flux in lb.ft^{-2}.hr^{-1}, d is the tube diameter in ft, and x_c is the critical quality. For high-flow region, the CHF is expressed as (in British units):

$$\frac{q_c}{10^6} = y_o\, d^{y_1} \left(\frac{G}{10^6} \right)^{y_2} - \frac{y_3}{4}\, d^{y_4} \left(\frac{G}{10^6} \right)^{y_5} G\, x_c\, d\, H_{fg} \tag{2.3}$$

where y_i are the pressure-dependent constants listed in Table 2.1. This correlation was superceded by the Thompson and Macbeth correlation (1964) and later by the Bowring correlation (1972) which is described in Section 2.3.1.3.

Table 2.1: Optimized Values of 'y' in the Macbeth Correlation.

Pressure (psia)	y_0	y_1	y_2	y_3	y_4	y_5
15	1.12	-0.211	-0.324	0.0010	-1.4	-1.05
250	1.77	-0.553	-0.260	0.0166	-1.4	-0.937
530	1.57	-0.566	-0.329	0.0127	-1.4	-0.737
1000	1.06	-0.487	-0.179	0.0085	-1.4	-0.555
1570	0.72	-0.527	0.024	0.0121	-1.4	-0.096
2000	0.627	-0.268	0.192	0.0093	-1.4	-0.343
2700	0.0124	-1.45	0.489	0.0097	-1.4	-0.529

2.3.1.2 The Biasi et al. Correlation

Biasi et al. (1967) derived two correlations for high- and low-quality regions, based on a relatively large number of experimental data. The correlation for low-quality flow is expressed as:

$$q_c = \frac{1.883 \cdot 10^3}{d^a \, G^{1/6}} \left(\frac{y(p)}{G^{1/6}} - x_c \right) \tag{2.4}$$

$$y(p) = 0.7249 + 0.099 \, p \, \exp(-0.032 p) \tag{2.5}$$

where G is the mass flux in kg.m^{-2}.s^{-1}, d is the tube diameter in metres, and p is the pressure in bars. The exponent 'a' depends on the tube diameter. It is 0.4 for tubes of diameter values greater than 0.01 m, and 0.6 otherwise. The correlation for high-quality flow is written in the form of:

Biasi et al. (1967) stated that these correlations predict their own data and the data of Macbeth (1963) and Becker (1965) with root-mean-square errors ranging from 6.5% to 11.3%.

$$q_c = \frac{3.78 \cdot 10^3 \, h(p)}{d^a \, G^{0.6}} \, (1 - x_c) \tag{2.6}$$

$$h(p) = -1.159 + 0.149 \, p \, \exp(-0.019 p) + \frac{8.99 p}{10 + p^2} \tag{2.7}$$

2.3.1.3 The Bowring Correlation

Bowring (1972) correlated the CHF in terms of inlet flow parameters (i.e., pressure, mass flux, inlet subcooling, and tube diameter). The correlation was based on the same form as that proposed by Thompson and Macbeth (1964). It is expressed as:

$$q_c = \frac{A + \frac{1}{4} d \, G \, \Delta H_{in}}{C + L} \tag{2.8}$$

where ΔH_{in} is the inlet subcooling in $J\cdot kg^{-1}$ and L is the tube length in metres. The expressions A and C are defined as

$$A = \frac{2.317 F_1 (\frac{1}{4} H_{fg} d G)}{1 + 0.0143 F_2 d^{0.5} G}$$
$$C = \frac{0.077 F_3 d G}{1 + 0.347 F_4 (7.4\times10^{-4} G)^{(2 - 0.0725 p)}} \tag{2.9}$$

where (for $R_p < 1$)

$$F_1 = \frac{R_p^{18.94} \exp(20.89 (1 - R_p)) + 0.917}{1.917}$$
$$F_2 = \frac{1.309 F_1}{R_p^{1.316} \exp(2.444 (1 - R_p)) + 0.309}$$
$$F_3 = \frac{R_p^{17.023} \exp(16.658 (1 - R_p)) + 0.667}{1.667} \tag{2.10}$$
$$F_4 = F_3 R_p^{1.649}$$
$$R_p = 2 - 0.5 p$$

where (for $Rp > 1$)

$$F_1 = R_p^{-0.368} \exp(0.648 (1 - R_p))$$
$$F_2 = F_1 R_p^{0.448} \exp(-0.245 (1 - R_p))$$
$$F_3 = R_p^{0.219} \tag{2.11}$$
$$F_4 = F_3 R_p^{1.649}$$
$$R_p = 2 - 0.5 p$$

2.3.1.4 The Doroschuk et al. Correlation

Doroschuk et al. (1980) developed a correlation with their 8-mm tube data covering pressures from 5 to 19.6 MPa and mass fluxes from 0.75 to 3 $Mg.m^{-2}.s^{-1}$. Their correlation is expressed as

$$q_c = \left(10.3 - 17.5\left(\frac{p}{98}\right) + 8.0\left(\frac{p}{98}\right)^2 \right) \exp(-1.5x_c) \left(\frac{G}{1000}\right)^{0.68(p/98) - 1.2x_c^{-0.3}} \tag{2.12}$$

A tube-diameter correction factor is used to extend this correlation to other tube-diameter values (from 4 to 16 mm). It is expressed as

$$\frac{q_{c,d}}{q_{c,0.008}} = \left(\frac{d}{0.008}\right)^{-1/2} \tag{2.13}$$

This correction factor applies to mass fluxes from 3 to 19.6 $Mg.m^{-2}s^{-1}$ and pressures from 0.75 to 5 MPa.

2.3.2 Semi-analytical Models

Semi-analytical models were developed with fundamental equations, and supplemented with closure relationships. They were primarily aimed at a specific dryout mechanism because of the uncertainties in the mechanism for DNB. To ease the modeling effort, many simplifying assumptions have been introduced. In most cases, this reduces the prediction accuracy of the modeling compared to the empirical correlations. However, the models can generally provide valid and realistic predictions outside the range of the data base. While many CHF models have been proposed, only representative examples will be discussed in this section.

2.3.2.1 The Becker Model

Becker (1965) presented an analysis on CHF prediction for vertical upward flow. The model postulated that dryout occurs at a position where liquid film is depleted. The location is independent of inlet subcooling and heated length, but depends on local parameters of pressure, heat flux, thermodynamic quality, mass flux, and tube diameter. The mass balance of the model involves liquid entrainment and droplet deposition, which are expressed by empirical functions. The correlation is expressed as:

$$\frac{1}{G^{0.5}\,(q_c/A)} = f(x_c,p) = \frac{B v_{fg}}{D H_{fg}} \tag{2.14}$$

where D is the droplet deposition rate. The parameter B is a complex function expressed in terms of critical quality, entrainment rate, and the parameter B itself. Therefore, a mathematical solution of this transcendental equation was derived. The CHF is calculated by solving this correlation together with the heat-balance equation.

2.3.2.2 The Tong Models

Tong (1968) postulated that the boiling crisis at subcooled conditions is primarily a hydrodynamic phenomenon. The process begins with stagnation under the bubbly boundary layer, which separates the bubbles from the heated wall. Due to the high heat flux from the surface, the stagnant liquid evaporates and forms a vapour blanket on the heated wall. Based on the formulation of Kutateladze and Leont'ev (1966) for the critical conditions of boundary layer separation from a flat plate with isothermal injection of the same fluid, Tong (1968) derived a CHF equation for subcooled flow boiling, which is expressed as

$$q_c = (1.76 - 7.433x_c + 12.222x_c^2)\, H_{fg}\, \rho_l\, U_o\, Re^{-0.6} \tag{2.15}$$

where U_o is the bulk-fluid velocity in $m \cdot s^{-1}$.

Tong (1972) developed a model for annular-film dryout, which relates liquid-film thickness to the rates of liquid entrainment, droplet deposition, and liquid evaporation. These rates are expressed as functions of mass flux, void fraction, heat flux and boiling length. The increase in local quality and steam velocity reduces liquid film thickness and hence decreases the dryout heat flux. The CHF is correlated as a function of pressure, thermodynamic quality, mass flux and tube diameter.

2.3.2.3 The Katto Correlation

Katto (1978) derived a simple dimensionless CHF correlation for vertical tube flow with subcooled fluid (no entrained vapour) at the inlet. The correlation postulates that hydrodynamic condition of two-phase vapour-liquid flow is responsible for CHF. A dimensional analysis was applied to derive the correlation by assuming at CHF condition there is a superficial vapour velocity ($q_c/\rho_v H_{fg}$) which is dependent to: the liquid velocity u; the densities of liquid and vapour which are related to inertia; the interfacial surface tension σ; the viscosities of the two phases which are related to viscous force, and the gravitational force which is related to buoyancy. The correlation in its basic form:

$$\frac{q_c}{G H_{fg}} = a \left(\frac{\rho_v}{\rho_l}\right) \left(\frac{\sigma \rho_l}{G^2 l}\right) \frac{1 - K x_c}{1 + K \left(\frac{\sigma \rho_l}{G^2 l}\right)^e \left(\frac{\rho_l}{\rho_v}\right)^m \left(\frac{\sigma \rho_l}{G^2 l}\right)^n \left(\frac{l}{d}\right)} \tag{2.16}$$

where a, b, c, e, m, n, and K are constants (correlated from experimental data) which vary corresponding to three different characteristic regimes dependent mainly on the range of mass fluxes.

The basic form of this dimensionless CHF correlation may be applicable to different types of fluids.

2.3.2.4 The Weisman and Pei Bubbly-Flow Model

Weisman and Pei (1983) derived a theoretical model for low-quality flows based on bubble crowding and vapour blanketing phenomena. Their model expects that the mass interchange between the core region and bubbly layer depends on the conditions of occurrence of a vapour blanket. It postulates on the buildup and thickening of a bubble layer along the channel until a region near the wall is filled up with bubbles where turbulent eddies are small in size and insufficient to move the bubbles. The CHF occurs at the region where the bubbly layer is thickest, when the void fraction in the bubbly layer exceeds a critical value such that an array of ellipsoidal bubbles cannot be maintained without significant contact between these bubbles. Weisman and Pei suggested a value of 0.82 for the critical void fraction after comparing the predictions of their model against a large number of data. The critical average bubble diameter was evaluated with the Levy (1966) model which was derived on the balances between the buoyancy and drag forces against surface tension.

The CHF in the Weisman and Pei model is expressed as

$$q_c = H_{fg}\, G\, (x_2 - x_1)\, i_b\, \psi\, \frac{H_f - H_{ld}}{H_l - H_{ld}} \tag{2.17}$$

$$i_b = 0.462\, Re^{-0.1}\, k^{0.6} \left(\frac{d_p}{d}\right)^{0.6} \left(1 + a\left(\frac{\rho_l - \rho_g}{\rho_g}\right)\right) \tag{2.18}$$

$$Re = \frac{G\, d}{\mu_l} \tag{2.19}$$

where ψ is a function of radial velocity created by vapour generation and the deviation of radial fluctuating velocity, d_p is the diameter of a bubble in metres, H_l and H_f are enthalpy values of the subcooled and saturated liquid, respectively, in J·kg^{-1}, H_{ld} is the liquid enthalpy at the point of bubble detachment in J·kg^{-1}, and ρ_l and ρ_g are densities of liquid and vapour, respectively, in kg·m^{-3}. An iterative scheme is used to calculate the CHF from these equations.

Agreement was apparent between predictions and the 1 500 data obtained with water flow in a uniformly heated tube. These data cover the following ranges: pressures from 2 to 20.5 MPa, mass fluxes from 1 to 13.6 Mg.m^{-2}.s^{-1}, heated lengths from 0.035 to 0.36 m, and tube diameters from 1.15 to 37.5 mm.

2.3.2.5 The Whalley et al. Model

Whalley et al. (1978) developed an annular-film dryout model for high-quality flow by evaluating the entrainment, deposition and evaporation rates from the liquid film. Critical heat flux is calculated based on a mass balance between liquid film flow rate and rates of entrainment and deposition. The variation of liquid-film flow rate is expressed as

$$\frac{dG_{lf}}{dz} = \frac{4}{d}\left(D - E - \frac{q}{H_{fg}} \right) \tag{2.20}$$

where G_{lf} is the mass flux of liquid film at the wall in kg.m^{-2}.s^{-1}, z is the tube length in metres, D is the liquid mass flux due to deposition in kg.m^{-2}.s^{-1}, and E is the liquid mass flux due to entrainment in kg.m^{-2}.s^{-1}. Both the entrainment and deposition mass fluxes were expressed in terms of a mass-transfer coefficient:

$$\begin{aligned} D &= k\,C \\ E &= k\,C_E \end{aligned} \tag{2.21}$$

The model requires a simultaneous solution of the liquid-film flow, liquid-film thickness and pressure drop, often referred to as the triangular relationship. Dryout was assumed to occur when the liquid film flow rate decreases to zero. The liquid-film thickness is calculated using

$$\delta = \frac{d}{4}\left(\frac{(dp/dz)_{lf}}{(dp/dz)} \right)^{0.5} \tag{2.22}$$

2.3.2.6 The Lee and Mudawwar Model

Lee and Mudawwar (1988) developed a CHF model for subcooled boiling based on the microlayer dryout theory. They postulated that CHF occurs as a result of Helmholtz instability if heat flux is sufficient for microlayer dryout. CHF is modeled as a function of microlayer thickness and velocity (determined from a force balance on the vapour blanket), and the length of vapour blanket (determined by the critical wavelength of the Helmholtz instability). The CHF is expressed as:

$$q_c = \frac{G_m \, \delta_m \, (H_{fg} + a C_p (T_{sat} - T_l))}{L_m} \tag{2.23}$$

where G_m is the mass flux of the microlayer in kg.m^{-2}.s^{-1}, δ_m is the microlayer thickness in metres, L_m is the length of the microlayer in metres, and T_l and T_{sat} are the local mean bulk temperature and saturation temperature, respectively, in °C. The microlayer thickness is expressed as

$$\delta_m = \frac{0.421 \, b \, Re^{(c-0.1)} \, G \, \rho_g \, H_{fg}^2 \, d_B}{(q_c - a \, h_{sc} (T_{sat} - T_l))^2} \left(1 + \frac{\delta_m}{\delta_m + d_B} \right) \left(\frac{L_m \, g \, \Delta\rho}{\rho_l \, C_d} \right)^{-0.5} \tag{2.24}$$

The bubble diameter is defined as

$$d_B = 0.015 \left(\frac{\sigma \, d}{\tau_w} \right)^{0.5} \tag{2.25}$$

and the drag coefficient is

$$C_d = \frac{2 \, d_{eB}}{3} \left(\frac{\sigma}{g \, \Delta\rho} \right)^{-0.5} \tag{2.26}$$

where d_{eB} is the equivalent bubble diameter. The length of the microlayer is determined with the critical wavelength of Helmholtz instability, and is expressed as

$$L_m = \frac{2\pi\sigma(\rho_l + \rho_g)}{\rho_l \rho_g U_B^2} \tag{2.27}$$

where U_B is the velocity of the vapour blanket in m·s^{-1}. The heat-transfer coefficient for subcooled boiling is expressed as

$$h_{sc} = \frac{230 q B_o^{0.5}}{(T_{sat} - T_m)(230 B_o^{0.5} - 1) + q/h_{FC}} \tag{2.28}$$

where h_{FC} is the heat-transfer coefficient for single-phase forced convection based on the Dittus and Boelter equation, which is expressed as

$$h_{FC} = \frac{k_l}{d} 0.023 Re^{0.8} Pr_l^{0.4} \tag{2.29}$$

The constants a, b and c were correlated with the Russian data. Numerical iterations are used to solve all these interrelated equations. This model was tested against experimental data of De Bortoli et al. (1958), Lee and Obertelli (1963), Matzner (1963), Thompson and Macbeth (1964), and Williams and Beus (1980).

2.3.2.7 The Katto Model

Katto (1990) developed a CHF model for subcooled boiling based on a theory of liquid sublayer dryout. This model was based on the similarity between subcooled flow boiling and pool boiling at dryout, and the CHF is expressed as

$$q_c = \frac{\delta_s \rho_l H_{fg} U_B}{L_B} \tag{2.30}$$

where L_B is the mean length of the vapour blanket in metres, and has the same definition as L_m

(Equation (2.24)) in the model of Lee and Mudawwar (1988). The sublayer thickness, δ_s, is calculated using a model by Haramura and Katto (1983) by taking into account the differences between forced and natural convection. It is written as

$$\delta_s = \frac{\pi (0.0584)^2}{2} \left(\frac{\rho_g}{\rho_l} \right)^{0.4} \left(1 + \frac{\rho_g}{\rho_l} \right) \frac{\sigma}{\rho_g} \left(\frac{\rho_g H_{fg}}{q_b} \right)^2 \tag{2.31}$$

$$\begin{aligned} q_b &= q - q_{FC} \\ q_{FC} &= h_{FC} (T_w - T_l) \end{aligned} \tag{2.32}$$

where q is the total heat flux in W·m^{-2}, q_{FC} is the heat-flux component for single-phase forced convection in W·m^{-2}, h_{FC} is the Dittus-Boelter heat-transfer coefficient for single-phase forced convection in W.m^{-2}.K^{-1}, σ is the surface tension in N·m^{-1}, and T_w is the surface temperature in °C. The single-phase heat-transfer coefficient is calculated using the Dittus-Boelter equation.

The mean velocity of the vapour blanket is defined as

$$U_B = k U_\delta \tag{2.33}$$

$$k = \frac{K_1}{1 + K_2 (\rho_v / \rho_l)^{K_3}} Re^{-0.8} \tag{2.34}$$

where K_1, K_2 and K_3 are void-fraction dependent coefficients. The local velocity of homogeneous two-phase flow is based on the Karman velocity distribution and is expressed as

$$U_\delta = U_\delta^+ \left(\frac{\tau_w}{\rho_{tp}} \right)^{0.5} \tag{2.35}$$

where ρ_{tp} is the two-phase homogeneous density in kg·m^{-3}. The wall shear stress is calculated using

$$\tau_w = \frac{f}{8} \rho_{tp} \left(\frac{G}{\rho_{tp}} \right)^2 \tag{2.36}$$

and the friction factor is evaluated using the Prandtl-Karman equation

$$\frac{1}{\sqrt{f}} = 2.0 \log_{10}(Re\sqrt{f}) - 0.8 \tag{2.37}$$

Since heat flux is required in the sublayer-thickness calculation, an iterative procedure is required to solve for the CHF.

2.3.2.8 The Megalla Model

Megalla (1990) developed a model to predict the liquid-film dryout location for annular and wispy-annular flow in vertical tubes. This model was based on a mass-transfer coefficient of the droplet deposition rate, which is expressed as a function of the Reynolds number of the vapour core and the relative motion between liquid droplets and vapour. The steady-state momentum equations for the droplets and vapour phase are expressed as functions of the droplet drag coefficient:

$$C_{dd} = Max\left(0.44, \frac{24}{Re_d} (1 + 0.15\, Re_d^{0.687}) \right) \tag{2.38}$$

The interfacial shear stress is calculated using the Wallis (1970) model. Similar to the Whalley et al. model (Section 2.3.2.5), the entrainment and deposition mass fluxes were expressed as functions of the droplet concentration and mass-transfer coefficient. Megalla employed separate coefficients and concentration values for deposition and entrainment, i.e.,

$$\begin{aligned} D &= k_D\, C_D \\ E &= k_E\, C_E \end{aligned} \tag{2.39}$$

The mass-transfer coefficient for entrainment, k_E, was calculated using the Katto correlation (1978). Megalla derived a correlation for the mass-transfer coefficient for deposition, k_D, which is written as

$$k_D = 1.15\, k_E \frac{\cosh(Re_d/7000)}{\cosh(Re_d/(1.1\cdot 10^6))} \tag{2.40}$$

2.3.2.9 The Sugawara Model

Sugawara (1990) developed a complex three-fluid (liquid film, vapour, entrained droplets suspended in vapour) model for vertical upward flow in tubes. This model includes the simulation of flow regions at entrance, transition between bubbly to slug flow, and liquid-vapour-droplet annular flow. Several correlations were used for deposition rate, entrainment rate, wall shear stress and droplet sizes. Sugawara showed that this model provides a closer agreement between predictions and data than other models (e.g., the Katto (1990) model).

2.3.2.10 The Lee et al. (1992) Model

Lee et al. (1992) modified the Katto (1990) model for liquid sublayer dryout. The main difference between these models is the evaluation of the vapour blanket velocity, which was calculated by solving conservative equations for mass, energy and momentum simultaneously in the model of Lee et al. (1992). Equation (2.21) was used to calculate the CHF.

2.3.3 CHF Look-up Tables

Both correlations and semi-analytical models are limited to a unique CHF mechanism, and often provide invalid predictions when extrapolated to other CHF mechanisms. A combination of several correlations or different models has been suggested to extend the range of application. However, this introduces a discontinuity in the transition regions. An approach was introduced by Doroshchuk et al. (1975), who tabulated the CHF values of about 5 000 data points at discrete values of pressure, mass flux and local critical quality. Despite a larger data base than those used in deriving either the correlations or the semi-analytical models, the range of application of this CHF look-up table remains limited.

Groeneveld et al. (1986) expanded the CHF look-up table of Doroshchuk et al. with over 15 000 data points. Since then, a number of look-up tables have been presented (Leung and Groeneveld, 1993), but the CHF table of Groeneveld et al. still provides the best prediction accuracy. Recently, Groeneveld et al. (1996) updated the 1986 table with a combined CHF data base of over 30 000 data points from the Institute of Physics and Power Engineering (of Russia) and Atomic Energy of Canada Limited (AECL). These data cover the following range of flow conditions: tube diameters from 0.620 to 92.40 mm, heated length values from 0.011 to 20.00 m, pressures from 0.1 to 21.20 MPa, mass fluxes from 0.006 to 24.27 $Mg.m^{-2}.s^{-1}$, local critical qualities from -1.652 to 1.577, and inlet subcooling values from -1211 to 2711 $kJ \cdot kg^{-1}$. Despite the large database, the availability of data remains scarce at the extreme conditions (e.g., high-flow and high-quality conditions). Therefore, the CHF look-up table of Groeneveld et al. (1996) is limited to the following range of flow conditions: pressures from 0.1 to 20 MPa, mass fluxes from 0 to 8 $Mg.m^{-2}.s^{-1}$, and dryout qualities from -0.5 to 1.

The CHF look-up table of Groeneveld et al. (1996) provides CHF values primarily for an 8-mm, uniformly heated tube with a vertical upward flow of steam-water mixture. Groeneveld et al. (1986) introduced a number of correction factors to extend the applications of the CHF look-up table to conditions and geometries other than the reference case. For the tube-diameter effect, the correction factor suggested by Doroshchuk et al. (1980) was used (i.e., Equation (2.11)).

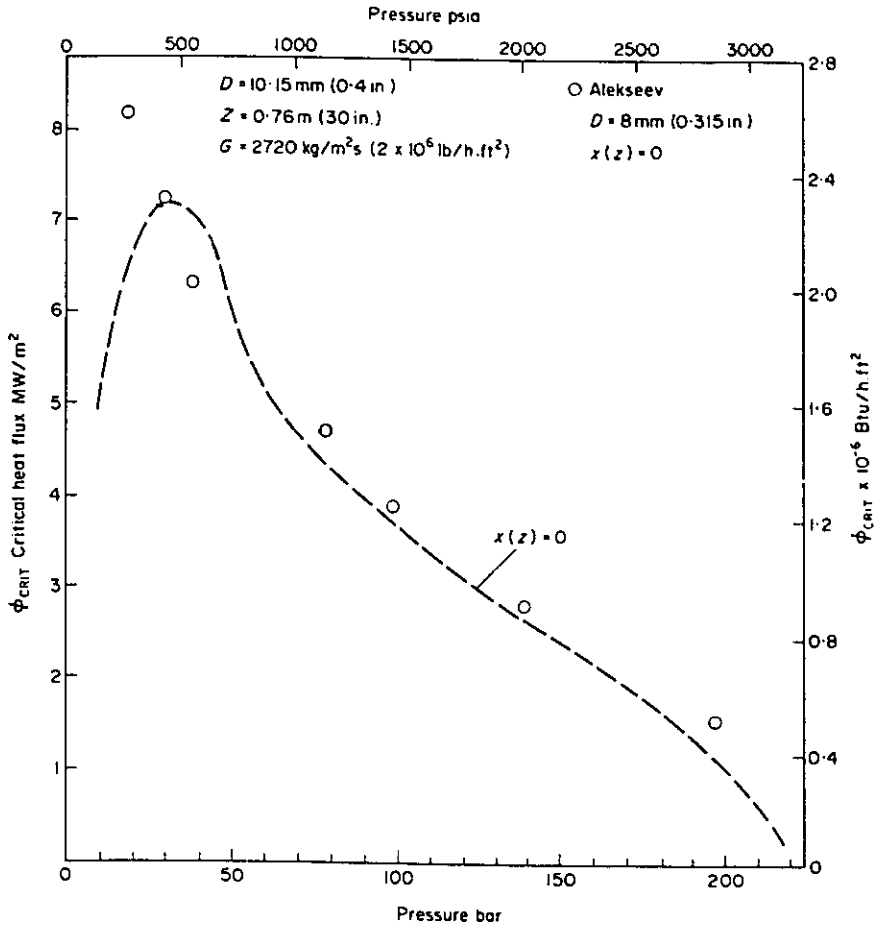

Figure 2.1: Relation Between Subcooled Flow CHF and Pressure Based on Constant Exit Quality (Collier 1972)

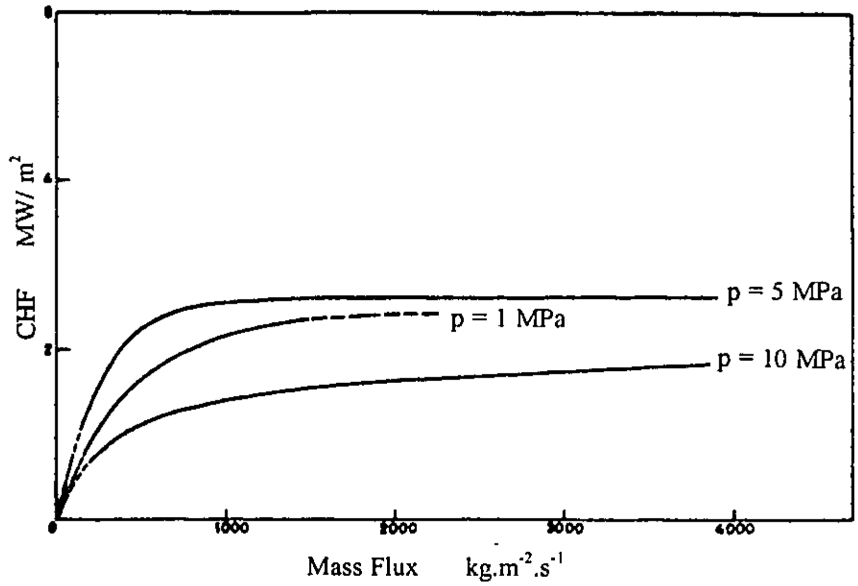

(Tube diameter 0.01 m, Length 1 m, Zero Inlet Subcooling)

Figure 2.2: Relation Between CHF and Mass Flux for Upward Flow in Tube Based on Constant Inlet Subcooling (Bowring 1972)

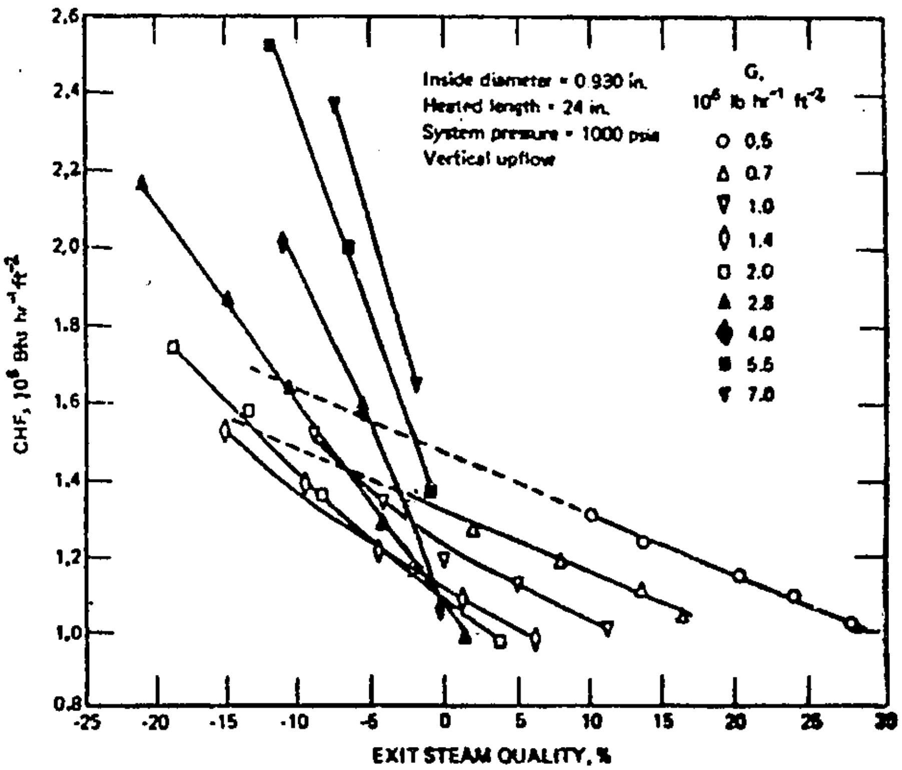

(Tube Diameter 23.6 mm, Pressure 6.9 MPa)

Figure 2.3: Relation Between CHF and Mass Flux for Upward Flow in Tube Based on Exit Quality (Griffel and Bonila 1965)

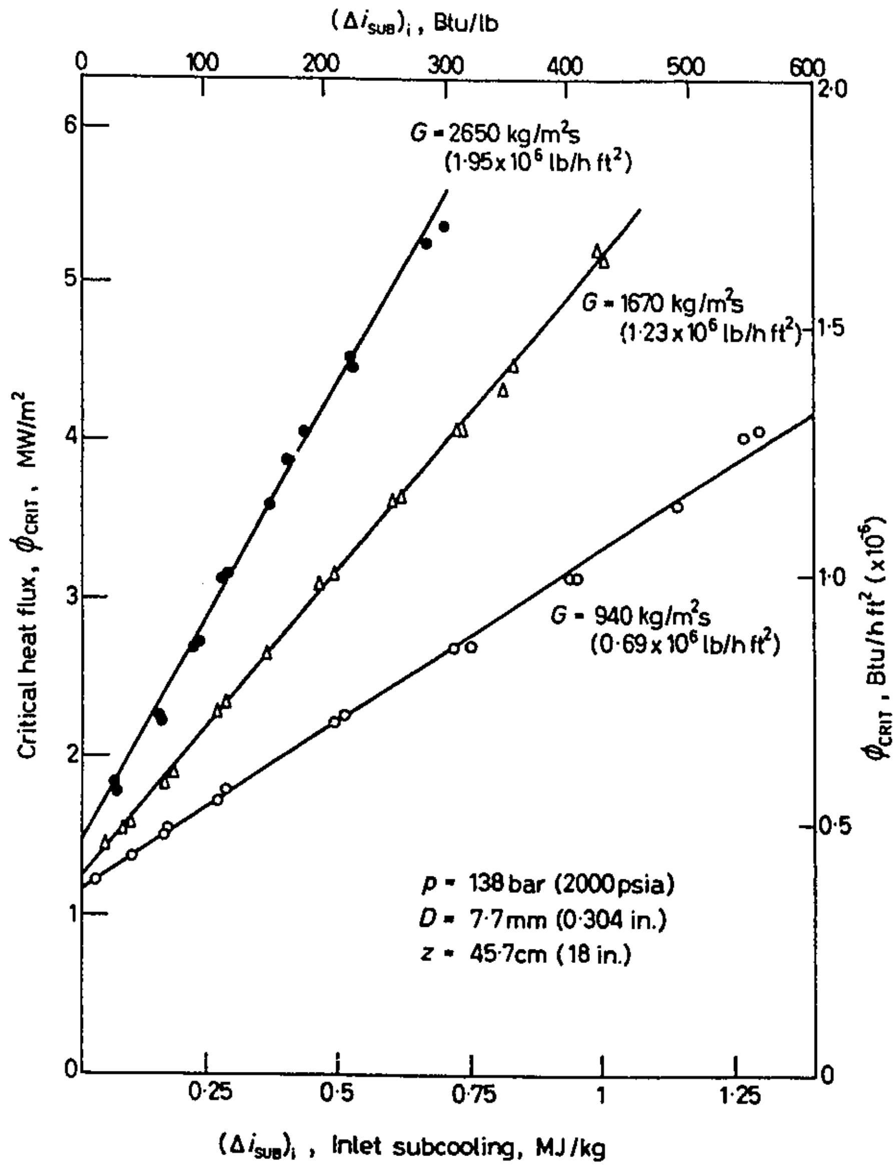

Figure 2.4: Effects of Inlet Subcooling on CHF (Collier 1972)

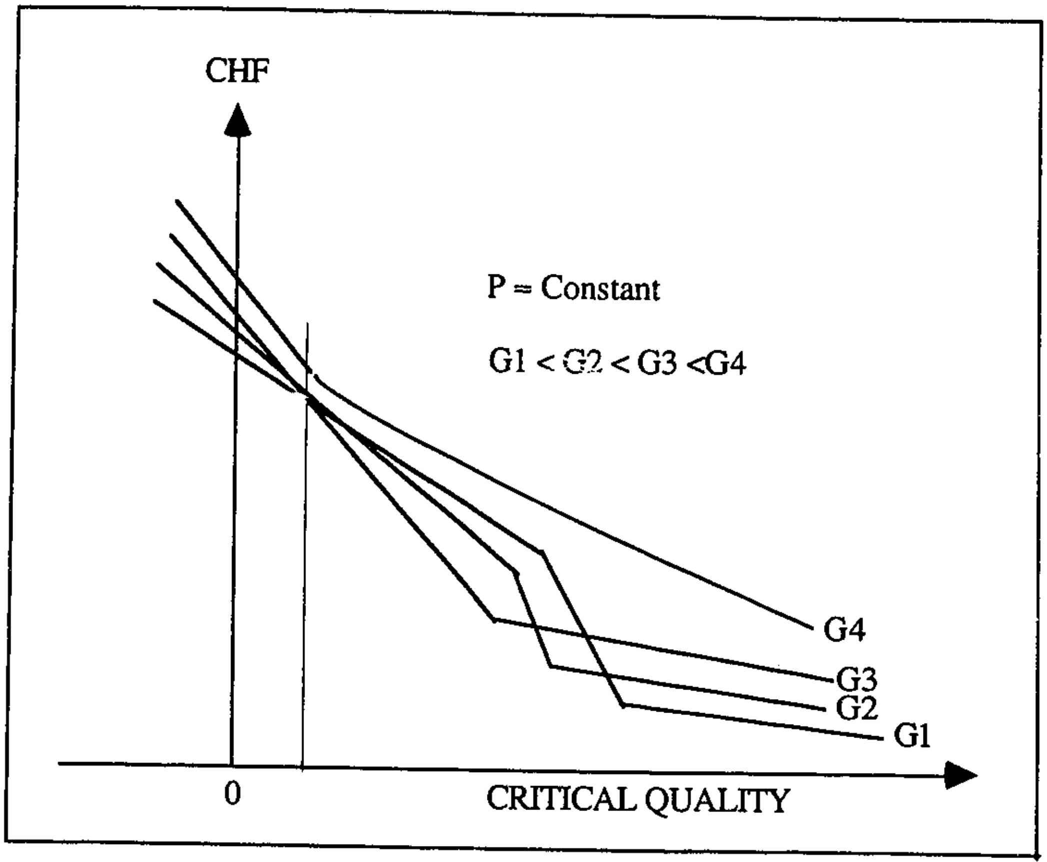

Figure 2.5: Qualitative Dependence of CHF on Critical Quality at Different Mass Fluxes (Boltenko 1989)

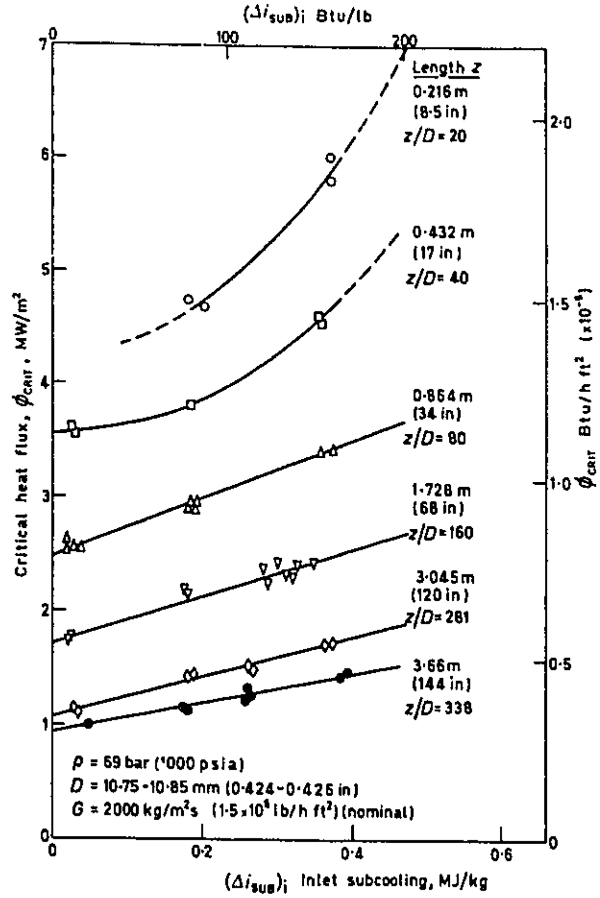

Figure 2.6: Effects of Tube Length on CHF at Fixed Inlet Conditions (Collier 1972)

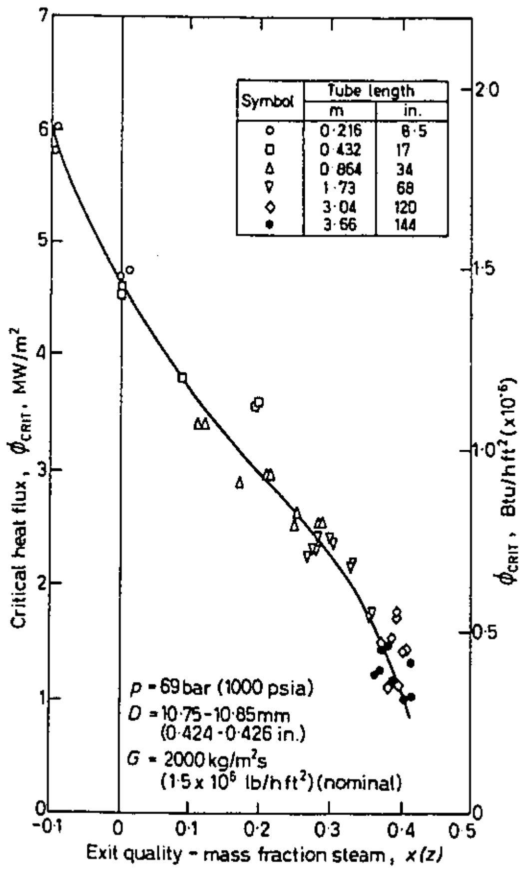

Figure 2.7: Effects of Tube Length on CHF at Fixed Exit Quality (Collier 1972)

3. LITERATURE SURVEY OF THE DIAMETER EFFECT ON CRITICAL HEAT FLUX

The effect of tube diameter on CHF in vertical flow has not been extensively studied, compared to flow parameters, which have a more dominant effect on CHF. The experimental data obtained from a single test facility usually cover only a limited range of flow conditions and tube diameters. As a result, most analyses and prediction methods pertaining to the diameter effect on CHF are suitable only for restricted applications. Nevertheless, the observations and conclusions drawn from a combination of these studies provide a good general view. This section describes some of the observations from experiments, empirical correlations and models that are related to the tube-diameter effect on CHF.

3.1 OBSERVATIONS FROM EXPERIMENTAL DATA

Experimental data obtained from test facilities suitable for the study of the diameter effect usually cover narrow ranges of local conditions, caused by the design limitation of the facility, such as power to the test section, cooling to the flow, and the pump head. As a result, the experiments focus on either a small variation of tube diameters or a narrow range of flow conditions. For most of the pre-1970 CHF experiments, data were presented for various diameters at constant inlet flow conditions. The effect of tube diameter on CHF cannot be examined because the effects of heated length were also involved. The use of constant local dryout conditions minimizes the effect of heated length and permits a more systematic study of the diameter effect.

A number of investigators have reported on the experimentally observed diameter effects on CHF. However, their analyses of the effects are scarce and often lack details. This chapter summarizes the relevant studies.

3.1.1 Lee and Obertelli Data

Lee and Obertelli (1963) obtained over 600 CHF data points at both subcooled and high-quality conditions. Their experiments covered pressures from 3.8 to 11 MPa, mass fluxes from 0.4 to 4.1 $Mg.m^{-2}.s^{-1}$, inlet subcoolings from 20 to 107°C, exit qualities from -0.2 to 0.95, and tube diameters from 5.6 to 11.5 mm (heated length to diameter ratio, L/d, from 20 to 360). Figure 3.1 shows the CHF data of the 5.6 and 10.8 mm tubes at a pressure of 6.9 MPa and mass fluxes from 1 to 4 $Mg.m^{-2}.s^{-1}$. The effect of tube diameter on CHF is observed from data of the high mass flux (4 $Mg.m^{-2}.s^{-1}$ or $3\cdot10^{6}$ $lb.ft^{-2}.hr^{-1}$); the CHF decreases with increasing tube diameter for constant dryout conditions. Due to the narrow range of local dryout conditions covered in other flow conditions, the tube-diameter effect cannot be directly examined. The same effect appears valid if the existing data trend is extrapolated.

3.1.2 Becker Data

Becker (1965) obtained a large amount of data that cover a wide range of flow conditions: pressures from 0.26 to 9.8 MPa, diameters from 4 to 25 mm, mass fluxes from 0.120 to 5.45 $Mg.m^{-2}.s^{-1}$, and local dryout qualities from 0 to 1. The effect of tube diameter on CHF was examined by comparing the experimental data against those of a 10-mm tube. Becker observed that the CHF is higher for tubes of diameter values smaller than 10 mm (e.g., about 20% higher for 4- and 6-mm tubes), but lower for tubes of diameter values larger than 10 mm (e.g., about 10% lower for a 25-mm tube). Figure 3.2 shows the relation between critical quality and the Becker burnout parameter (which is presented in Equation (2.12) and is inversely proportional to CHF) for a pressure of 7 MPa. At a constant critical quality, the burnout parameter increases (or the CHF decreases) with increasing tube diameter values.

A correction factor for the tube-diameter effect on CHF was described by Becker (1965). It represents the CHF ratio between a tube of interest to one of 10-mm inside diameter. Based on the experimental data, Becker presented graphically the correction factor for tubes of diameter values from 4 to 25 mm (Figure 3.3). The correction factor (and hence CHF) generally decreases with increasing diameter for tube diameters greater than 5 mm. An opposing trend appears, however, for a 4-mm tube where the correction factor becomes smaller than that of a 5-mm tube. No data was obtained for tube diameters smaller than 4 mm, and thus extrapolation of the correction factor to smaller tube diameters is not recommended. This correction factor has been validated with the Columbia and Winfrith data, which were predicted with an average error of 3% and 6%, respectively, using the Becker correlation.

3.1.3 Bergles Data

Bergles (1963) obtained subcooled CHF data with tubes of 1.2 to 2.4 mm in diameter. These data covered mass fluxes from 0.5 to 1.1 $Mg.m^{-2}.s^{-1}$ at a pressure of 0.2 MPa. Figure 3.4 shows that the CHF increases with decreasing tube diameter based on constant exit conditions. The tube-diameter effect appears to diminish for large diameter tubes (d > 6 mm (or 0.24 in)). The same trend was exhibited in the Becker correction factor, but a reduction in the tube diameter effect is observed for tubes of diameters larger than 25 mm. Unlike the Becker correction factor, Bergles showed consistently an increasing trend of CHF for small diameter tubes (down to 0.5 mm). However, the data scatter increases considerably as the tube diameter decreases.

Bergles et al. (1967) expanded the experiments to obtain CHF data at the positive-quality region. About 200 data points were collected; they covered pressures from 0.07 to 0.76 MPa, mass fluxes from 0.68 to 2 $Mg.m^{-2}.s^{-1}$, and tube diameters of 2, 2.4 and 6 mm. These data correspond to bubbly or slug flow at qualities lower than 0.02, and fully developed annular flow for qualities up to 0.7. Figure 3.5 shows the CHF data with respect to critical quality. Increase in CHF with increasing critical quality at a low-quality condition is caused by the unstable characteristic of slug and churn flow. Despite the large uncertainty among these data, the effect of tube diameter on CHF is clearly displayed by the data for the 2.4- and 6.1-mm tubes (0.094 in and 0.242 in, respectively). For the same critical quality, the CHF is higher for the 2.4-mm tube than for the 6.1-mm tube (e.g., a reduction of 40% in CHF was noticed at 25% quality). A comparison against data of the 2-mm tube cannot be made because of the differences in exit pressure (80 psia compared to 40 psia).

3.1.4 Ornatskiy Data

Ornatskiy (1969) obtained CHF data in tubes of diameter values from 0.5 to 12 mm. These data covered pressures from 1 to 21.6 MPa, mass fluxes from 0.75 to 90 $Mg.m^{-2}.s^{-1}$, and inlet subcoolings from 0 to 250 K. As Figure 3.6 shows, the CHF generally decreases with increasing tube diameter at small diameter tubes. Similar to the trend of the Bergles data, the tube-diameter effect diminishes for tubes of large diameter values. The critical diameter value (i.e., at which the diameter effect on CHF becomes negligible), however, appears to be affected by mass flux and quality. It is about 1.5 mm at a mass flux of 50 $Mg.m^{-2}.s^{-1}$, and 4 mm for mass fluxes less than 20 $Mg.m^{-2}.s^{-1}$.

3.1.5 Combined Data of Lee and Obertelli, and Matzner

Collier (1972) showed the diameter effect on CHF using data of Lee and Obertelli (1963) and Matzner (1963). These data were obtained at a pressure of 6.9 MPa and a mass flux of 2 $Mg.m^{-2}.s^{-1}$. Figure 3.7 shows the CHF values for various tube diameters with respect to critical quality. Except for the 5.6-mm tube, overlapping CHF conditions were observed for tubes of diameter range from 9.35 to 37.5 mm. In all cases, the decreasing CHF trend is clearly displayed with increasing tube diameter at constant dryout conditions. This trend is shown for both positive quality and subcooled conditions.

3.1.6 Levitan et al. Data

Levitan et al. (1981) obtained CHF data with tubes of various diameters (4, 6, 8 and 10 mm). These data covered pressures from 4.9 to 13.7 MPa, mass fluxes from 0.75 to 5 $Mg.m^{-2}.s^{-1}$, and a wide range of critical qualities. They correspond primarily to the dispersed annular-film dryout region. Although a large amount of data were obtained, the effect of tube diameter on CHF cannot be examined clearly from most data because the dryout conditions are different. Figure 3.8 illustrates the comparison of CHF data of Levitan for various tube diameters at the same dryout conditions. The general trend of increasing CHF with decreasing tube diameter is observed among the presented data. However, the magnitude of the increase is difficult to determine because a sharp decrease in CHF is found at certain qualities. Levitan termed these qualities the "boundary vapour content", which is encountered mainly at low-pressure and low-flow conditions. Levitan showed that the tube-diameter effect can be represented with the correction factor, Equation (2.11).

$$\frac{q_{c,d}}{q_{c,0.008}} = \left(\frac{d}{0.008}\right)^{-1/2} \qquad (3.1)$$

3.1.7 Smolin and Semenovker Data

Smolin and Semenovker (1981) obtained CHF data over a wide range of pressure, critical quality and tube diameters. Figure 3.9 shows the comparison of CHF data obtained in tubes of various diameters at a mass flux of 1 $Mg.m^{-2}.s^{-1}$ and pressures of 10, 12, 14 and 18 MPa. While the gradient of CHF with respect to critical quality is steeper at high qualities than low qualities, it is less drastic than those exhibited in the Levitan data. The "boundary vapour content", as referred to by Levitan, is encountered only at pressures of 9.8 and 12 MPa in the 8-mm tube and at a pressure of 11.8 MPa in the 10.8-mm tube.

An additional transition can be observed at the low-quality region in the 10.8-mm tube. The gradient of CHF with respect to critical quality is steep at the low-quality region where flow is likely bubbly, gradual at the mid-quality region where annular flow is expected, and becomes steep again at the high-quality region where annular flow with entrainment is anticipated.

The effect of tube diameter on CHF is displayed clearly at various pressures; the CHF for the

8-mm tube is generally higher than those for either the 10-mm or the 10.8-mm tubes. However, this relation is limited to data of the same flow regime only. Comparing data of different flow regimes (at low qualities), the CHF for the 8-mm tube becomes lower than that for the 10.8-mm tube at the same dryout conditions.

3.1.8 Nariai et al. Data

Nariai et al. (1987) obtained subcooled CHF data with water at low pressures and high mass fluxes (range from 7 to 20 $Mg.m^{-2}.s^{-1}$) in tubes of 1, 2 and 3 mm diameter and of 0.01 to 0.1 m in length. Since the tube length was relatively short compared to the tube diameter (length-to-diameter ratios from 3 to 50), a strong entrance effect on CHF is anticipated (Collier, 1972). This is reflected in Figure 3.10 where an increase in CHF is observed with decreasing tube diameter and heated length for the same dryout conditions. The effect of tube diameter on CHF is shown in Figure 3.11. It is strong for small length-to-diameter ratios, but becomes less significant for large ratios.

3.1.9 Boltenko et al. Data

Boltenko et al. (1988) observed that the diameter effect on CHF is affected by a change in dryout mechanism at various flow regimes. CHF appears to increase with increasing tube diameter at low quality or subcooled conditions, but reverses at high qualities. Between the low- and the high-quality regions, a transition exists and the diameter effect is small. The CHF data are shown in Figure 3.12 for tube diameters of 3.8, 6.1, and 8 mm at a pressure of 14.7 MPa and a mass flux of 4 $Mg.m^{-2}.s^{-1}$.

3.1.10 Cheng et al. Data

Cheng et al. (1992) presented their CHF data obtained with Freon flow in tubes of 4, 8, and 12 mm (ratios of heated-length to diameter from 86 to 165). These data are shown in Figure

3.13; they covered pressures from 1 to 3 MPa and mass fluxes from 1 to 6 $Mg.m^{-2}.s^{-1}$. The effect of diameter on CHF is significant at subcooled conditions, but diminishes at saturated conditions (above -10% critical quality). At subcooled conditions, an increase in CHF was observed for decreasing tube diameter. The diameter effect appears to be functions of pressure and mass flux. At high mass fluxes and pressures, a much stronger effect was observed. Furthermore, this effect may also depend on the diameter size.

3.1.11 Celata et al. Data

A large data bank of subcooled CHF data was compiled by Celata et al. (1993) for low-pressure and high heat-flux conditions (pressures from 0.1 to 5.5 MPa, diameters from 0.3 to 15 mm, heated lengths from 0.0021 to 0.3 m, mass fluxes from 2 to 40.5 $Mg.m^{-2}.s^{-1}$ and fluid subcoolings from 900 to 230 K). Ornatski (1969), Bergles (1977) and Vandervort et al. (1990) show that CHF increases significantly with decreasing tube diameters. The effect of diameter on CHF is also affected by mass flux. Combining their data with that of Nariai et al. (Figure 3.10), Celata et al. (1993) showed that the CHF decreases consistently with increasing diameter at subcooled conditions for tube diameter ranges from 2.5 to 8 mm (Figure 3.14). A diminishing diameter effect is also observed in large-diameter tubes.

3.2 CORRELATIONS AND PHYSICAL MODELS

The predicted CHF trends with respect to tube diameters of various correlations and semi-analytical models are examined. For empirical correlations, they usually represent the general trend of data and hence are limited to a specific range of conditions. For semi-analytical models, on the other hand, the tube diameter effect is commonly based on the parametric trends of the closure relations and is often difficult to review. The trends exhibited by the correlations and models can be used to substantiate the tube-diameter effect on CHF in regions where experimental data are unavailable.

3.2.1 The Macbeth Correlations

The Macbeth (1963) correlations are derived separately for low-flow and high-flow conditions. For low-flow conditions, the CHF is proportional to $d^{-0.1}$ for the same dryout conditions (Equation (2.2)). A more complex diameter effect on CHF is shown for high-flow conditions (Equation (2.3)). The diameter parameter in the second term is proportional to $d^{-0.4}$, while the exponent 'y_1' for the diameter parameter in the first term varies from -0.211 to -1.45 for pressures from 0.1 to 18.6 MPa. The variation of CHF with respect to critical quality and diameter is illustrated in Figure 3.15 for the Macbeth correlations.

3.2.2 The Biasi et al. Correlations

The correlations of Biasi et al. (1967) are derived for low- and high-quality regions. At constant dryout conditions, the effect of diameter on CHF is proportional to d^{-a}. However, the value of exponent 'a' depends also on the diameter; it is 0.4 for tube diameters less than 10 mm and 0.6 for tube diameters larger than 10 mm.

3.2.3 The Tong Models

The Tong model (1968) includes the diameter effect in the Reynolds number term (Equation (2.13)), which is proportional to $d^{-0.6}$. This function was derived from the interfacial friction factor based on the average value between laminar and turbulent flow in a smooth tube. As described in Section 2.3.2.2, this Tong model (1968) is valid for subcooled conditions only.

For annular flow, Tong (1972) postulated that CHF is affected by the thickness of liquid film at the wall. The thickness of the liquid film depends on the rates of liquid entrainment, droplet deposition, and liquid evaporation. These rates are influenced by mass velocity, bulk void fraction, heat flux, and boiling length. The increase in local quality and steam velocity reduce the liquid film thickness, thus decreasing the dryout heat flux. Tong correlated the CHF as functions of pressure, critical quality, mass flux and tube diameter. The CHF was shown proportional to $d^{-1/2}$.

3.2.4 The Doroschuk et al. Correlation

Doroschuk et al. (1975) derived a correction factor for the diameter effect, which is expressed as

$$\frac{q_{c,d}}{q_{c,0.008}} = \left(\frac{d}{0.008}\right)^{-1/2} \tag{3.2}$$

This correction factor was established with data obtained in tubes of 4 to 16 mm in diameter.

3.2.5 The Whalley et al. Model

The Whalley et al. (1978) model is based on a complex set of equations relating the rates of entrainment, deposition and evaporation. A number of closure relations have been suggested for this model; most of them are strongly dependent on tube diameter. In general, the entrainment rate is the driving mechanism for CHF. It is affected by the liquid film thickness, which in turn depends on the tube diameter. In small-diameter tubes, the liquid film thickness is thin. This reduces the entrainment rate and hence leads to an increase in CHF. This effect is described in detail in Chapter 5.

3.2.6 The Weisman and Pei Model

The effect of diameter on CHF is included primarily in the bubble-interchange parameter, i_b, in the Weisman and Pei (1983) model (Equation (2.15)). Assuming that the other parameters are independent of tube diameter, the predicted CHF is proportional to $d^{-0.7}$ for constant dryout conditions.

3.2.7 The CHF Look-up Table

Groeneveld et al. (1986) employed the same approach as Doroschuk et al. (1975) to correct CHF for the tube diameter effect. They observed a strong effect of quality on the exponent 'n' at some flow conditions, but the overall trend was inconclusive. By assessing the correction factor with their CHF database (over 15 000 data points), the exponent in Equation (3.2) was modified to -1/3 for tube diameters from 2 to 16 mm, i.e.,

$$\frac{q_{c,d}}{q_{c,0.008}} = \left(\frac{d}{0.008}\right)^{-1/3} \tag{3.3}$$

This correction factor was validated with the data of Becker (1965) and Doroschuk et al. (1980). For tube diameters greater than 16 mm, Becker and Soderquist (1992) suggested using an exponent that is much smaller than -1/2, but Doroschuk (1980) showed that values larger than -1/2 are more appropriate. Recently, Groeneveld et al. (1996) included the data bank of IPPE in their analysis and suggested a value of -1/2 for the exponent.

3.2.8 The Lee and Mudawwar Model

The diameter effect exhibited in the Lee and Mudawwar (1988) model cannot be easily examined. It affects mainly the calculation of the microlayer thickness in Equation (2.20). Within this calculation (Equation (2.21)), however, it has an impact on the Reynolds number, the bubble diameter, the drag coefficient, and the heat-transfer coefficient for subcooled boiling. A comparison between predictions of this model and experimental data for various tube diameter was shown by Lee and Mudawwar (Figure 3.16). Except for the 4-mm tube, the model predictions agreed closely with the data. Overall, the CHF predictions can be expressed as a function of $d^{-0.5}$.

3.2.9 The Boltenko et al. Correlations

Boltenko et al. (1988) showed that the diameter effect on CHF is a function of flow regime based on observations from experimental data. From the observed trends the data showed, the quality range was separated and categorized into five flow regimes: highly subcooled boiling, nucleate boiling, dispersed annular flow, transition region, and dispersed flow. Several correlations based on mass flux and pressure were derived to predict the flow-regime transitions.

Based on the diameter correction factor suggested by Levitan and Lanstman (1975) (i.e., Equation (3.2)), Boltenko et al. introduced a flow-regime dependent exponent. A positive exponent (n = +1/5) is recommended for highly subcooled flow. In addition, the correction factor is expressed as a function of quality, i.e.,

$$\frac{q_{c,d}}{q_{c,0.008}} = (1 - x_c)\left(\frac{d}{0.008}\right)^n \tag{3.4}$$

A similar function is used for dispersed annular flow, except a negative coefficient is suggested (i.e., n = -1/5). For dispersed annular flow where deposition is dominating, the quality effect is not present (Equation (3.2)) and the exponent 'n' is -1/3.

Later, Boltenko et al. (1989) modified their recommendation by neglecting the quality effect in the exponent. Several pressure and flow-regime dependent exponents were suggested. They are tabulated in the following table:

Pressure	Exponent n for: $CHF_d / CHF_8 = (d/8)^n$		
(MPa)	Subcooled & Nucleate Boiling	Dispersed Annular Flow	Dispersed Flow
1 to 6	0.188	-0.068	-0.266
6 to 14	0.263	-0.164	-0.197
14 to 20	0.418	n/a	-0.163

A revised set of pressure-dependent correlations were also introduced to predict the transitions between various flow regimes.

3.2.10 The Katto Model

The Katto (1990) model was also based on the microlayer dryout theory, as in the Lee and Mudawwar model. Due to its complexity, the effect of tube diameter on CHF cannot be clearly established. Katto compared the model predictions against data presented by Thompson and Macbeth (1964). These data covered the subcooled conditions at a pressure of 13.8 MPa, mass flux of 2 $Mg.m^{-2}.s^{-1}$, quality of -0.146, and tube diameters of 4, 8 and 12 mm. Figure 3.17 shows good agreement between the predictions and data. Similar to the Lee and Mudawwar model, the predicted CHF values appears to follow the trend of $d^{-0.5}$.

3.2.11 The Levitan Correlation

Levitan (1990) postulated that CHF at subcooled conditions is affected by the rates of bubble formation and removal at the wall layer. An increase in intensity of bubble removal, coupled with the decrease in intensity of bubble formation, leads to an increase in heat-removal rate and results in an increase in CHF. For flow in vertical tubes, vapour bubbles are primarily removed by the drag force, which is proportional to the velocity gradient in the wall layer, dU/dy. Bubble formation at the wall, on the other hand, depends on the wall layer temperature gradient; a steep temperature gradient causes a reduction of bubble formation. Since the tube diameter strongly affects the velocity and temperature gradient in the wall layer, it also has a significant impact on bubble formation and removal, and hence CHF.

For a turbulent subcooled liquid flow, the velocity profile of the wall layer of thickness y may be approximated as linear from zero at the wall to U_0, and at the liquid core $U = U_0$ = constant. Kutateladze (1966) suggested that:

$$\frac{\Delta\delta}{d} = Re^{-0.7} \tag{3.5}$$

where δ is the thickness of the laminar sublayer in metres. The velocity gradient is expressed as

$$\frac{dU}{dy} = \frac{U_o}{\Delta\delta} \propto \frac{Re^{0.7}}{d} \propto d^{-0.3} \tag{3.6}$$

and similarly,

$$\frac{dT}{dy} = \frac{T_w - T_o}{\Delta\delta} \propto d^{-0.3} \tag{3.7}$$

Since CHF increases with an increasing rate of bubble removal (from a higher wall velocity gradient, dU/dy) and a decreasing rate of bubble generation (from a steeper temperature gradient, dT/dy), the CHF can be approximated to:

$$q_c \propto \frac{dU}{dy}\frac{dT}{dy} \propto d^{-0.6} \tag{3.8}$$

Levitan showed that this proportionality agrees with the data trend of Rybin (1963) for tubes of 2 to 13 mm in diameter, where the CHF is proportional to $d^{-0.5}$ for a subcooled water and steam-water mixture (steam qualities from 0 to 0.1).

A similar analogy was made for dryout in annular dispersed flow with bubble entrainment. The liquid film is considered to be a single-phase flow because the film thickness is many times thicker than a viscous quasi-laminar flow. An increase in the temperature gradient in small-diameter tubes reduces the liquid superheat in the film and hence increases the CHF.

3.2.12 The Celata et al. Model

The Celata et al. (1994) model was developed for high subcooling and high mass-flux conditions. It exhibits an increasing CHF trend with decreasing tube diameter (Figure 3.18). Similar to other models, the CHF is proportional to $d^{-0.5}$.

3.3 SUMMARY

A complex effect of tube diameter on CHF has been shown among the experimental data. While a simple correction factor was suggested by a number of authors, this effect appears to be strongly affected by the flow conditions (and flow regimes). Tables 3.1 and 3.2 summarize the observations in CHF variation with tube diameter and the available prediction methods. Most studies showed an increasing CHF trend with decreasing tube diameter for both subcooled and saturated conditions. A few exceptions (e.g., Boltenko et al. (1988)) observed a reverse trend in subcooled boiling where CHF increases with increasing tube diameter.

3.3.1 Models for Subcooled and Low-quality Conditions

A number of models have been derived to predict CHF in bubbly flow. One of these models relates the diameter effect to the size of vapour bubbles and the thickness of bubble vapour layer adjacent to the wall. For small-diameter tubes, heat transferred from the liquid to the vapour bubbles is higher since the distance from the vapour bubble layer to the subcooled liquid flow at the core is reduced. This improves the rate of condensation of the growing vapour bubbles, and leads to a reduction in both bubble size and bubble boundary-layer thickness. The effective condensation also causes the vapour bubbles to collapse within the vapour layer. As a result, the CHF increases as the tube diameter decreases.

Another model postulated that void fraction within the bubble layer, along with the relative thickness of the bubble boundary layer, decreases when the tube diameter is smaller. This increases the amount of liquid re-entry for replenishment under the bubble layer, and raises the supply of liquid for condensation, and hence increases the CHF.

One theory postulated that the throughput velocity of the liquid core, or the velocity gradient at the two-phase boundary layer, increases as tube diameter decreases. This enhances the rate of detachment for the growing bubbles from the bubble layer into the liquid core, and reduces the size of the vapour patches. It is also suggested that the temperature gradient in the near-wall region increases for small-diameter tubes, and this improves heat transfer between bubbles and liquid, which in turn decreases the rate of bubble generation. As a result of the better heat-transfer rate and faster detachment of the bubbles, CHF becomes higher in narrow tubes.

Another theory considered the hydrodynamic phenomenon where CHF increases as a result of changes in the interfacial friction between the two phases. Since interfacial friction is inversely proportional to tube diameter (via the Reynolds number), CHF increases when the tube diameter is decreased (because the friction factor is greater).

3.3.2 Models for High-quality Conditions

The observations from virtually all experimental data suggested that the CHF is generally higher for smaller-diameter tubes at high-quality flow. For annular film flow, dryout occurs when the liquid film becomes too thin and breaks down into dry patches. Therefore, CHF depends strongly on the liquid film thickness, which in turn is affected by the rates of liquid entrainment, droplet deposition, and liquid evaporation. These rates are influenced by mass velocity, bulk void fraction, heat flux, and boiling length. Most annular-film dryout models were derived to calculate the variation in film thickness, by employing empirical equations for rates of liquid entrainment, liquid evaporation, and droplet deposition. These empirical equations are mostly functions of tube diameter (e.g., the deposition rate has been correlated with $d^{-0.5}$). At most conditions, the entrainment rate is the driving force for CHF, and depends strongly on the liquid film thickness. With decreasing tube diameter, the liquid film is relatively thinner and hence the height of the waves along the liquid film surface is reduced. The relative amount of wave-tips being torn off by the vapour flow and entrained into the vapour core may in effect reduces. This leads to a relative reduction in the entrainment rate and hence an increase in the CHF.

Another model developed for high-quality dryout was based on the analogy to the subcooled flow burnout by assuming a single-phase flow of liquid film. The increase in temperature gradient at the near-wall fluid in small-diameter tubes lowers the liquid superheat in the liquid film and increases the CHF.

Table 3.1: Summary Of Suggested Phenomenon and Mechanisms for Tube-Diameter Effect.

	Phenomenon in Small-diameter Tubes	Mechanisms for CHF Increase
Subcooled and low-quality flow	- smaller vapour bubble size - thinner vapour bubble boundary layer	- better heat transfer because of core flow closer to wall
	- void fraction within bubble layer decreases	- re-entry of liquid replenishment easier
	- velocity gradient of 2-phase boundary layer increases	- growing vapour bubble detaches easier before forming vapour patches at wall
	- temperature gradient of wall layer higher	- bubble generation slower, due to high condensation rate at the tip of the bubbles
	- interfacial friction inversely proportional to Reynolds number	- increase friction at two-phase boundary and increase heat transfer
High-quality, annular flow	- flow of liquid layer at wall thinner	- boiling is suppressed in the liquid film
	- lower entrainment rate	- liquid film thickness increases
	- temperature gradient of liquid film at wall increases	- liquid superheat in the film is reduced
	- rate of liquid deposition increases	- liquid film thickness increases

Table 3.2: Summary Of Correction Factors For Tube-Diameter Effect on CHF.

Diameter Effect and Prediction (same dryout conditions)	Reference	Validity Range
$CHF_d / CHF_{10} = f(d)$ $f(d) = 1.18$ to 0.9	Becker (1965)	d from 4 to 25 mm, P from 0.27 to 10 MPa, G from 0.12 to 5.4 $Mg \cdot m^{-2} \cdot s^{-1}$, x from 0 to 0.5
$CHF \propto d^{-0.4}$ (d >10 mm) $CHF \propto d^{-0.6}$ (d <10 mm)	Biasi et al. (1967)	d from 3 to 37.5 mm, P from 0.27 to 14 MPa, G from 0.2 to 6 $Mg \cdot m^{-2} \cdot s^{-1}$
$CHF \propto d^{-0.6}$	Tong (1968)	subcooled and low-quality flow
$CHF \propto d^{-0.5}$	Doroschuk et al. (1975)	d from 4 to 16 mm, correlation based on CHF data of 8-mm diameter tubes
$CHF \propto d^{-0.7}$	Weisman and Pei (1983)	d from 1 to 37.5 mm, P from 2 to 21 MPa, G from 0.1 to 13.6 $Mg \cdot m^{-2} \cdot s^{-1}$
$CHF_d / CHF_8 = \text{Max}(0.63, (d/8)^{-1/3})$	Groeneveld et al. (1986)	d from 2 to 32 mm
$CHF_d / CHF_8 = (d/8)^{0.2}(1+x)$ for subcooled and low qualities flow, $CHF_d / CHF_8 = (d/8)^{-0.2}(1+x)$ for dispersed annular flow, $CHF_d / CHF_8 = (d/8)^{-1/3}$ for transition, $CHF_d / CHF_8 = (d/8)^{-0.2}(1+x)$ for dispersed flow	Boltenko et al. (1988)	d from 4 to 20 mm, correlation based on CHF data of 8-mm diameter tubes
$CHF_d / CHF_8 = (d/8)^n$ $n=f(P, G, x)$	Boltenko et al. (1990)	x from -0.5 to 0.5, G from 1 to 6 $Mg \cdot m^{-2} \cdot s^{-1}$
$CHF \propto d^{-0.6}$	Levitan (1990)	

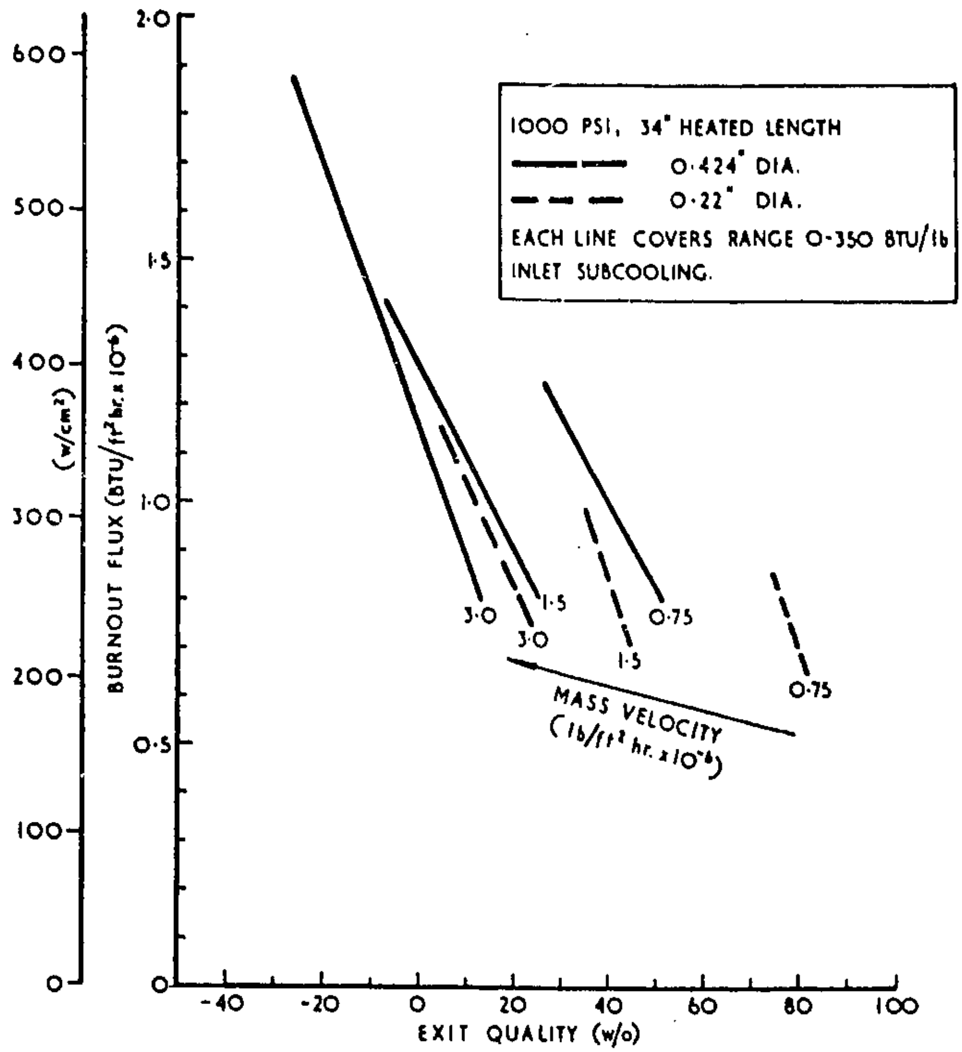

Figure 3.1: Diameter Effect Based on Exit Quality (Lee and Obertelli 1963)
(Diameter=5.6 and 10.8 mm, Pressure=6.9 MPa,
Mass flux=1 to 4 $Mg.m^{-2}.s^{-1}$)

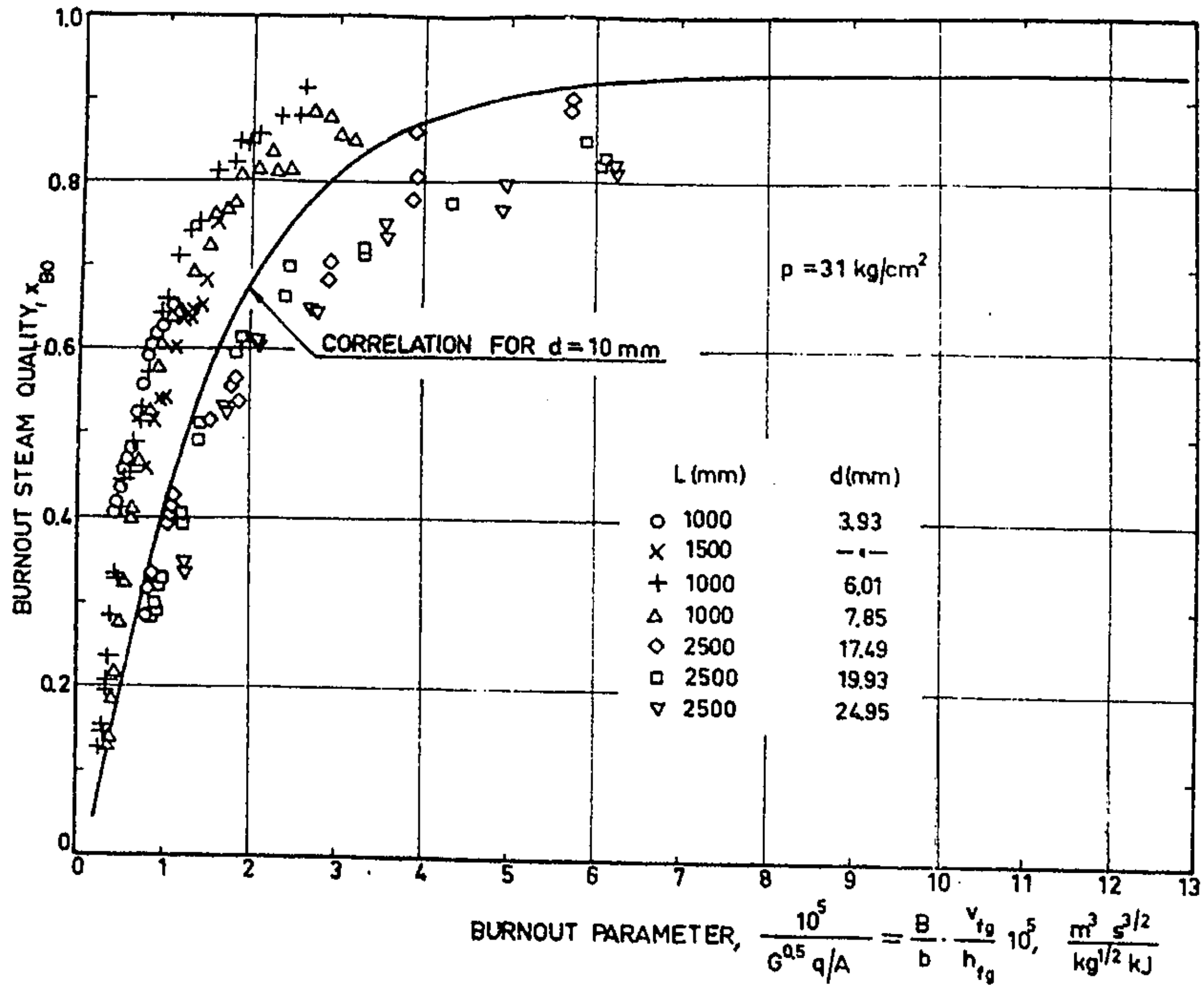

Figure 3.2: Experimental Data and Correlation Showing the Diameter Effect (Becker 1965)
(Diameter=3.9 and 25 mm, Pressure=3 MPa)

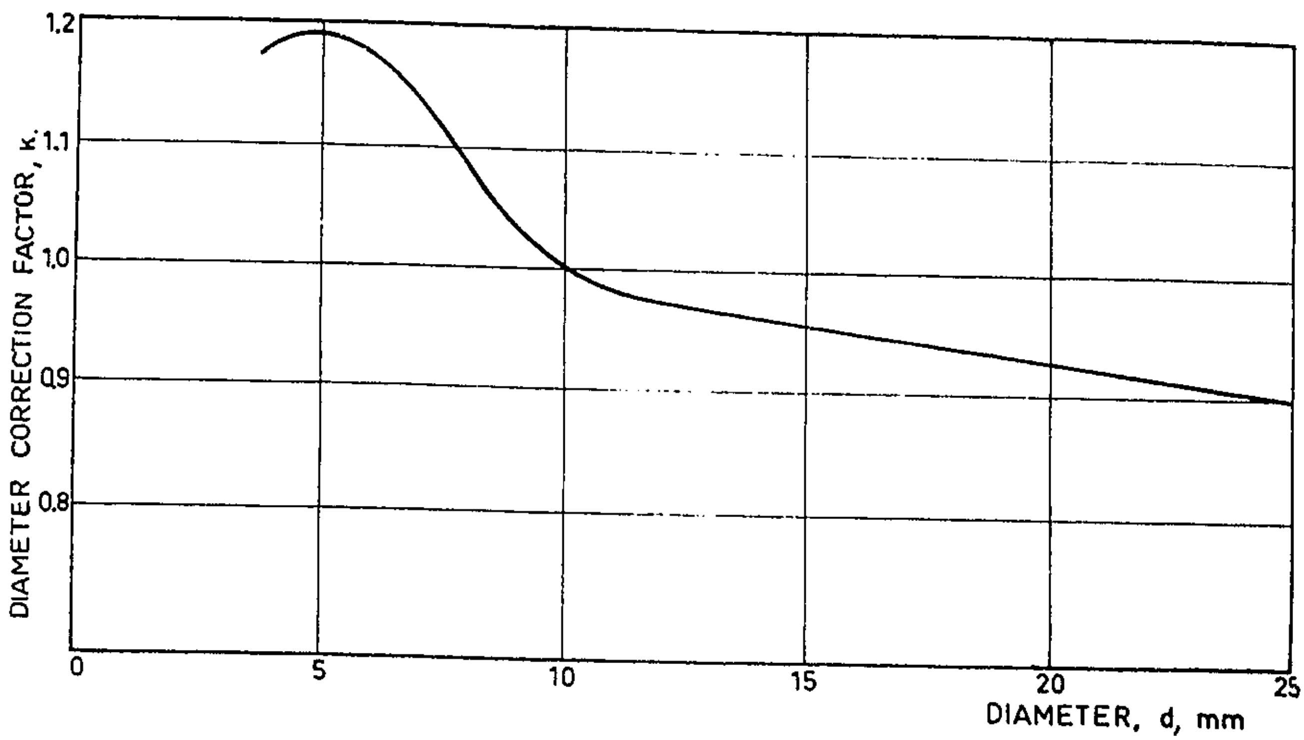

Figure 3.3: Diameter Correction Factor Correlated from Experimental Data (Becker 1965)

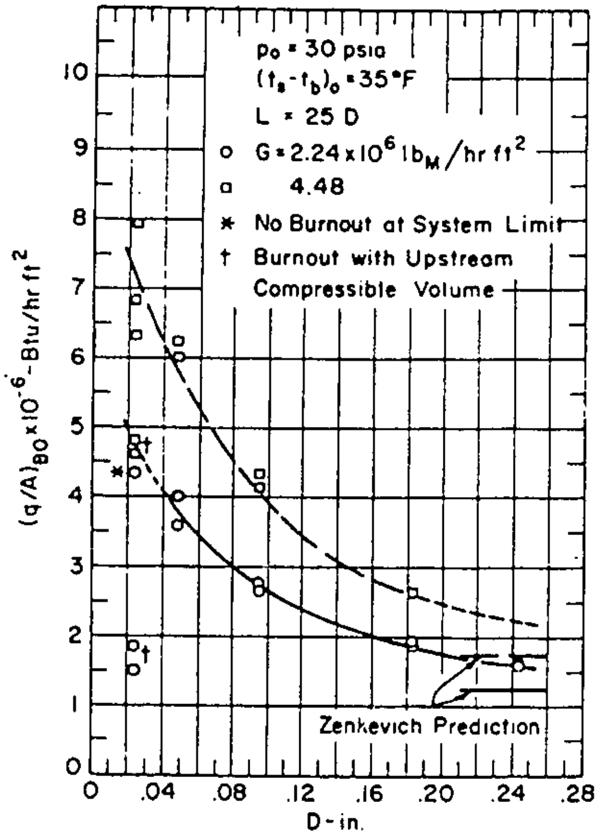

Figure 3.4: Experimental Data Showing the Diameter Effect for Low-pressure Flow Based on Constant Inlet Subcooling (Bergles 1963) (Diameter=0.58 to 6 mm, Pressure=0.2 MPa, Mass Flux=3 and 6 $Mg.m^{-2}.s^{-1}$)

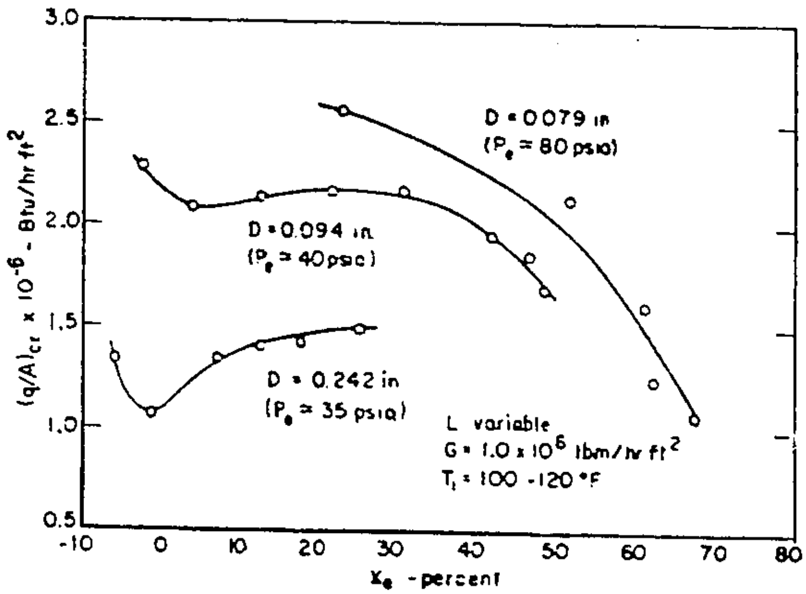

Figure 3.5: Experimental Data Showing the Diameter Effect Based on Quality (Bergles 1967)
(Diameter=2, 2.4, and 6 mm, Pressure=0.24 to 0.55 MPa, Mass Flux=1.35 $Mg.m^{-2}.s^{-1}$)

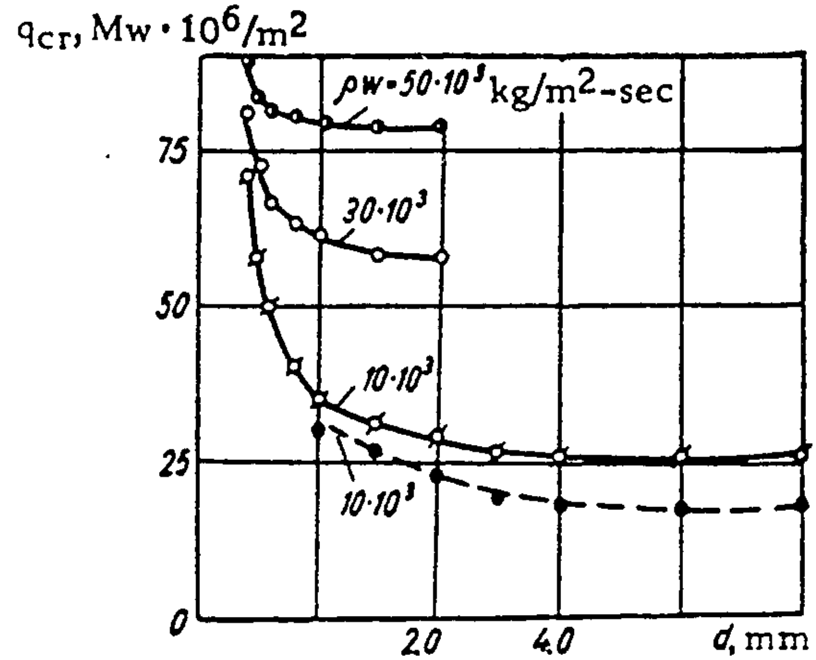

Figure 3.6: Experimental Data Showing the Diameter Effect Based on Constant Inlet Conditions (Ornatskiy 1969)
(Pressure=2.5 MPa, Inlet Subcooling=60 and 100°K, Mass Flux=1 to 5 $Mg.m^{-2}.s^{-1}$)

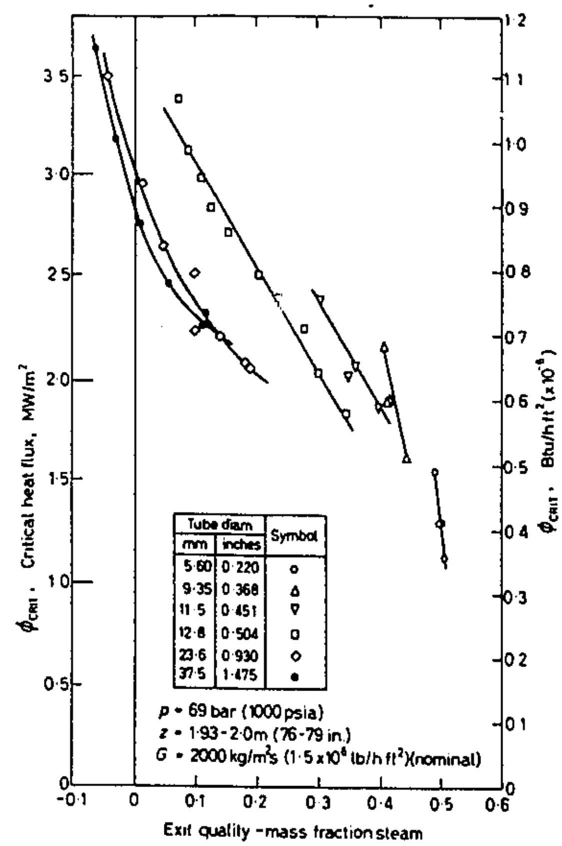

Figure 3.7: Experimental Data Showing the Diameter Effect Based on Quality (Collier 1972)
(Diameter=5.6 to 37.5 mm, Pressure=6.9 MPa, Mass Flux=2 $Mg.m^{-2}.s^{-1}$)

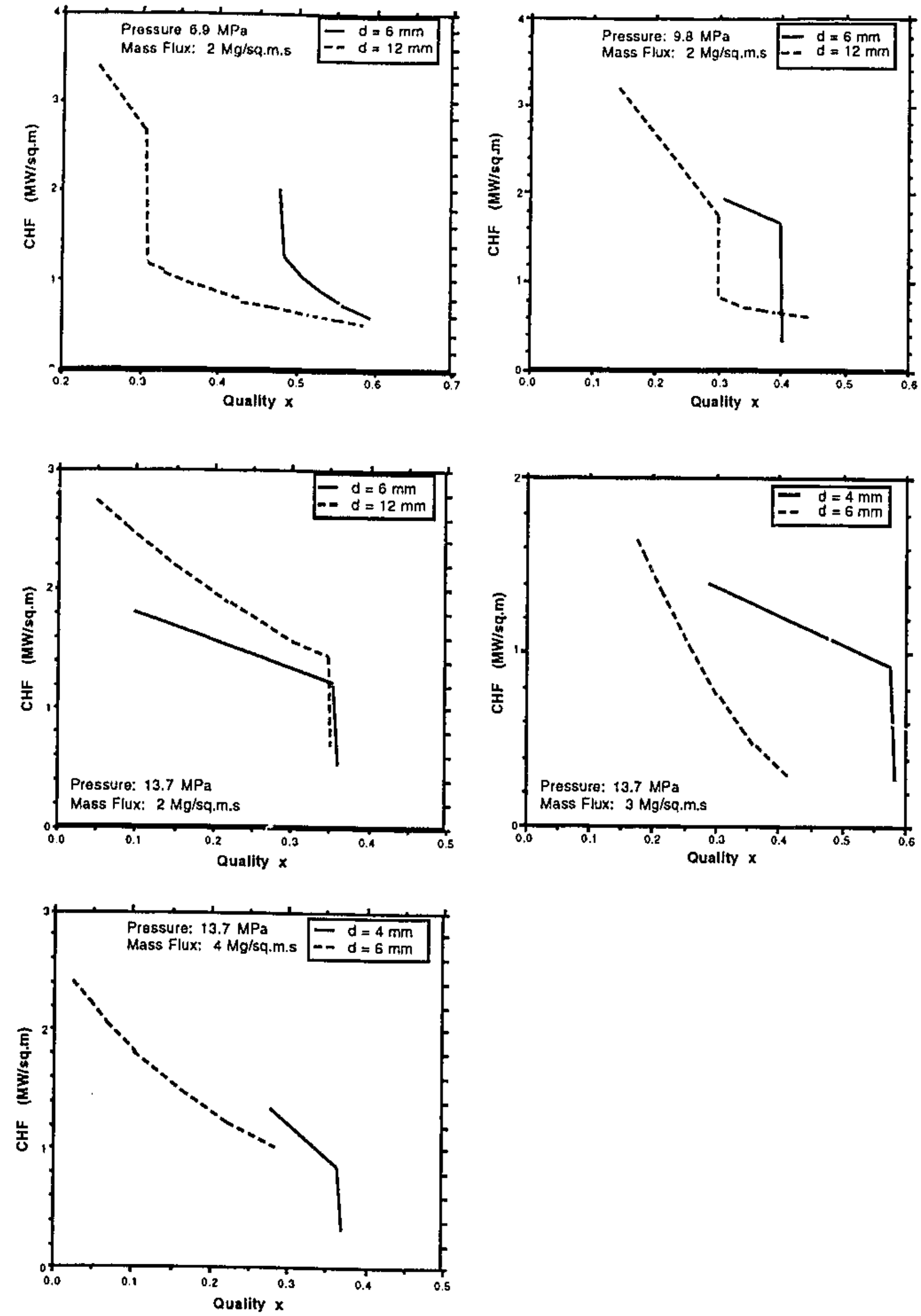

Figure 3.8: Best-fit Curves from Experimental Data Showing the Diameter Effect Based on Exit Quality (Levitan 1981)
(Pressure=6.9, 9.8, and 13.7 MPa, Mass Flux=2, 3, and 4 $Mg.m^{-2}.s^{-1}$)

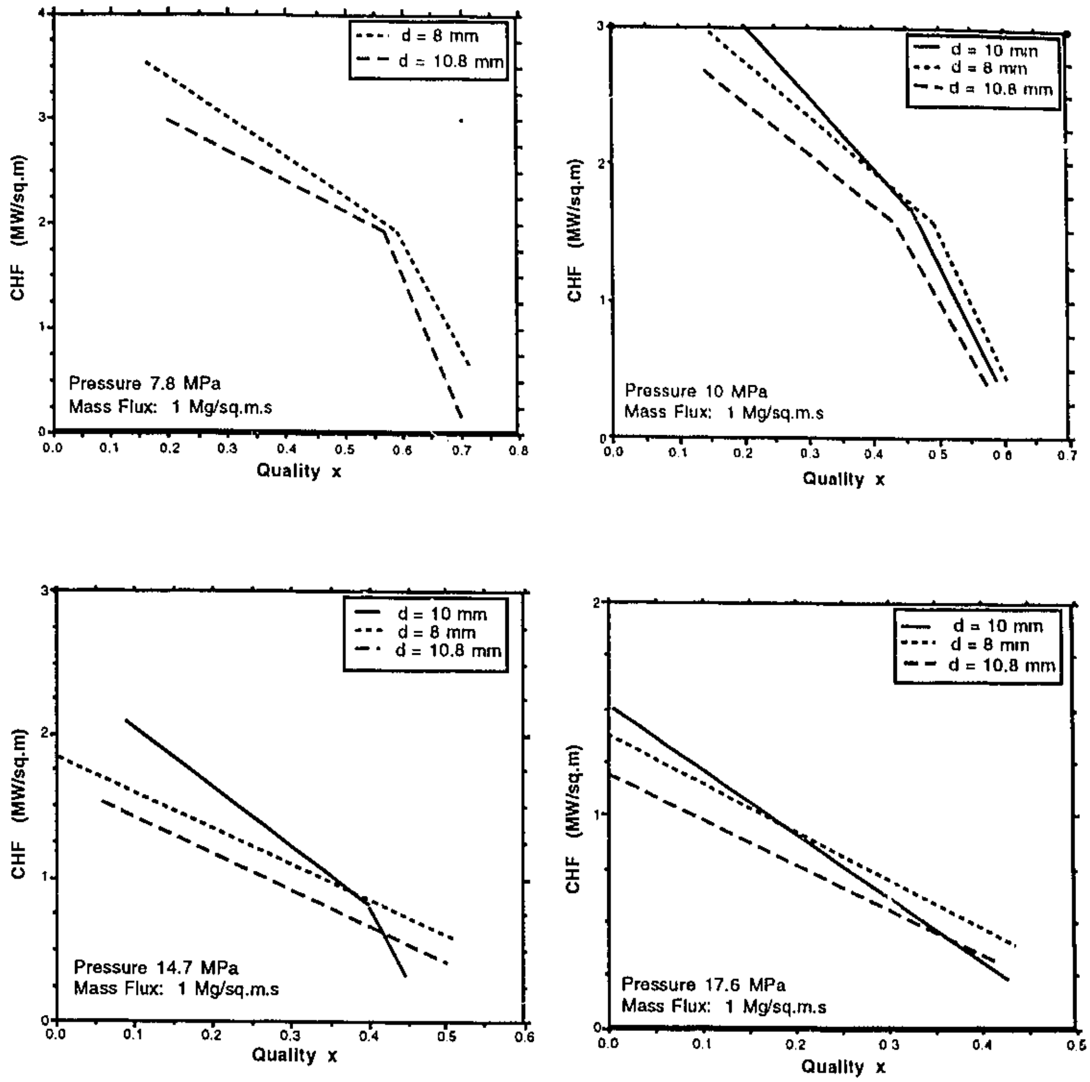

Figure 3.9: Best-fit Curves from Experimental Data Showing the Diameter Effect Based on Exit Quality for Mass Flux of 1 $Mg.m^{-2}.s^{-1}$ (Smolin 1981) (Pressure=7.8, 10, 14.7, and 17.6 MPa)

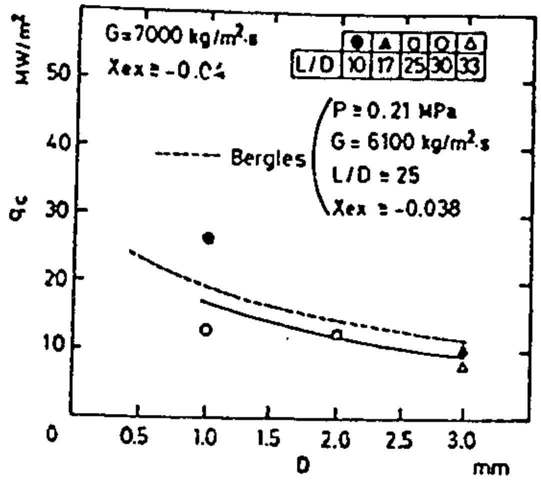

Effect of Diameter on CHF Shown By Experimental Data of Nariai et al. and Bergles (Mass Flux=6.1 $Mg.m^{-2}.s^{-1}$, Exit Quality= -0.04)

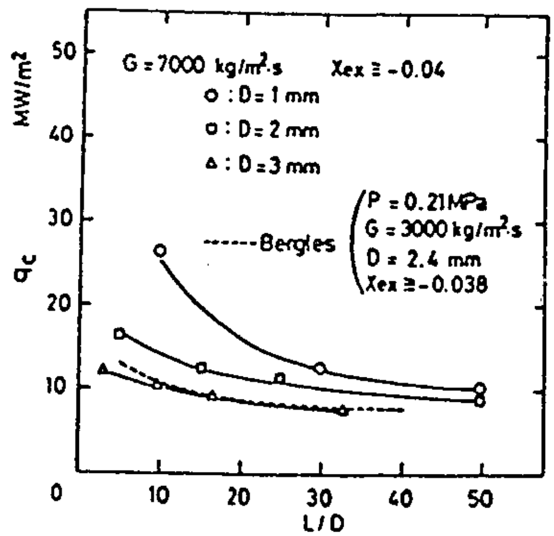

Effect of Length / Diameter Ratio Shown By Experimental Data of Nariai et al. and Bergles (Mass Flux=3 $Mg.m^{-2}.s^{-1}$, Exit Quality= -0.04)

Figure 3.10: The Diameter and Length / Diameter Effect at Low-pressure Based on Exit Quality (Nariai et al. 1987) (Diameter=1 to 3 mm, Pressure= 0.21 MPa)

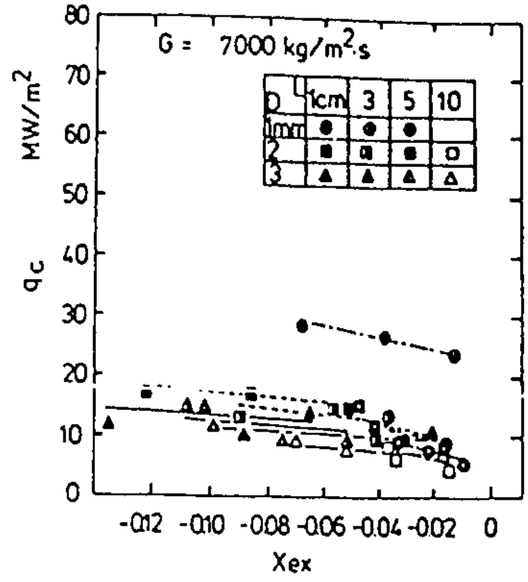

Mass Flux=7 $Mg.m^{-2}s^{-1}$

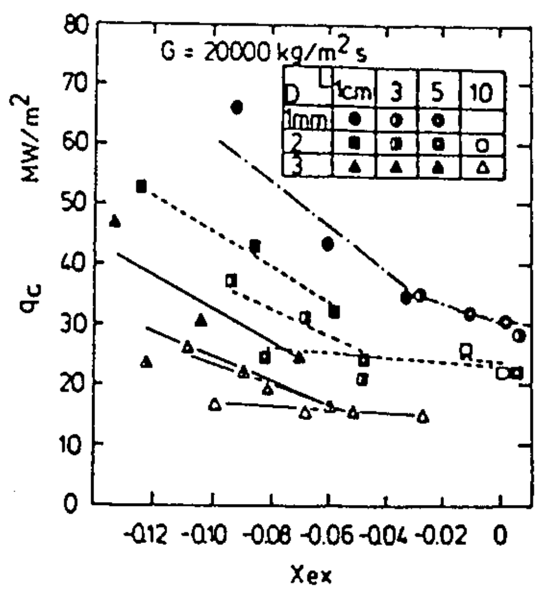

Mass Flux=20 $Mg.m^{-2}s^{-1}$

Figure 3.11: Experimental Data Showing the Diameter Effect at Low-pressure Based on Exit Quality (Nariai 1987) (Diameter=1 to 3 mm, Mass Flux=7 and 20 $Mg.m^{-2}s^{-1}$)

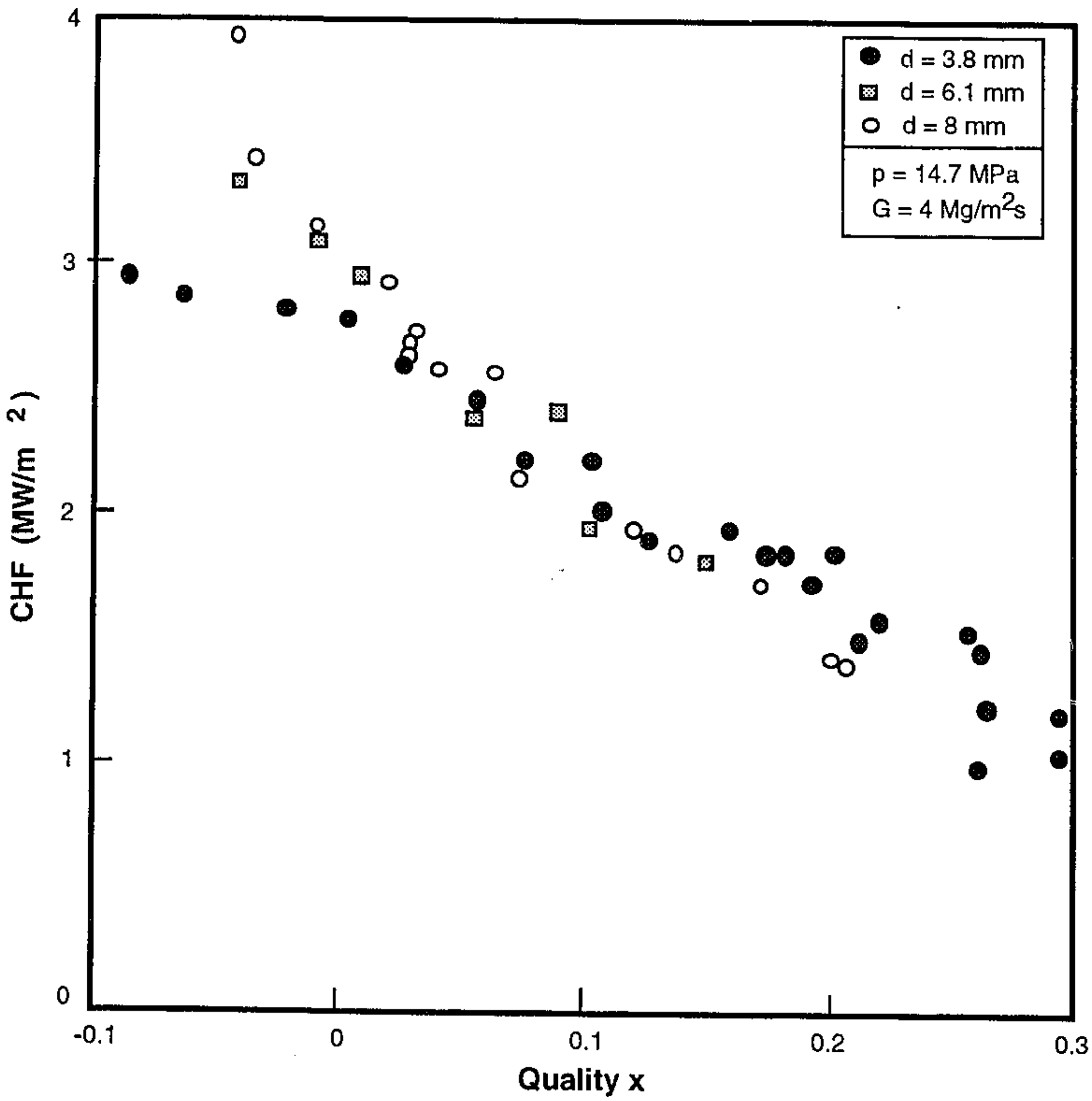

Figure 3.12: Experimental Data Showing the Diameter Effect Based on Exit Quality (Boltenko 1988)
(Diameter=3.8, 6.1, and 8 mm, Pressure=14.7 MPa, Mass Flux=4 $Mg.m^{-2}.s^{-1}$)

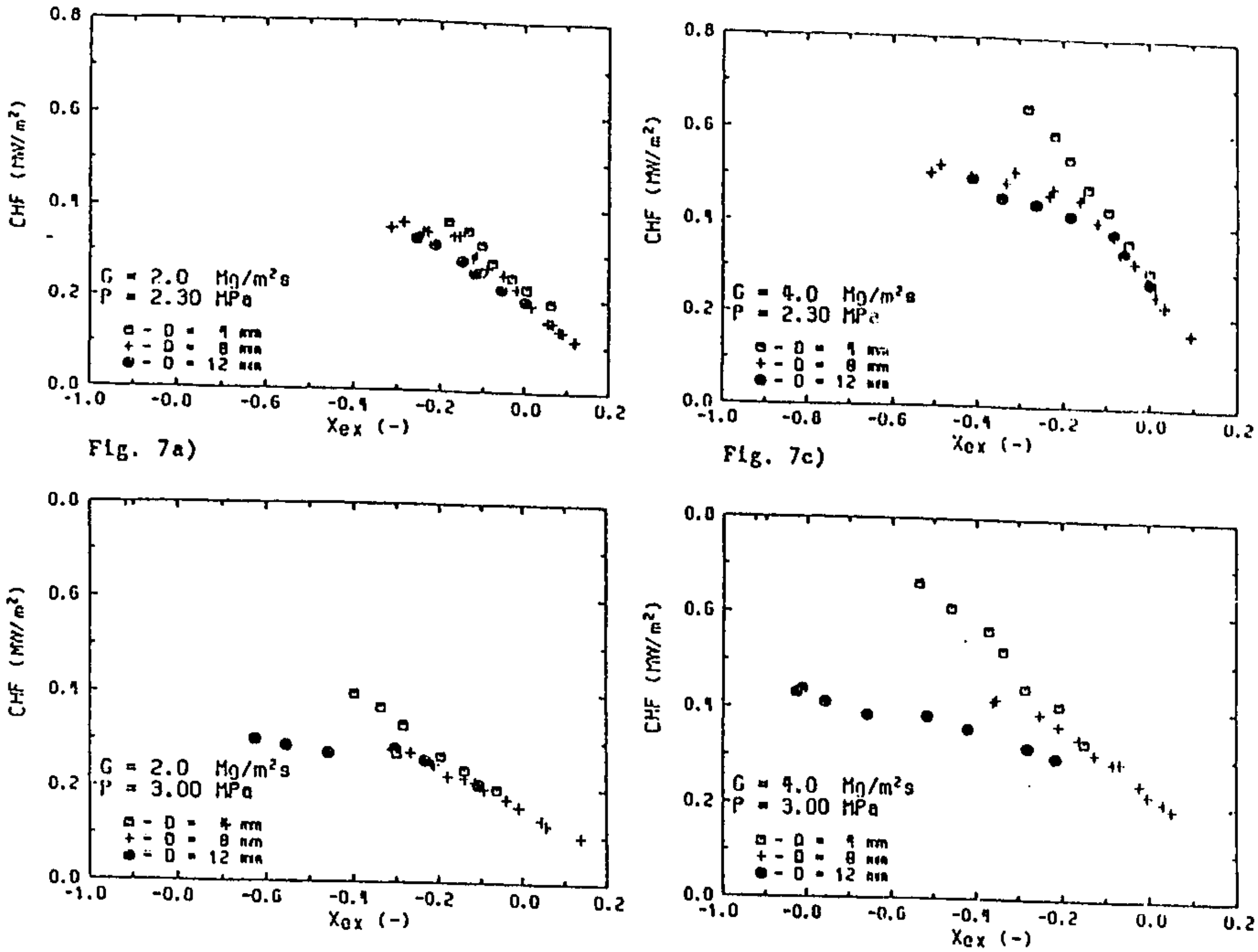

Figure 3.13: Experimental Data Showing the Diameter Effect Based on Exit Quality (Cheng et al. 1992)
(Diameter=4, 8, and 12 mm, Pressure=2.3 and 3 MPa, Mass Flux=2 and 4 $Mg.m^{-2}s^{-1}$)

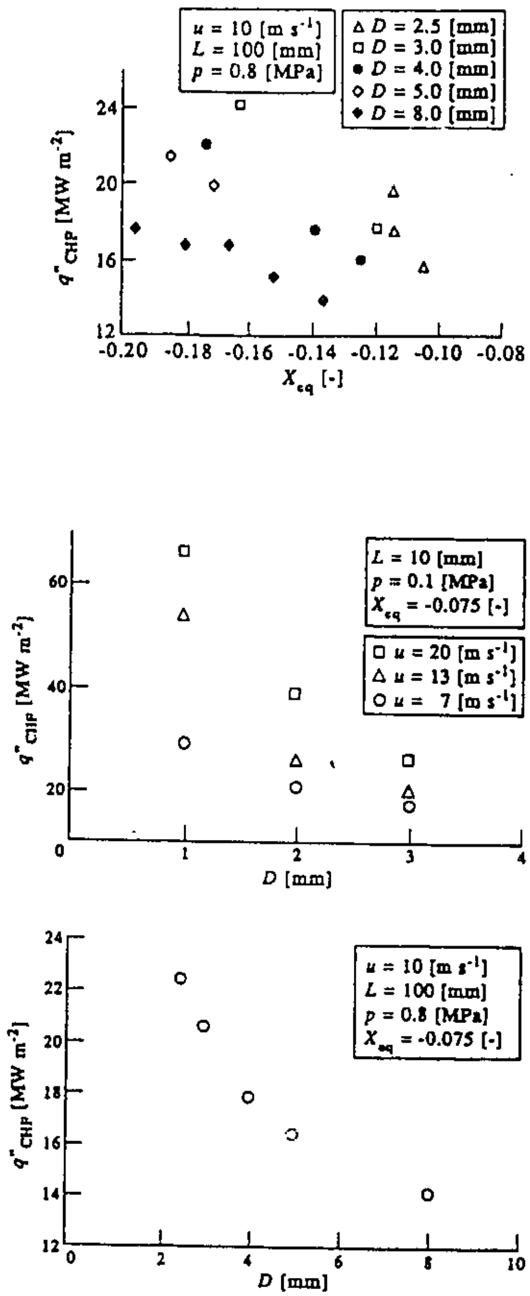

Figure 3.14: Experimental Data from Celata et al. (1992) and Nariai (1987) Showing Diameter Effect Based on Exit Quality (Celata et al. 1992)
(Diameter=2.5 to 8 mm, Pressure=0.1 and 0.8 MPa, Flow Velocity=7 to 20 $m.s^{-1}$)

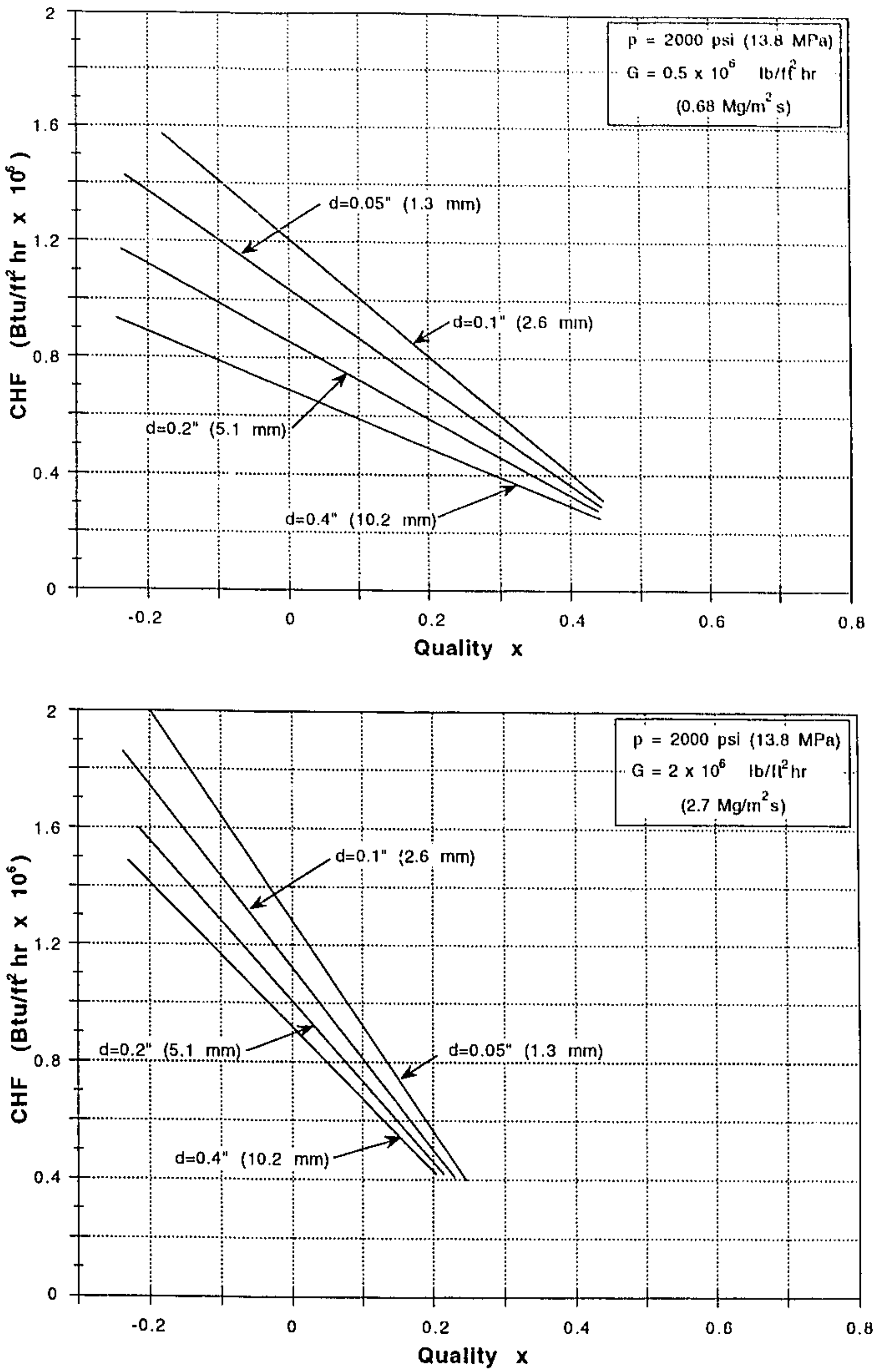

Figure 3.15 : Diameter Effect Correlated from Experimental Data (Macbeth 1963) (Diameter=1.3, 2.6, 5.1, and 10.2 mm, Pressure=13.8 MPa, Mass Flux=0.68 and 2.7 $Mg.m^{-2}.s^{-1}$)

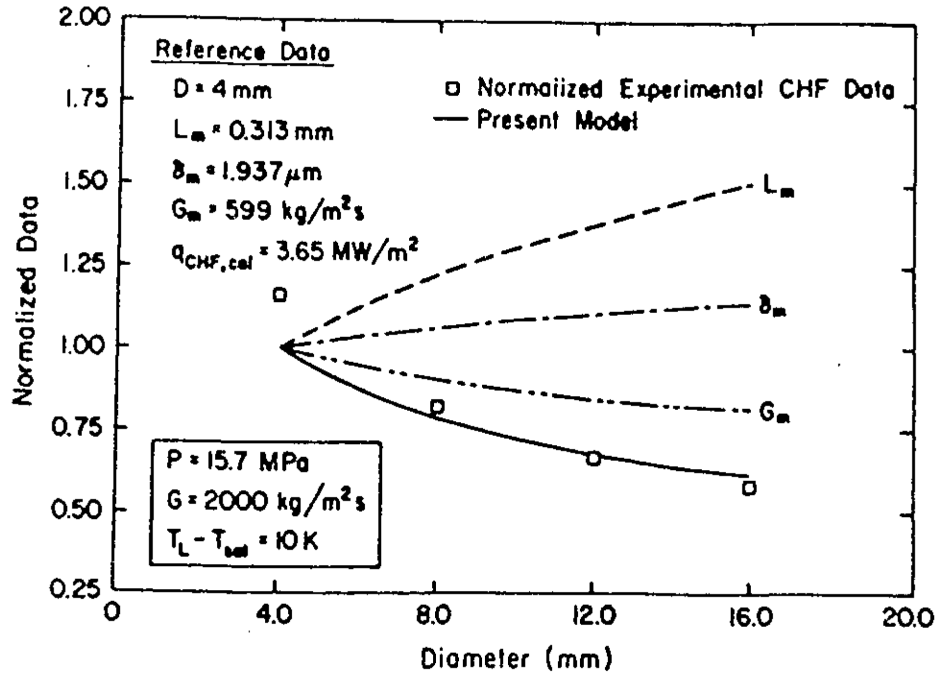

Figure 3.16: Experimental Data Showing the Diameter Effect Based on Inlet Subcooling (Lee and Mudawwar 1988)
(Diameter=4, 8, 12, and 16 mm, Pressure=15.7 MPa,
Mass Flux=2 $Mg.m^{-2}s^{-1}$, Subcooling=10°K)

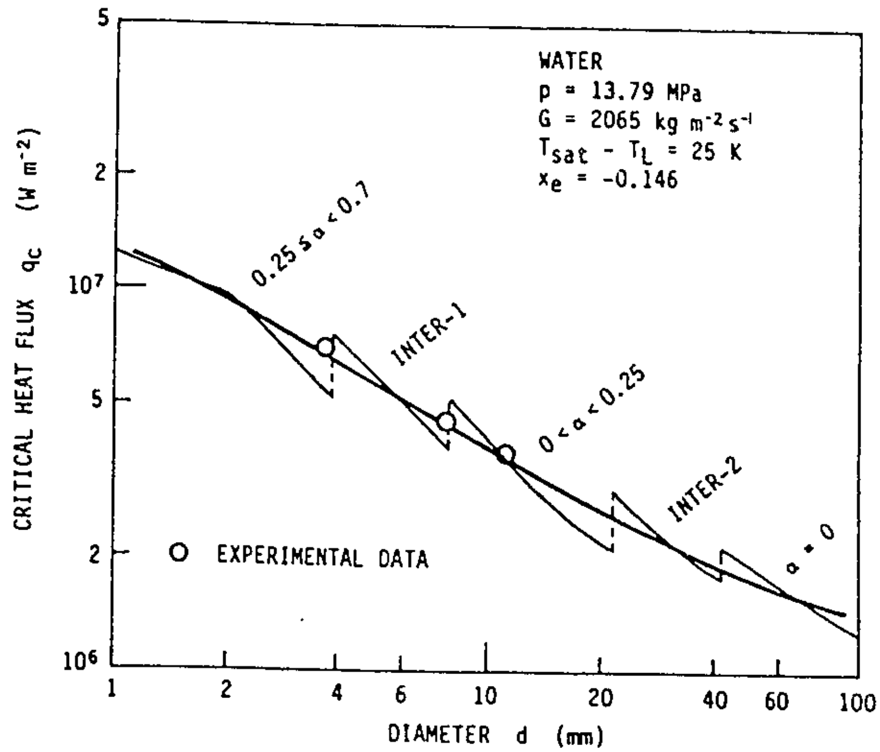

Figure 3.17: Experimental Data from Thompson and Macbeth (1964) and Katto Model Prediction Showing the Diameter Effect Based on Exit Quality (Katto 1990) (Pressure=13.8 MPa, Mass Flux= 2 $Mg.m^{-2}s^{-1}$, Exit Quality= -0.146)

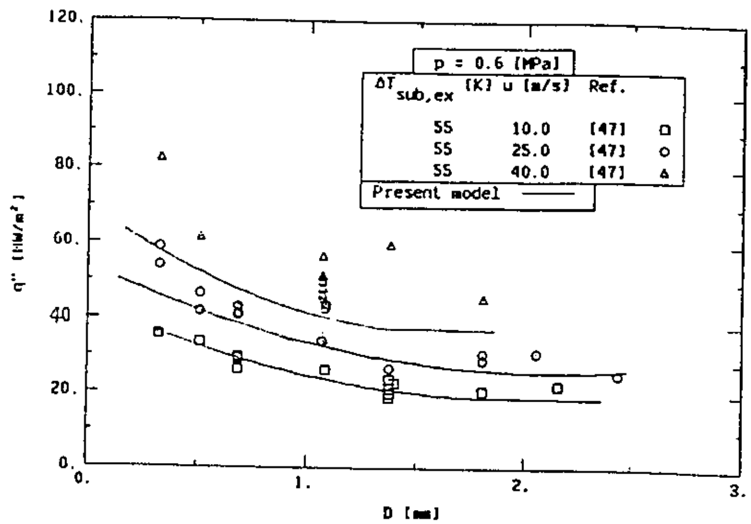

Figure 3.18: Diameter Effect Based on Exit Quality Shown by Experimental Data and Analytical Model (Celata et al. 1994)
(Diameter=0.3 to 2.5 mm, Pressure=0.6 MPa, Flow Velocity=10 to 40 $m.s^{-1}$)

4. OVERALL EFFECT OF DIAMETER ON CHF BASED ON THE AECL DATA BANK

The effect of tube diameter was studied by examining the parametric trend of experimental data. While a large amount of CHF data has been obtained for tube flow, only a few experimental studies focused on the diameter effect (see Chapter 3). In addition, their data covered only a limited range of flow conditions and this further hampered the development of a generalized prediction method. The present analysis examined the trend over a wide range of flow conditions by combining a large amount of collected data. This expanded the comparison beyond the range of any individual data set and led to a better understanding of this complex phenomenon.

The AECL CHF data bank contains the largest amount of data for upward flow of water in tubes (over 27 000 data points from about 40 data sets compiled by sources from different countries). However, many data were obtained at extreme flow conditions, which are beyond the scope of this study. A screening process was initiated to select appropriate data based on the following criteria:

(1) single-phase liquid at the entrance of the heated section (to avoid any phase distribution for two-phase flow),

(2) ratio of length to diameter larger than or close to 100 (to avoid flow entrance and tube length effects), and

(3) critical quality less than 1 (to avoid unrealistic data probably caused by heat-balance uncertainty).

A total of 23 500 data points were selected from this screening process. Table 4.1 lists the sources and range of flow conditions for these data. Data points at similar flow conditions (i.e., approximately the same pressure and mass flux) were grouped and analyzed by comparing their CHF values based on critical quality and tube diameters. Neglected are some data obtained at isolated flow conditions (e.g., with only a single tube diameter).

4.1 CHF TRENDS EXHIBITED IN THE AECL DATA BANK WITH RESPECT TO TUBE DIAMETER

CHF data obtained at each group of nominal pressure and mass flux were presented as functions of critical quality and tube diameter. Overall, data for the following range of nominal conditions have been examined:

Pressure, p:	3, 5, 6.9, 7.9, 9.8, 11.8, 14.7, 15.7, 17.8, 19.6 MPa
Mass flux, G:	1 to 5 $Mg.m^{-2}.s^{-1}$
Critical quality, x:	-0.3 to 0.9
Tube diameter, d:	4 to 20 mm

Data at other flow conditions were not analyzed because (1) the amount of data is too small, (2) the scatter among data is excessive, or (3) the data obtained were from tubes of the same diameter.

4.1.1 Data Obtained at a Pressure of 3 MPa

Figure 4.1 compares CHF data for a pressure of 3 MPa and mass fluxes of 1, 1.5, 2.7, 3.2, 4 and 5 $Mg.m^{-2}.s^{-1}$. These data covered a range of tube diameters from 4 to 20 mm, and qualities from -0.2 to 0.7. In general, the CHF data are consistent with respect to critical quality; a decrease in CHF is observed with increasing critical quality. Most data were obtained at the low mass-flux regions, where a strong tube diameter effect is shown. An increasing trend of CHF is observed with decreasing tube diameter. At high mass fluxes, however, the diameter effect appears to diminish somewhat, as CHF values are almost the same for different tube diameters at the same critical quality. Due to the lack of data (only for 8 and 10 mm tubes at a mass flux of 5 $Mg.m^{-2}.s^{-1}$), this trend for the high mass flux is not conclusive.

4.1.2 Data Obtained at a Pressure of 5 MPa

Figure 4.2 shows the CHF data for qualities from 0 to 0.8 and mass fluxes from 1 to 4 $Mg.m^{-2}.s^{-1}$ at a pressure of 5 MPa. The tube diameters covering these conditions are 4, 6, 8, 10, 12, 13, and 20 mm. While most data show an appropriate trend with respect to quality, a large scatter is observed at high qualities in the 8-mm tubes with a mass flux of 1 $Mg.m^{-2}.s^{-1}$. In fact, all data for the 8-mm tubes exhibit much non-uniformity in CHF with respect to quality than those for other tubes. The effect of tube diameter remains the same with higher CHF values for smaller diameter tubes. However, the variation in CHF observed in the 8-mm tubes results in a wide fluctuation of CHF ratio based on the same dryout conditions. For example, at a mass flux of 4 $Mg.m^{-2}.s^{-1}$, the CHF ratio between the 5.6 and 8 mm tubes is about 1.25 at a quality of 0, but it is reduced to about 1 at a quality of 0.2. When comparing the data between the 5.6 and 12.8 mm tubes, on the other hand, the CHF ratio is consistently at about 1.7 at qualities between 0 and 0.1. This illustrates not only the complexity of the tube-diameter effect, but also the importance of data reliability.

4.1.3 Data Obtained at a Pressure of 6.9 MPa

A much larger scatter is observed among data obtained at a pressure of 6.9 MPa (Figure 4.3) than at other low pressures. Except for the data of Bertoletti et al. (1964), most data exhibit a correct CHF trend with quality. Bertoletti et al. (1964) noted that their data were affected by a strong flow oscillation and hence are considered unreliable. These data were shown for illustration purposes and have not been included in the present analysis. The effect of tube diameter on CHF is not clearly shown, but the trend of higher CHF for smaller diameter tubes is generally observed. Due to the uncertainty in individual data sets, this trend is not definitely identified. For example, at a mass flux of 3.3 $Mg.m^{-2}.s^{-1}$, the CHF data of Mayinger for the 7-mm tube are higher than those of Kirillov for the 6-mm tubes. Moreover, the data of Kirillov also indicated an effect of heated length on CHF at the mass flux of 5 $Mg.m^{-2}.s^{-1}$, even though the length-to-diameter ratios are much larger than 100 (up to 1000). Other than these abnormalities, the effect of tube diameter is relatively strong at low qualities and diminishes with increasing quality.

4.1.4 Data Obtained at a Pressure of 7.9 MPa

Figure 4.4 shows the CHF data for mass fluxes from 1 to 5 $Mg.m^{-2}.s^{-1}$ and qualities from -0.3 to 0.7 at a pressure of 7.9 MPa. The tube-diameter range varies from 4 to 11 mm. These CHF data show much less scatter than those of 7 MPa and decrease with increasing quality. As for other pressures, they are generally higher for small-diameter tubes. The tube-diameter effect on CHF is stronger in small-diameter tubes at low qualities, but reduces as the tube diameter and quality increase.

4.1.5 Data Obtained at a Pressure of 9.8 MPa

At a pressure of 9.8 MPa (Figure 4.5), CHF data are available for mass fluxes from 1 to 5 $Mg.m^{-2}.s^{-1}$ and qualities from -0.1 to 0.8 covering tube diameters of 6, 7, 8, 9, 10, 11, 12, 13, 15 and 16 mm. Except for a relatively large scatter observed for the data at a mass flux of 1 $Mg.m^{-2}.s^{-1}$, the CHF data decrease consistently with increasing quality. The tube-diameter effect, on the other hand, is significantly reduced over the present quality range. A higher CHF is shown for small-diameter tubes at low qualities, but there is practically no diameter effect for various tubes at high qualities. The uncertainty remains high in several data sets: a large difference is observed between the data of Mayinger and those of Kirillov for tubes of 7 mm at a mass flux of 3.3 $Mg.m^{-2}.s^{-1}$. In addition, both sets of CHF data are higher than those of Kirillov's for the 6-mm tube, and Borodin's data (a 9-mm tube) lie between the 7-mm and 6-mm data of Kirillov. The data of Kirillov for the 4-mm tube are consistently higher than those for all other tubes; those of Tong for the 13-mm tube are systematically lower than all the other data.

4.1.6 Data Obtained at a Pressure of 11.8 MPa

Figure 4.6 shows the CHF data for mass fluxes from 1 to 5 $Mg.m^{-2}.s^{-1}$ and qualities between -0.1 to 0.55 at a pressure of 11.8 MPa. These data were obtained in tubes of 2, 4, 5, 6, 8, 10, 11, 14, 15 and 28 mm in diameter. A large data scatter is observed at high qualities for a mass flux of

1 $Mg.m^{-2}.s^{-1}$ in the 8-mm tubes. Large variation of CHF values are shown for qualities between 0.4 and 0.5. This set of data is therefore questionable. Other data sets appear to be more reliable as they exhibit a decreasing trend with increasing qualities. Similar to the data of 9.8 MPa, the effect of tube diameter on CHF appears strong at low quality and low mass flux conditions, and diminishes with increasing quality and mass flux. Again, this effect is almost absent at high mass-flux conditions. The large-diameter tube data of Lee and Obertelli (1963) are consistently lower than those of smaller tubes. An unusual trend is also observed for the 2-mm tube data of Thompson and Macbeth; these CHF data are much lower than those of large-diameter tubes. This cannot be confirmed since the data cover an extremely narrow range of qualities (mainly at -0.05).

4.1.7 Data Obtained at a Pressure of 14.7 MPa

Figure 4.7 shows the CHF data for mass fluxes from 1 to 5 $Mg.m^{-2}.s^{-1}$ and qualities from -0.1 to 0.55 at a pressure of 14.7 MPa. These data covered tube diameters of 4, 6, 8, 10, 11, 15 and 16 mm. The data scatter remains large at a mass flux of 1 $Mg.m^{-2}.s^{-1}$. Other data exhibit the expected trend with quality. At a high positive quality region, a small tube-diameter effect can still be observed for small-diameter tubes, but the effect is not present for large-diameter tubes. At subcooled and low-quality (less than 0.1) conditions, these data exhibit a systematic trend where the CHF values are lower for small-diameter tubes (a reverse trend compared to those observed so far at low pressures), and it is maintained for all mass fluxes. It is anticipated that this reverse trend is caused by differences in flow regime encountered in tubes of different sizes. The quality at which the CHF trend reverses appears to be a function of mass flux and diameter.

4.1.8 Data Obtained at a Pressure of 15.7 MPa

The CHF data at a pressure of 15.7 MPa exhibit a more consistent trend with respect to quality and tube diameter (Figure 4.8). They were obtained at mass fluxes from 1 to 5 $Mg.m^{-2}.s^{-1}$, tube diameters of 6, 8, 11 and 15 mm, and qualities from -0.15 to 0.5. Unlike the CHF data shown for a pressure of 14.7 MPa, these data present the common trend of increasing CHF with decreasing tube diameter, and no reversal at subcooled and low-quality conditions. In addition, the tube-diameter effect appears to be stronger than for lower pressures at the high-quality region.

4.1.9 Data Obtained at a Pressure of 17.8 MPa

Figure 4.9 shows the CHF data for mass fluxes from 1 to 5 $Mg.m^{-2}.s^{-1}$ and qualities from -0.6 to 0.6 at a pressure of 17.8 MPa. These data were obtained in tubes of 6, 7, 8, 10, 11, 15 and 16 mm in diameter. A large scatter is observed among these data over the complete range of mass fluxes. The averages of these scattered data show that there is practically no tube-diameter effect on CHF over the entire range of flow conditions at this pressure. The only exception is the data of a 4-mm tube which appears to show a similar reverse CHF trend to that observed at a pressure of 14.7 MPa. This, however, is not supported by data of other tube diameters. For example, at a mass flux of 5 $Mg.m^{-2}.s^{-1}$, the CHF data for the 8-mm tubes are lower than those for the 6-mm tubes over the same flow conditions of the 4-mm tube data.

4.1.10 Data Obtained at a Pressure of 19.6 MPa

Figure 4.10 shows the CHF data for mass fluxes from 1 to 3.3 $Mg.m^{-2}.s^{-1}$, tube diameters of 6, 8, 11 and 15 mm, and qualities from -0.6 to 0.6 at a pressure of 19.6 MPa. There is not much data obtained at similar flow conditions, except those for a mass flux of 1.5 $Mg.m^{-2}.s^{-1}$ but some of them quite scattered. The commonly observed tube-diameter effect appears to prevail among most of the data at this pressure, and the reverse trend is less evident than the other high pressure data such as 17.8 MPa (section 4.1.9) as an example.

4.1.11 Summary of CHF Trends with respect to Tube Diameter Exhibited in the AECL Data Bank

CHF trends with respect to tube diameter are summarized below based on the examination of the AECL data bank. The selected data groups cover mainly pressures from 3 to 20 MPa and mass fluxes from 1 to 5 $Mg.m^{-2}.s^{-1}$.

- Most data exhibit a common parametric trend with respect to critical quality. However, relatively large scatter was observed in several data sets.
- A complex phenomenon was shown in this examination where the tube-diameter effect is affected by not only the tube diameter itself, but may also be by the flow regime (which depends on pressure, mass flux and critical quality).
- The effect of tube diameter on CHF is stronger at low pressures, low mass fluxes, and high qualities, but appears to diminish as the pressure and mass flux increase.
- In general, the CHF increases with decreasing tube diameter. This trend was observed in both subcooled and saturated conditions at pressures lower than 14.7 MPa. A reversed trend was found at subcooled and low-quality conditions for some high pressures. However, except at a pressure of 14.7 MPa, this trend is inconclusive.
- Systematic differences have been noted among data of different sources. A few data sets were identified as questionable, but the uncertainty cannot be verified unless more data were obtained.

4.2 A COMPARISON OF CHF VALUES OF VARIOUS TUBE DIAMETERS TO THOSE OF AN 8-MM TUBE

The influence of various flow parameters on the tube-diameter effect is examined by comparing the CHF values of various tube diameters to those of an 8-mm tube at the same flow conditions. The 8-mm tube data are selected as the reference because they represent the largest number and cover the widest range of flow conditions in the AECL data bank. However, these data do not always cover all corresponding conditions for data of other tube diameters.

In this comparison, a polynomial function of CHF based on critical quality was derived with the 8-mm tube data for each set of nominal pressure and mass flux (corresponding to Figures 4.1 to 4.10). The CHF ratios were calculated between the CHF data of any tube diameters (other than 8-mm) and the experimental CHF values of an 8-mm diameter tube expressed as continuous functions (i.e., best-fit from the AECL data bank data of an 8-mm tube) at the same pressure, mass flux and qualities. All these calculations were applied only to conditions where the 8-mm tube data are available, or in other words, these functions of CHF ratios were not extrapolated over the ranges where the 8-mm tube data were absent. These best-fit continuous functions are assumed to be valid only for the ranges covered by experimental data; any extension may result in large errors.

4.2.1 CHF Ratios at Various Nominal Flow Conditions

Figures 4.11 to 4.18 show the CHF ratios between tubes of diameters of interest and those of the 8-mm diameter for various pressures. In each figure, the mean values of the correction factor for diameter effect (in place of the exponent -1/2 as presented by Doroschuk et al. (1975) in Equation (3.2)) are also shown for various sets of data.

At a pressure of 3 MPa (Figure 4.11), the CHF ratio decreases consistently with increasing tube diameter. For tubes of diameter larger than 8 mm, it is also a function of critical quality, where a smaller ratio (stronger diameter effect) is observed for higher quality. The quality effect, however, is reduced as the mass flux is increased. Data of the 6-mm tubes appear to show a similar trend that the diameter effect is stronger at higher quality (CHF ratio larger). On average, the exponent in the correction factor varies from -0.96 to -2.48 for various tube diameters.

Figure 4.12 shows the CHF ratios at a pressure of 5 MPa. All ratios are larger than 1 for tube diameter values smaller than 8 mm, while smaller than 1 for diameters larger than 8 mm. Unlike those ratios at a pressure of 3 MPa, they are not affected significantly by either quality or mass flux at these conditions. Various exponents (from -0.476 to -2.38) have been optimized with these ratios.

A large scatter among CHF ratios is observed in Figure 4.13 for data obtained at a pressure of 7 MPa. Although an overall increasing trend of CHF ratio is shown with decreasing diameter, there are a few exceptional cases. For example, the ratios are consistently larger than 1 for the data of a 9.4-mm tube, while the data of a 20-mm tube lie between those of the 12.8-mm and 15-mm tubes at a mass flux of 1 $Mg.m^{-2}.s^{-1}$. The data scatter is especially significant for small-diameter tubes, where a mixed effect is observed at mass fluxes of both 3.3 and 4 $Mg.m^{-2}.s^{-1}$. A range of exponents from 0.03 to -2.03 is obtained for the correction factor.

The CHF ratios for data obtained at a pressure of 8 MPa are shown in Figure 4.14. Except for a relatively large variation in CHF ratios with respect to quality at low mass-flux conditions, the quality effect appears to be insignificant. The effect of mass flux is also quite small. Overall, the CHF ratios remain larger for small-diameter ratios. The exponent varies from -0.075 to -1.31.

Figure 4.15 shows the CHF ratios for a pressure of 9.8 MPa. Similar to those obtained at 7 MPa, a large variation of ratios is observed with respect to quality. The trend is not systematic; some show an increasing trend whereas others indicate a decreasing trend. Except for the 9-mm tube data, a larger ratio is shown for small-diameter tubes. The ratios are larger than 1 for the 9-mm tube, but they cover only a narrow range of flow conditions. The average values for the exponent cover a range from 2.21 to -3.35.

The CHF ratios for a pressure of 11.8 MPa are shown in Figure 4.16. They reduce considerably at a mass flux of 1 $Mg.m^{-2}.s^{-1}$ with increasing quality, but vary little at other flow conditions. At high mass-flux conditions, the ratios approach 1. The exponent varies from 0.34 to -1.7.

Figure 4.17 shows a variation in CHF ratios with respect to quality at a pressure of 14.7 MPa. The 11-mm tube data, the most obvious examples, show a systematic decreasing trend of CHF ratio with increasing quality. The ratio varies from 1.5 to 0.75 over the quality range from subcooled to saturated conditions. Furthermore, the tube-diameter effect is considerably reduced at mass fluxes higher than 1 $Mg.m^{-2}.s^{-1}$. The mean values of the exponents vary from 0.133 to -0.663.

A different trend of CHF ratios is shown in Figure 4.18 at a pressure of 15.7 MPa, compared to that in Figure 4.17. The increasing ratio displayed at a low-quality region in Figure 4.17 has not been observed in Figure 4.18 at similar flow conditions (e.g., 1 $Mg.m^{-2}.s^{-1}$). Except at high-quality conditions, the CHF ratios are relatively constant with respect to quality. At high mass fluxes, the CHF ratio appears to increase with decreasing quality. However, the trend observed in general seems quite different from what the other data showed; most CHF ratios for the 11-mm tube are larger than 1 at a mass flux of 3.3 $Mg.m^{-2}.s^{-1}$. The exponent varies from -0.950 to 0.347.

The same trend of CHF ratio as for the pressure of 14.7 MPa is displayed for data at a pressure of 17.8 MPa (Figure 4.19). The data for both the 10-mm and 11-mm tubes exhibit the decreasing trend with increasing quality at low mass fluxes. At high qualities, however, an increasing trend is shown for the same tubes. The exponent varies from 0.503 to -0.85. In general, the diameter effect appears to be reversing towards the lower qualities that CHF gradually becomes increasing with increasing diameter.

4.2.2 Summary of the Variations in CHF Ratios

Tables 4.2 to 4.4 summarize the range of CHF ratios (together with the average values) calculated for various tube diameters with respect to each data source. A large variation in CHF ratios has been shown at various flow conditions for the same tube diameters. Figure 4.20 shows the variations of CHF ratios for specific tube-diameter values (i.e., 4, 6 and 10-mm), where a relatively large amount of data is available (other than the 8-mm tubes). Although the scatter among these data is large, a few general observations can be made. For tube diameters of 4 mm, the CHF ratios appear to increase with increasing quality. Except for the data at a pressure of 15 MPa, the effect of pressure and mass flux on CHF ratio is relatively small. The average CHF ratio for the 4-mm tubes is approximately 1.4 over these flow conditions. For tube diameters of 6 mm, the CHF ratios are relatively constant at the low-quality region, but decrease as the quality increases. Overall, the CHF ratio is influenced also by pressure and mass flux; a large ratio is generally observed for low mass-flux and low-pressure conditions. Over these flow conditions, the average CHF ratio is about 1.1. A similar trend to that of the 6-mm tubes is observed for the 10-mm tubes, with relatively constant CHF ratios at low-quality regions but a large scatter at high qualities. The CHF ratios are also higher for low mass-flux and low-pressure conditions. On average, the CHF ratio is about 0.9.

Figure 4.21 compares of CHF ratios for various tube diameters and pressures over a small range of mass fluxes. As described in previous sections, the CHF ratios are generally larger for small-diameter tubes. These figures also illustrate that the CHF ratio is a function of pressure: larger CHF ratios are shown for lower pressures.

4.3 CORRECTION FACTORS FOR TUBE-DIAMETER EFFECT ON CHF BASED ON THE AECL DATA BANK

A literature review of existing prediction methods for the tube-diameter effect on CHF was described in Chapter 3. The methodology commonly used to account for this effect is based on the correction factor recommended by Doroschuk et al. (1975) (i.e., Equation (3.2)). Most studies suggested using a constant value for the exponent 'n' (e.g., Doroschuk et al. (1975) used a value of -1/2 and Groeneveld et al. (1986) suggested a value of -1/3). This recommendation appears to have the support of several analytical models, where the predictions can be similarly expressed in term of a similar function as the correction factor of Doroschuk et al. (1975).

Section 4.2.3 clearly showed a more complex tube-diameter effect on CHF, which cannot be accounted for with a simple constant value as the exponent. Tables 4.2 to 4.4 list the calculated exponent 'n' at various flow conditions for various sources of data. Overall, the exponent varies from -5.547 to 4.604, and is a function of pressure, mass flux and quality. Although more complex correction factors were proposed by Boltenko et al. (1988 and 1989), they appear to exhibit different trends from the experimental data shown in Section 4.2.2. The recommended use of positive values for the exponent at the low-quality region was not supported by most data. In addition, the exponents of Boltenko et al. (1988 and 1989) introduced discontinuity over the transition region; this may not be acceptable for some computer-code applications. Hence, an improved correction factor is needed for thermalhydraulic analysis.

The improvement to the prediction of the tube diameter effect on CHF follows the same approach suggested by Doroschuk et al. (1975), which is consistent with existing prediction methodology. A correction factor to the CHF of an 8-mm tube is used to predict the CHF of tubes of other diameter values, and is presented as a function of the diameter ratio. It is expressed as

$$\frac{q_{c,d}}{q_{c,0.008}} = \left(\frac{d}{0.008}\right)^{n} \tag{4.1}$$

In the present study, a flow-dependent exponent, n, is introduced to account for the effect of flow parameters on the correction factor, and is expressed in terms of pressure, mass flux and quality. Two approaches were used to derive the exponent: one based on average calculated values referenced to the data of the 8-mm tube in the AECL data bank, and one based on the best-fit values of individual data set at various flow conditions. The main difference between these two approaches lies in the data selection for each set of nominal flow conditions. The first approach considered the data bank essentially a single source (it disregarded the identity of each data except in identifying the reference), and deduced the tube-diameter effect over the complete flow range. This approach provides the largest data base, but also the largest scatter, due to the inherent uncertainty associated with each data set. The second approach examined only data contained in each individual source. This reduces significantly the number of data, but minimizes the uncertainty related to loop, design and operation.

4.3.1 Correction Factors Based on CHF Ratios Referenced to 8-mm Tube

An expression of the exponent, n, in Equation (4.1) is derived with the experimental data for various flow conditions (calculated exponents previously shown in Figures 4.11 to 4.19 and in Tables 4.2 to 4.4). It is expressed in terms of pressure, mass flux and critical quality, and a number of constants optimized with the data base. To simplify the analysis, the optimization is based on the average exponent calculated over each quality range for a nominal set of pressure and mass flux. Figure 4.22 shows the average CHF ratios calculated for various tube diameters and nominal flow conditions based on the data in Figures 4.11 to 4.19. The CHF ratios appear to be quite consistent over these ranges of flow conditions for various qualities. Figure 4.23 shows the corresponding exponents at the same flow conditions, and a much larger scatter is observed. The general trend is that the exponent is closer to 0 (CHF ratio nearer to 1) at low qualities and decreases (CHF ratio lesser or larger than 1 respectively for diameters larger than or smaller than 8 mm) with increasing quality. Figure 4.24 illustrates the complexity of the pressure and mass-flux effects on the CHF ratio at a pressure of 13 MPa. The mass-flux effect is relatively consistent with larger CHF ratios for higher mass-flux conditions; the pressure effect is inconclusive in this particular case.

Table 4.5 lists the calculated average values of exponent for various diameters and flow conditions. Based on these average values, a best-fit expression of exponent, n, is empirically derived. It is written as

$$n = -0.7 + 0.477\exp(-1.215 + 0.115p - 2.7x_c - 0.1G) \qquad (4.2)$$

where p is the pressure in MPa, G is the mass flux in $Mg.m^{-2}.s^{-1}$, and x_c is the critical quality in fraction. This equation is limited to flow conditions of water flow only, and should not be extrapolated to other fluids or flow conditions outside of the data base. An attempt was made to use non-dimensional parameters in the correlation. However, most non-dimensional parameters for mass flux were also expressed in a function of diameter. This will result in an implicit equation which is difficult to solve. Therefore, as a simplification, the dimensional parameters are employed.

Figure 4.25 shows the parametric trend of the correction factor (based on the exponent n of Equation (4.2)) with respect to diameter at a pressure of 10 MPa and mass fluxes of 1, 3 and 4.5 $Mg.m^{-2}.s^{-1}$. In general, the CHF ratio or CHF increases (negative value for the exponent n in Equations (4.1) and (4.2)) with decreasing tube diameter, for any constant critical quality. As critical quality increases, value of the CHF ratio gradually changes and shifts more away from unity (exponent n more negative) for any one tube diameter, showing the increase in diameter effect. For comparison, the average CHF ratios based on experimental data of the databank are also shown in the same figure. They are well predicted with the correction factor (Equations

(4.1) and (4.2)), except for the data having large scattering.

4.3.2 Correction Factors Based on Data of Individual Data Set

The correlation for the exponent, n, (Equations (4.1) and (4.2)) is dependent on the data of the 8-mm tubes, because the CHF ratio was calculated with reference to these data. As shown in Figures 4.2 to 4.10, the scattering among some of the 8-mm tube data, especially for combined data from different sources, shows certain degree of uncertainty and that can have a large impact on the accuracy of the correlation. To minimize the effect, the exponent, n, was again determined with data in individual data sets for specific flow conditions. This eliminates certain uncertainties associated with different test facilities and experimental procedures.

The present analysis focused mainly on data sets with a large number of data and multiple tube diameters. These data sets included Becker (1965), Bennett et al. (1965), Griffel (1965), Lee (1965 and 1966), Tong (1964), Zenkevich et al. (1969), Smolin et al. (1979) and Kirillov (1992). The compilation of data provided by Kirillov (1992) contains data from Zenkevich, Smolin, Alekseev and Kirillov. CHF data in each data set were divided into various groups, according to the nominal pressure and mass flux. These data were used to optimize the coefficients in the following equation:

$$q_c = f(x)\ d^n \tag{4.3}$$

where f(x) is a polynomial function in terms of the critical quality. The exact form of the function is not crucial because the main purpose of this optimization is to determine the exponent, n. The slight variations with respect to critical quality of the exponent, n, is neglected over each nominal flow condition.

Figure 4.26 compares the equations with the optimized correction factors to the smoothed experimental data for various tube diameters at nominal sets of pressures and mass fluxes. The optimized exponent for these conditions is shown in the same figure. Appendix I presents the comparisons for other flow conditions and data sets. Table 4.6 summarizes the optimized exponents for various flow conditions and data sets. The overall range of the exponents is between -1.2 and 0, with the majority being from -0.7 to -0.5. As anticipated, the flow conditions covered in this approach are much narrower than those of the previous approach (i.e., based on all data in the AECL data bank). The optimized exponents are shown in Figure 4.27 over various ranges of quality at each set of nominal conditions. They vary with both quality and mass flux, but do not appear to be significantly affected by pressure (other than data scatter). The pressure effect shown in the previous approach was encountered mainly at high-pressure conditions, which are not covered in the present data sets. Figure 4.28 shows the overall variation of the optimized exponent for all data sets.

Based on the nominal flow conditions, an expression for the exponent is derived and is written in the form of

$$n = -0.58\ (1 - 0.25 e^{2x_c})\ (1 - 0.015G) \qquad (4.4)$$

where G is the mass flux in $Mg.m^{-2}.s^{-1}$ and x_c is the critical quality in fractions. Probably due to the lesser amount of applicable data in the optimization process as compared to section 4.3.1, the pressure effect was not observed to be as significant and hence not included as a component in equation 4.4. As explained above (for Equation (4.2)), non-dimensional parameters for mass flux are not used because they are also a function of diameter.

4.4 ASSESSMENT OF CORRELATIONS FOR THE EXPONENT OF THE TUBE-DIAMETER CORRECTION FACTOR

The introduction of the newly derived correction factors (exponent n) into the CHF correlation is assessed with data in the AECL data bank. Although these correction factors only represent the values of the exponent n, the comparison between their predicted CHF values and the experimental values is assessed, since the accuracy in terms of CHF is the main interest. The CHF is predicted using Equation (4.1) based on the diameter ratio to the power n. As established earlier, the CHF values for the 8-mm tube data were used as a reference.

4.4.1 CHF Look-up Table Based on Data Obtained in Tubes of Diameter Between 7 and 9 mm

The CHF look-up table of Groeneveld et al. (1996) was derived for 8-mm tubes. However, the table entries were updated with data of other diameter tubes using the correction factor with an exponent value of -1/2, to improve the prediction accuracy of the table. The use of this table, therefore, introduces a bias toward this exponent value. To avoid the bias, the preliminary CHF look-up table (Leung 1996), derived only with data obtained in tubes of diameters between 7 and 9 mm, is used to provide the reference CHF value in this assessment. It covers a much narrower range of flow conditions than the final table of Groeneveld et al. (1996). The comparison of predictions against experimental data is made only for flow conditions where CHF values are available in the preliminary CHF table. This further reduces the number of data for this assessment.

4.4.2 Results of the Comparison

The comparison is carried out under constant dryout conditions, to show the closeness of fit for the correlations (i.e., Equations (4.2) and (4.4)). Based on the experimental conditions of pressure, mass flux and critical quality, the CHF value for an 8-mm tube is calculated using the preliminary CHF look-up table, and the corresponding exponent, n, is evaluated using either Equation (4.2) or (4.4). The CHF value for the tube of interest is obtained by correcting the CHF value of an 8-mm tube with the diameter ratio to the power n. It is then compared against the experimental CHF value to assess the prediction error. In this study, the prediction error is defined as

$$Error = \frac{PredictedCHF - MeasuredCHF}{MeasuredCHF} \qquad (4.5)$$

the overall average error is defined as

$$Average\ Error\ (Avg.) = \frac{1}{N}\sum_{i=1}^{N}(Error)_i \tag{4.6}$$

and the overall root-mean-square error is defined as

$$Root\text{-}mean\text{-}square\ Error\ (rms) = \sqrt{\frac{1}{N}\sum_{i=1}^{N}(Error)_i^2} \tag{4.7}$$

The predicted CHF values using Equation (4.2) for the exponent results in an overall average error of -0.67% and a rms error of 17.6% for 15 862 data points. About 1 900 data points have been neglected in this analysis, due to the extremely large prediction error (beyond ±50%). These rejected data are believed to be questionable mainly because the parametric trends they showed are opposite to the generally observed. Using Equation (4.4) for the exponent provides a slight improvement in prediction accuracy: the average error is -0.28% and the rms error is 17.4% for also 15 862 data points. Figure 4.29 shows the distributions of prediction error for these correlations at various error ranges (over a 5% interval). The error distributions are about the same for both correlations, with more than 50% of the total data predicted within the ±10% error range. However, the use of Equation (4.4) results in slightly more data being predicted within the ±5% range. Therefore for this point in time, Equation (4.4) is recommended over Equation (4.2).

4.4.3 Comparison Against Other Exponent-based Correlations

Several existing methods of predicting the exponent in the tube-diameter correction factor (see Chapter 3) were assessed with the same data base. They include the diameter-dependent exponent of Becker (1965), the constant values of -1/2 of Doroschuk et al. (1975) and -1/3 of Groeneveld et al. (1986), and the flow-regime-dependent exponents of Kirillov et al. (1989 and 1991). These methods were selected in this assessment because they were based on a large number of data and hence applicable over a wide range of flow conditions.

Table 4.7 lists the prediction accuracy of CHF for various prediction methods. The accuracies for Equations (4.2) and (4.4) are also shown for comparison. Among the existing methods, the constant-exponent approach of either Doroschuk et al. (1975) or Groeneveld et al. (1986) provides the best prediction accuracy. In addition, more data are predicted within the ±50% error range with this approach than with the others. The complex flow-regime-dependent exponents of Kirillov et al. (1989 and 1991) give a less satisfactory prediction accuracy than others. This is probably because of the uncertainty in the flow-regime transition, which limits the application of these equations. The diameter-dependent exponents of Becker (1965) yield a reasonable prediction of CHF. Table 4.8 lists the accuracies of these prediction methods based on each data set.

The prediction accuracy of Equation (4.4), which is recommended over Equation (4.2), is practically the same as that of Doroschuk et al. (1975), with close to 0% average error and 17.5% rms error, and is better than the others. However, slightly more data are predicted within the ±50% error range (as well as the ±5% error range) for Equation (4.4) than that of Doroschuk et al. (1975) (15 862 data points for the former compared to 15 816 data points for the latter). The error distributions of various methods are compared against that of Equation (4.4) in Figure 4.30. For all cases, more data are predicted within the ±5% error range with Equation (4.4).

4.5 SUMMARY OF THE TUBE-DIAMETER EFFECT ON CHF AND THE DERIVATION OF A CORRELATION FOR PREDICTING THE EXPONENT N

The tube-diameter effect on CHF has been examined with the AECL data bank. As described in Chapter 3, the diameter effect is a complex phenomena which is affected by pressure, mass flux and quality. In general, higher CHF values are observed for small-diameter tubes. A large variation in the CHF ratio is shown when the CHF value of the 8-mm tubes is used as a reference value. The ratios are strongly affected by quality and mass flux. The pressure effect is not significant at low-pressure conditions, but becomes strong in the low-quality region as the pressure increases.

The tube-diameter correction factor, used to modify the CHF values of an 8-mm tube, has been rederived with the AECL data bank. It is based on the same method suggested by Doroschuk et al. (1975), but the exponent is expressed in terms of flow parameters. Two approaches have been used to derive the correlation for the exponent: one based on trends of the complete AECL data bank (Equation (4.2)), and one based on trends of individual data sets (Equation (4.4)). The latter approach has been shown to provide the best correlation. Furthermore, it results in a simpler form of correlation than the first approach.

The recommended correlation, Equation (4.4), has been assessed against the AECL data bank, and compared against the predictions of several existing methods. This assessment showed that the recommended correlation provides the best prediction accuracy and predicts the most data within both the ±50% and the ±5% error ranges.

Table 4.1: Range of Conditions Covered by Various Sources in the AECL Data Bank.

Source	No. of points	Diameter (mm)	Pressure (MPa)	Mass flux ($Mg \cdot m^{-2} \cdot s^{-1}$)
Alekseev (Kirillov, 1992)	1108	10	9.8 to 19.6	0.2 to 7.5
Becker et al. (1962, 1963)	2378	4, 6, 7.8, 10, 13, 20	0.3 to 4.1	0.1 to 3.2
Becker et al. (1965)	1227	4, 5.6, 8.6, 9.4, 10, 11.5, 12.8, 17.5, 20, 23.6, 25	1.1 to 9.9	0.2 to 5.5
Becker and Ling (1970)	116	2.4, 3, 3.6	3.05 to 7.1	0.03 to 0.98
Becker et al. (1971)	1379	10	3 to 20	0.2 to 8
Bennett et al. (1965)	201	9.5, 12.6	4 to 5.2	0.6 to 5.5
Bertoletti et al. (1964)	352	5, 8, 9.2	5 to 8.9	1 to 4
Borodin and MacDonald (1984)	465	9	8.3 to 10.3	1.2 to 6.9
Dell et al. (1969)	82	6.2	6.9	1.3 to 4.1
Era et al. (1967)	62	6	7	1.1 to 3
Griffel (1965)	402	6.2, 12.8, 23.6, 37.5	3.5 to 10.3	0.6 to 18.6
Groeneveld (1985)	118	10	8 to 20	0.28 to 2.8
Hassid et al. (1967)	168	25	3 and 5	0.37 to 3.8
Hewitt et al. (1965)	263	9.3	0.11 to 0.2	0.09 to 0.3
Jens and Lottes (1951)	47	5.7	3.4 to 13.8	1.3 to 10.5
Judd and Wilson (1967)	49	11.3	7 to 13.8	0.67 to 3.4
Kirillov et al. (1984)	2470	7.8, 8	7 to 17.7	0.5 to 6
Lee and Obertelli (1963)	239	5.6, 10.8	4.1 to 11	0.68 to 4.4
Lee (1965)	264	9.2, 9.5, 10.8, 11.8	6.9	2 to 5.5
Lee (1966)	243	14, 22, 28, 45	8.6 to 12.5	0.33 to 3.4
Lowdermilk et al. (1958)	64	4, 4.8	0.1	0.07 to 2.4
Matzner et al. (1965)	99	10	6.9	1.2 to 9.5
Mayinger (1967)	50	7	7 to 10.3	2.5 to 3.5
Nguyen and Yin (1975)	56	12.6	7 and 8	0.93 to 3.8
Rudzinski (1994)	106	8	3.1 to 10	1.2 to 7.8
Smolin (1962, Kirillov (1992))	666	4, 5, 6, 7.4, 8, 10	7.8 to 19.6	0.5 to 7.5
Smolin (1979, Kirillov (1992))	3009	3.8, 6.1, 8, 11, 16	3 to 17.7	0.5 to 7.5
Snoek (1988)	13	12	9.6	1 to 5
Swenson (1962)	25	10.5	13.8	0.67 to 1.8
Teyssedou et al. (1995)	68	8	0.5 to 3	1 to 4
Thompson and Macbeth (1964)	945	1, 2, 5.6, 7.8, 9.4, 10.8, 11.5, 12.8, 23.6, 37.5	1 to 19	0.2 to 18.5
Tong (1964)	253	6.2, 10.5, 11.2, 12.8	5.2 to 13.8	0.68 to 14
Yin et al. (1988)	287	13.4	1 to 20	2
Zenkevich et al. (1969)	5033	4, 5.8, 6.8, 8, 11, 15	5.9 to 19.6	0.5 to 5
Zenkevich et al. (1971)	392	8	6.9 to 17.5	1 to 2.8
Zenkevich et al. (1974)	840	5, 6, 7, 8, 9, 10, 11, 12.6	6 to 20	0.5 to 6.7

Table 4.2: CHF Ratios and Exponents 'n' for Various Sources (diameter from 2 to 6 mm).

Dia. (mm)	P (MPa)	G $(Mg \cdot m^{-2} \cdot s^{-1})$	x	CHF_d/CHF_8	CHF_d/CHF_8 (average)	n	n (average)	Source
2	12	3.3	0	1.16	1.16	-0.11	-0.11	Thompson
4	5	2.7	.34 to .38	1.47 to 1.50	1.483	-0.556 to -0.292	-0.568	Becker
	5	3.2	.25 to .33	1.41 to 1.55	1.457	-0.496 to -0.632	-0.543	Becker
	7	2.8	.3 to .35	1.54 to 1.574	1.557	-0.623 to -0.654	-0.639	Becker
	7	3.3	0.23	1.24	1.24	-0.307	-0.307	Becker
	7	5	.1 to .15	1.28 to 1.53	1.41	-0.356 to -0.614	-0.495	Becker
	8	4	.15 to .25	1.44 to 1.5	1.444	-0.526 to -0.585	-0.53	Kirillov
	8	5	.1 to .25	1.71 to 1.58	1.629	-0.774 to -0.660	-0.704	Kirillov
	10	5	.05 to .2	1.33 to 1.76	1.531	-0.411 to -0.816	-0.614	Kirillov
	15	4	-.03 to .25	.77 to 1.18	1.017	0.377 to -0.239	-0.023	Kirillov
	15	5	0 to .2	.9 to 1.1	1.020	0.9 to -0.138	-0.027	Kirillov
4.5	7	4	0 to .05	1.37 to 1.5	1.433	-0.547 to -0.585	-0.625	Kirillov
5	7	3.3	.1 to .15	1.443 to 1.50	1.471	-0.780 to -0.705	-0.821	Kirillov
	12	4	.1 to .15	1.02 to .95	0.985	-0.042 to 0.109	0.032	Kirillov
5.6	5	4	.08 to .28	1.37 to 1.11	1.18	-0.883 to -0.222	-0.476	Thompson
	7	4	.05 to .25	1.524 to 1.16	1.336	-1.181 to -0.416	-0.812	Kirillov
6	3	1.5	.5 to .55	1.22 to 1.92	1.513	-0.691 to -1.829	-1.44	Becker
	7	2.8	.13 to .2	1.36 to 1.46	1.4	-1.069 to -1.315	-1.172	Mayinger
	7	3.3	.05 to .30	1.28 to 1.08	1.14	-0.858 to -0.268	-0.456	Kirillov
	7	4	.1 to .15	1.55 to 1.44	1.496	-1.523 to -1.268	-1.4	Tong
	7	5	.05 to .25	1.24 to 1.04	1.114	-0.748 to -0.136	-0.375	Kirillov
	8	2.8	0 to .25	1.08 to .98	1.022	-0.268 to 0.070	-0.075	Kirillov
	8	3.3	.05 to .3	1.21 to 1.027	1.11	-0.663 to -0.093	-0.369	Kirillov
	8	4	.05 to .2	1.09 to 1.13	1.124	-0.300 to -0.425	-0.407	Kirillov
	8	5	0 to .2	1.27 to 1.15	1.192	-0.831 to -0.486	-0.61	Kirillov
	10	2.8	0 to .15	1.13 to 1.36	1.233	-0.425 to -1.069	-0.727	Kirillov
	10	3.3	.1 to .35	1.12 to 1.08	1.099	-0.394 to -0.268	-0.329	Kirillov
	10	2.8	0 to .15	1.13 to 1.36	1.233	-0.425 to -1.069	-0.727	Tong
	10	4	0 to .15	1.09 to 1.086	1.09	-0.300 to -0.287	-0.3	Kirillov
	10	5	0 to .15	1.21 to 1.1	1.119	-0.663 to -0.331	-0.391	Tong
	12	3.3	0 to .3	1.12 to .99	1.162	-0.394 to 0.035	-0.522	Kirillov
	12	5	.05 to .15	1.07 to 1.03	1.045	-0.235 to -0.103	-0.153	Kirillov
	15	1	.3 to .38	1.28 to 1.14	1.205	-0.858 to -0.455	-0.648	Kirillov
	15	2.7	0 to .18	1.1 to 1.17	1.146	-0.331 to -0.546	-0.474	Kirillov
	15	3.2	-.1 to .33	1.09 to .82	1.005	-0.300 to 0.690	-0.017	Kirillov
	15	4	-.05 to .17	.88 to 1.01	0.962	0.444 to -0.035	0.133	Kirillov
	15	5	0 to .27	1.18 to .85	1.012	-0.575 to 0.565	-.0415	Kirillov
	16	1.5	.05 to .45	.97 to .69	0.937	0.106 to 1.290	0.226	Kirillov
	16	3.3	0 to .35	1.18 to .98	1.073	-0.575 to 0.070	-0.245	Kirillov

Table 4.3: CHF Ratios and Exponents 'n' for Various Sources (diameter from 7 to 10.4 mm).

Dia. (mm)	P (MPa)	G ($Mg \cdot m^{-2} \cdot s^{-1}$)	x	CHF_d/CHF_8	CHF_d/CHF_8 (average)	n	n (average)	Source
7	7	2.8	.15 to .25	1.19 to 1.35	1.27	-1.303 to -1.043	-1.79	Mayinger
	7	3.3	.1 to .2	1.21 to 1.26	1.216	-1.428 to -1.731	-1.465	Mayinger
	10	3.3	.2 to .35	1.23 to 1.93	1.564	-1.550 to -4.924	-3.35	Kirillov
	10	3.3	.1 to .2	1.23 to 1.55	1.379	-1.550 to -3.282	-2.41	Mayinger
9	7	2.8	.3 to .4	.96 to .84	0.9	-0.347 to 1.306	-0.904	Kirillov
	8	2.8	0.4	0.928	0.928	-0.634 to -0.634	-0.632	Borodin
	10	2.8	.25 to .35	1.18 to .92	1.074	1.405 to -0.708	0.606	Borodin
	10	3.3	.25 to .35	1.25 to 1.34	1.297	1.895 to 2.485	2.21	Borodin
9.5	7	1	.62 to .74	1.23 to 1.72	1.388	1.205 to 4.604	2.031	Kirillov
10	3	1	.45 to .65	1.04 to .42	0.791	0.176 to -3.888	-1.051	Becker
	3	1.5	.43 to .53	.79 to .29	0.575	-1.056 to -5.547	-2.48	Becker
	3	2.7	.2 to .38	.89 to .55	0.786	-0.522 to -2.679	-1.08	Becker
	3	3.2	.13 to .35	.9 to .63	0.807	-0.472 to -2.071	-0.96	Becker
	5	1	.58 to .73	.68 to .582	0.587	-1.728 to -2.426	-2.38	Becker
	5	2.7	.25 to .375	.895 to .938	0.868	-0.497 to -0.287	-0.632	Becker
	5	3.2	.18 to .3	.91 to .88	0.876	-0.423 to -0.573	-0.592	Becker
	7	1	.4 to .65	.955 to .84	0.826	-0.206 to -0.781	-0.855	Becker
	7	2.8	.1 to .15	.99 to .861	0.925	-0.045 to -0.671	-0.349	Becker
	7	3.3	.1 to .3	.84 to .91	0.889	-0.781 to -0.423	-0.527	Becker
	7	4	0 to .25	1.36 to .95	1.007	1.378 to -0.230	0.031	Kirillov
	7	5	.05 to .25	1 to .91	0.97	0 to -0.423	-0.137	Becker
	8	1	.3 to .58	.92 to .81	0.855	-0.374 to -0.944	-0.7	Becker
	8	3.3	.05 to .075	.98 to .88	0.932	-0.091 to -0.573	-0.316	Becker
	10	1	.225 to .55	1.13 to .53	0.92	-0.548 to -2.845	-0.376	Becker
	10	3.3	.1 to .35	.84 to 1.14	0.981	-0.781 to 0.587	-0.086	Becker
	10	4	-.05 to .225	1 to .932	0.978	0 to -0.316	-0.1	Becker
	10	5	.05 to .1	1	1	0	0	Kirillov
	12	1	.3 to .46	1.14 to .42	0.973	0.587 to -3.888	-0.121	Kirillov
	12	2.8	.1 to .3	.89 to 1.16	0.95	-0.522 to 0.665	-0.263	Kirillov
	12	3.3	.1 to .3	.98 to 1.18	1.079	-0.091 to 0.742	-0.34	Kirillov
	12	4	.1 to .15	.98 to .99	0.986	-0.091 to -0.045	-0.063	Kirillov
	12	5	.05 to .15	1.04 to .95	0.996	0.176 to -0.230	-0.018	Kirillov
10.4	15	3.2	.07 to .2	.88 to .93	0.919	-0.487 to -0.325	-0.32	Kirillov

Table 4.4: CHF Ratios and Exponents 'n' for Various Sources (diameter from 11 to 20 mm).

Dia. (mm)	P (MPa)	G ($Mg \cdot m^{-2} \cdot s^{-1}$)	x	CHF_d/CHF_8	CHF_d/CHF_8 (average)	n	n verage)	Source
11	7	1	.27 to .714	.957 to .489	0.847	-0.138 to -2.727	-0.522	Kirillov
	7	2.8	.05 to .15	.856 to .86	0.855	-0.488 to -0.474	-0.492	Kirillov
	7	3.3	.05 to .15	.77 to .84	0.803	-0.821 to -0.547	-0.69	Kirillov
	8	1	.2 to .7	.9 to .48	0.764	-0.331 to -2.305	-0.844	Kirillov
	8	2.8	-.05 to .05	.956 to .83	0.907	-0.141 to -0.585	-0.305	Kirillov
	10	1	.125 to .5	.88 to .465	0.751	-0.401 to -2.404	-0.897	Kirillov
	10	2.8	.35	0.921	0.921	-0.258	-0.258	Kirillov
	12	1	.3 to .46	.85 to 0.34	0.581	-0.510 to 0.340	-1.703	Kirillov
	12	2.8	0 to .3	.89 to 1.07	0.878	-0.366 to 0.212	-0.4	Kirillov
	15	1	-.05 to .48	1.4	1.4	1.057	-0.46	Kirillov
	15	2.7	0 to .33	1.07 to .88	0.979	0.212 to -0.401	-0.083	Kirillov
	15	3.3	.25 to .3	.92 to .96	0.926	-0.262 to -0.128	-0.241	Kirillov
	16	1	.15 to .53	.77 to 1.19	0.835	-0.821 to 0.546	-0.567	Kirillov
	16	1.5	.05 to .33	.71 to .60	0.739	-1.075 to -1.604	-0.948	Kirillov
	16	2	.03 to .35	.91 to 1.03	0.9	-0.296 to 0.093	-0.328	Kirillov
	16	2.8	0 to .35	.95 to .67	0.862	-0.161 to -1.258	-0.467	Kirillov
13	3	1	.5 to .58	.72 to .46	0.600	-0.677 to -2.438	-1.052	Becker
	5	2.7	.125 to .3	.754 to .737	0.752	-0.582 to -0.629	-0.608	Tong
	5	4	.03 to .1	.759 to .814	0.788	-0.568 to -0.424	-0.508	Tong
	7	1	.513 to .6	.763 to .802	0.801	-0.557 to -0.454	-0.472	Kirillov
	7	2.8	.05 to .3	.90 to .803	0.833	-0.217 to -0.452	-0.376	Kirillov
	7	4	0 to .05	.89 to .75	0.82	-0.240 to -0.593	-0.82	Tong
	8	2.8	.05 to .2	0.734 to .68	0.709	-0.637 to -0.794	-0.709	Tong
	10	2.8	0 to .15	.684 to .662	0.677	-0.782 to -0.850	-0.803	Tong
	10	4	0 to .1	.826 to .75	0.79	-0.394 to -0.593	-0.486	Tong
14	12	2.8	.1 to .15	.78 to .71	0.75	-0.444 to -0.705	-0.51	Lee
	12	3.3	0 to .05	0.923	0.923	-0.143	-0.143	Lee
15	7	1	.6 to .625	.417 to 0.341	0.379	-1.391 to -1.923	-1.54	Kirillov
	15	1	.28 to .43	0.749	0.749	-0.46	-0.46	Kirillov
	16	1	.25 to .4	.75 to .69	0.731	-0.458 to -0.590	-0.5	Kirillov
	16	1.5	.25 to .35	.81 to .72	0.742	-0.335 to -0.523	-0.475	Kirillov
	16	2	.28 to .35	1.1 to 1.33	1.244	0.152 to 0.454	0.347	Kirillov
16	10	1	.47 to .49	.35 to .32	0.331	-1.515 to -1.813	-1.596	Kirillov
	15	1	.37 to .47	0.632	0.632	-0.663	-0.663	Kirillov
20	5	1	.43 to .48	.579 to .526	0.553	-0.596 to -0.701	-0.646	Becker
	7	1	.35 to .4	.645 to .563	0.603	-0.479 to -0.627	-0.552	Becker

Table 4.5: Average Values of Exponent 'n' at Various Nominal Pressures and Mass Fluxes.

	p = 3 MPa, x from 0.02 to 0.72				p = 5 MPa, x from 0.02 to 0.73				p = 7 MPa, x from 0 to 0.4			
G =	1	1.5	2.7	3.2	1	2.7	3.2	4	2.8	3.3	4	5
d(mm)												
4						-0.568	-0.543		-0.639			-0.5
4.5											-0.625	
5										-0.821	-0.49	
5.5								-0.476			-0.812	
6		-1.44							-0.172	-0.456	-1.4	-0.38
7									-0.179	-1.46		
9									-0.904			
10	-1.05	-2.48	-1.08	-0.96		-2.38	-0.632	-0.592		-0.349	-0.527	-0.03
11										-0.492	-0.69	
13	-1.05					-0.608		-0.508	-0.376		-0.409	
20					-0.646							

	p = 8 MPa, x from -0.05 to 0.3				p = 10 MPa, x from -0.05 to 0.38			
G =	2.8	3.3	4	5	2.8	3.3	4	5
d(mm)								
4			-0.53	-0.704				-0.614
4.5								
5								
5.5								
6	-0.075	-0.369	-0.407	-0.61	-0.727	-0.329	-0.3	-0.606
7						-3.1		
9	-0.632	-1.31			-0.606	2.21		
10	-0.14		-0.316			-0.086	-0.100	0
11	-0.31				-0.256			
13	-0.709				-0.803		-0.46	
20								

	p = 12 MPa, x from 0 to 0.3				p = 15 MPa, x from -0.07 to 0.48				
G =	2.8	3.3	4	5	1	2.8	3.2	4	5
d(mm)									
2		-0.11							
4								-0.023	-0.027
5			-0.032						
6.		-0.522		-0.153	-0.648	-0.474	-0.017	0.133	-0.042
7									
10	-0.26	0.340	-0.063	-0.016			-0.32		
11	-0.4				-0.117	-0.083	-0.241		
14	-0.51	-0.145							
15					-0.46				
16					-0.663				

	p = 16 MPa, x from 0 to 0.45					p = 18 MPa, x from -0.15 to 0.48				
G =	1	1.5	2	2.8	3.3	1	2.8	3.3	4	5
d(mm)										
2										
4									0.112	0.02
5										
6.		0.226			1.073	0.167	0.102	-0.153	0.102	-0.654
7									0.503	
10						-0.85	0.031	0.446	0.307	
11	-0.567	-0.948	-0.328	-0.467		-0.825	-0.231			
14										
15	-0.5	-0.475	0.347			-0.69				
16										

Table 4.6: Prediction Accuracies of CHF from Various Exponent-based Prediction Methods.

Method	No. of Data	Error (%)	
		mean	rms
Becker (1965)	15657	0.9	18.2
Doroschuk et al. (1975)	15816	0.3	17.5
Groeneveld et al. (1986)	15816	1.3	17.6
Kirillov et al. (1989)	15641	2.3	18.7
Kirillov et al. (1991)	15660	2.3	19.1
Equation (4.2)	15862	-0.67	17.6
Equation (4.4)	15862	-0.28	17.4

Table 4.7: Optimized Exponents for Various Flow Conditions and Data Sets.

Becker (1965)	P = 3, G = 0.5 0.45 < x < 0.9 6 < d < 25 **n = -0.8**	P = 3, G = 1.0 0.45 < x< 0.75 6 < d < 8 **n = -0.4**	P = 3, G = 1.5 0.3 < x < 0.7 4 < d < 20 **n = -0.45**	P = 3, G = 2 0.2 < x < 0.55 4 < d < 17.5 **n = -0.5**	P = 5, G = 0.5 0.75 < x < 0.9 7 < d < 10 **n = -0.55**	P = 5, G = 1 0.35 < x< 0.65 7 < d < 20 **n = -0.9**	P = 5, G = 2.3 0.1 < x <0.5 3.93 < d < 10 **n = -1.2**	P = 5, G = 4 0. < x <0.3 3.93 < d < 6 **n = -0.35**	P = 7, G = 1 0.2 < x <0.8 6 < d < 24 **n = -0.6**
Becker (1965)	P = 7, G = 2 0 < x <0.5 4 < d < 24 **n = -0.6**	P = 7, G = 4 0.05 < x <0.35 4 < d < 24 **n = -0.6**							
Bennett et al. (1965)	P = 7, G = 1.3 0.35 < x <0.6 9.5 < d < 13 **n = -0.5**	P = 7, G = 2 0.1 < x <0.5 9.5 < d < 13 **n = -0.9**	P = 7, G = 2.7 0.1 < x <0.45 9.5 < d < 13 **n = -0.6**	P = 7, G = 4 0 < x <0.45 9.5 < d < 13 **n = -0.5**					
Griffel (1965)	P = 7, G =0.95 0 < x <0.6 13 < d < 38 **n = -0.5**	P = 7, G =1.35 -0.1 < x <0.45 13 < d < 38 **n = -0.4**	P = 7, G = 1.9 -0.05 < x <0.4 6 < d < 38 **n = -0.4**	P = 7, G = 2.7 -0.2 < x <0.25 6 < d < 38 **n = -0.5**	P = 7, G = 3.8 -0.15 < x <0.2 6 < d < 38 **n = -0.4**	P = 7, G = 5.5 -0.15 < x <0.2 6 < d < 38 **n = -0.4**	P = 7, G = 7.5 -0.05 <x<0.15 6 < d < 38 **n = -0.4**		
Lee and Obertelli (1963)	P = 7, G = 1 0.5 < x <0.8 6 < d < 12 **n = -0.9**	P = 7, G = 2 0.15 < x <0.5 6 < d < 12 **n = -0.5**	P = 7, G = 4 0 < x <0.3 6 < d < 12 **n = -0.5**						
Lee (1966)	P = 11, G = 1 0.1 < x <0.4 9.4 < d < 28 **n = -0.5**	P =11, G=1.35 0 < x <0.3 11.5 < d < 28 **n = -0.8**	P = 11, G = 2 0.05 < x <0.25 9.4 < d < 14 **n = -0.5**	P = 11, G =2.7 0.05< x <0.15 11.5 < d < 14 **n = -0.85**	P = 12, G =0.5 0.4 < x <0.5 14 < d < 28 **n = -0.8**	P = 12, G = 1 0.15 < x <0.25 14 < d < 28 **n = -1.0**	P = 12, G =1.4 0.05 < x <0.2 14 < d < 28 **n = -0.8**		
Zenkevich et al. (1969)	P = 7, G =2.75 0.3 < x <0.4 9.5 < d < 12.6 **n = -0.85**								
Zenkevich (1974)	P = 12, G =1.5 0.25 < x <0.4 7.7 < d < 10.4 **n = -1.2**	P = 12, G = 2 0.15 < x <0.35 7.7 < d < 10.4 **n = -0.85**	P = 12, G =2.5 0.1 < x <0.3 7.7 < d < 10.4 **n = -0.9**						
Kirillov (1992)	P = 7, G =0.5 0.7 < x <0.9 8 < d < 12.6 **n = -0.6**	P = 7, G =2 0.15 < x <0.45 8 < d < 12.6 **n = -0.5**	P = 7, G =4 0.05 < x <0.35 8 < d < 9.5 **n = -0.5**						
Tong (1964)	P = 7, G =1.5 0.1 < x <0.2 10 < d < 13 **n = -0.5**	P = 7, G =1.9 0.2 < x <0.3 6 < d < 13 **n = -0.6**	P = 7, G =2.7 0.1 < x <0.25 6 < d < 13 **n = -0.85**	P = 7, G =3.8 0.05 < x <0.2 6 < d < 13 **n = -0.8**	P = 7, G =5.5 0 < x <0.1 6 < d < 13 **n = -0.85**	P = 7, G =7.5 0 < x <0.08 6 < d < 13 **n = -0.8**	P = 7, G =9.5 0 < x <0.1 6 < d < 13 **n = -0.5**		
Tong (1964)	P = 10, G =2.7 0 < x <0.15 6 < d < 13 **n = -0.7**	P = 10, G =3.7 0 < x <0.1 6 < d < 13 **n = -0.85**	P = 10, G =5.3 0 < x <0.1 6 < d < 13 **n = -0.7**	P = 10, G =7.6 -0.05 < x <0.1 6 < d < 11 **n = -0.5**	P = 10, G =9 0 < x <0.12 6 < d < 11 **n = -0.5**				
Smolin et al. (1979)	P = 8, G =1 0.6 < x <0.7 8 < d < 11 **n = -0.8**	P = 8, G =1.5 0.45 < x <0.55 8 < d < 11 **n = -0.5**	P = 8, G =2.7 0.1 < x <0.4 8 < d < 11 **n = -0.5**	P = 12, G =1.5 0 < x <0.25 6 < d < 8 **n = -0.5**	P = 12, G =2.2 -0.05 < x <0.3 6 < d < 11 **n = -0.5**	P = 12, G =2.7 -0.02 < x <0.3 6 < d < 11 **n = -0.5**	P = 12, G =4 -0.05 <x<0.15 6 < d < 8 **n = 0**	P = 12, G =5 0 < x <0.15 6 < d < 8 **n = -0.1**	
Kirillov (1992)	P = 10, G =0.5 0.4 < x <0.95 8 < d < 10 **n = 0**	P = 10, G =1 0.2 < x <0.6 8 < d < 10 **n = 0**	P = 10, G =1.5 0 < x <0.4 6 < d < 11 **n = -0.6**	P = 10, G =2 -0.05 < x <0.4 6 < d < 11 **n = -0.5**	P = 10, G =2.5 0.05 < x <0.35 6 < d < 11 **n = -0.5**	P = 10, G =2.7 0 < x <0.35 8 < d < 11 **n = -0.35**	P = 10, G =3 0 < x <0.3 6 < d < 10 **n = -0.45**	P = 10, G =4 0 < x <0.4 4 < d < 10 **n = -0.45**	P = 10, G =0.5 0 < x <0.15 6 < d < 8 **n = -0.5**

Table 4.8: Prediction Accuracies of CHF Correlations vs. Data Sets of AECL Data Bank

Source of Experimental Data	Year	Correlations											
		Equation (4.2)			Equation (4.4)			Kirrilov (1989)			Kirrilov (1991)		
		mean error	rms error	no. of data	mean error	rms error	no. of data	mean error	rms error	no. of data	mean error	rms error	no. of data
Alekseev	1992	-0.063	0.186	843	-0.086	0.191	839	-0.028	0.183	841	-0.013	0.185	842
Becker	1963	-0.074	0.230	1967	-0.044	0.223	1991	0.014	0.223	1961	0.002	0.221	1983
Becker	1965	-0.084	0.193	1158	-0.065	0.188	1150	0.000	0.230	1111	-0.003	0.226	1108
Becker	1970	0.053	0.142	54	-0.076	0.159	56	0.257	0.358	62	0.251	0.371	61
Becker	1971	-0.058	0.181	1080	-0.072	0.183	1071	-0.013	0.175	1070	-0.001	0.175	1070
Bennett	1965	-0.011	0.161	188	0.028	0.165	186	0.104	0.201	176	0.107	0.201	175
Borodin	1984	-0.034	0.117	464	-0.021	0.115	464	0.002	0.118	464	0.007	0.117	464
Dell	1969	0.000	0.144	67	-0.014	0.170	70	-0.060	0.174	70	-0.070	0.191	72
ERA	1967	0.206	0.289	25	0.183	0.275	27	0.165	0.276	32	0.164	0.275	35
Griffel	1965	-0.112	0.183	196	-0.074	0.172	196	0.088	0.253	201	0.091	0.267	187
Hassid	1967	-0.136	0.175	158	-0.018	0.137	161	0.315	0.363	116	0.273	0.342	134
Jens	1951	-0.255	0.273	13	-0.173	0.187	13	-0.319	0.324	13	-0.333	0.338	13
Judd	1967	0.103	0.175	49	0.108	0.169	49	0.216	0.246	46	0.228	0.260	46
Lee	1963	-0.167	0.203	189	-0.154	0.193	189	-0.098	0.162	186	-0.089	0.158	183
Lee	1965	-0.030	0.144	261	-0.013	0.136	257	0.035	0.137	250	0.040	0.140	250
Lee	1966	0.015	0.101	120	0.006	0.087	120	0.170	0.196	120	0.193	0.220	120
Matzner	1965	-0.046	0.197	59	-0.027	0.189	58	0.031	0.194	57	0.034	0.194	57
Mayinger	1967	-0.185	0.225	38	-0.187	0.220	37	-0.215	0.242	37	-0.215	0.242	37
Rudzinski		-0.092	0.158	87	-0.092	0.158	87	-0.092	0.158	87	-0.092	0.158	87
Smolin	1962	0.072	0.152	612	0.062	0.156	606	0.021	0.155	613	0.018	0.173	610
Smolin	1979	0.036	0.125	2778	0.040	0.132	2783	0.017	0.125	2751	0.012	0.129	2748
Snoek	1988	0.016	0.127	14	0.034	0.130	14	0.122	0.145	13	0.184	0.228	14
Tong	1964	-0.084	0.185	135	-0.073	0.180	135	-0.006	0.237	134	-0.005	0.240	135
Yin	1988	-0.098	0.247	219	-0.124	0.281	211	-0.068	0.223	185	-0.030	0.230	195
Zenkevich	1969	0.048	0.175	4101	0.042	0.168	4114	0.038	0.185	4079	0.036	0.193	4069
Zenkevich	1971	0.043	0.211	203	0.044	0.211	203	0.043	0.212	203	0.043	0.212	203
Zenkevich	1974	0.054	0.163	784	0.047	0.157	775	0.089	0.188	763	0.100	0.200	762
All		-0.0067	0.176	15862	-0.0028	0.174	15862	0.0233	0.187	15641	0.0232	0.191	15660

Source of Experimental Data	Year	Correlations								
		Becker			Groeneveld (1986)			Doroschuk et al.(1975)		
		mean error	rms error	no. of data	mean error	rms error	no. of data	mean error	rms error	no. of data
Alekseev	1992	-0.087	0.194	840	-0.066	0.188	840	-0.092	0.195	839
Becker	1963	-0.008	0.219	1971	-0.007	0.221	1997	-0.039	0.223	2001
Becker	1965	-0.015	0.232	1103	-0.033	0.200	1133	-0.065	0.188	1150
Becker	1970	-0.264	0.335	28	0.224	0.274	58	0.078	0.176	57
Becker	1971	-0.055	0.178	1066	-0.049	0.176	1065	-0.077	0.186	1071
Bennett	1965	0.087	0.196	179	0.064	0.175	179	0.022	0.170	186
Borodin	1984	-0.012	0.115	464	-0.007	0.116	464	-0.025	0.116	464
Dell	1969	-0.062	0.180	71	-0.053	0.168	70	-0.011	0.167	70
ERA	1967	0.185	0.290	35	0.173	0.274	31	0.186	0.277	27
Griffel	1965	0.045	0.251	200	-0.022	0.191	197	-0.096	0.177	197
Hassid	1967	0.312	0.371	120	0.129	0.210	164	-0.053	0.123	160
Jens	1951	-0.210	0.221	13	-0.187	0.199	13	-0.140	0.159	13
Judd	1967	0.177	0.222	49	0.161	0.208	49	0.096	0.158	49
Lee	1963	-0.118	0.166	183	-0.125	0.171	186	-0.158	0.195	189
Lee	1965	0.014	0.144	255	0.013	0.140	255	-0.018	0.139	258
Lee	1966	0.156	0.182	120	0.080	0.119	120	-0.017	0.081	120
Matzner	1965	0.001	0.185	57	-0.001	0.185	57	0.074	0.273	37
Mayinger	1967	-0.206	0.235	37	-0.201	0.231	37	-0.183	0.217	37
Rudzinski		-0.096	0.160	87	-0.092	0.158	87	-0.092	0.158	87
Smolin	1962	0.012	0.149	613	0.048	0.150	610	0.063	0.153	597
Smolin	1979	0.020	0.126	2757	0.035	0.128	2768	0.042	0.132	2773
Snoek	1988	0.077	0.114	13	0.052	0.097	13	0.014	0.133	14
Tong	1964	-0.029	0.211	134	-0.046	0.199	134	-0.084	0.184	134
Yin	1988	-0.070	0.233	189	-0.079	0.262	203	-0.132	0.284	211
Zenkevich	1969	0.036	0.173	4101	0.044	0.172	4117	0.045	0.168	4100
Zenkevich	1971	0.041	0.212	204	0.044	0.211	203	0.044	0.211	203
Zenkevich	1974	0.064	0.172	768	0.061	0.165	766	0.044	0.156	772
All		0.0094	0.182	15657	0.0126	0.176	15816	-0.0027	0.175	15816

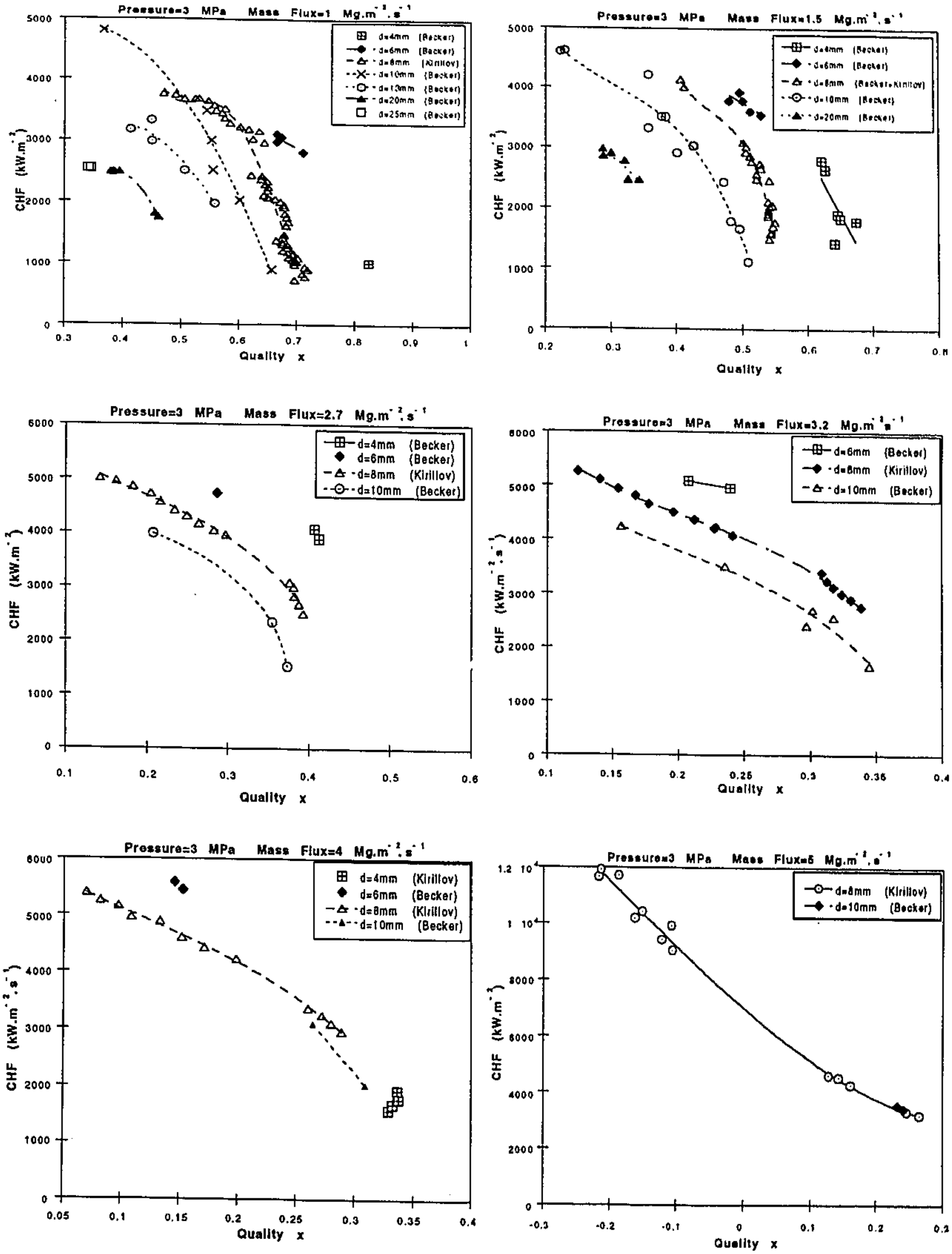

Figure 4.1: CHF vs. Quality for Data from Different Sources (Pressure 3 MPa)

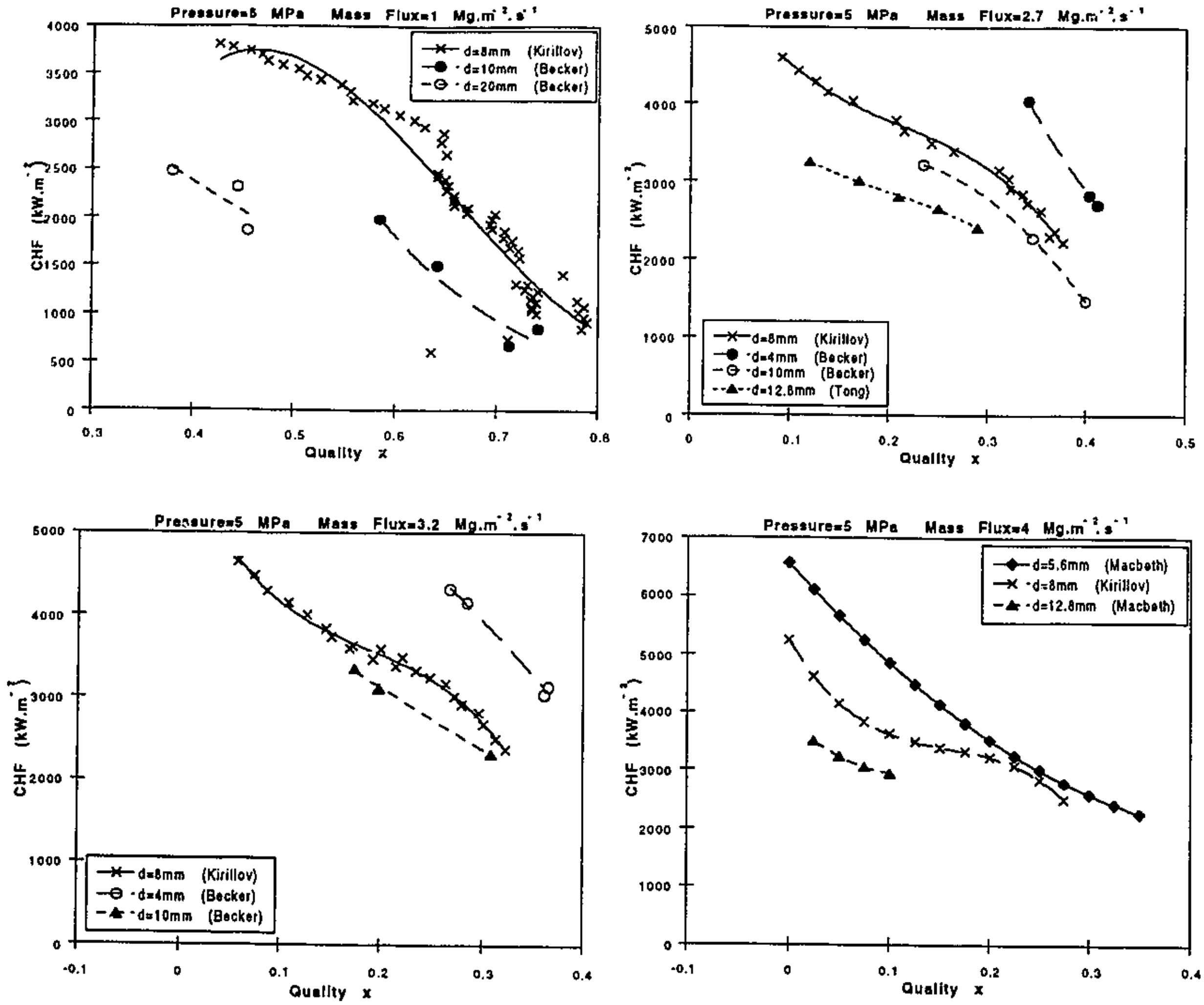

Figure 4.2: CHF vs. Quality for Data from Different Sources (Pressure 5 MPa)

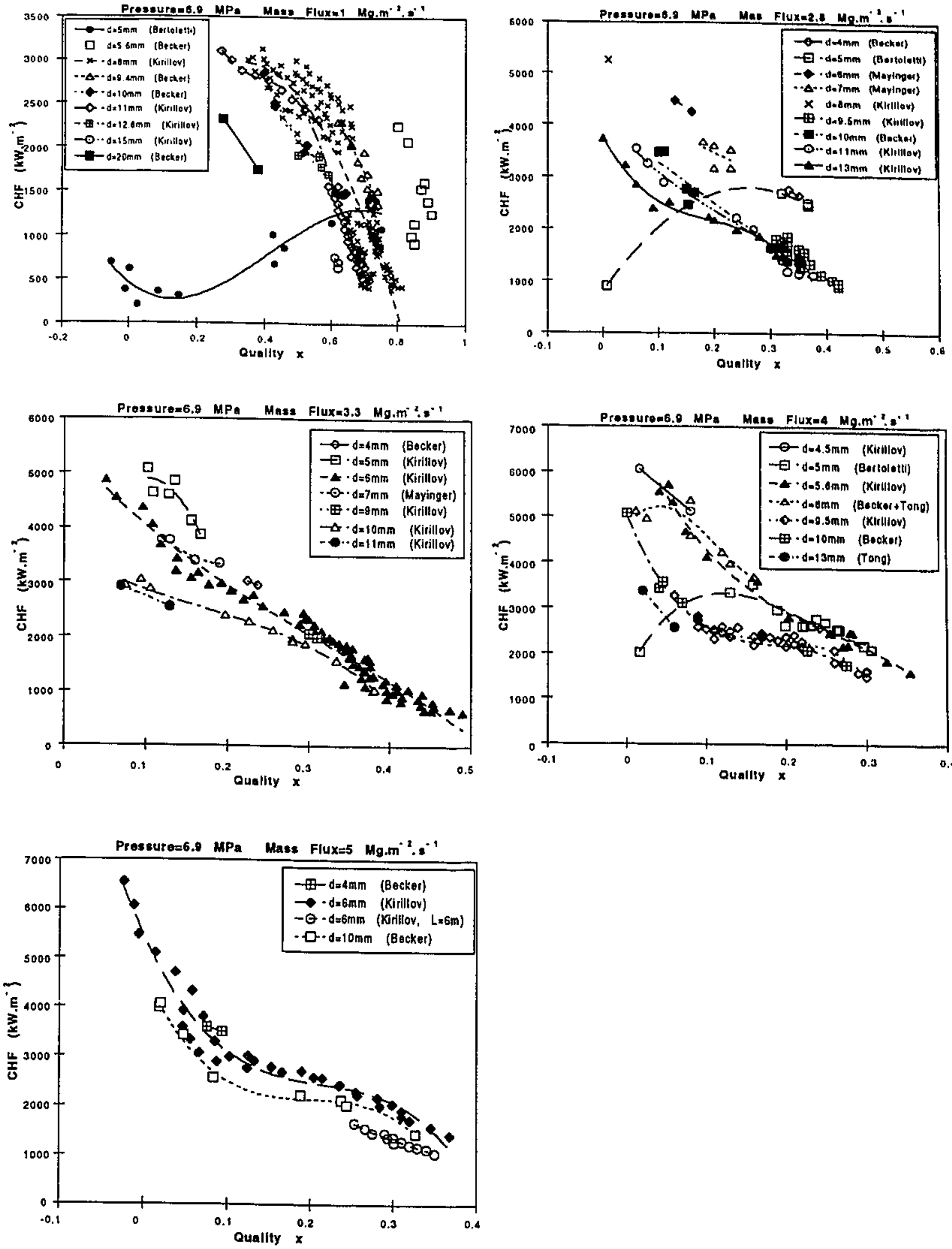

Figure 4.3: CHF vs. Quality for Data from Different Sources (Pressure 6.9 MPa)

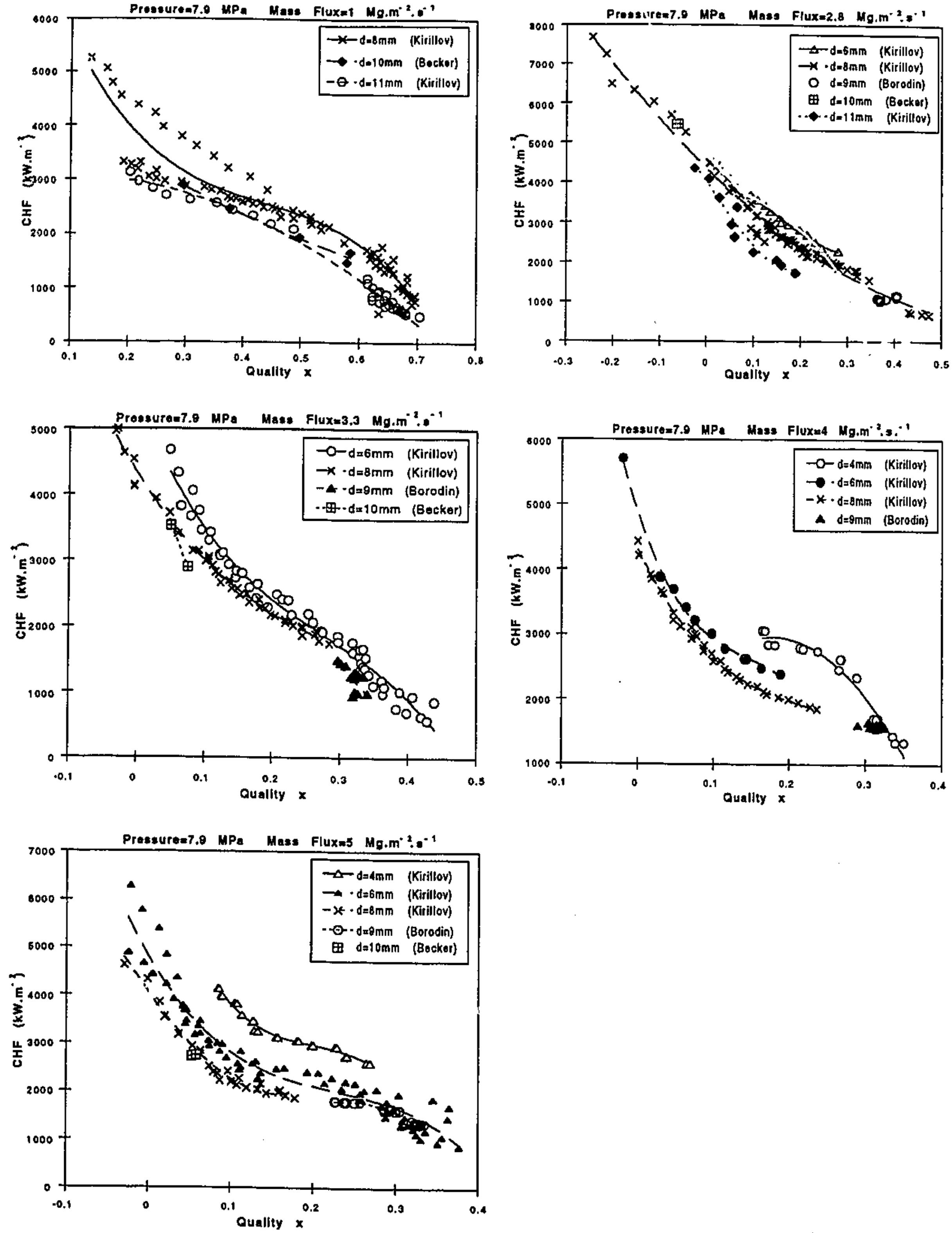

Figure 4.4: CHF vs. Quality for Data from Different Sources (Pressure 7.9 MPa)

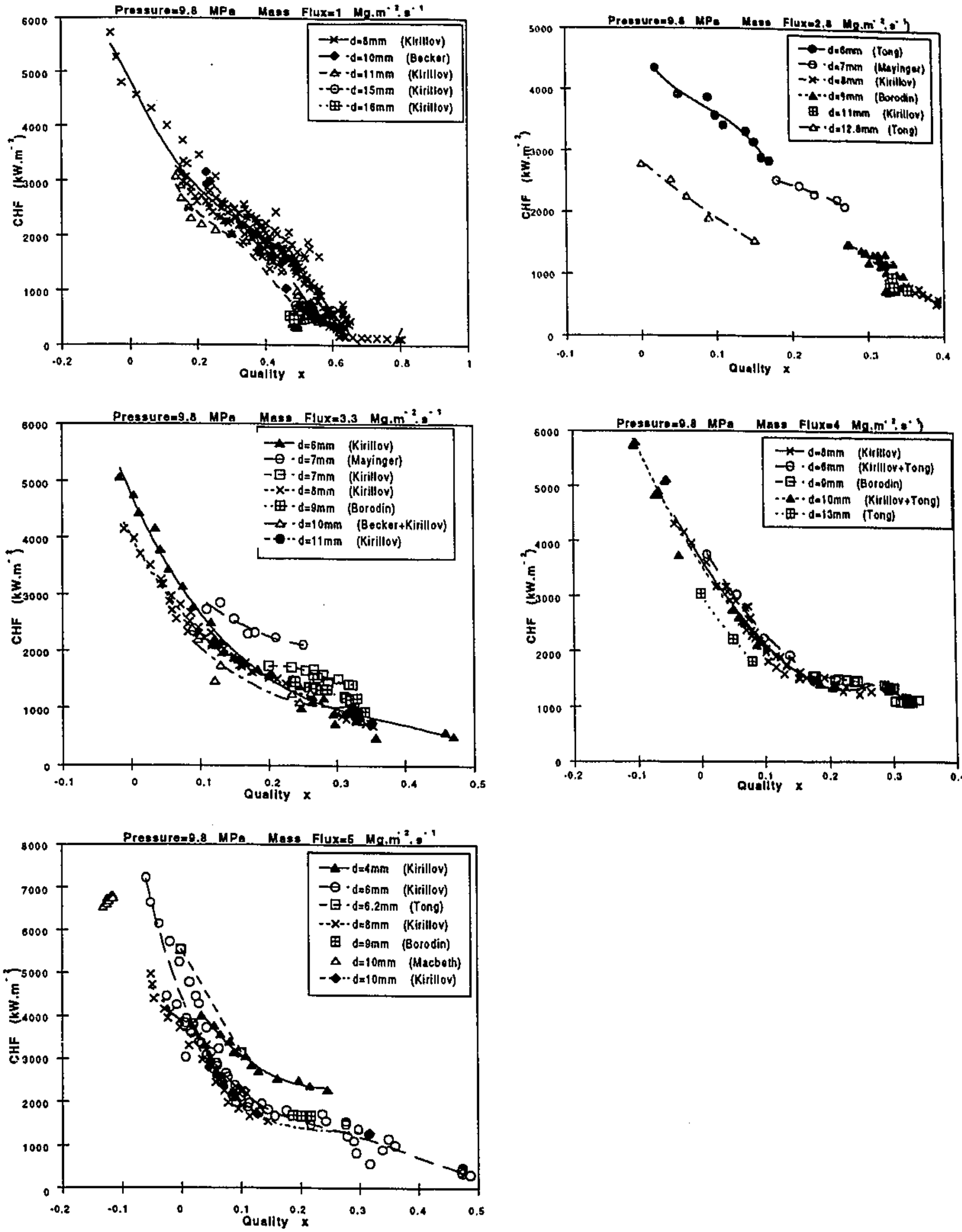

Figure 4.5: CHF vs. Quality for Data from Different Sources (Pressure 9.8 MPa)

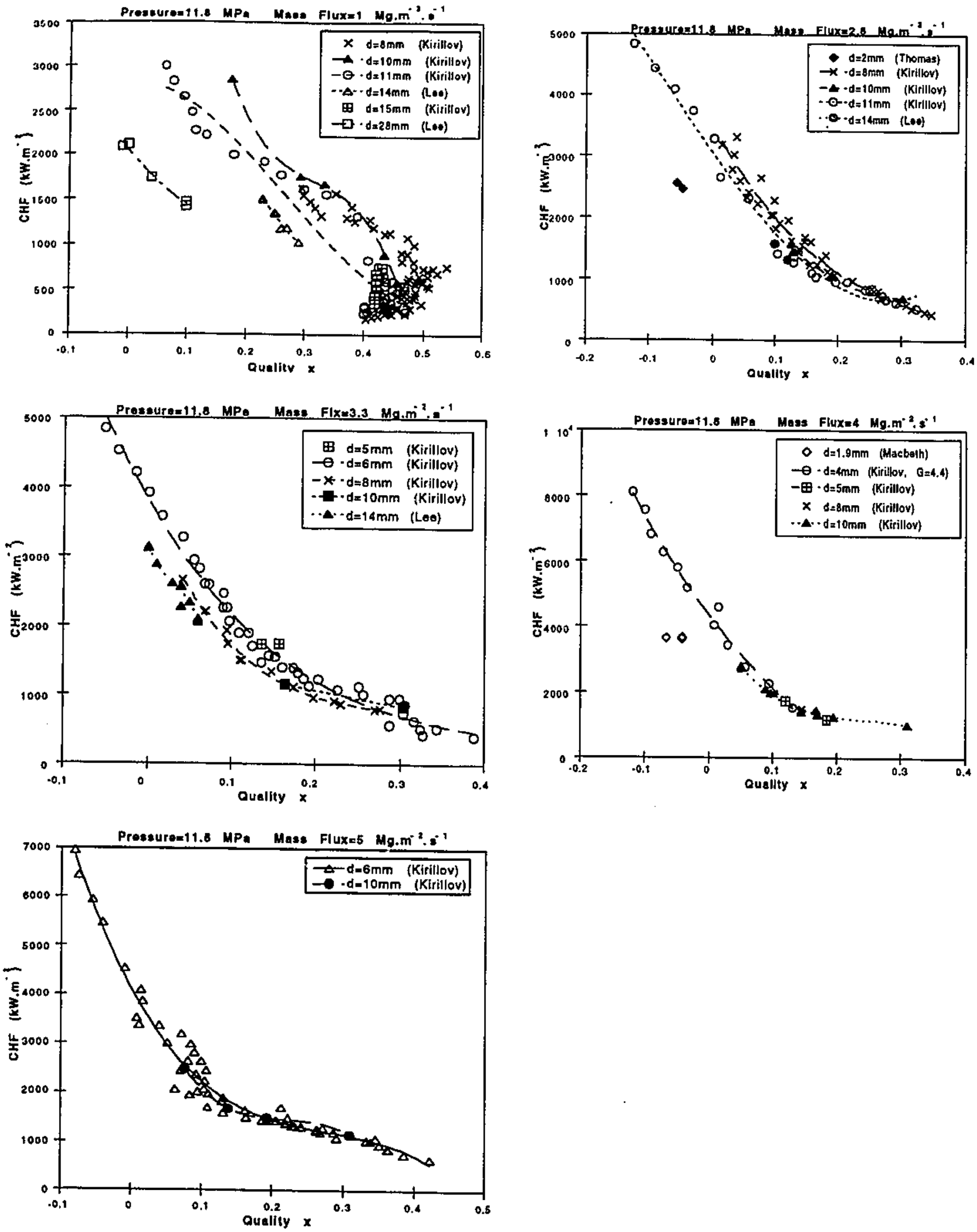

Figure 4.6: CHF vs. Quality for Data from Different Sources (Pressure 11.8 MPa)

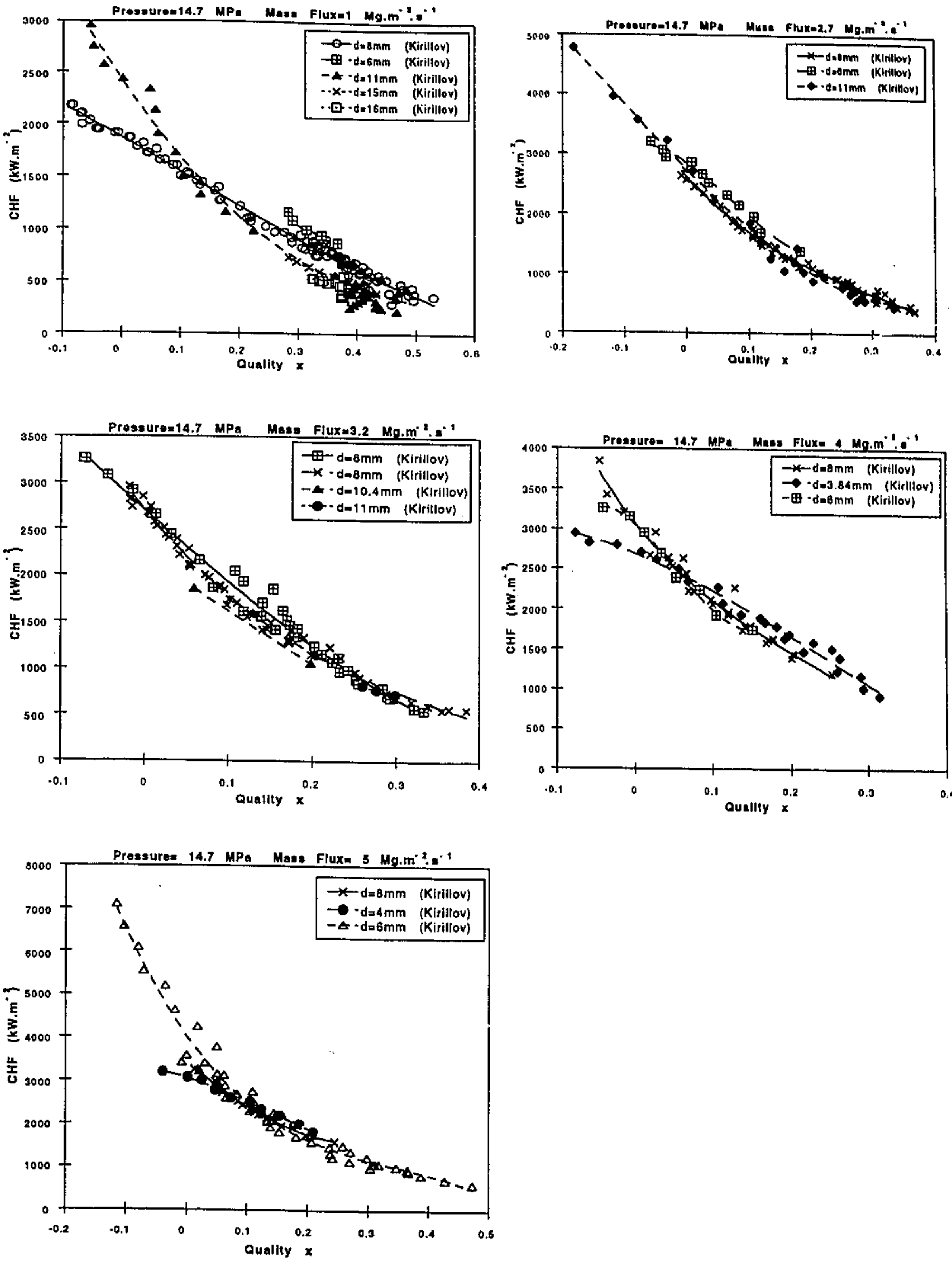

Figure 4.7: CHF vs. Quality for Data from Different Sources (Pressure 14.7 MPa)

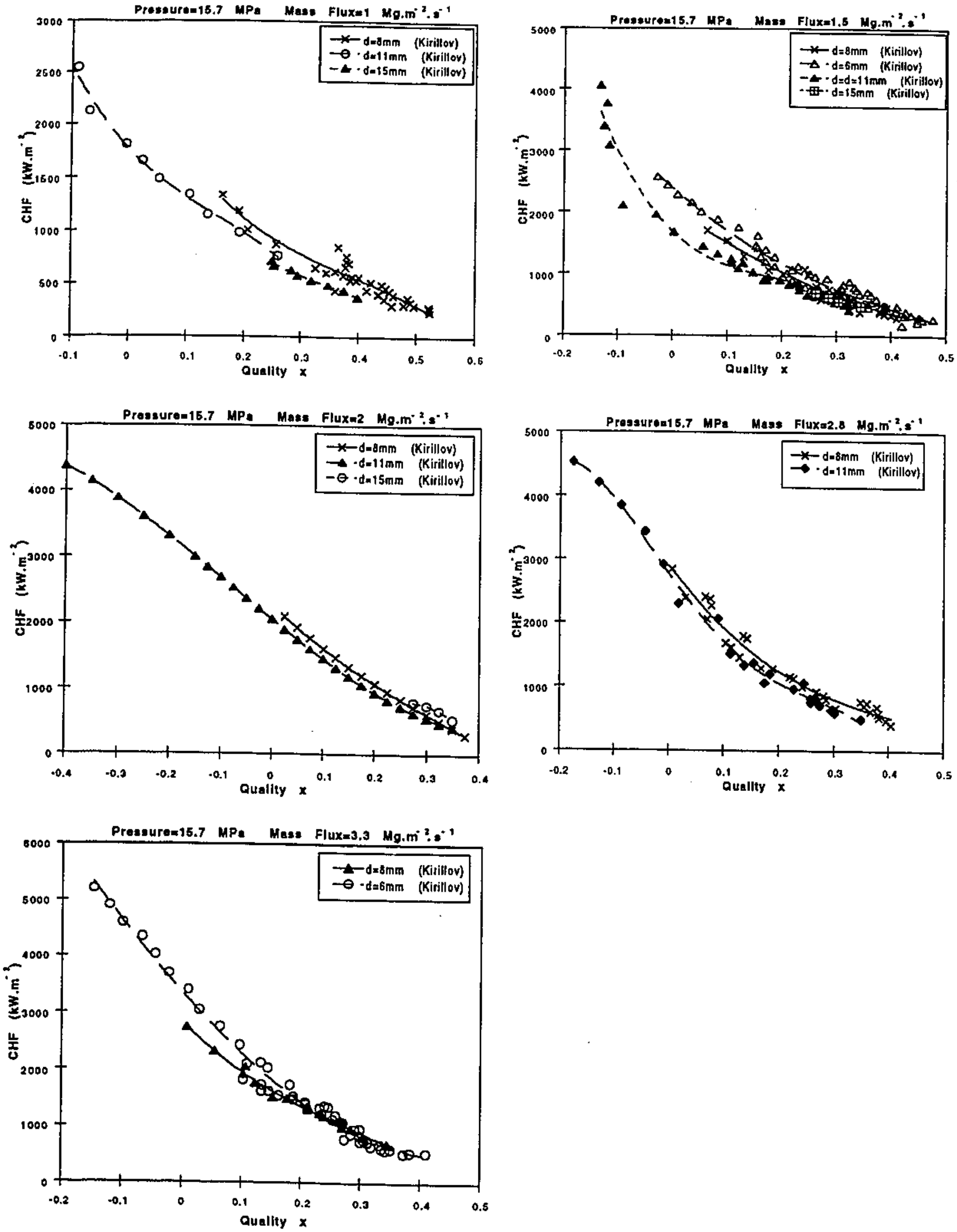

Figure 4.8: CHF vs. Quality for Data from Different Sources (Pressure 15.7 MPa)

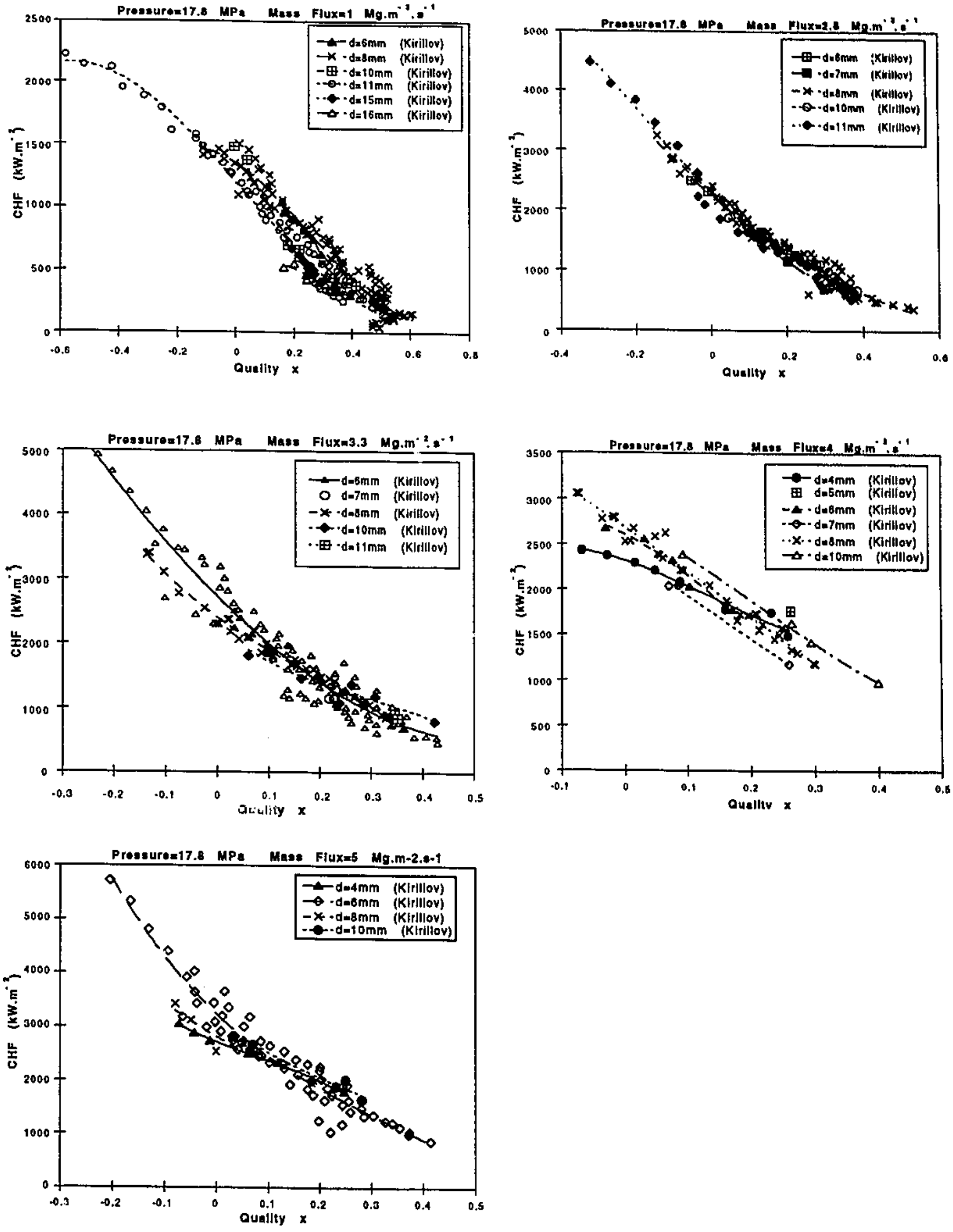

Figure 4.9: CHF vs. Quality for Data from Different Sources (Pressure 17.8 MPa)

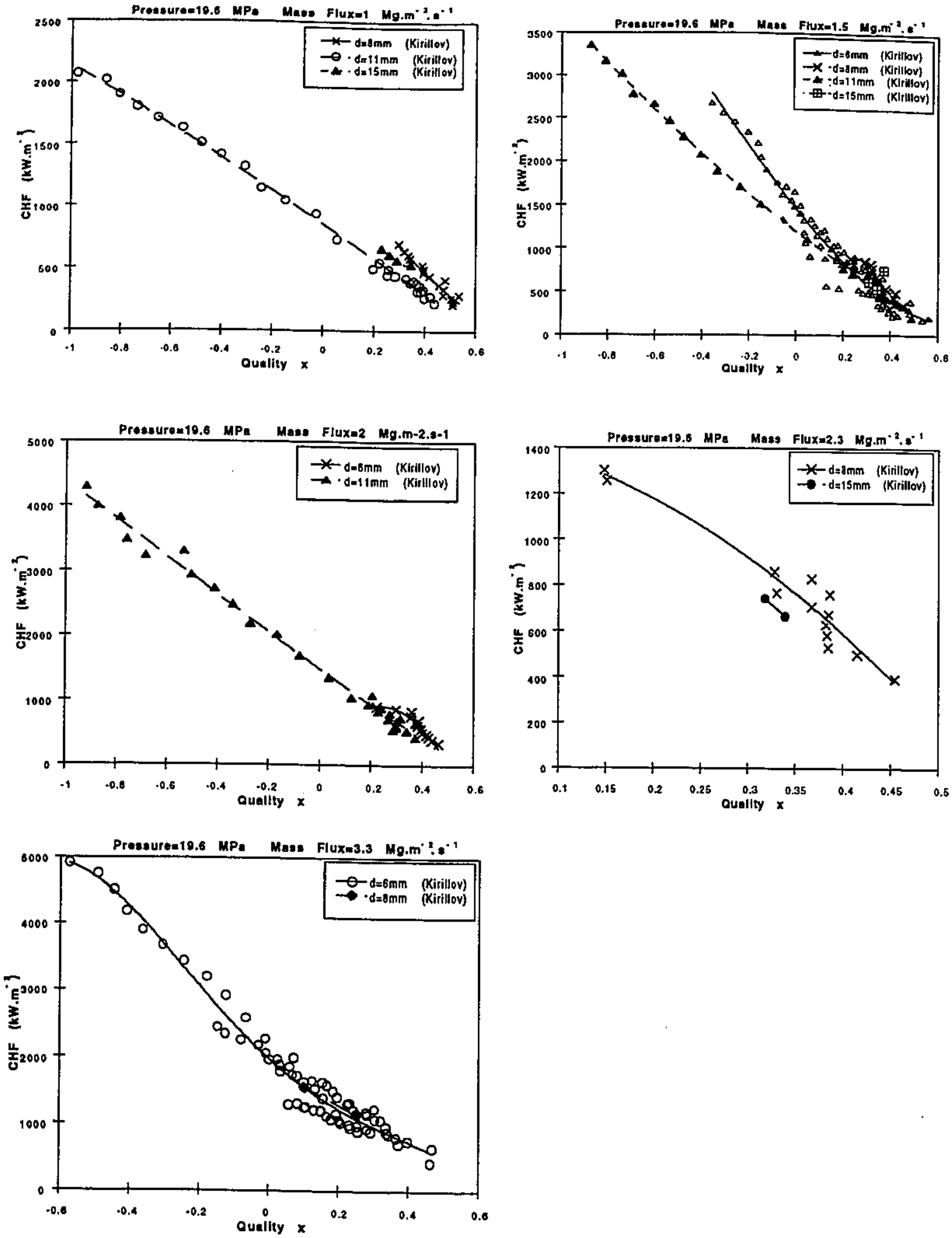

Figure 4.10: CHF vs. Quality for Data from Different Sources (Pressure 19.6 MPa)

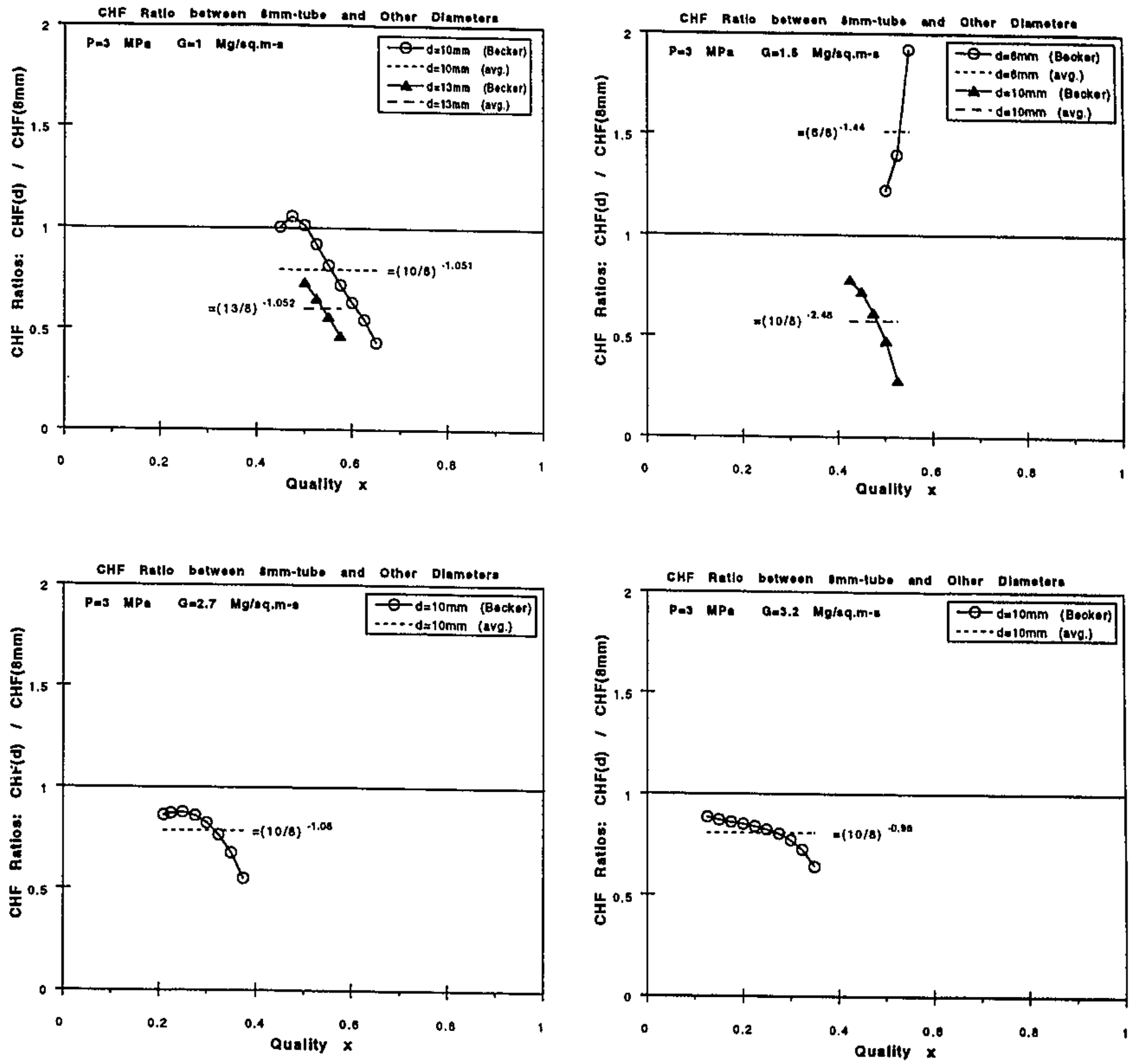

Figure 4.11: Ratios of CHF vs. Quality Between 8 mm Tube to Other Diameters (Pressure 3 MPa)

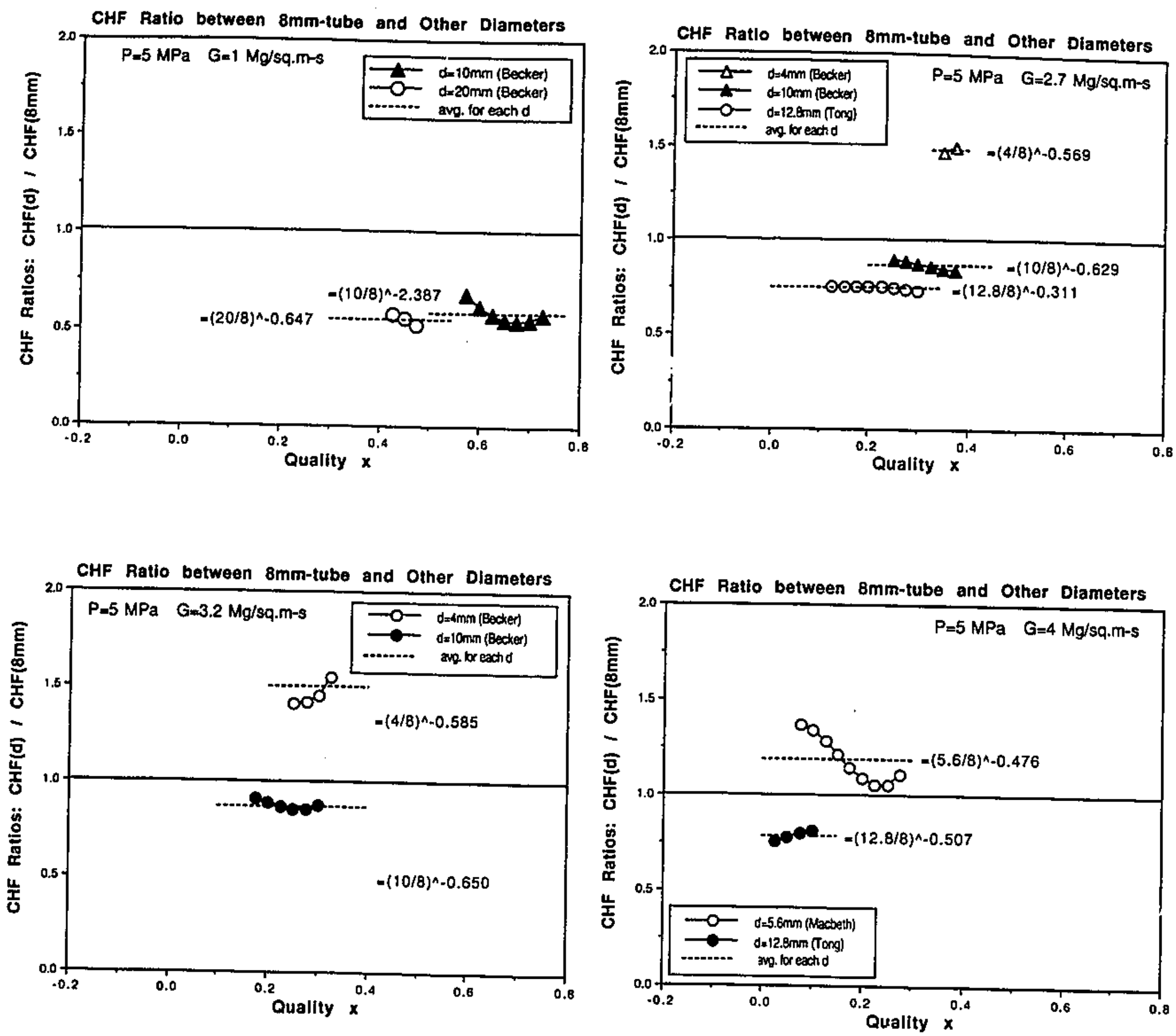

Figure 4.12: Ratios of CHF vs. Quality Between 8 mm Tube to Other Diameters (Pressure: 5 MPa)

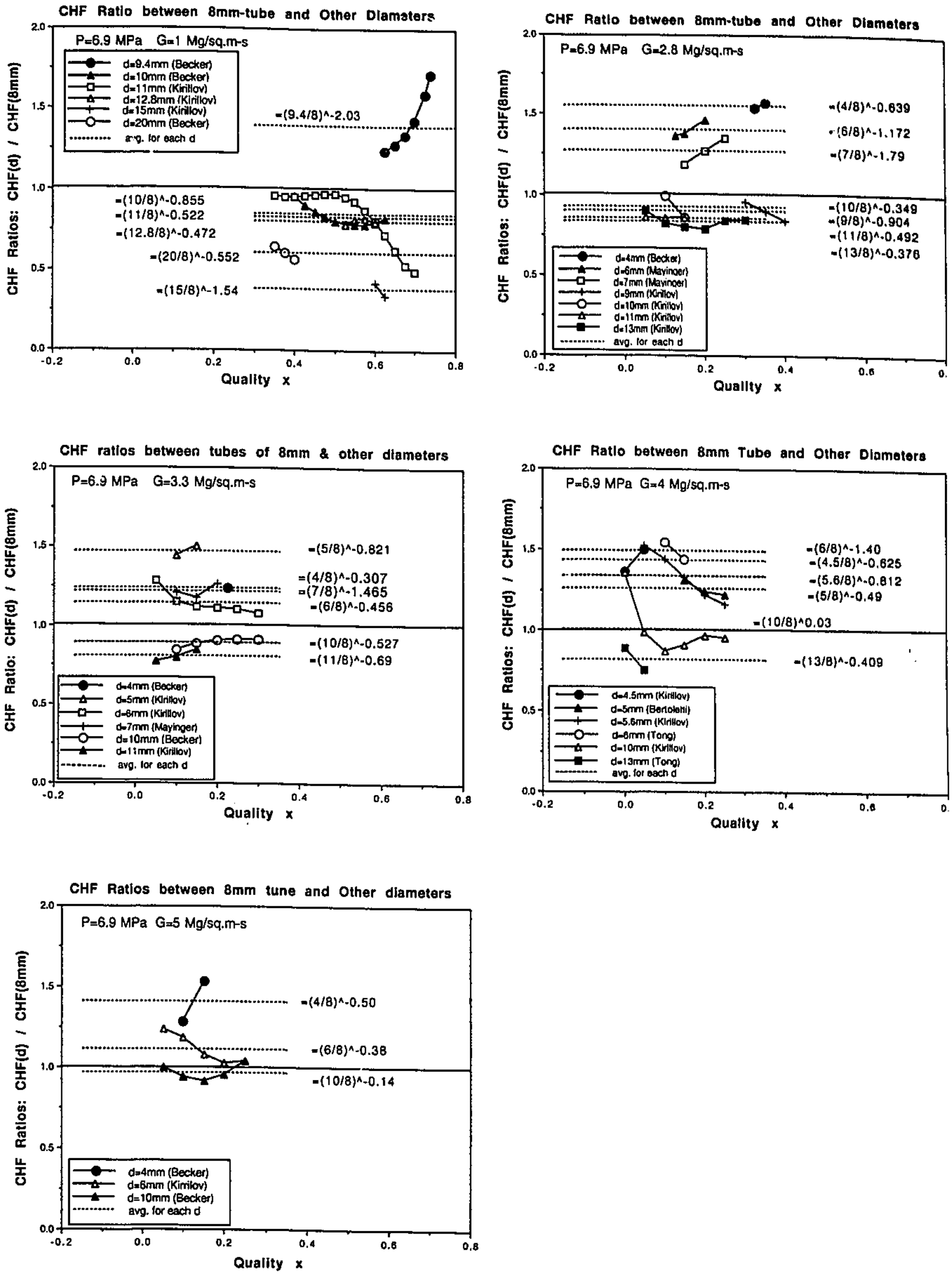

Figure 4.13: Ratios of CHF vs. Quality Between 8 mm Tube to Other Diameters
(Pressure: 6.9 MPa)

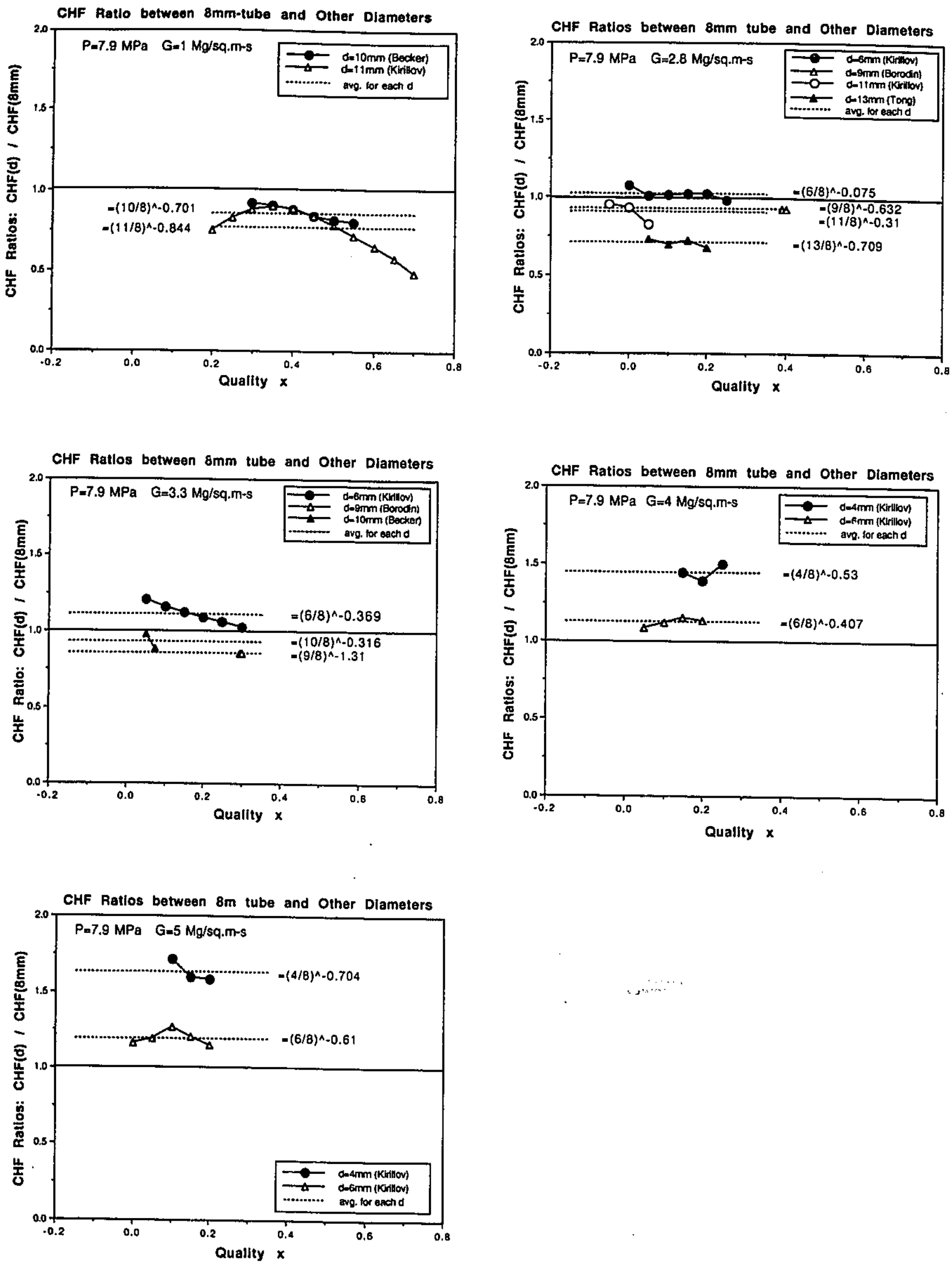

Figure 4.14: Ratios of CHF vs. Quality Between 8 mm Tube to Other Diameters (Pressure: 7.9 MPa)

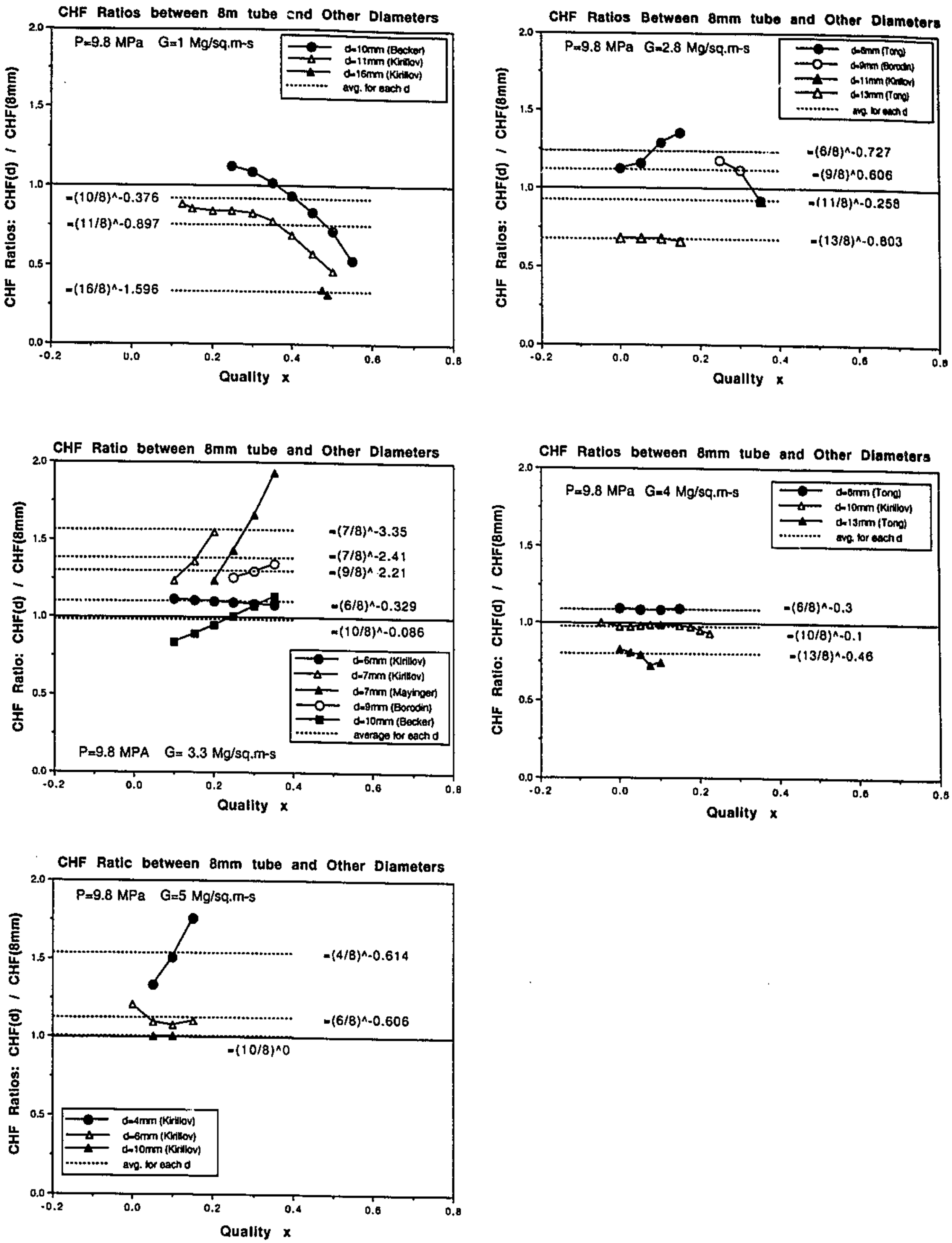

Figure 4.15: Ratios of CHF vs. Quality Between 8 mm Tube to Other Diameters (Pressure: 9.8 MPa)

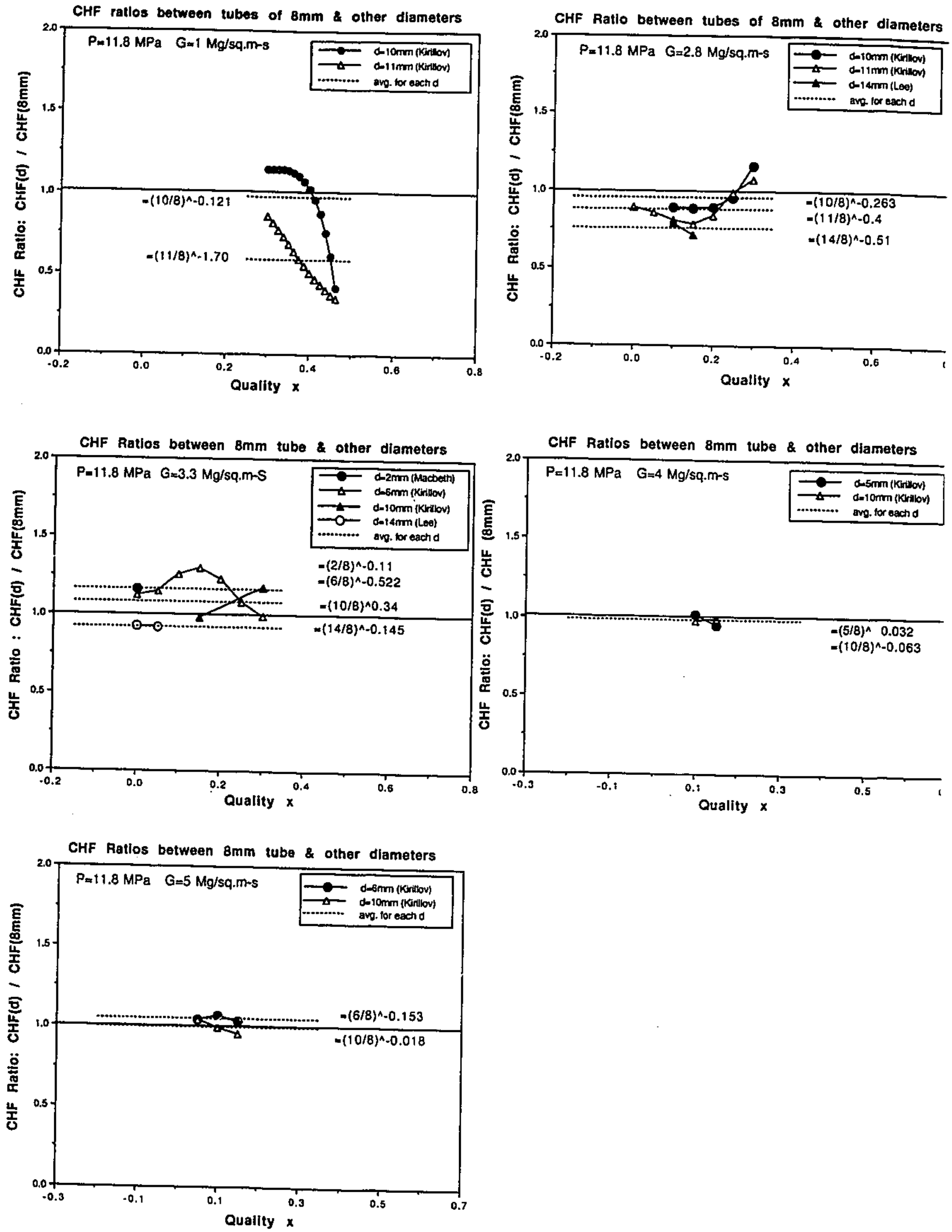

Figure 4.16: Ratios of CHF vs. Quality Between 8 mm Tube to Other Diameters (Pressure: 11.8 MPa)

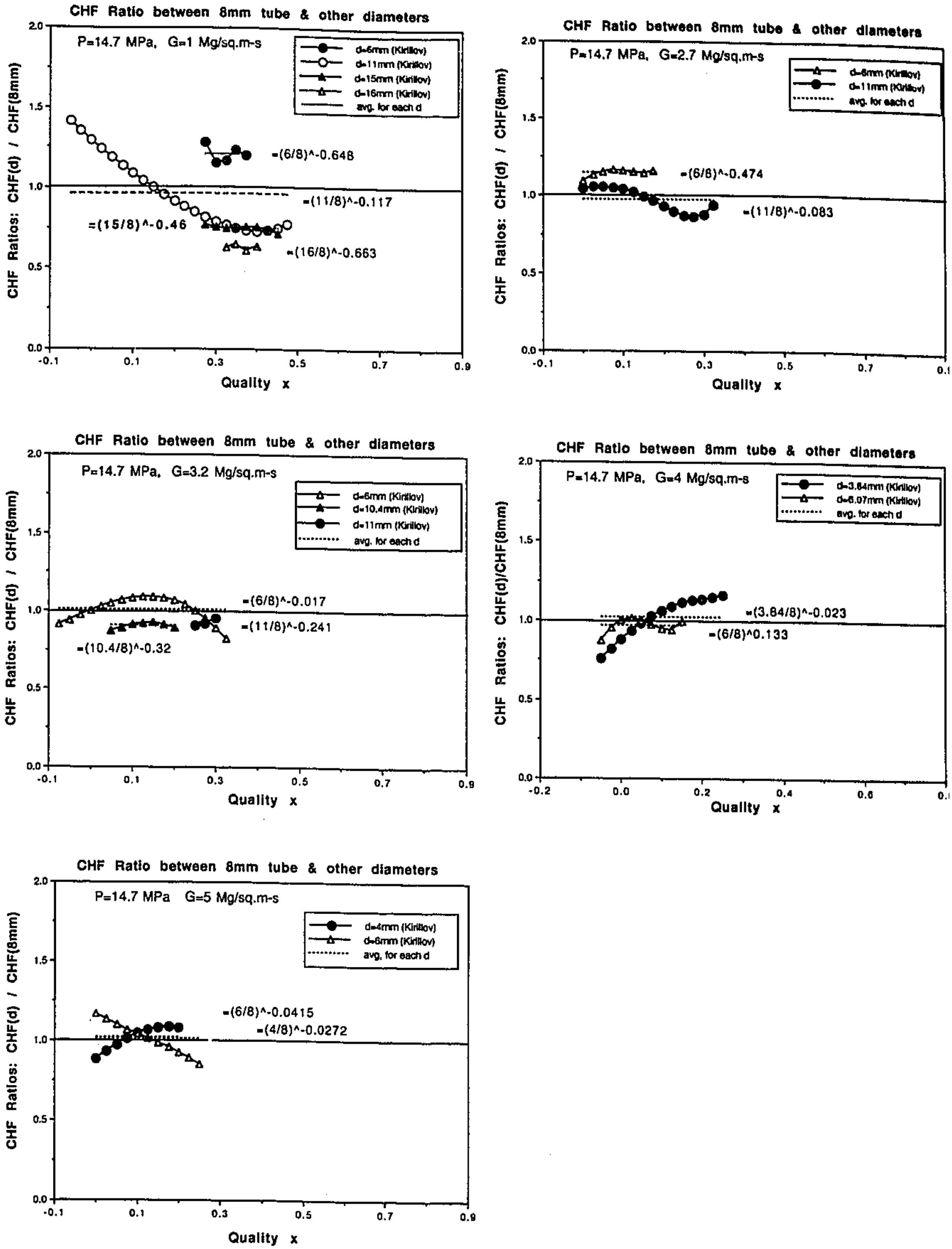

Figure 4.17: Ratios of CHF vs. Quality Between 8 mm Tube to Other Diameters (Pressure: 14.7 MPa)

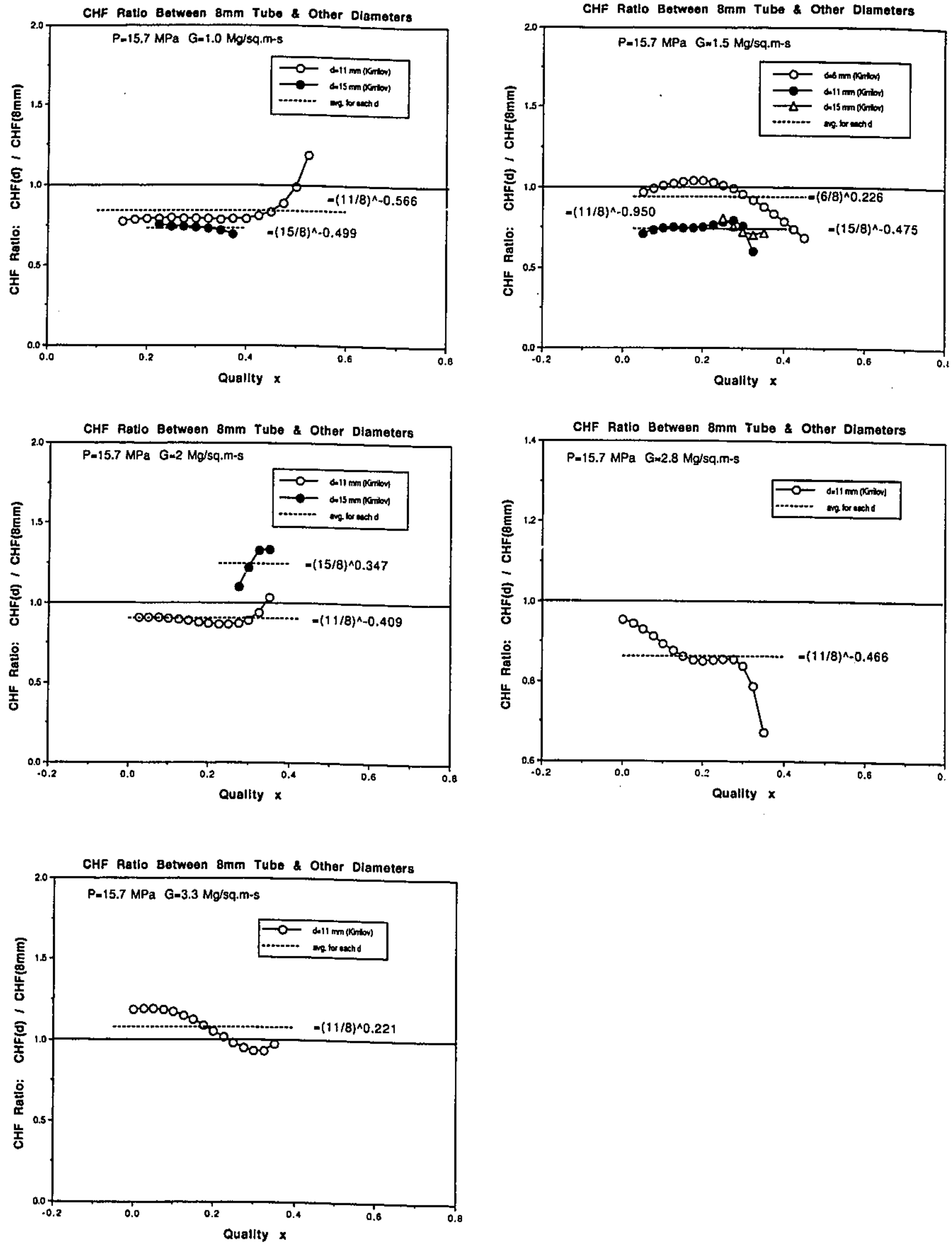

Figure 4.18: Ratios of CHF vs. Quality Between 8 mm Tube to Other Diameters (Pressure: 15.7 MPa)

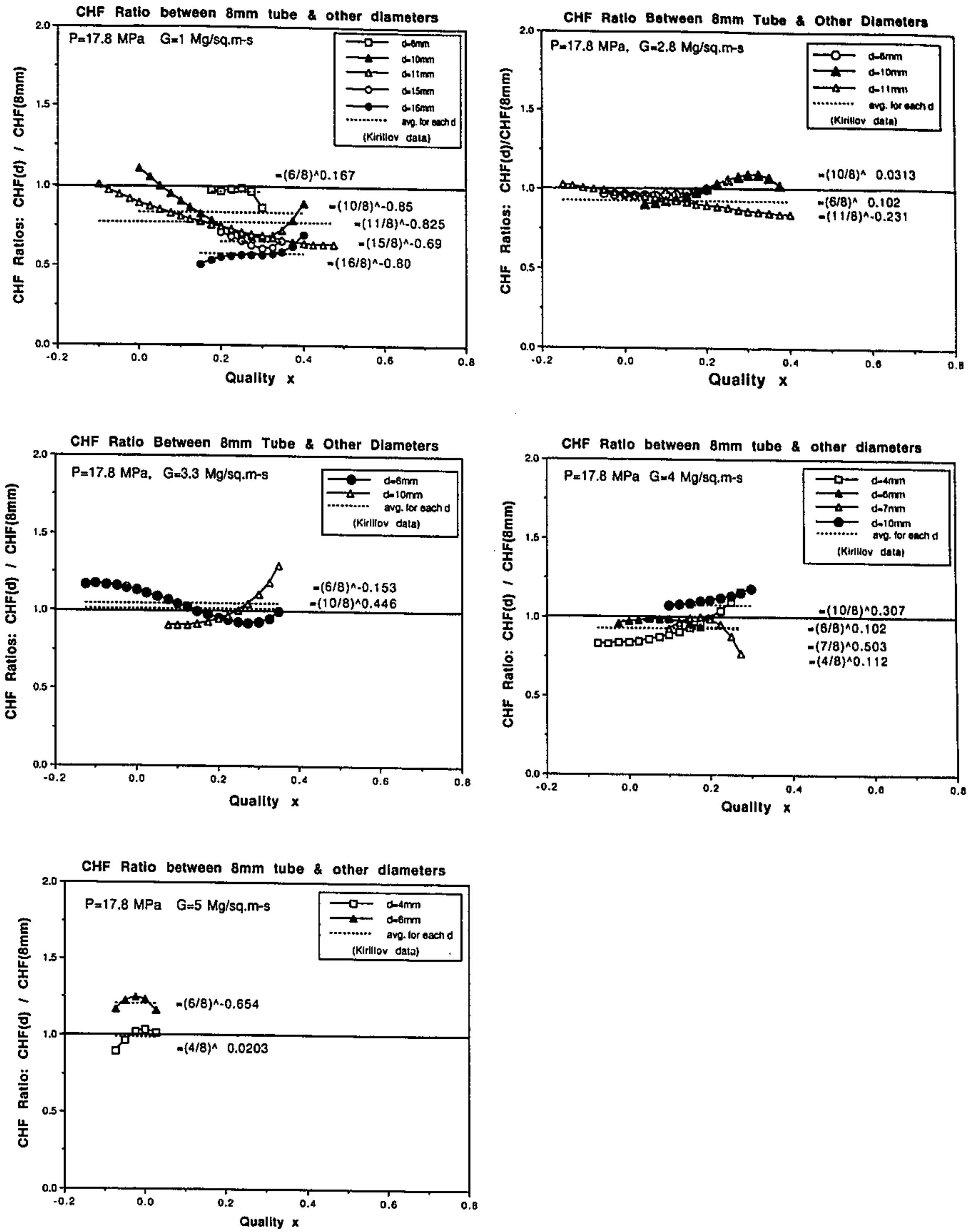

Figure 4.19: Ratios of CHF vs. Quality Between 8 mm Tube to Other Diameters (Pressure: 17.8 MPa)

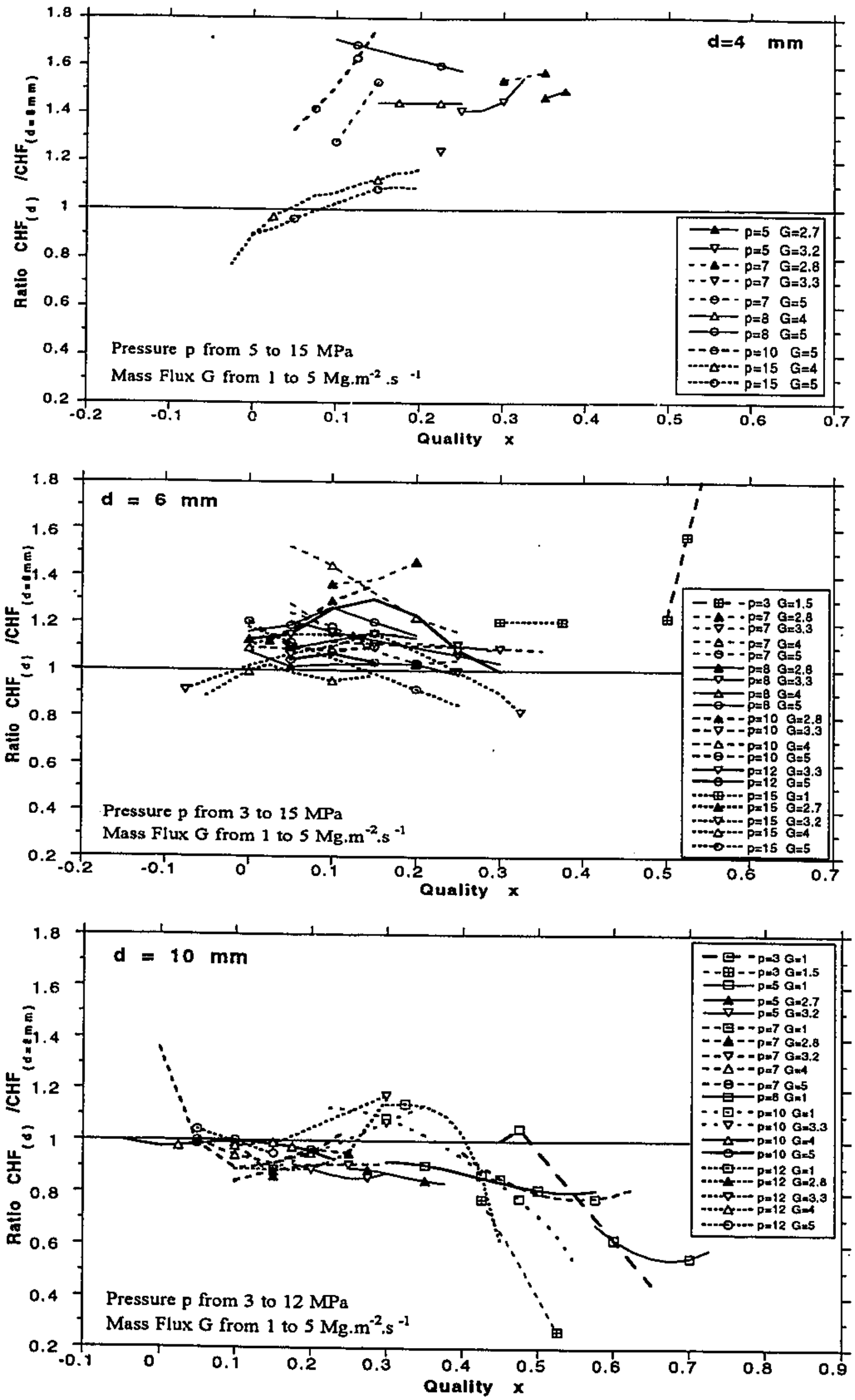

Figure 4.20: CHF Ratios Between AECL Data Bank's Data of 8-mm Diameter to Data of 4-mm, 6-mm, and 10-mm Diameters at Various Pressures and Mass Fluxes

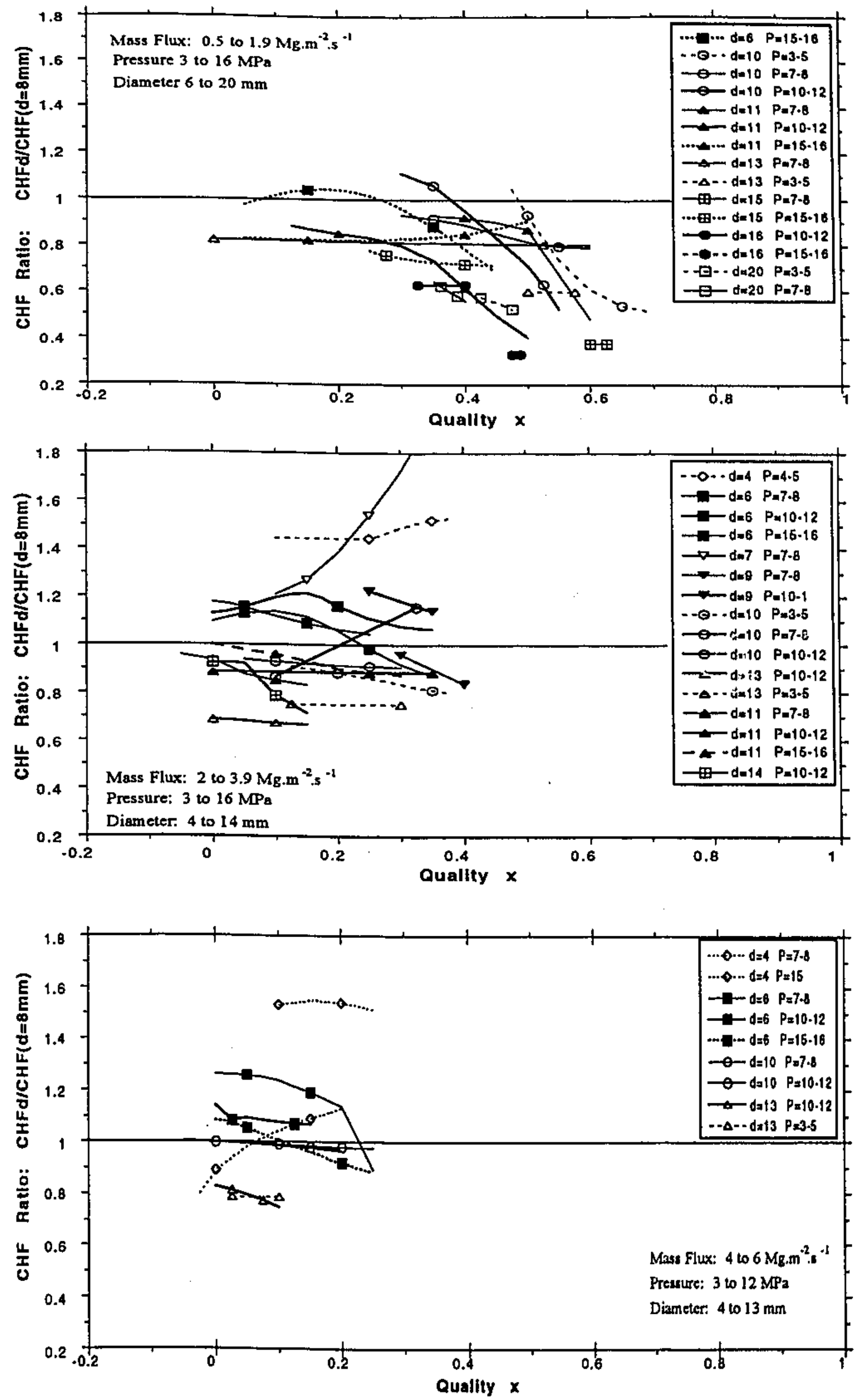

Figure 4.21: CHF Ratios Between AECL Data Bank's Data of 8-mm Diameter to Data of Other Diameters For Mass Flux: (a) 0 to 1.9 (b) 2 to 3.9 (c) 4 to 6 Mg.m^{-2}.s^{-1}

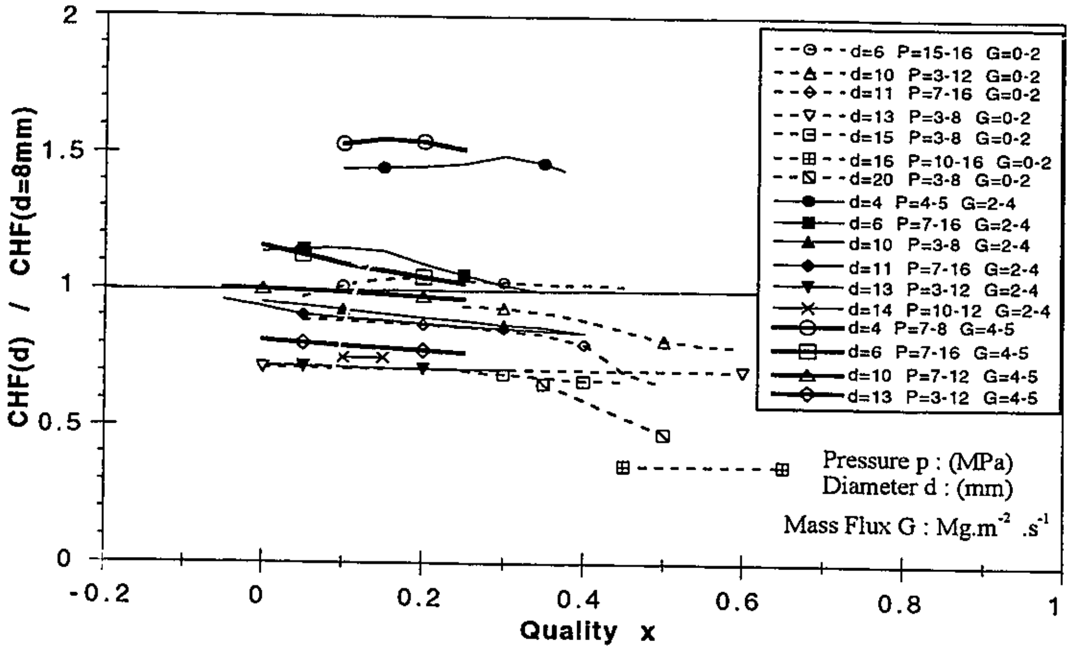

Figure 4.22: CHF Ratios for Average Pressures Between 8-mm Diameter Tube and Other Diameters for Ranges of Mass Fluxes

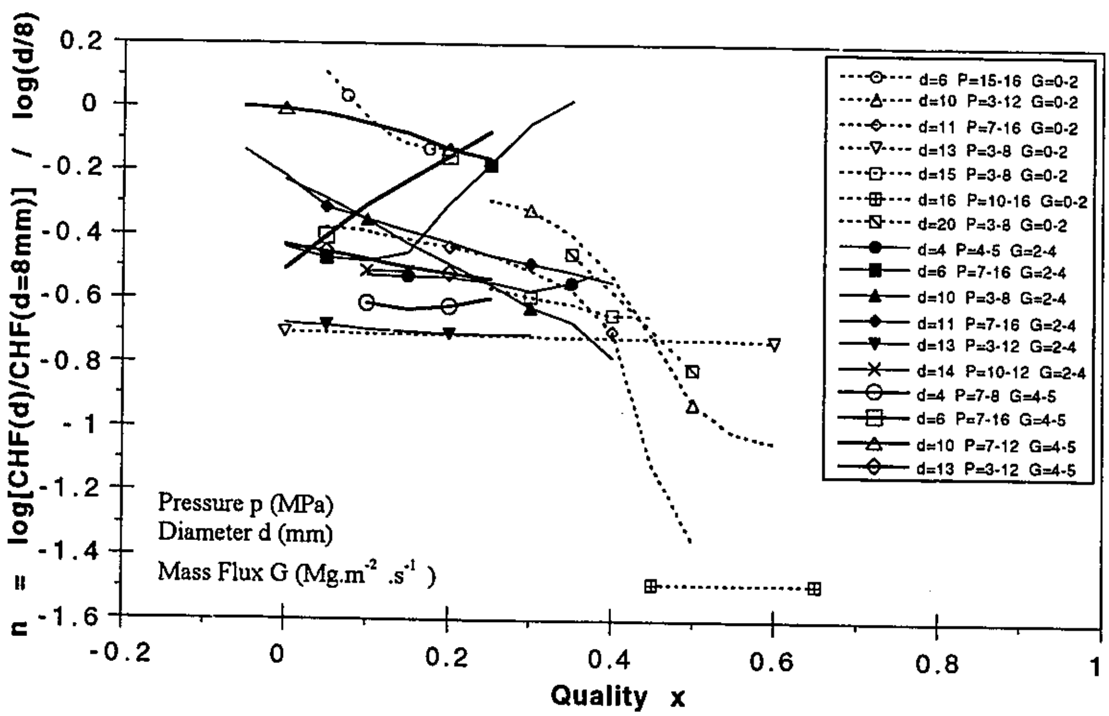

Figure 4.23: n (from $CHF_{(d)} = CHF_{(d=8mm)} (d/8)^n$) Calculated from Figure 4.22 as Function of Quality

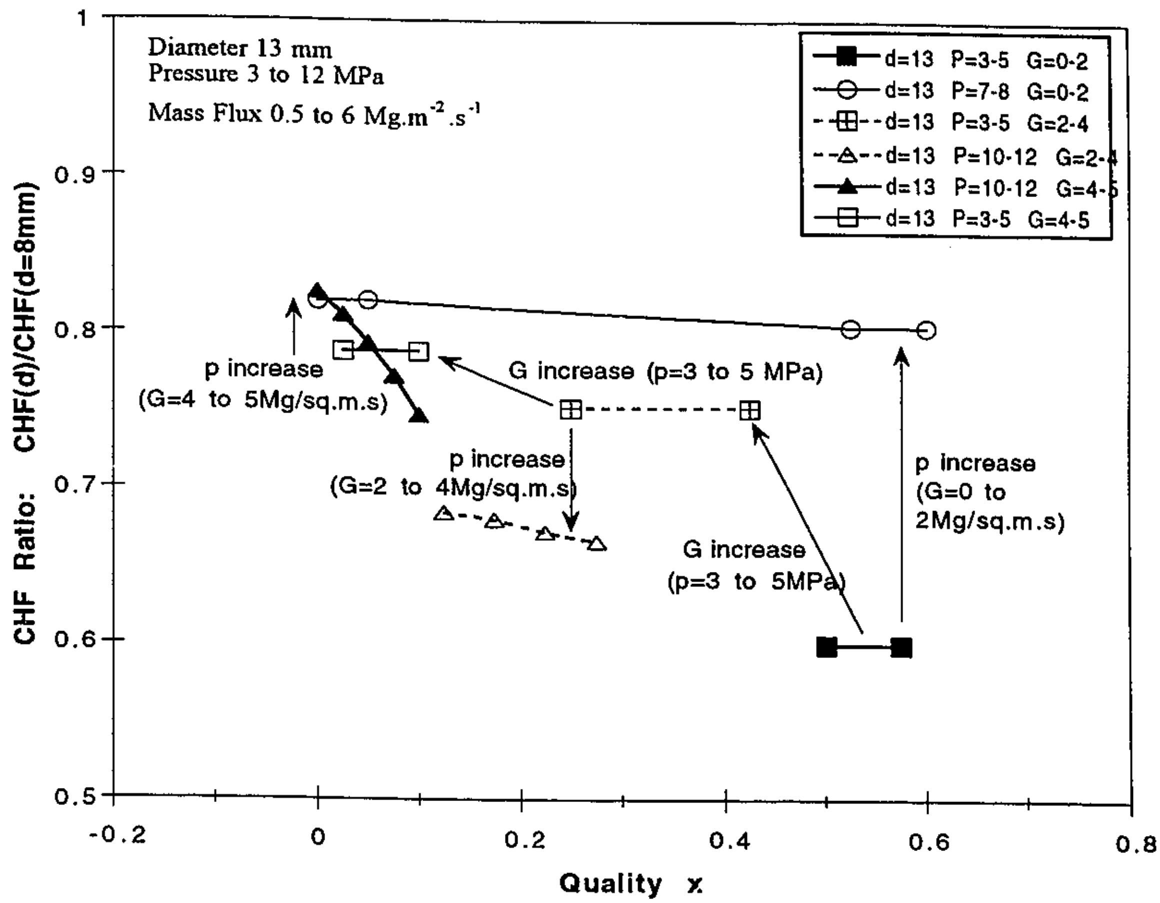

Figure 4.24: Evaluation of Effects of Pressure and Mass Flux to CHF Ratios Between Data of 13-mm and 8-mm Diameter Tubes

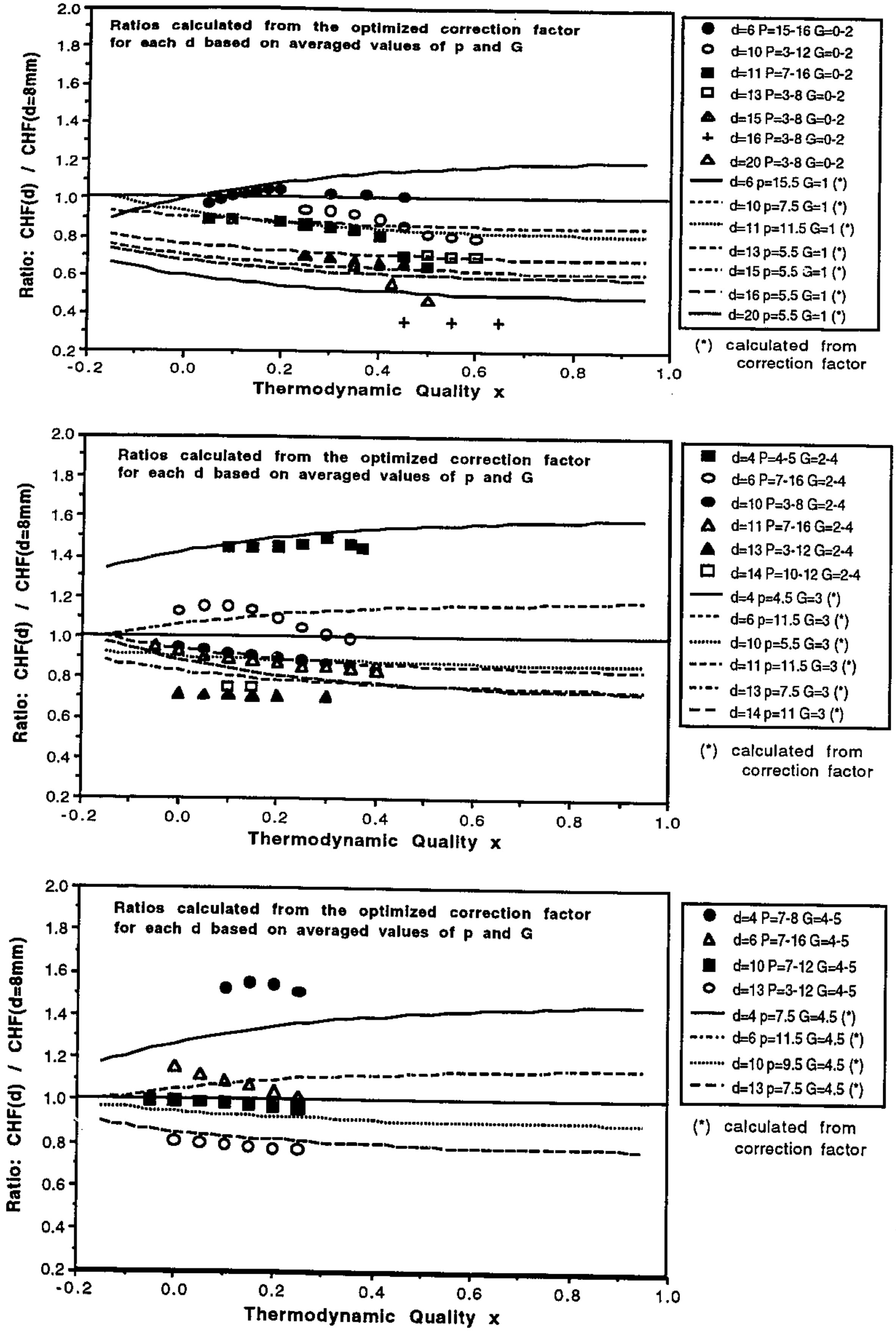

Figure 4.25 : Correlated Ratio $(d/8)^n = CHF_{(d)}/CHF_{(d=8mm)}$ as Functions of Quality Based on Average Pressure and Mass Fluxes of 1, 3, andd 4.5 $Mg.m^{-2}.s^{-1}$

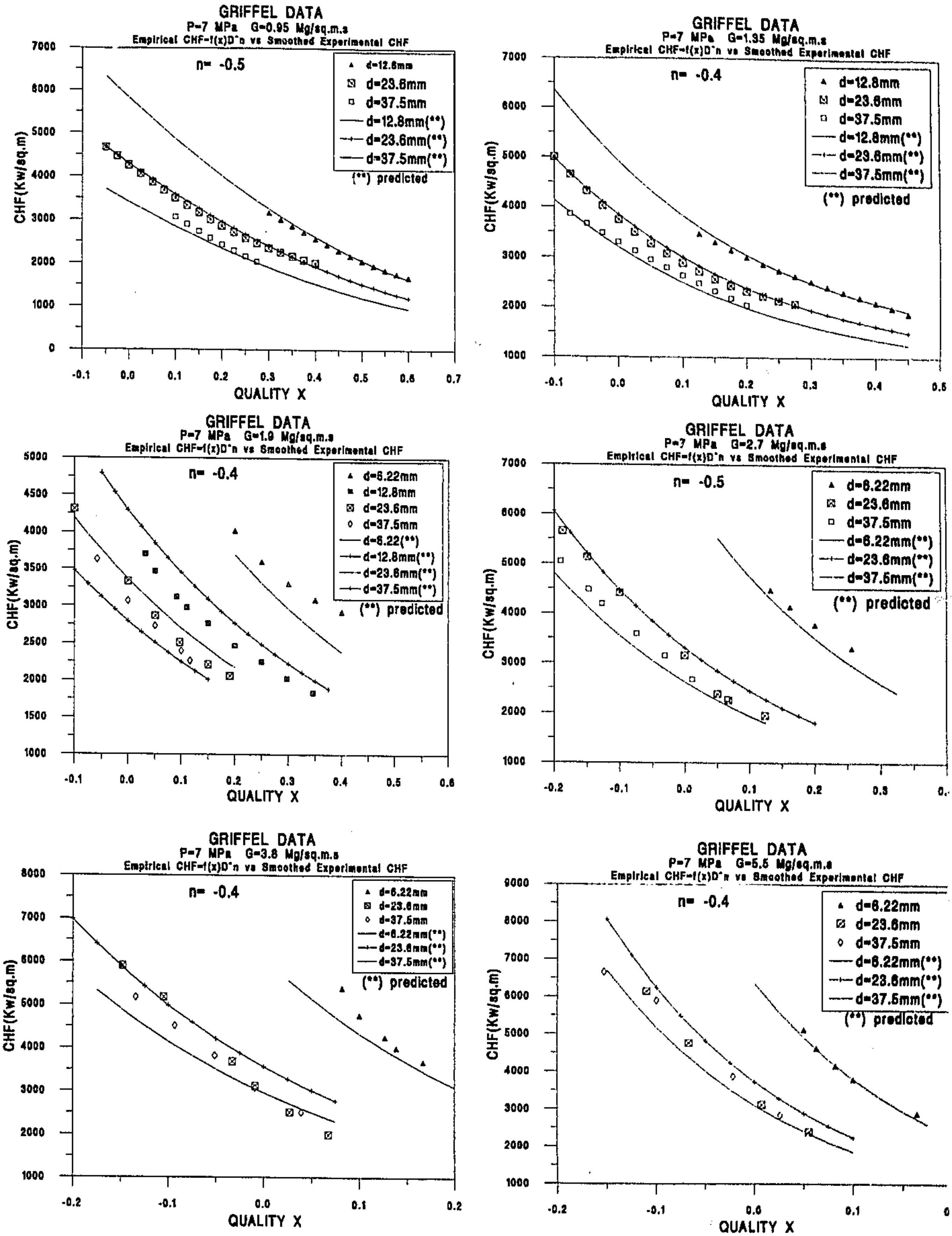

Figure 4.26: Experimental Data (Griffel) vs. Fitted Function $q_c = f(x)\, d^n$ (Pressure = 7 MPa)

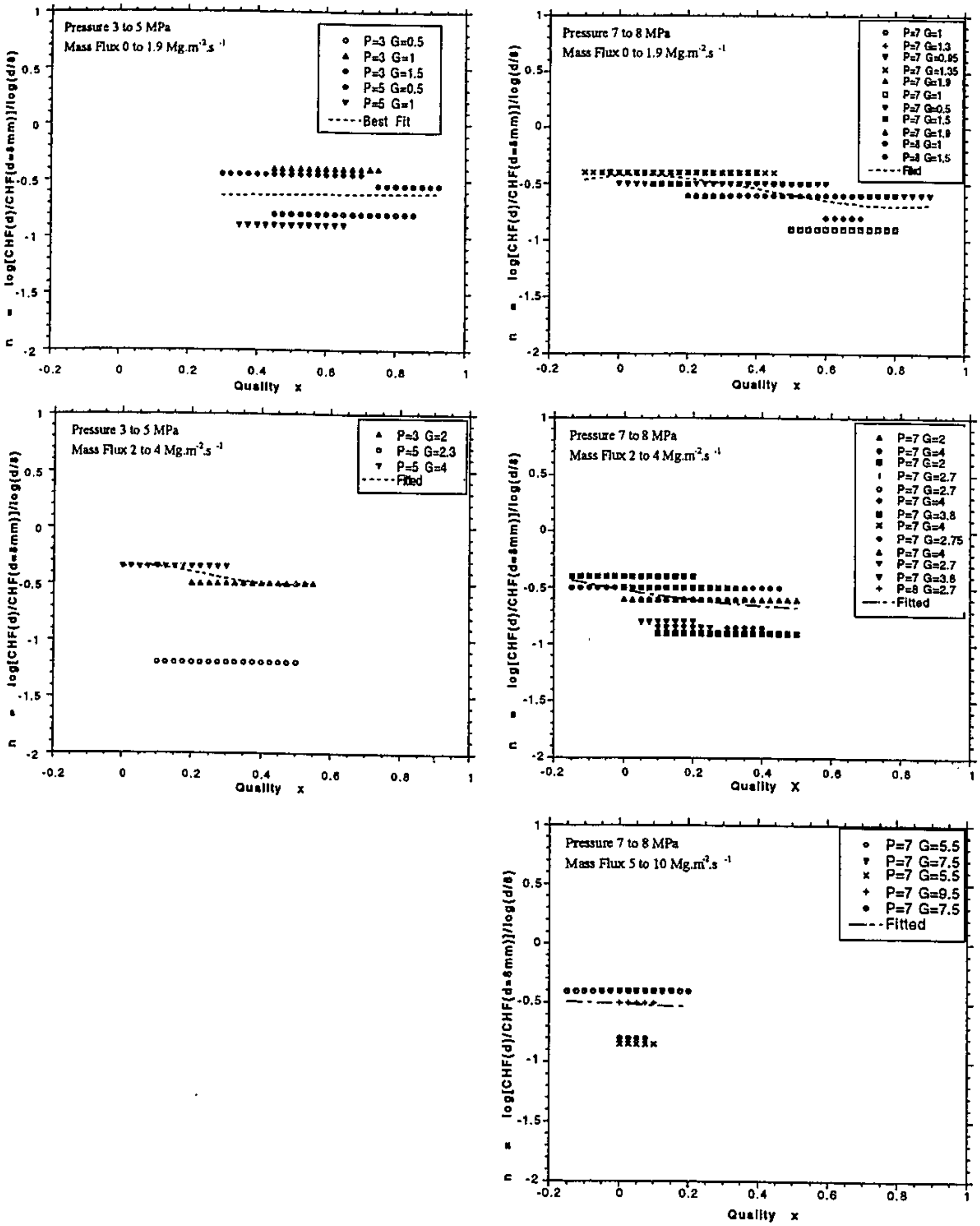

Figure 4.27: Constant Valued n (for $CHF=f(x)d^n$) from Comparing Data from Same Sources
(a) Pressure=3 to 5 MPa, Mass Flux=0.5 to 4 $Mg.m^{-2}.s^{-1}$
(b) Pressure=7 to 8 MPa, Mass Flux=0.5 to 10 $Mg.m^{-2}.s^{-1}$

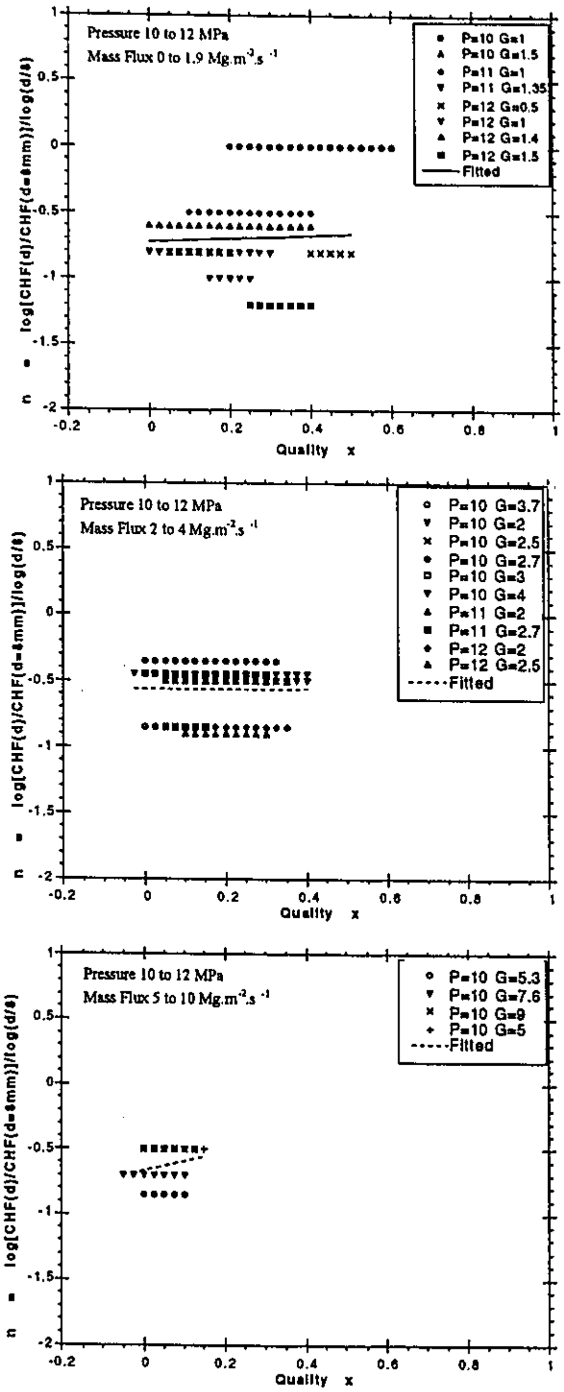

Figure 4.27: Constant Valued n (for CHF=f(x)d^n) from Comparing Data from Same Sources
(c) Pressure=10 to 12 MPa, Mass Flux=0.5 to 10 $Mg.m^{-2}.s^{-1}$

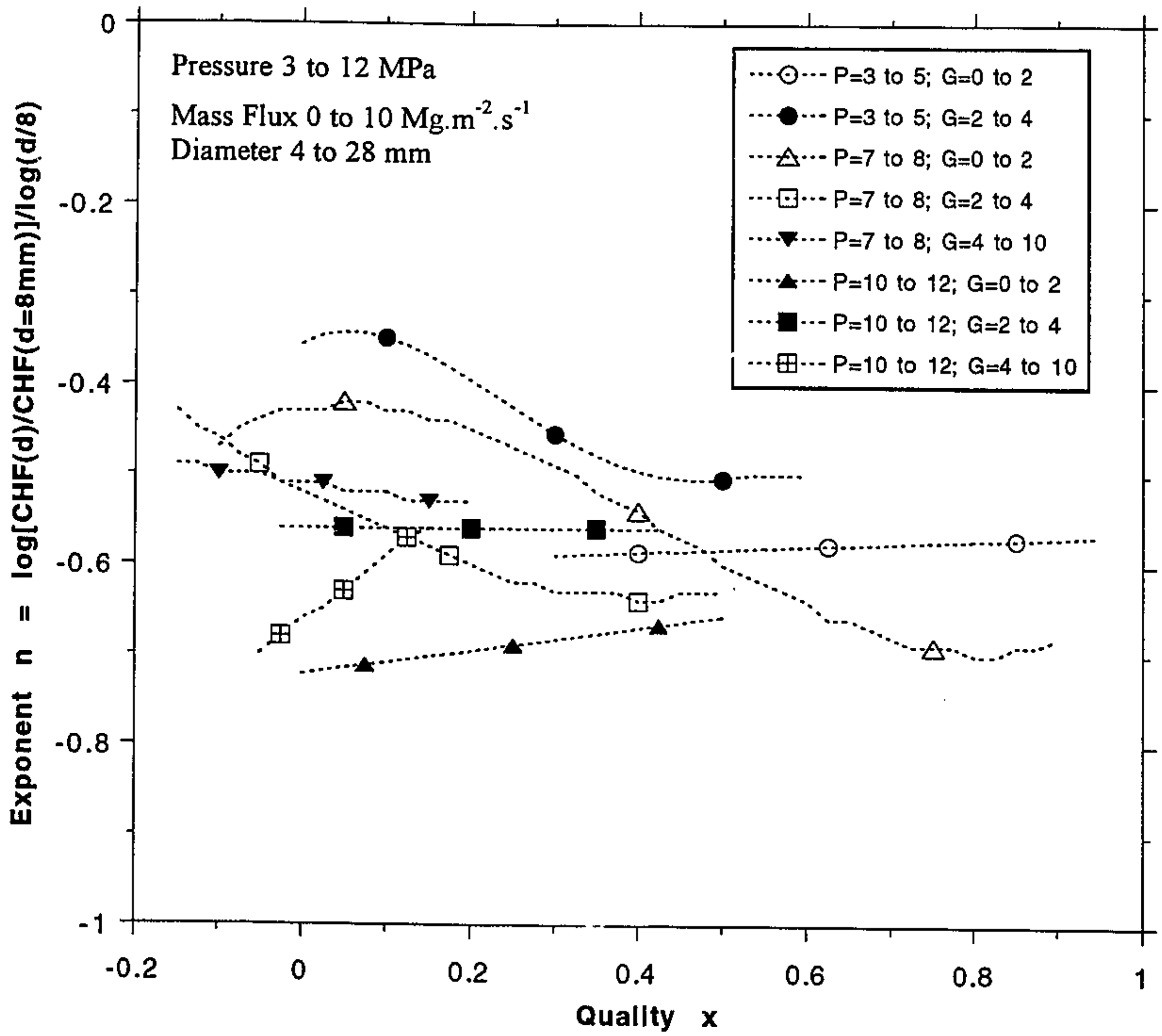

Figure 4.28: Values of Exponent n (for $CHF=f(x)d^n$) from Comparing Data from Same Sources

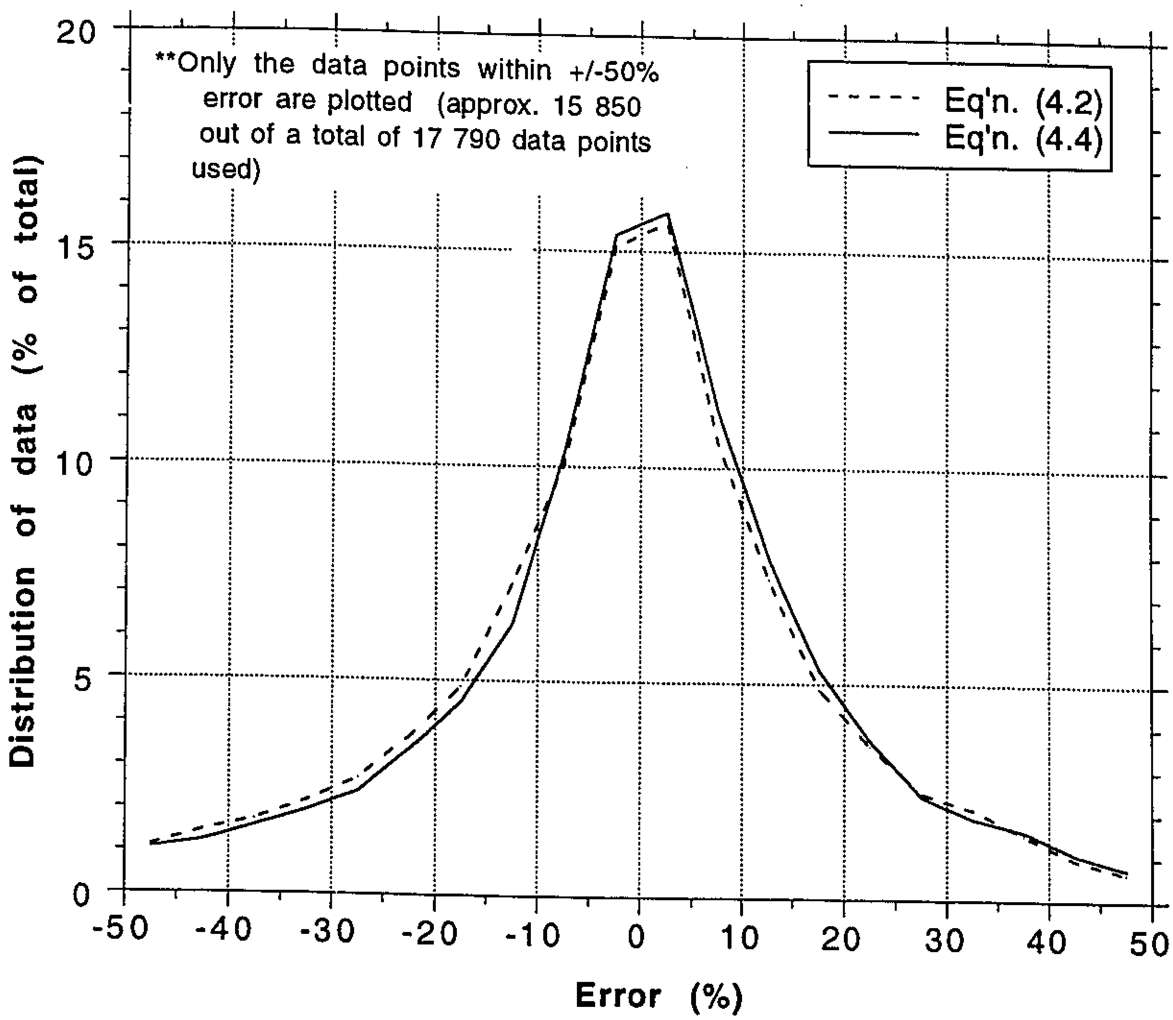

Figure 4.29: Error-distributions of Predicted CHF from Equations (4.2) and (4.4) Based on Experimental Data from AECL Data Bank

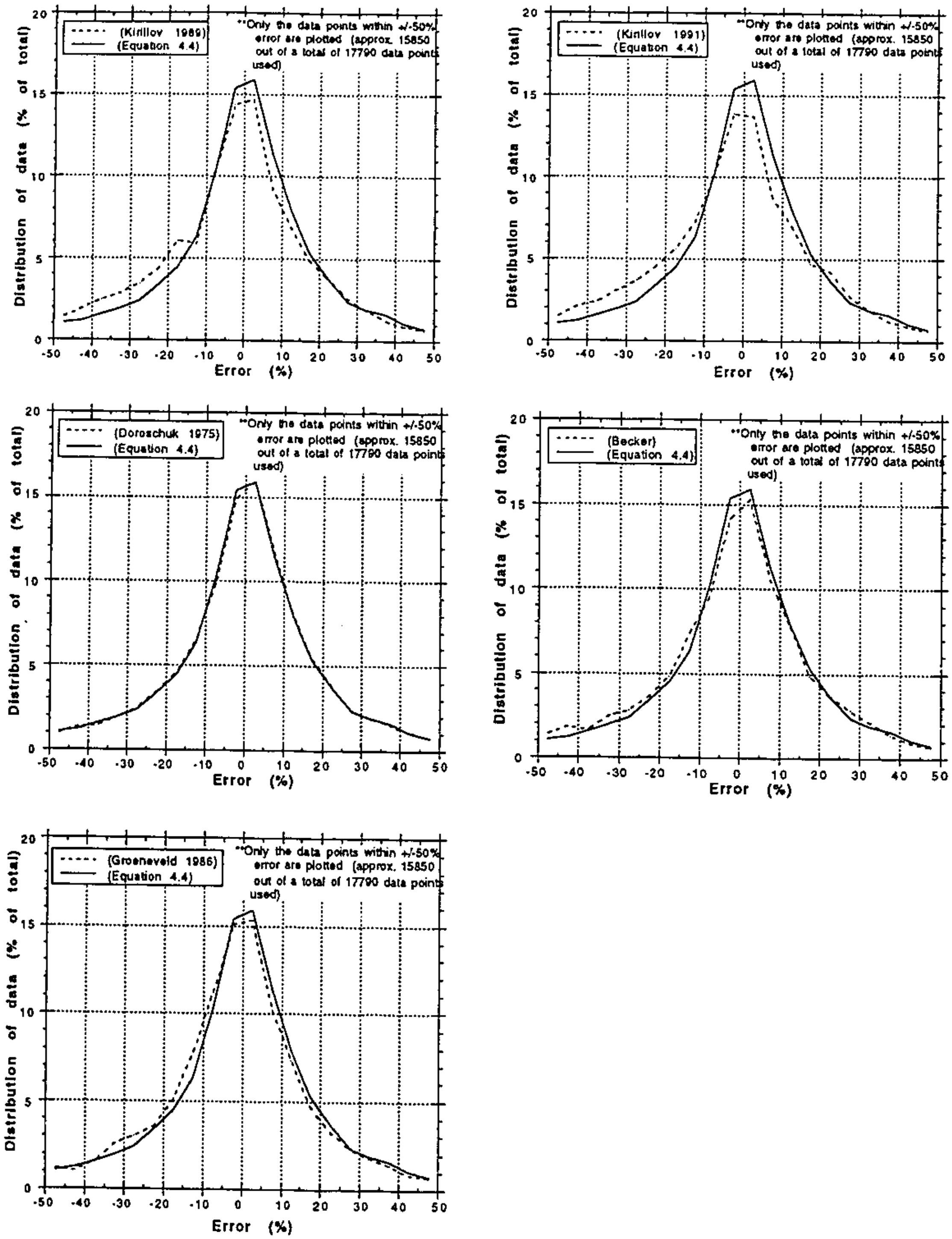

Figure 4.30: Comparisons of Error-distributions (vs. Data from AECL Data Bank) Between Equation (4.4) and Other Correlations

5. ASSESSMENT OF MODELS ON DIAMETER EFFECTS

Appropriate accounting for the tube-diameter effect on CHF is crucial for the success of a physical model or correlation. It is unlikely that a single model is capable of modelling the CHF mechanisms in different flow regimes. Two semi-analytical models are examined to enhance the understanding of the physical mechanisms pertinent to the diameter effect on CHF. These models cover two different regimes: bubbly flow at subcooled and low-quality conditions, and annular-film flow at high qualities. They are the homogenous flow model based on the Reynolds analogy for subcooled and low-quality flow and the annular-film dryout model for high-quality flow.

5.1 REYNOLDS ANALOGY FOR SUBCOOLED AND LOW-QUALITY FLOW

5.1.1 Introduction

The Reynolds analogy relates the similarity of heat transfer in pipe flow to friction at the wall. Based on this theory, Tong (1968) and Thorgenson et al. (1974) related the heat transfer and CHF for subcooled flow in tubes to a critical friction factor or Reynolds number. Their semi-analytical models express CHF in terms of a Reynolds number, which is a function of the tube diameter. Therefore, they provide the basis to account for the tube-diameter effect on CHF.

5.1.2 Concept Background

In subcooled flow, nucleate boiling occurs when a thin layer of liquid next to the heated wall is superheated sufficiently for bubble formation. These bubbles grow and approach the subcooled liquid from the main stream and subsequently collapse while transferring their latent heat to the colder fluid. The growth and collapse process is repeated. Although there is no net flow of vapour from the heat-transfer surface, there is a certain volume of vapour in the proximity of the surface at any time. Heat transfer is caused by the phase change of the liquid next to the tube wall: vaporization occurs at the base of the vapour bubbles while condensation takes place at their top.

Jordan and Lepppert (1962) applied the Reynolds analogy to subcooled nucleate-boiling heat transfer. The vapour bubbles at the wall are considered to be the wall roughness which affects the thermal boundary layer of the liquid core. The flow structure is illustrated schematically in Figure 5.1. Assuming that the heat-transfer mechanism from the top of the bubbles to the bulk subcooled flow is entirely turbulent convection, the heat transfer can be related to a friction factor based on the Reynolds analogy. The Stanton number is written as

$$St = \frac{Nu}{Re\,Pr} = \frac{h}{\rho C_p U} = \frac{f}{2} \tag{5.1}$$

where Nu is the Nusselt number, Re is the Reynolds number, Pr is the Prandtl number and f is the friction factor. The heat-transfer coefficient is then written as

$$h = \frac{f}{2} \rho\, C_p\, U \tag{5.2}$$

and the surface heat flux becomes

$$q = h\,\Delta T = \frac{f}{2} \rho\, C_p\, U\, \Delta T \tag{5.3}$$

This equation is applicable for flow conditions of the Prandtl number close to 1 (Pr ~ 1, at water temperatures between 170°C to 210°C). The Colburn analogy (or modified Reynolds analogy) is to be applied for other Prandtl numbers (i.e., Pr ≠ 1), and the heat flux is expressed as

$$q = h\,\Delta T = \frac{f}{2}\rho\, C_p\, U\,\Delta T Pr^{-2/3} \qquad (5.4)$$

5.1.3 Reynolds Analogy for CHF in Subcooled Tube Flow

In subcooled boiling, the liquid next to the tube wall is being vaporized into bubbles, which in turn are being condensed at their top next to the subcooled flow core. At the onset of CHF, vigorous nucleate boiling is present and heat transferred from the wall relies more by vaporization than by forced convection. CHF is expected to occur when the heat-transfer rate is limited either by the vaporization at the tube wall or by the turbulent transport from the bubbles. In the first case, liquid is prevented from reaching the wall for the vaporization process to continue, and in the second case vapour is restricted from leaving the wall at the critical condition. Vaporization controls the heat-transfer process at the low subcooling or saturated boiling conditions, while turbulent transport dominates at the high subcooled region. Based on Equation (5.3), the critical heat flux is expressed as

$$q_c = \frac{f_c}{2}\rho\, C_p\, U\,\Delta T_w \qquad (5.5)$$

where ΔT_w is the temperature difference between the heated surface and bulk stream, and the critical friction factor:

$$f_c = \Delta P \frac{d}{2L\,\rho_l\, U^2} \qquad (5.6)$$

where ΔP is the pressure drop at CHF and ρ_l is the density of the bulk liquid stream. A similar equation for CHF can be written with Equation (5.4) based on the Colburn analogy.

Thorgerson et al. (1974) obtained pressure-drop and CHF data with an annular channel at low pressure (0.3 MPa or 40 psig). Figure 5.2 shows the pressure-drop measurements against the coolant subcooling. The critical friction factor calculated from the pressure drop was presented as

$$f_c(annulus) = 0.694\,Re^{-0.386} \tag{5.7}$$

Figure 5.3 shows the relation between the friction factor and the Reynolds number from the experiment. The same figure shows the friction factors corresponding to various relative-roughness (ε/d) values in commercial pipes. They were used to evaluate the equivalent roughness or the size of the bubbles for the vapour blanket. The data showed that the equivalent roughness or bubble size decreases with increasing flow velocity. Chang et al. (1961) expressed the radius of the detaching bubbles as

$$r_b = \frac{k\sigma_l}{\rho_l U^2} \tag{5.8}$$

Equation (5.7) was extended by Thorgerson to CHF in round tubes by the relation:

$$f_c(annulus) = \left(\frac{d_i}{d_o + d_i}\right) f_c(tube) + \left(\frac{d_i}{d_o + d_i}\right) f \tag{5.9}$$

where f is the non-boiling friction factor from the Moody Chart. The friction factor for a round tube at CHF is calculated from Equation (5.9):

$$f_c = 7.413\,Re^{-0.545} \tag{5.10}$$

This friction factor correlation represents the boiling effects for a round tube, and is shown in Figure 5.4.

CHF is predicted using Equations (5.7) for annulus and Equation (5.10) for tube. The tube wall temperature is calculated using the Weatherhead (1963) correlation, which is expressed as

$$T_w - T_{sat} = (47.7 - 0.127T_{sat})\ (q \cdot 10^{-0.6})^{0.25} \tag{5.11}$$

This analogy shows that the boiling contribution and the rate of vaporization are important only in influencing turbulence at the wall, and that the heat transferred can be related to a corresponding friction factor. Thorgerson applied this analogy and the friction factors, Equations (5.7) and (5.10), to compare against his experimental CHF data for annular channels and round tubes, and his predictions were within 10% of accuracy.

The Thorgerson data were obtained at low-pressure conditions only and may not be applicable for high pressures, because the calculations for both the surface temperature and frictional pressure drop are also affected by pressure. Since the CHF is predicted to be proportional to the Reynolds number (i.e., CHF $\propto Re^{-0.545}$), the effect of tube diameter on the CHF is similar (i.e., CHF $\propto d^{-0.545}$) for constant dryout conditions. This agrees closely with the trend exhibited among data in the AECL data bank for both low- and high-pressure conditions (see Chapter 4), where the exponent n varies from -0.3 to -0.8 (or an average of -0.55).

Tong (1968) postulated the occurrence of CHF at subcooled conditions due to flow stagnation under the boundary layer (separating the vapour from the heated wall). The stagnant liquid vaporizes to form a vapour blanket next to the wall. Kutateladze and Leont'ev (1966) suggested that an injection stream normal to the main flow arises from vapour generation at the wall in nucleate boiling. At critical conditions, the injection stream causes a local stagnation to the boiling two-phase boundary layer, resulting in dryout at the stagnation point. The criterion for flow stagnation with wall injection of a fluid into the stream of the source fluid is expressed as

$$G_{inj} = 2 f_{nb}\, G_{stream} \tag{5.12}$$

or

$$\rho_j U_j = 2 f_{nb} \rho_o U_o \tag{5.13}$$

where subscript j and o denote injection and the stream, and f_{nb} is the friction with no injection or boiling. By equating the momentum of the critical injection to the momentum of the vapour generated by boiling, Tong expressed the criteria as

$$\frac{1}{\rho}\left(\frac{q_c}{H_{fg}}\right)^2 = \rho_j U_j^2 = \rho_l U_o^2 (2f)^2 \left(\frac{\rho_l}{\rho_j}\right) \tag{5.14}$$

or

$$q_c = 2 f H_{fg} \rho_l U_o \tag{5.15}$$

The velocity distribution and the friction factor in a tube experiencing subcooled CHF were assumed to be similar to that of a tube with a rough surface. The velocity profile for turbulent flow in a rough tube has been shown to be in-between those for turbulent and laminar flow in a smooth tube. The friction factor for a fully developed turbulent flow is expressed as

$$f_T \propto Re^{-0.2} \tag{5.16}$$

while for a fully developed laminar flow it is

$$f_L \propto Re^{-1.0} \tag{5.17}$$

Tong assumed a mean friction factor of these values for the boiling flow, which is expressed as

$$f_{2\text{-}phase} \propto Re^{-0.6} \tag{5.18}$$

where

$$Re = \frac{\rho_l U_o d}{\mu_{sat}} \tag{5.19}$$

After substitution, Equation (5.15) becomes:

$$q_c = C H_{fg} \rho_l U_o Re^{-0.6} \tag{5.20}$$

where C is an empirical factor expressed in terms of bulk quality or subcooling. Based on the same derivation presented above, the tube diameter effect on CHF is shown to be $d^{-0.6}$ rather than $d^{-0.545}$.

5.1.4 Discussion of the Subcooled Flow Model

The subcooled-flow models examined in this section express CHF as a function of the friction factor at the vapour-liquid interface. Since friction factor is proportional to the Reynolds number, this implies that CHF at constant dryout conditions is related to the tube diameter through

$$q_c \propto d^n \tag{5.21}$$

The exponent, n, is slightly different, depending on the models (either -0.545 or -0.6). This basically agrees with the general trend exhibited among data of the AECL data bank (Chapter 4). While these models showed a simple tube-diameter effect on CHF, a more complex relation was exhibited upon the examination of the AECL data bank. The observation, however, is primarily valid for high-quality conditions, because the available data for subcooled and low-quality conditions are limited. A high-quality model is described in the next section.

5.2 ANNULAR FLOW MODEL FOR HIGH QUALITY

CHF at high-quality flow in general corresponds to the annular-film dryout phenomenon. Many models have been developed for annular-film dryout; they were mostly based on the basic model of Whalley et al. (1978). Modifications were introduced to various closure relationships which are needed to complete the prediction scheme. They are anticipated to be continuously updated when more experimental data become available and better analytical approaches are derived. The effect of tube-diameter on CHF for the latest model is examined in detail in this section.

5.2.1 Background

Annular flow is characterized by a thin liquid film flowing along the tube wall while a continuous vapour flows with a significant amount of liquid entrainment in the core of the tube. CHF generally occurs at sufficiently high qualities where the liquid film dries out. Thinning of the liquid film is caused by liquid evaporation and also liquid entrainment into the vapour core. Part of the lost liquid is replenished by the droplet deposition process from the flow core.

For most analyses, the flows of both the liquid film and vapour are turbulent, and hence most annular-film dryout models are semi-analytically based. In addition, a number of closure relationships (such as entrainment rate, deposition rate, etc.) for these models are mostly empirical.

5.2.2 Governing Equations

Figure 5.5 shows a control volume of the annular flow regime. To simplify the derivation of the equations, the following assumptions are made:

- constant fluid properties (i.e., no flashing),
- no vapour present in the liquid film, and
- flow of liquid droplets and vapour in the tube core is homogeneous.

Mass Continuity:

$$\frac{\delta((1-\alpha)\rho_l)}{\delta t} + \frac{\delta G_{lf}}{\delta z} = \frac{4}{d}\left(D - E - \frac{q}{H_{fg}} \right) \tag{5.23}$$

$$\frac{\delta(\alpha(1-\alpha')\rho_l)}{\delta t} + \frac{\delta G_{lf}}{\delta z} = \frac{4}{d}(E - D) \tag{5.24}$$

$$\frac{\delta(\alpha\alpha'\rho_v)}{\delta t} + \frac{\delta G_v}{\delta z} = \frac{4}{d}\left(\frac{q}{H_{fg}} \right) \tag{5.25}$$

Overall heat balance:

$$\frac{\delta}{\delta z}(H_l G_{lf} + H_l G_{le}) + \frac{\delta}{\delta t}((1-\alpha)\rho_l u_l + \alpha(1-\alpha')\rho_l u_l + \alpha\alpha'\rho_v u_v) = \frac{4q}{d} \tag{5.26}$$

where G is the mass flux based on the flow area of tube, D is the deposition rate, E is the entrainment rate, d is the tube diameter, f is the friction factor, H is the enthalpy, q is the heat flux, u is the velocity, x is the quality, z is the tube length, α is the fraction of tube cross-section occupied by the vapour and droplets, α' is the fraction of the vapour/droplet core occupied by the vapour, δ is the liquid film thickness, δz is the incremental tube length, μ is the viscosity, and τ is the shear stress.

The subscripts *le, lf, lfc, fg, i, l, v,* and *vc* refer to liquid entrainment, liquid film, critical liquid film for entrainment, the difference between saturated vapour and saturated liquid, liquid-vapour interface, liquid, vapour, and vapour core, respectively.

For the approximation of α, and denoting δ as the thickness of the liquid film,

$$\alpha \approx 1 - \frac{4\delta}{d} + \frac{4\delta^2}{d} \qquad (5.27)$$

By assuming $\delta/d << 1$, then $\alpha \approx 1$, and

$$1 - \alpha \approx \frac{4\delta}{d} \qquad (5.28)$$

Use C as the concentration of liquid droplets in the vapour/droplet core,

$$C = (1 - \alpha')\,\rho_l \qquad (5.29)$$

Since C/ρ_l is usually so small that α' is close to 1, then $\alpha\alpha'$ for the above equations can be assumed to be unity. At steady state, Equation (5.26) becomes:

$$\frac{\delta}{\delta z}(H_l G_{lf} + H_l G_{le} + H_v G_v) = \frac{4q}{d} \qquad (5.30)$$

By substituting Equations (5.32) to (5.34), the energy Equation (5.30) can be written as:

$$0 = -\frac{d}{4H_{fg}}\left(G_l\left(\frac{dH_l}{dp}\right) + G_v\left(\frac{dH_v}{dp}\right)\right)\frac{dp}{dz} \qquad (5.31)$$

At steady state, Equations (5.23) to (5.25) become:

$$\frac{\delta G_{lf}}{\delta z} = \frac{4}{d}\left(D - E - \frac{q}{H_{fg}}\right) \qquad (5.32)$$

$$\frac{\delta G_{le}}{\delta z} = \frac{4}{d}(E - D) \tag{5.33}$$

$$\frac{\delta G_v}{\delta z} = \frac{4}{d}\left(\frac{q}{H_{fg}}\right) \tag{5.34}$$

A triangular relationship is derived to solve simultaneously for the liquid film thickness (δ), liquid/vapour interfacial shear (τ_i), and liquid film mass-flow rate (G_{lf}). The triangular relationship is described in the following equations.

From Turner and Wallis (1965):

$$1 - \alpha = \sqrt{\frac{(dp/dz)_{lf}}{dp/dz}} \approx \frac{4\delta}{d} \tag{5.35}$$

$$\delta \approx \frac{d}{4}\left(\sqrt{\frac{(dp/dz)_{lf}}{dp/dz}}\right) \tag{5.36}$$

where dp/dz is the two-phase pressure gradient:

$$\frac{dp}{dz} = \frac{2\tau_i}{d/2 - \delta} \tag{5.37}$$

and $(dp/dz)_{lf}$ is the frictional pressure drop, as if a liquid film flows alone in a tube:

$$\left(\frac{dp}{dz}\right)_{lf} = \frac{2 f_l G_{lf}^2}{\rho \alpha_v d} \tag{5.38}$$

The solution of the interfacial shear is found from the relationship between the interfacial friction factor correlated by Whalley and Hewitt (1978):

$$f_i = f_{vc} = f_v \left(1 + 24 \left(\frac{\rho_l}{\rho_v} \right)^{1/3} \left(\frac{\delta}{d} \right) \right) \tag{5.39}$$

and

$$\tau_i = \frac{1}{2} f_{vc} \rho_{vc} \frac{u_{vc}^2}{2} \tag{5.40}$$

Defining

$$Re_{lf} = \frac{G_{lf} d}{\mu_{lf}} \tag{5.41}$$

$$Re_{vc} = \frac{(G_v + G_{le} d)}{\mu_v} \tag{5.42}$$

For the laminar case (f_l is the liquid film friction factor depending on liqid film Reynold's number):

$$\rho_{vc} = \frac{G_{le} + G_v}{G_{le}/\rho_{le} + G_v/\rho_v} \tag{5.43}$$

and

$$f_l = \frac{16}{Re_{lf}} \tag{5.44}$$

For the turbulent case, the Blasius correlation (White (1991)):

$$f_l = 0.079\,Re_{lf}^{-0.25} \tag{5.45}$$

and

$$f_v = 0.079\,Re_{vc}^{-0.25} \tag{5.46}$$

The correlations for entrainment and deposition used by the Whalley et al. (1978) annular flow model can be replaced by the most recent E/D model of Hewitt and Govan (1990) as in the following:

$$D = kC \tag{5.47}$$

$$E = kC_E \tag{5.48}$$

Since the vapour and droplet core is assumed to be homogeneous, the velocity, u_{le}, of the droplets in the vapour core is assumed to have the same velocity, u_{vc}, as the vapour.

$$u_{vc} = \frac{G_{le}}{\rho_l} + \frac{G_v}{\rho_v} \tag{5.49}$$

The concentration factor for deposition is:

$$C = \frac{G_{le}}{u_{vc}} = \frac{G_{le}}{G_{le}/\rho_l + G_v/\rho_v} = \rho_l(1-\alpha_{vc}) \tag{5.50}$$

The deposition rate coefficient is:

$$\begin{aligned} k &= 0.1815\sqrt{\frac{\sigma}{\rho_v d}} & C/\rho_v \le 0.3 \\ k &= 0.083\sqrt{\frac{\sigma}{\rho_v d}}\left(\frac{C}{\rho_v}\right)^{-0.65} & C/\rho_v > 0.3 \end{aligned} \tag{5.51}$$

The entrainment rate (the subscript *lfc* denotes critical liquid film for onset of entrainment) is:

$$E = G_v\left(5.75\cdot10^{-5}\left((G_{lf}-G_{lfc})^2\frac{d\rho_l}{\sigma\rho_v^2}\right)^{0.316}\right) \tag{5.52}$$

for $G_{lf} > G_{lfc}$, and

$$E = 0 \tag{5.53}$$

for $G_{lf} \le G_{lfc}$, where

$$G_{lfc} = \left(\frac{\mu_l}{d}\right)Re_{lfc} = \left(\frac{\mu_l}{d}\right)\exp\left(5.85+0.4249\left(\frac{\mu_v}{\mu_l}\right)\sqrt{\frac{\rho_l}{\rho_v}}\right) \tag{5.54}$$

To solve the annular flow model, the initial conditions for the liquid film, the vapour core, and the location at the onset of annular flow are required. The initial condition for the onset of annular flow is assumed to be at local quality of 1%, and the rate of liquid entrainment is assumed to be at 99% of the total liquid flow (Whalley et al. (1978)).

At the onset of annular flow:

$$x = 0.01$$
$$\frac{G_{le}}{G_l} = 0.99 = E_f \tag{5.55}$$

Mass fluxes are calculated as follows:

$$\begin{aligned} G_v &= G(x) \\ G_l &= G - G_v \\ G_{le} &= G_l(E_f) \\ G_{lf} &= G_l - G_{le} \end{aligned} \tag{5.56}$$

The balances of mass fluxes are iterated in steps, using:

$$\begin{aligned} G_v &= G_v + \frac{dG_v}{dz}dz \\ G_l &= G - G_v \\ G_{le} &= G_l - G_{lf} \\ G_{lf} &= G_{lf} + \frac{dG_{lf}}{dz}dz \end{aligned} \tag{5.57}$$

CHF occurs when the liquid-film flow is zero ($G_{lf} \leq 0$). The local dryout quality and the location along the tube can be calculated from:

$$x_c = \frac{4 q_c z}{H_{fg} G d} - x_{in} \tag{5.58}$$

where

$$x_{in} = \frac{\Delta H_{in}}{H_{fg}} \tag{5.59}$$

and

$$z = x_{in} H_{fg} d \frac{G}{4 q_c} \tag{5.60}$$

5.2.3 Prediction of the Annular Flow Model

The model described in Section 5.2.2 has been incorporated into a computer program by Chin (1984). The newer E/D correlation from Hewitt and Govan (1990) was added to the program by Vaitekunas et al. (1995).

The computer program (1995) was used for sample runs to calculate CHF for a pressure of 3 MPa and mass fluxes of 0.5 and 2 $Mg.m^{-2}.s^{-1}$; for a pressure of 7 MPa and mass fluxes of 1 and 9.5 $Mg.m^{-2}.s^{-1}$; and a pressure of 15 MPa and mass fluxes of 1.5 and 2.7 $Mg.m^{-2}.s^{-1}$. CHF is calculated for tube diameters from 4 mm to 37.5 mm; and the local dryout quality from 0 to 1. The results were plotted for CHF vs. quality and are shown in Figures 5.6 to 5.11. Experimental CHF data from the AECL data bank are also shown in these figures.

The figures also show the curves in the form of $q_c = f(x)d^n$ for various tube diameters to correlate with the program predictions. For each flow condition, the curves were generated by the best-fit of a polynomial function f(x) and by the exponent n for all the different diameters. Illustrated by the plots, the trend of the diameter effects on CHF are similar between the model prediction and the fitted CHF. Values of n for these correlations are between -0.5 to -0.6; i.e., -0.55 and -0.6 for the the two low-pressure (3 MPa) cases; -0.5 and -0.6 for the 7 MPa cases; and -0.5 for the two high-pressure (15 MPa) cases.

In the same figures, experimental data from the AECL data bank (smoothed by best-fit) were also shown. These CHF data were also correlated by another function $f1(x)d^n$ for the various diameters, to show quantitatively their relation to diameter. The best-fit values of n are between -0.5 to -0.8.

However, the experimental data are consistently higher than the corresponding CHF values predicted by the model. In other words, the annular flow model underpredicts CHF at most conditions.

5.2.4 Tube-Diameter Effect on CHF As Predicted with the Annular-Film Dryout Model

The effect of diameter on CHF as shown by both the experimental data and prediction by the annular-flow model is very similar, and especially can be closely correlated by the function $q_c = f(x)d^n$ (or $q_c \propto d^n$), where n is between -0.5 to -0.8.

The annular model was derived for the balances of mass flows and energy. The annular-flow regime is complex, because it involves several types of mass and heat transfer, such as the liquid film at the wall, the vapour core, the liquid entrainment, the droplet deposition, and the vaporization near the wall. The turbulent nature of these mass flows rules out the possibility of a completely theoretical derivation of the model. There are few alternatives but the use of empirical correlations for frictional shear at the vapour/liquid fim interface, entrainment, and droplet deposition. Due to these complexities, the relation of the diameter's effect on CHF is not explicit from the model's equations. The relation of the diameter to some of the governing equations is examined in this section.

Equation (5.30 to 5.34) involves the balance of the mass-transfer flow rates. Rearrangement of the equations results in:

$$\frac{q}{H_{fg}} = D - E - \frac{\partial G_{lf}}{\partial z}\left(\frac{d}{4}\right)$$

For entrainment, Equation (5.52), for a liquid film flow rate (G_{lf}) higher than a critical rate (G_{lfc}):

$$E = G_v\left(5.75 \cdot 10^{-5}\left((G_{lf} - G_{lfc})^2 \frac{d\rho_l}{\sigma \rho_v^2}\right)^{0.316}\right)$$

The critical liquid film flow rate (5.54) is given by:

$$G_{lfc} = \left(\frac{\mu_l}{d}\right) Re_{lfc} = \left(\frac{\mu_l}{d}\right)\exp\left(5.85 + 0.4249\left(\frac{\mu_v}{\mu_l}\right)\sqrt{\frac{\rho_l}{\rho_v}}\right)$$

The deposition rate, Equation (5.47), depends on Equations (5.48), (5.49), and (5.50) as follows:

The concentration factor for deposition is

$$C = \frac{G_{le}}{u_{vc}} = \frac{G_{le}}{G_{le}/\rho_l + G_v/\rho_v} = \rho_l(1 - \alpha_{vc})$$

The deposition rate coefficient, Equations (5.50) and (5.51), is

$$k = 0.1815\sqrt{\frac{\sigma}{\rho_v d}} \qquad C/\rho_v \le 0.3$$

$$k = 0.083\sqrt{\frac{\sigma}{\rho_v d}}\left(\frac{C}{\rho_v}\right)^{-0.65} \qquad C/\rho_v > 0.3$$

Hence for the same liquid concentration, the deposition rate, Equation (5.47), is a function of $d^{-0.5}$. Thus the liquid film will be replenished more slowly for larger diameters. In addition, for larger diameters, the film depletion will be increased by an increased entrainment rate, since entrainment is a function of $d^{0.316}$ from Equation (5.52). Hence both the parameters, the deposition and the entrainment, have an integral effect on the film flow rate and lower the CHF. These integral effects and hence the effect of diameter are embodied in the annular-flow model.

The model clearly shows an increase in CHF with a decrease in diameter, and the examples are shown in Figures 5.6 to 5.11. On the other hand, no obvious influence of mass flux and pressure on the diameter effect is evident from these figures.

In summary, the annular-flow model predicts CHF with the diameter effect similar to that the experimental data showed in Chapter 4. CHF occurrence appears to be controlled by entrainment and deposition near the critical condition, and both the rates of entrainment and deposition (empirical) are empirically correlated to the diameter in the form of d^n.

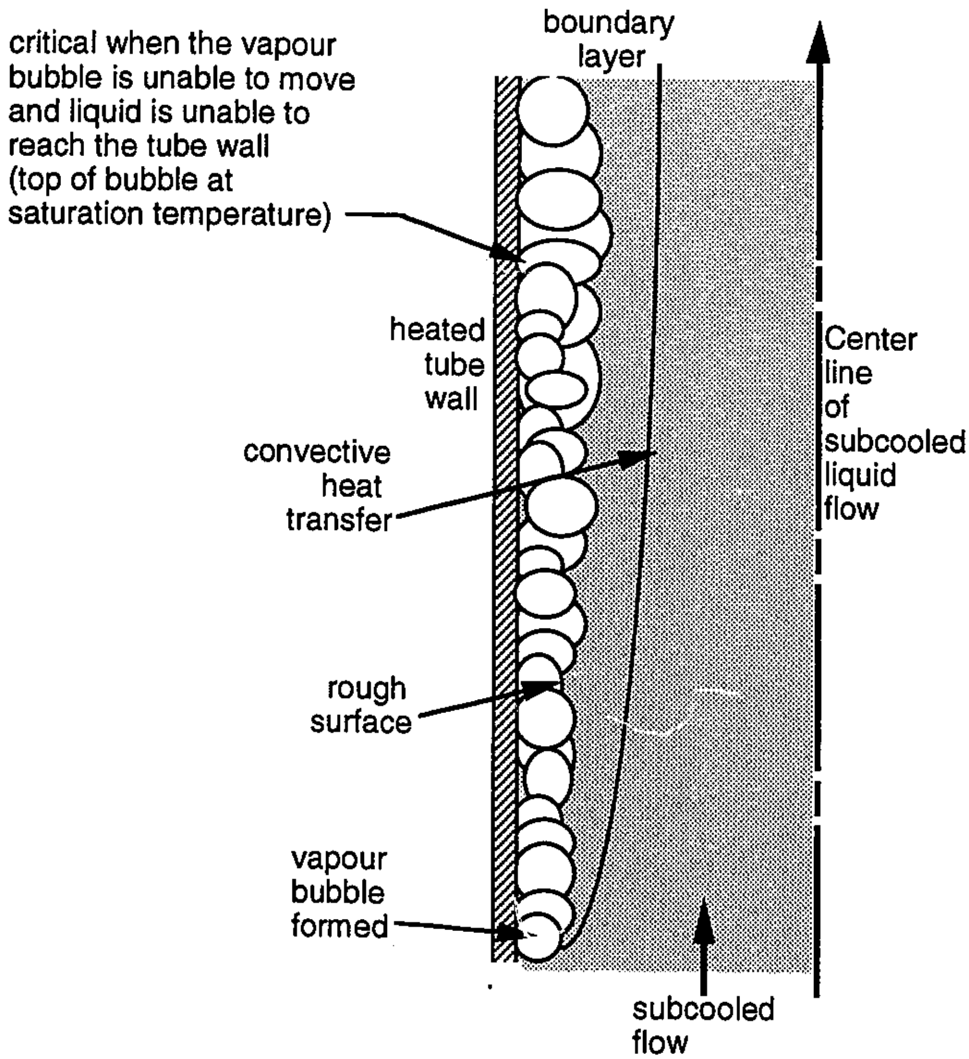

Figure 5.1: Upward Flow Subcooled Boiling in Tube

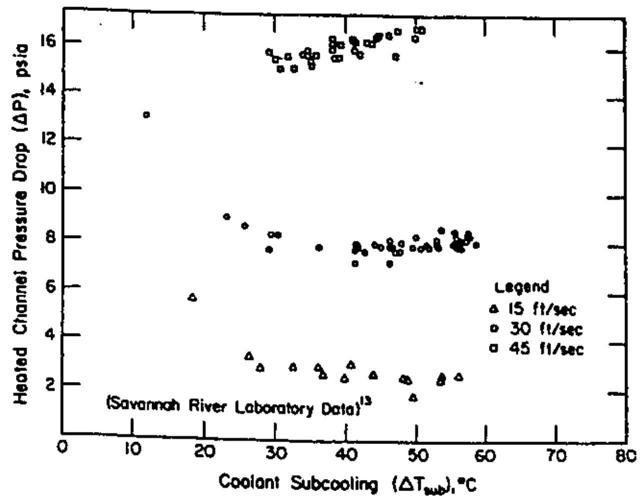

Figure 5.2: Pressure Drop vs. Subcooling at Burnout from Experiment (Thorgenson et al. 1974)

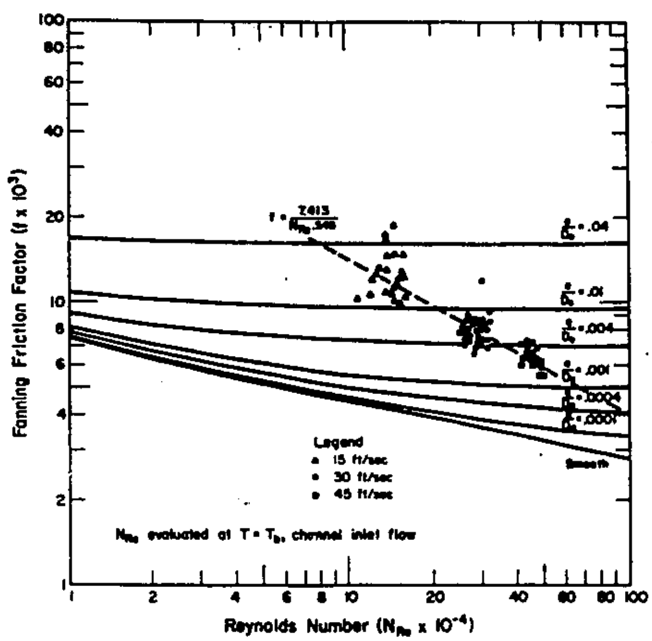

Figure 5.3: Experimental Friction Factor as Function of Reynolds Number for Annular Channel (Thorgenson et al. 1974)

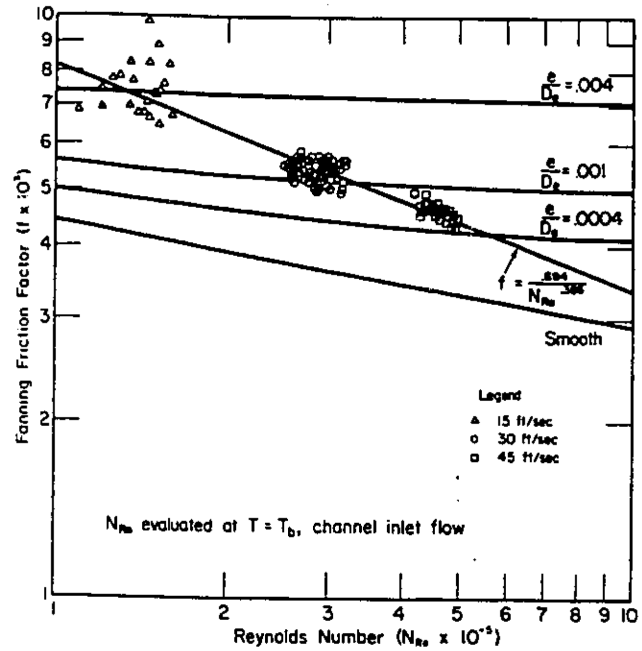

Figure 5.4: Experimental Friction Factor as Function of Reynolds Number for Tube Correlated from Annular Channel Data (Thorgenson et al. 1974)

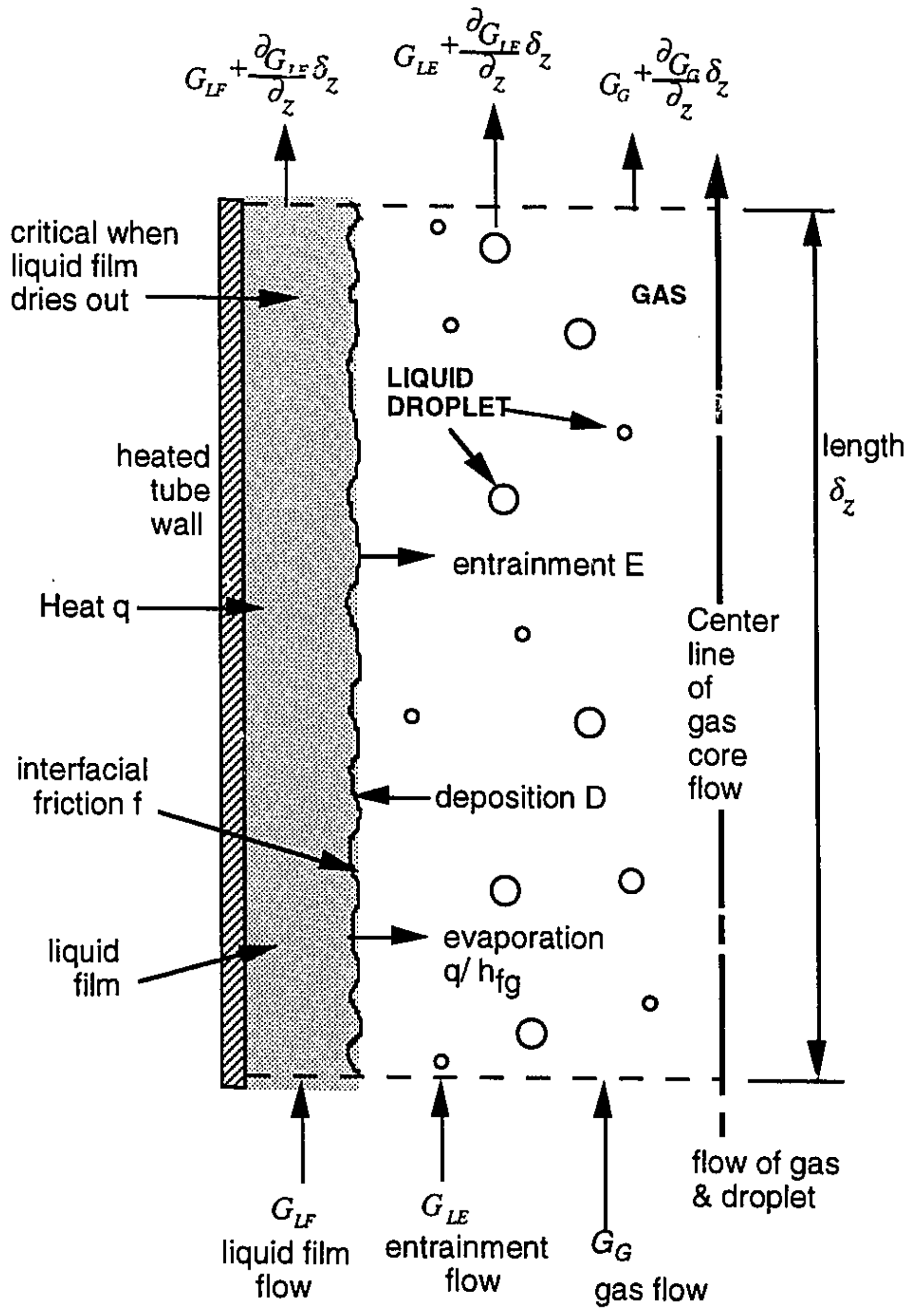

Figure 5.5: A Control Volume of Annular Flow Regime for a Vertical Pipe

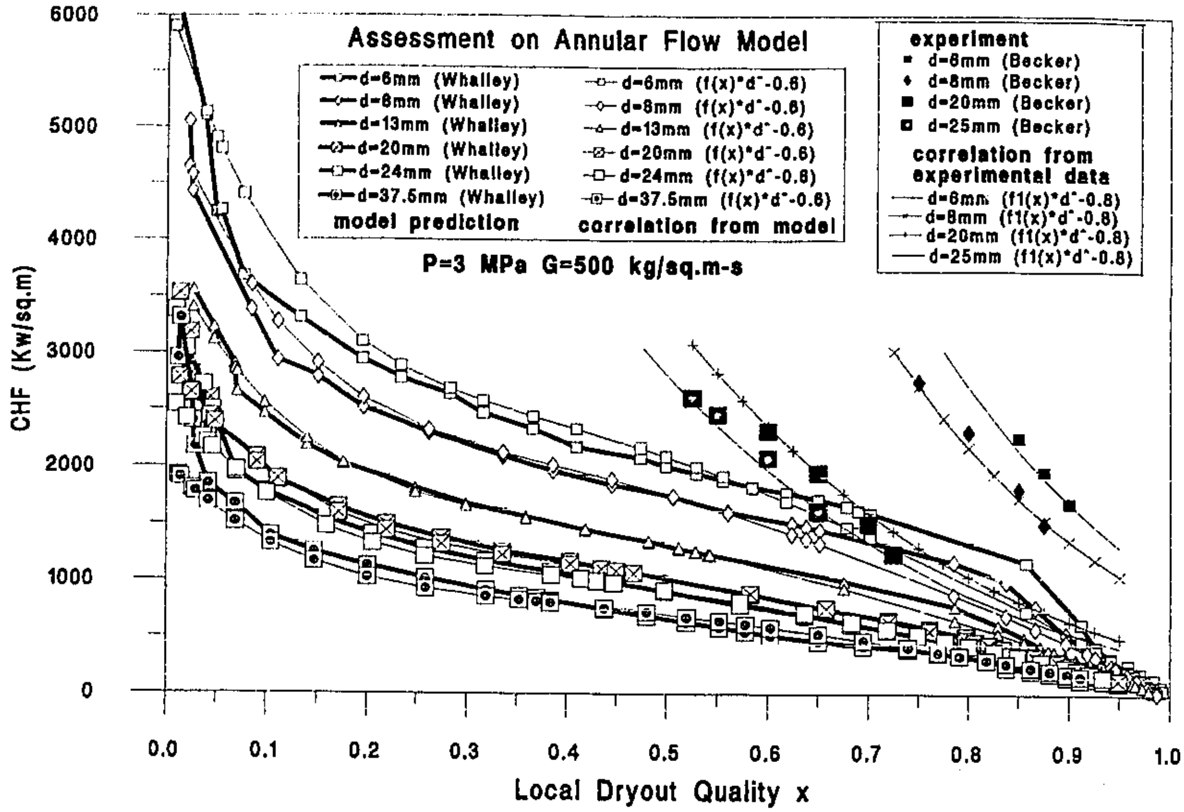

Figure 5.6: Diameter Effect: Annular Film Model Prediction vs. Experimental Data (Pressure=3 MPa, Mass Flux=0.5 Mg.m^{-2}.s^{-1})

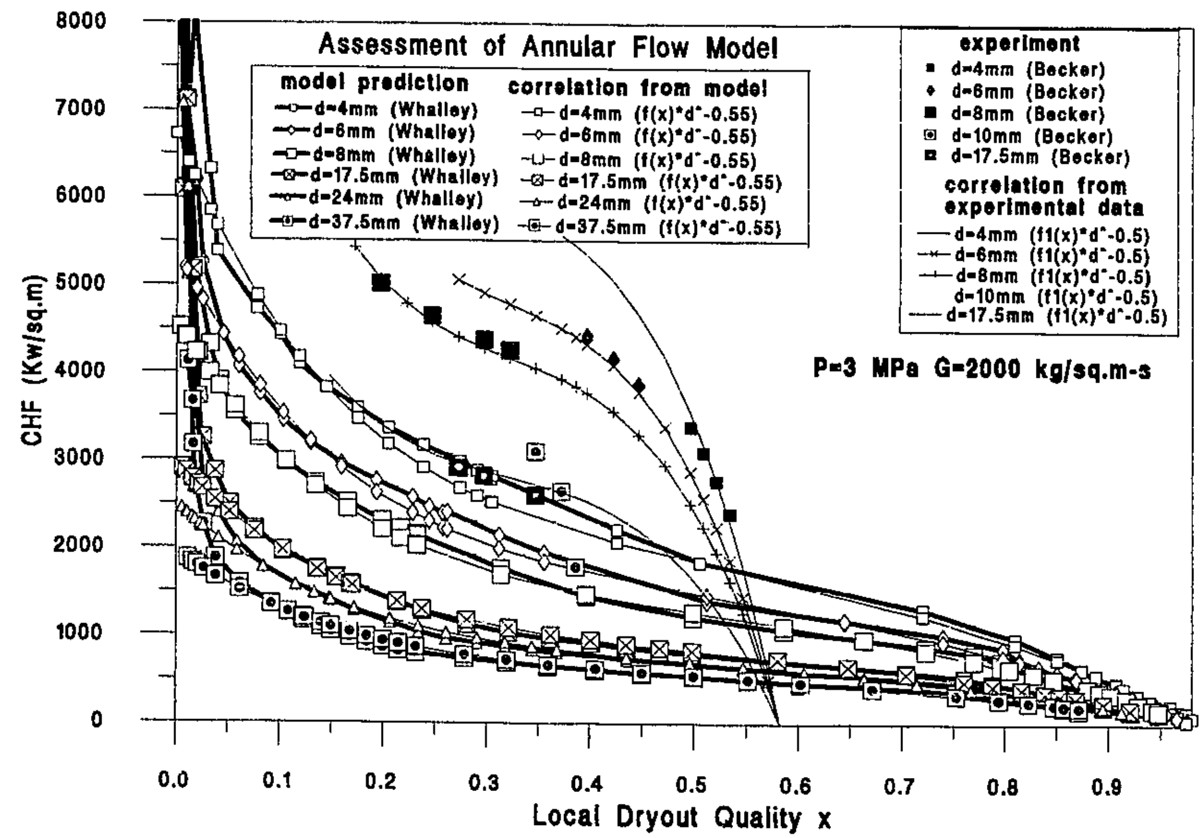

Figure 5.7: Diameter Effect: Annular Film Model Prediction vs. Experimental Data (Pressure=3 MPa, Mass Flux=2 Mg.m^{-2}.s^{-1})

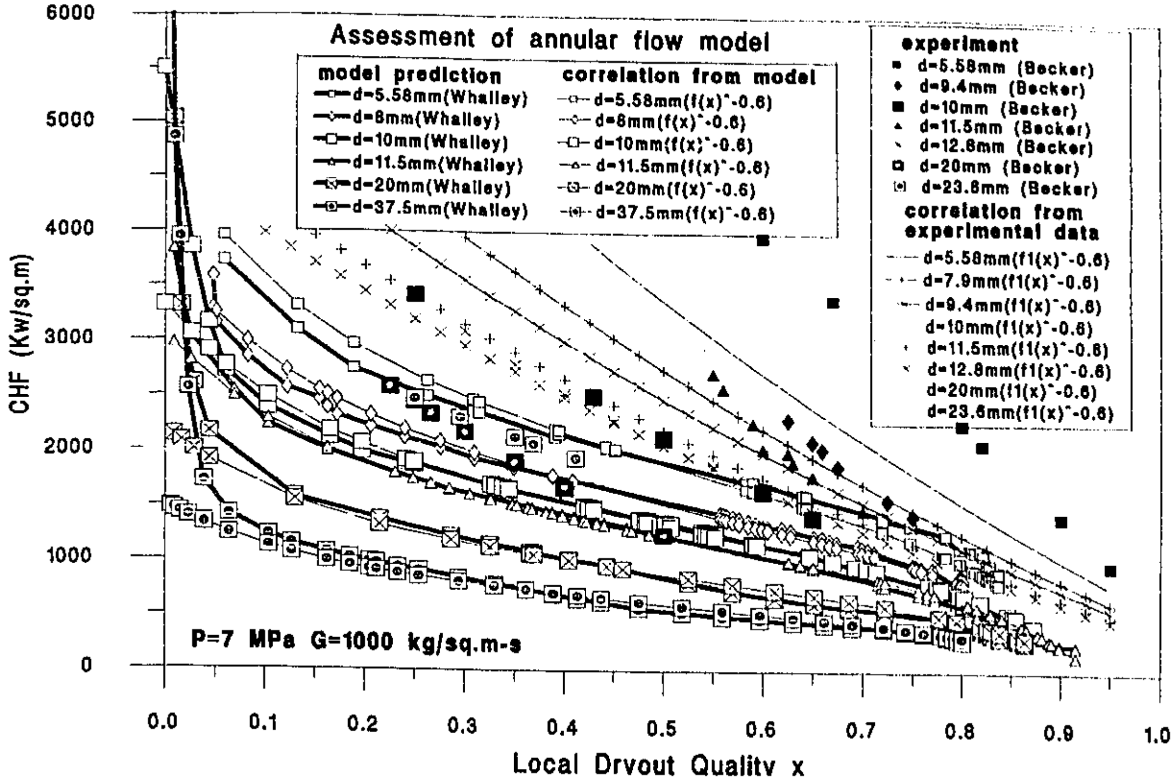

Figure 5.8: Diameter Effect: Annular Film Model Prediction vs. Experimental Data (Pressure=7 MPa, Mass Flux=1 $Mg.m^{-2}.s^{-1}$)

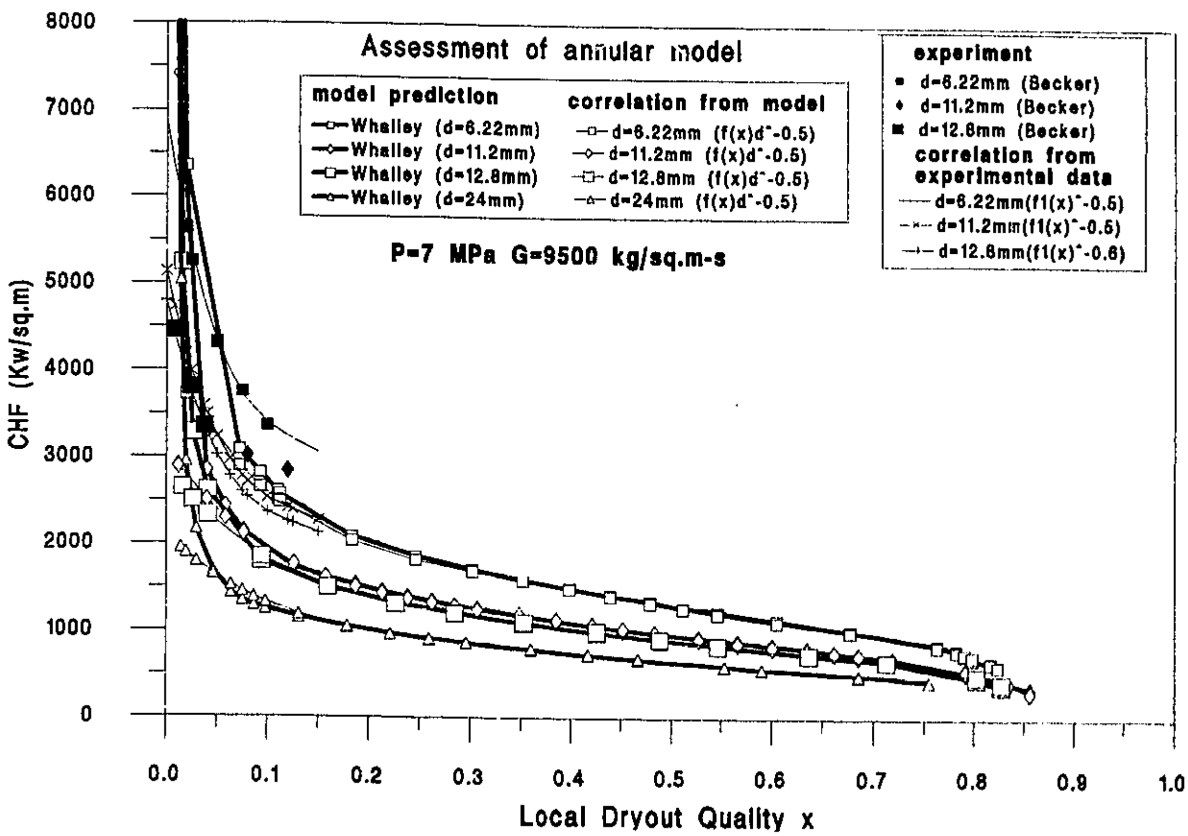

Figure 5.9: Diameter Effect: Annular Film Model Prediction vs. Experimental Data (Pressure=7 MPa, Mass Flux=9.5 $Mg.m^{-2}.s^{-1}$)

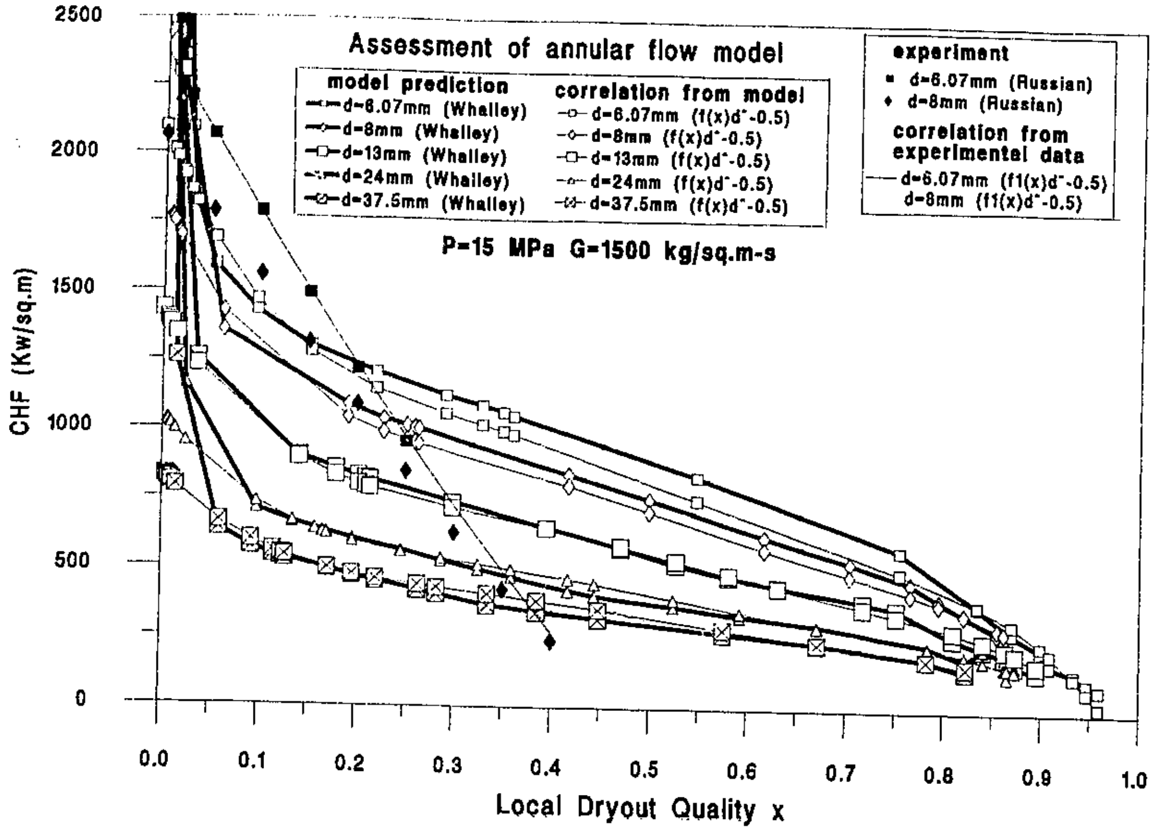

Figure 5.10: Diameter Effect: Annular Film Model Prediction vs. Experimental Data (Pressure=15 MPa, Mass Flux=1.5 Mg.m^{-2}.s^{-1})

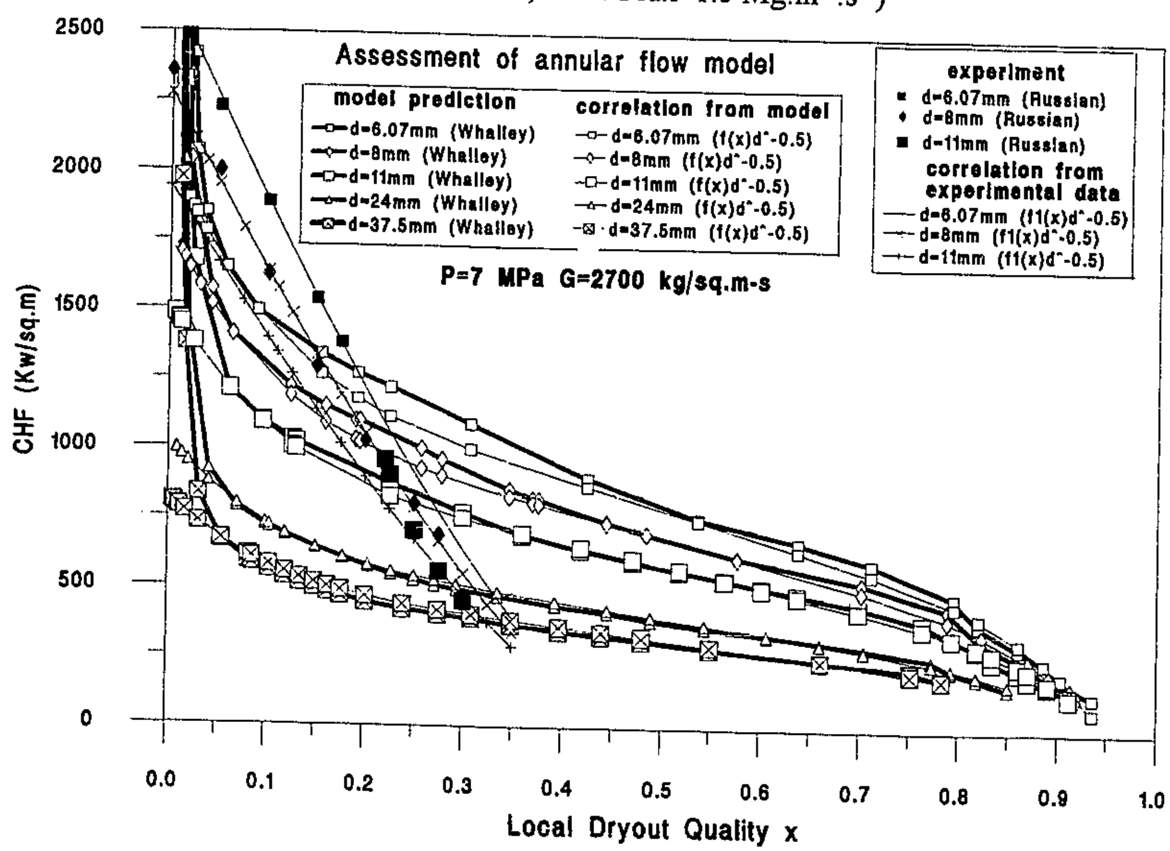

Figure 5.11: Diameter Effect: Annular Film Model Prediction vs. Experimental Data (Pressure=15 MPa, Mass Flux=2.7 Mg.m^{-2}.s^{-1})

6. VALIDATION OF CORRELATION FOR EXPONENT IN TUBE-DIAMETER CORRECTION FACTOR

A correlation has been derived for improving the exponent, n, in the tube-diameter correction correlation for CHF (i.e., Equation (4.1)). It was described in Chapter 4, as Equation (4.4), and has been assessed against data in the AECL data bank. Since these data were used in developing the correlation, this assessment is considered part of the verification process only. To ensure that the correlation is valid outside the development data base, a validation exercise has been introduced. This chapter describes the experimental program to obtain validation data and the comparison of predictions based on the correlation against the experimental data.

6.1 DESCRIPTION OF EXPERIMENT

An experiment was introduced to obtain CHF data with upward steam-water flow at high-pressure conditions in vertical tubes. It was carried out at the Chalk River Laboratories and covered a wide range of flow conditions. In addition to the CHF data, this experiment was used to obtain pressure-drop measurements in heated channels. A detailed description of the test loop and test sections has been provided by Leung (1994).

6.1.1 Test Loop

The experiment was carried out in the MR-1 FLARE Loop of the Fuel Channel Thermalhydraulics Branch at the Chalk River Laboratories. A schematic diagram of the MR-1 loop is shown in Figure 6.1. The loop consists of the following main components:

- two boilers - to maintain system pressure,
- a condenser - to condense vapour generated from the test section,
- a pre-heater - raises the temperature of the flow at the inlet of the test section to a pre-set temperature,
- two circulating pumps - to circulate water through the loop, and

- 350 kW power supply (175 VDC and 2000A) - to heat up the test section.

A control loop, consisting of a catch tank and a heat exchanger, automatically regulates the flow conditions by controlling the pressure and level of water at the condenser and the two boilers. The catch tank is used to relieve over-pressure at the boiler. The heat exchanger removes excess heat from the main loop flow to maintain the same water temperature as at the inlet of the test section. A make-up pump supplies make-up water to the loop, and a bleed valve purges the system.

The flow rate to the test section is adjusted through a control valve in the loop. Three orifice plates with low, medium and high ranges are used to measure the flow rate. A resistance-temperature device (RTD) measures the temperature of flow at the orifice plates for correction in flow calculation.

6.1.2 Test Sections

The test sections were constructed of Inconel-600 tubes having inside diameters of 5.45 and 8.94 mm (wall thicknesses of 1.25 and 1.88 mm, respectively). They were heated over a length of 2.5 m. Two ungrounded chromel-alumel thermocouples were installed at both the inlet and the outlet ends to measure the fluid temperature. Both test sections were insulated with fibreglass to reduce heat loss. The setup of the test section is shown schematically in Figure 6.2.

6.1.3 Data Acquisition System

A Concurrent mini-computer (Model 3212) collected the data during the experiment through analog/digital convertors. The following parameters were monitored:

- water flow rate through the test section,
- external power supplied to the test section,
- pressure at the outlet of the test section,
- fluid temperatures at the inlet and outlet of the test section,

- ambient temperature, and
- surface temperatures along the test section.

6.1.4 Experimental Procedure

The loop was stabilized at a pre-set pressure, and the desired flow rate was adjusted. Power was applied to the test section and increased gradually until a sharp rise in temperature at the outlet of the test section was detected. This implied that critical heat flux had been reached. Power at this level was then reduced by approximately 2 kW, and subsequently increased in increments of 1 kW until the critical heat flux reoccurred. This confirmed the events of critical heat flux for each test. All parameters to be monitored were scanned and recorded seven times in 10-second intervals. The flow conditions were adjusted for the subsequent test. A number of tests were repeated to check the accuracy of the measurements and the repeatability of the experiment.

6.2 EXPERIMENTAL DATA

6.2.1 Descriptions of Data

A number of test parameters were obtained with the data acquisition system. However, only some of them are required for the present study. They include the pressure, mass flow rate, inlet fluid temperature and power. Appendix II lists the measurements for each run number. These measurements were used together with the geometry of each test section to calculate the correlated parameters, which are mass flux, heat flux and exit thermodynamic quality at CHF. Based on the tube diameter, the flow area is calculated using

$$A_f = \frac{\pi d^2}{4} \tag{6.1}$$

and the heated area is calculated using the tube diameter and heated length

$$A_h = \pi d L_h \tag{6.2}$$

The mass flux is determined using the mass flow rate and flow area,

$$G = \frac{W}{A_f} \tag{6.3}$$

The exit thermodynamic quality is calculated using

$$x_c = \frac{1}{H_{fg}}\left(\frac{Power}{W} + H_{in} - H_f\right) \tag{6.4}$$

The critical heat flux is obtained from

$$q_c = \frac{PoweratCHF}{A_h} \tag{6.5}$$

The calculated parameters corresponding to the measurements are listed in Tables 6.1 and 6.2 for the 8.94- and 5.45-mm diameter tubes, respectively. They covers the following range of flow conditions:

Pressure:	7 and 9.5 MPa
Mass flux:	1, 2, 3, 4.3, 6, 7, 7.5, 8.5 and 10 $Mg.m^{-2}.s^{-1}$
Inlet subcooling:	~0 to 325 $kJ \cdot kg^{-1}$
Critical heat flux:	0.7 to 3.250 $MW \cdot m^{-2}$

An examination of the data's consistency was carried out based on the relation between critical heat flux and inlet subcooling. Collier (1972) showed that the critical heat flux is linearly proportional to inlet subcooling at the same pressure and mass flux for tubes of large ratios of heated length to diameter (>100) (Figure 2.6). Figures 6.3 and 6.4 show, respectively, the comparison of critical heat flux and inlet subcooling for data obtained from the 8.94-mm and the 5.45-mm tubes. The data are generally consistent over the present range of flow conditions, especially for those of the 8.94-mm tubes. They are also repeatable, as shown in the figures (where multiple points are shown at the same flow conditions). The scatter among data obtained at mass fluxes of 4.2 and 6 $Mg.m^{-2}.s^{-1}$ in the 5.45-mm tube are caused by the variations in mass flow rate, which is about ±5% of the nominal values. A systematic increasing CHF trend with increasing mass flux is also displayed at all pressures for a constant inlet subcooling.

6.2.2 Error Analysis on Data

A simple analysis to provide estimates of the sizes of error associated with the experiment is presented in Appendix III. The statistical concepts used for the analysis mostly were well established and have been previously applied to experiments performed in AECL's MR-1 Loop. The following is a summary of the errors or uncertainties, valid for the range of flow conditions of the experiment performed for this thesis:

	uncertainty (%)
outlet pressure	0.4
mass flux	7.
heat flux	4.3
outlet quality	9.

6.3 ANALYSIS OF EXPERIMENTAL DATA

The present set of experimental data were analyzed using the constant dryout quality approach. Due to the limitation of the experimental setup, there is only a narrow range of overlapping conditions for both the 5.45-mm and the 8.94-mm tube data. To extend the ranges, the analysis of the diameter effect is presented with reference to the preliminary CHF look-up table based on the 7-mm to 9-mm tube data (see Chapter 4). In addition, several data points of Snoek (1988) are shown for comparison. Snoek's (1988) data were obtained at the same facility with an Inconel-600 tube of 11.9-mm inside diameter, and hence are comparable with the present set of data.

6.3.1 Effect of Critical Quality and Mass Flux on Critical Heat Flux

Figures 6.5 and 6.6 show, respectively, for the 8.94-mm and the 5.45-mm tubes, the variation of critical heat flux as functions of critical quality and mass fluxes. At pressures of both 9.55 and

7 MPa for the 8.94-mm tube (Figure 6.5), the critical heat flux generally increases with decreasing quality, except for the data scatter at low mass-flux conditions. A sharp decrease in CHF is shown at low mass-flux conditions. At qualities where data are available for several mass fluxes, the critical heat flux increases with increasing mass flux. Comparing data of different pressures, a higher CHF value is shown for lower pressure (7 MPa).

A much larger data scatter is observed at a pressure of 9.55 MPa for the data of the 5.45-mm tube (Figure 6.6). In general, the increasing trend of CHF with decreasing quality and increasing mass flux is displayed. As indicated in Section 6.2, the data scatter is probably caused by the deviation in mass flow rate from the nominal conditions. A higher CHF is also indicated for the low pressure at the same mass flux and quality.

6.3.2 Effect of Tube Diameter on Critical Heat Flux

The effect of tube diameter on critical heat flux is examined by comparing data obtained at the same flow conditions with various diameter tubes. The CHF values presented in the preliminary CHF look-up table and those of Snoek (1988) are shown for comparison.

Figure 6.7 shows the CHF data obtained in all three diameter tubes at a pressure of 9.55 MPa and mass fluxes of 2 and 3 $Mg.m^{-2}.s^{-1}$. The effect of tube diameter on critical heat flux cannot be examined directly, because there are no overlapping conditions; however, it is observed by comparing the data against values of the CHF look-up table (i.e., 8-mm tube data). The data of 8.94 and 11.9-mm tubes are systematically lower than those of the 8-mm tube, and the differences between data and table values increase with increasing tube diameter. This agrees with the trends previously described in Chapters 3 and 4. The single data point of the 5.45-mm tube is also lower than that of the 8-mm tube, which is contrary to the anticipated trend. However, the variation in CHF is drastic at these conditions (as presented for the data of the 8.94-mm tube), and has not been shown in the CHF look-up table (or the 8-mm tube data). This high uncertainty, together with the large data scatter, may have a large impact on the trend of the data at these conditions.

Figure 6.8 compares critical heat flux values at a pressure of 9.55 MPa and mass fluxes of 1 and 4 $Mg.m^{-2}.s^{-1}$ where the data were obtained in both the 5.45- and 11.9-mm tubes. The effect of tube diameter is clearly demonstrated by comparing the 8-mm tube data. Compared against the 8-mm tube data at the same flow conditions, the CHF is larger for the 5.45-mm tube and smaller for the 11.9-mm tube. One of the 11.9-mm tube data points (marked in the figure) is questionable: it shows an incorrect trend of a decrease in CHF with a decrease in quality. This can be confirmed in Figure 6.9, which shows the relation between CHF and inlet subcooling for the 11.9-mm tube data (Snoek 1988). This data point (at a mass flux of 1 $Mg.m^{-2}.s^{-1}$ and inlet subcooling 350 kJ) also shows a drop in CHF with increasing subcooling, contrary to all other data for higher mass fluxes.

Figure 6.10 shows the CHF data at a pressure of 9.55 MPa and mass fluxes of 4.4 and 6 $Mg.m^{-2}.s^{-1}$. The effect of tube diameter cannot be directly recognized, since the quality range is different between the 5.45-mm and the 8.94-mm tube data. However, the 8-mm tube data values lie between the two sets of data. Hence a trend can be visualized showing that CHF is likely to be higher for the 5.45-mm than the 8.95-mm tube data.

Figure 6.11 shows the data at a pressure of 9.55 MPa and a mass flux of 7.5 $Mg.m^{-2}.s^{-1}$. At a quality of 0.25, CHF for the 5.45-mm is higher.

Figure 6.12 shows the data obtained at two mass fluxes at a pressure of 7 MPa. In general, they exhibit the same trends as those at a pressure of 9.55 MPa, and hence are not discussed further.

6.4 VALIDATION OF EQUATION (4.4)

The present set of experimental data are used to validate the correlation derived to predict the exponent in the tube-diameter correction factor (i.e., Equation (4.4)). This validation procedure is described in Section 4.4. The prediction error, average error and rms error were defined in Equations (4.5) to (4.7).

The CHF values predicted using Equation (4.4) are listed together with the experimental data in

Tables 6.1 and 6.2. Overall, these correlations predict with the experimental data quite well. For the recommended correlation, Equation (4.4), the overall average error is -6.18% and the rms error is 9.57% when compared to the 39 data points of the 8.95-mm tube; and 6.22% and 9.39% respectively, for 37 data points of the 5.45-mm tube. Figure 6.13 shows the comparison between the predicted and measured values of critical heat flux. For both diameters, most data are overpredicted, but are within the ±10% error range. The overall prediction accuracy is about the same when Equation (4.2) is used.

The predictions based on the recommended correlation are also shown in Figures 6.7 to 6.12 (except for Figure 6.9), for comparison. In comparison, the agreements between predictions and experimental data are better for high mass-flux conditions.

6.5 SUMMARY

A set of tube data have been obtained to validate of the correlation with the newly derived tube-diameter correction factor. Analysis shows that the data are reliable and consistent with trends exhibited by data from other sources. A diameter effect on critical heat flux has been observed from the experiment data, based mainly on a comparison against the reference 8-mm tube data of the CHF look-up table. The critical heat flux is generally higher for the tube of a smaller diameter. This trend is supported by the 11.8-mm tube data of Snoek (1988).

A comparison of the predicted against measured CHF values showed that the correlation provides good prediction accuracy for the present set of data. The combined average error and rms error are 6.2% and 9.54%, respectively, for a total of 76 data points from the 5.45 mm and the 8.94 mm tubes.

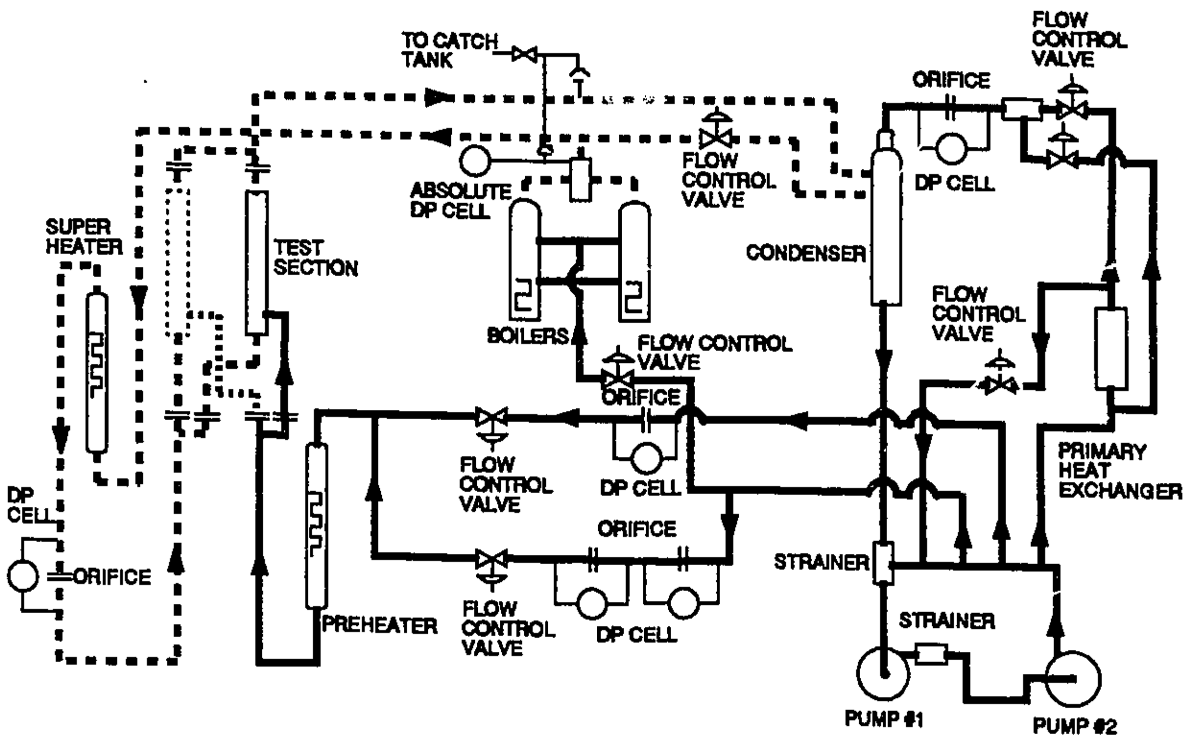

Figure 6.1: The MR1-Loop Test Facility

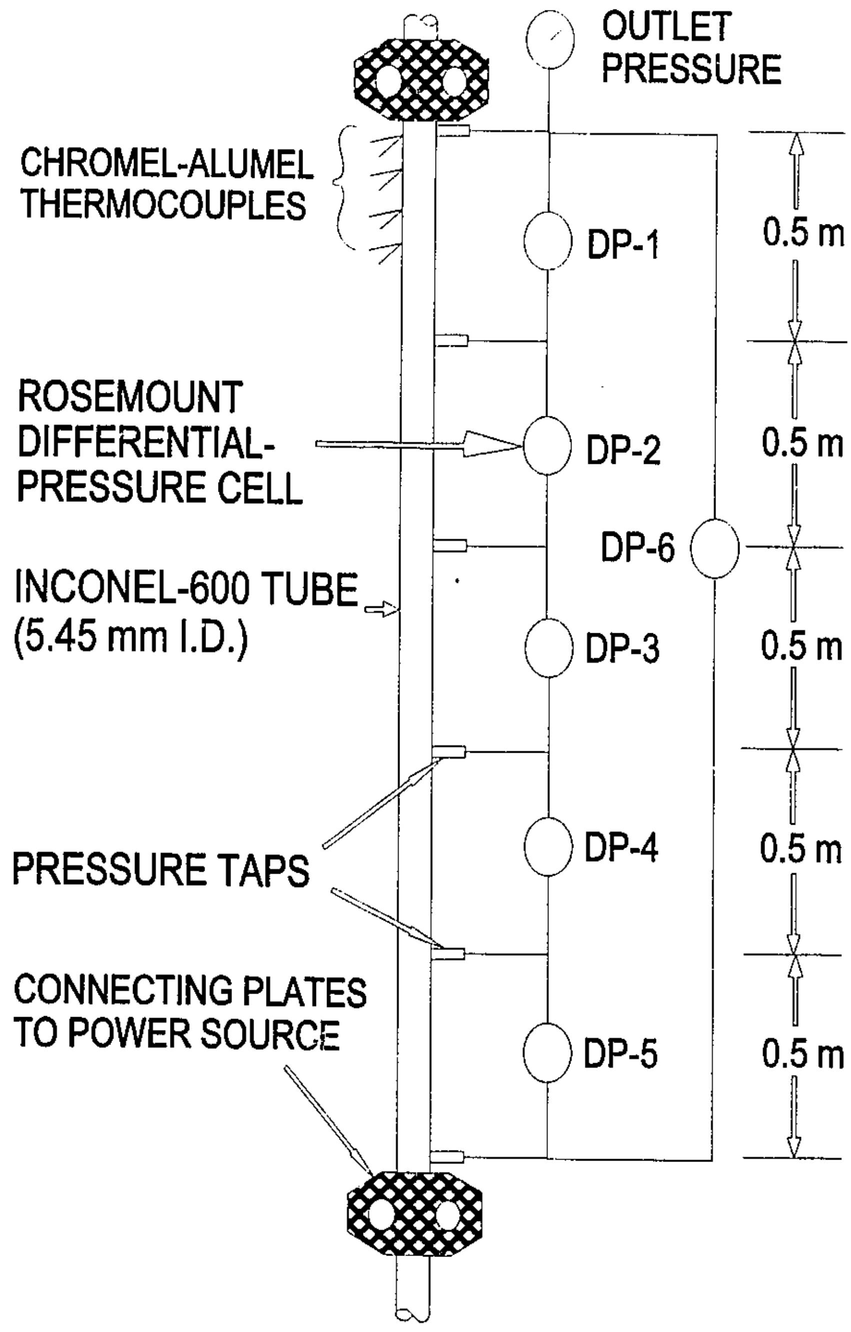

Figure 6.2: Test Section and the Setup Schematics

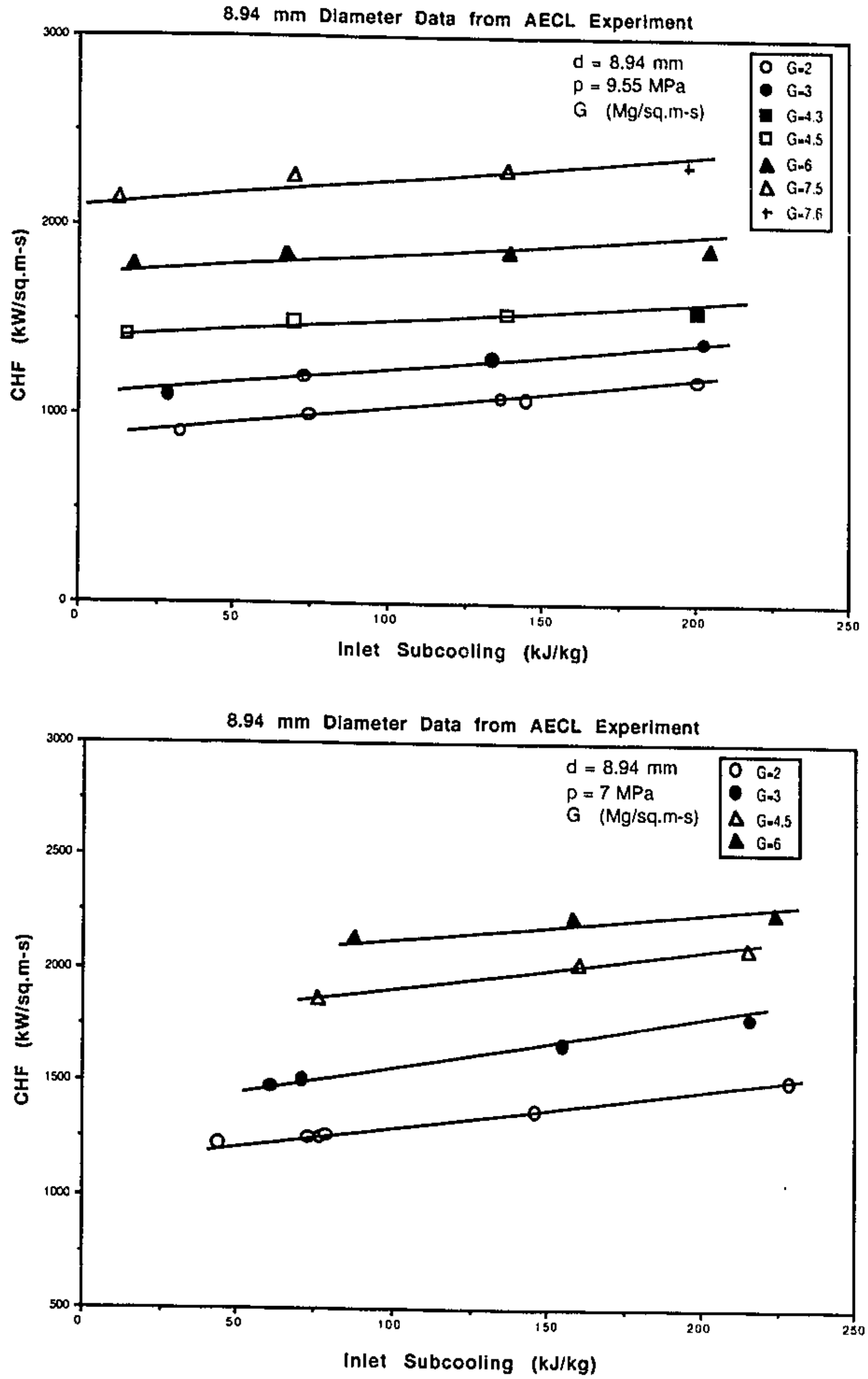

Figure 6.3: CHF vs. Inlet Subcooling for Various Mass Fluxes at Pressures 9.55 MPa and 7 MPa (AECL Experiment for 8.94 mm Diameter Tube)

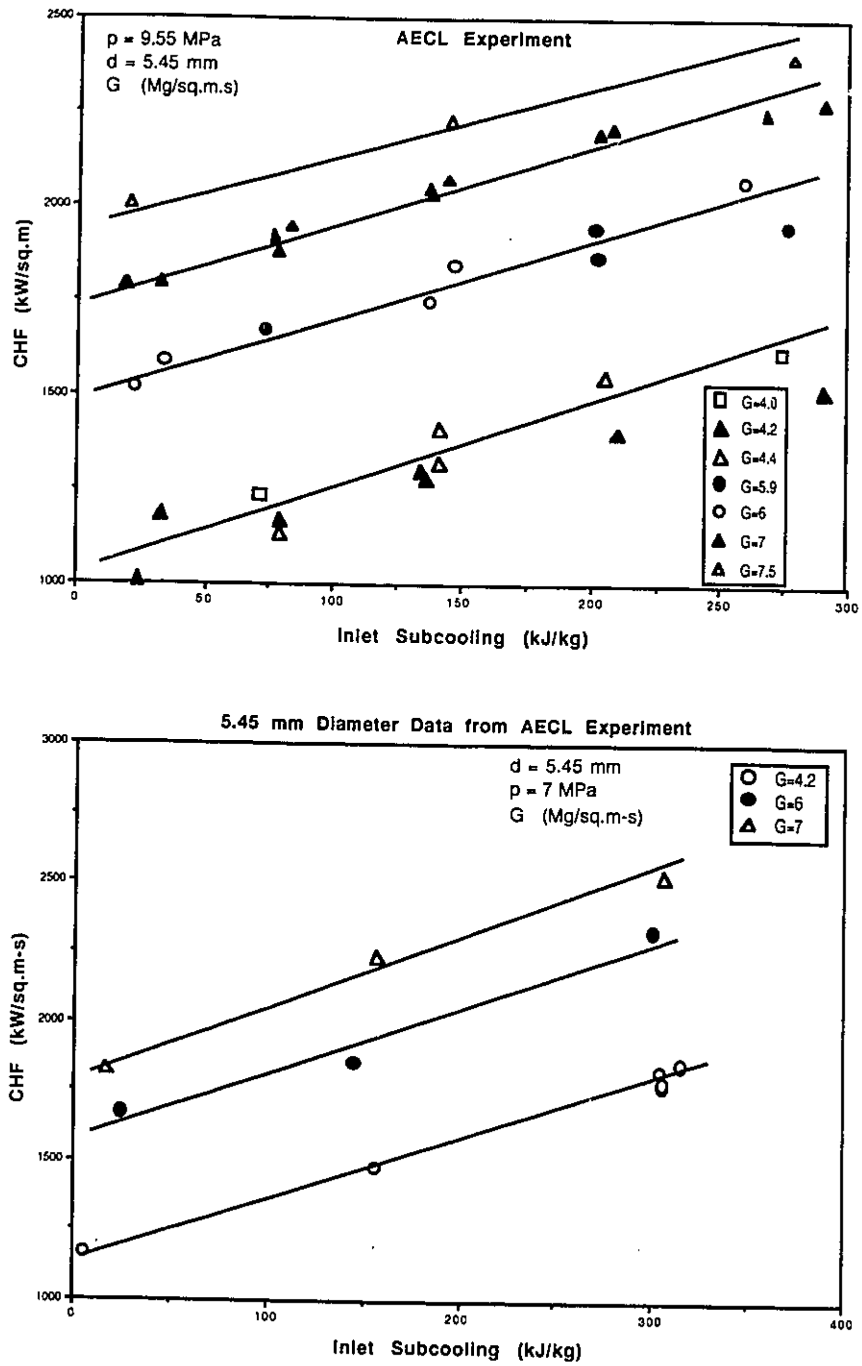

Figure 6.4: CHF vs. Inlet Subcooling for Various Mass Fluxes at Pressures 9.55 MPa and 7 MPa (AECL Experiment for 5.45 mm Diameter Tube)

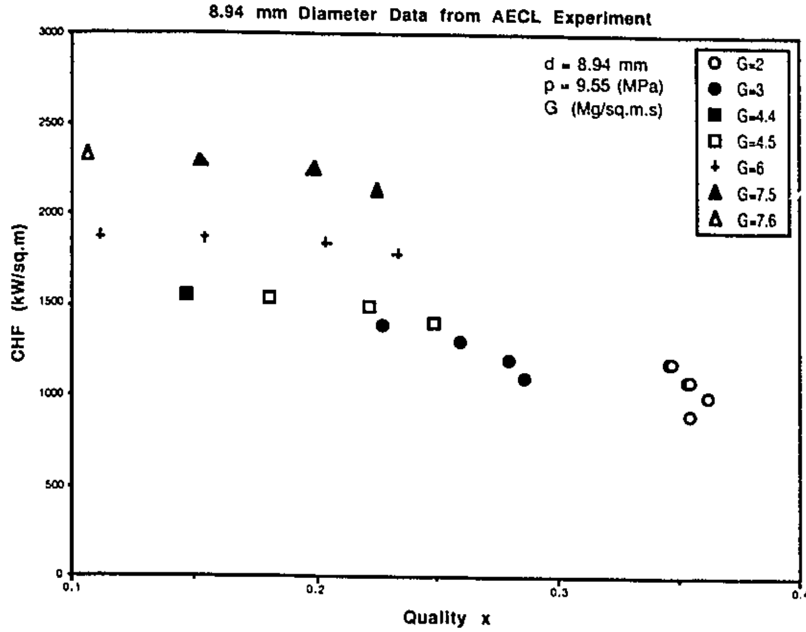

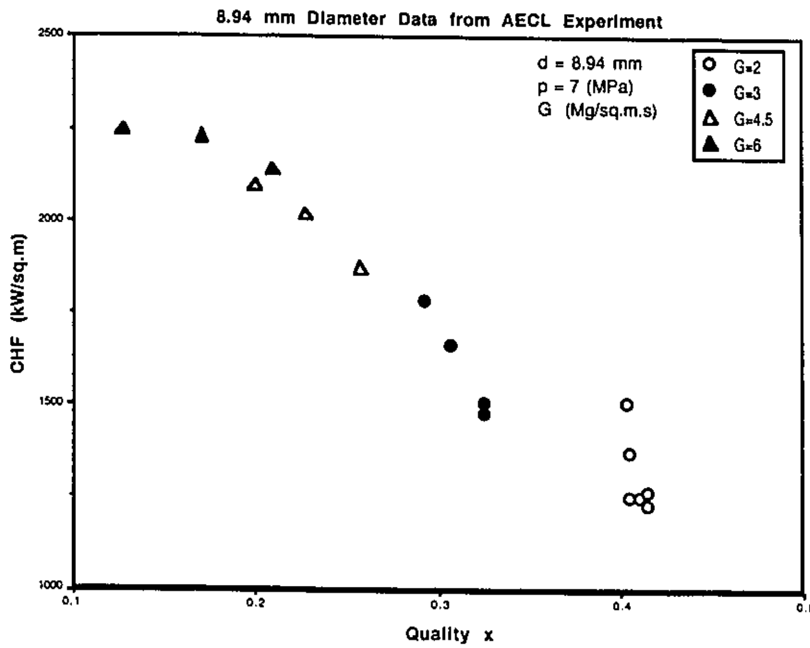

Figure 6.5: CHF vs. Quality for Various Mass Fluxes at Pressures 9.55 MPa and 7 MPa (AECL Experiment for 8.94 mm Diameter Tube)

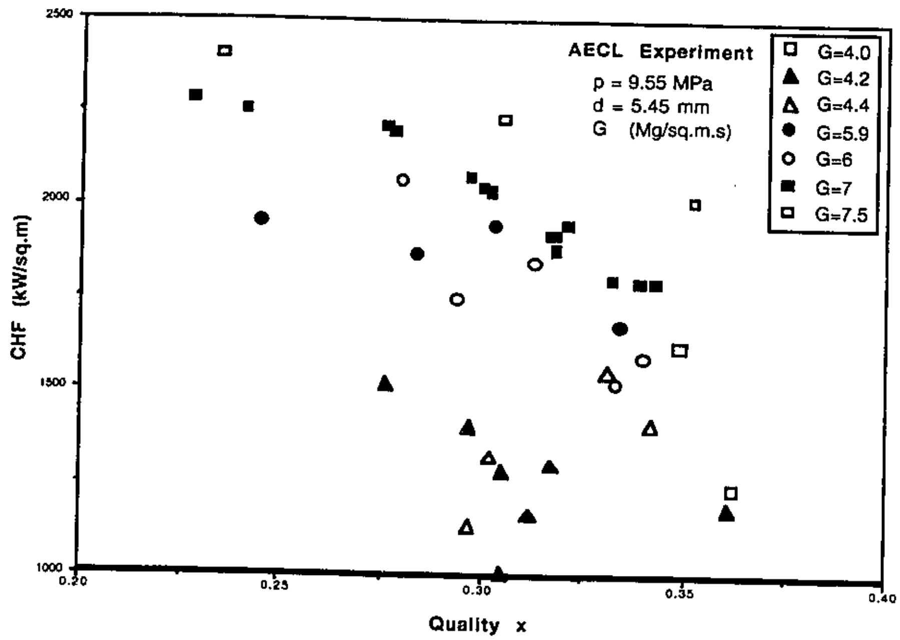

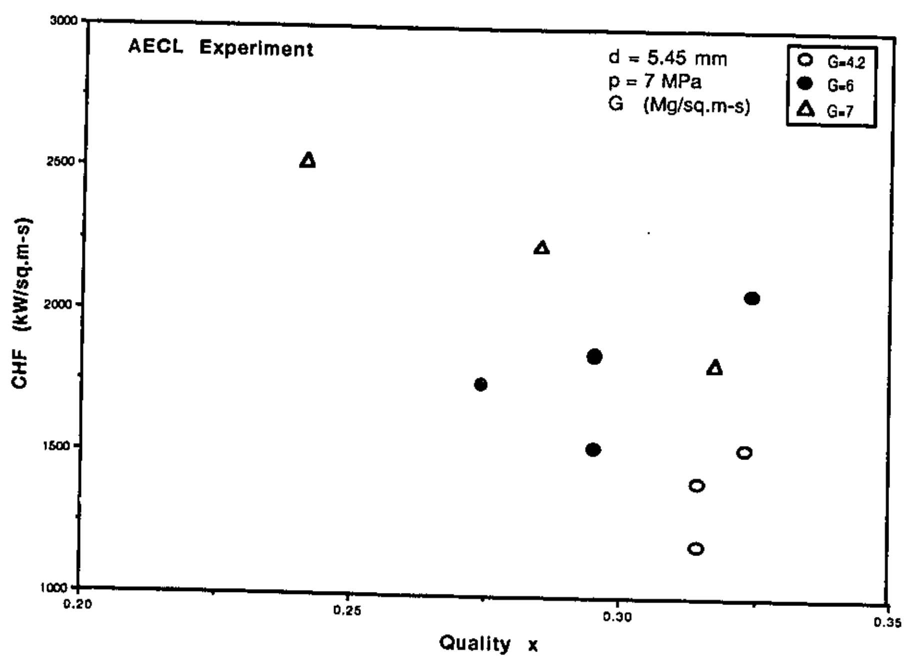

Figure 6.6: CHF vs. Quality for Various Mass Fluxes at Pressures 9.55 MPa and 7 MPa (AECL Experiment for 5.45 mm Diameter Tube)

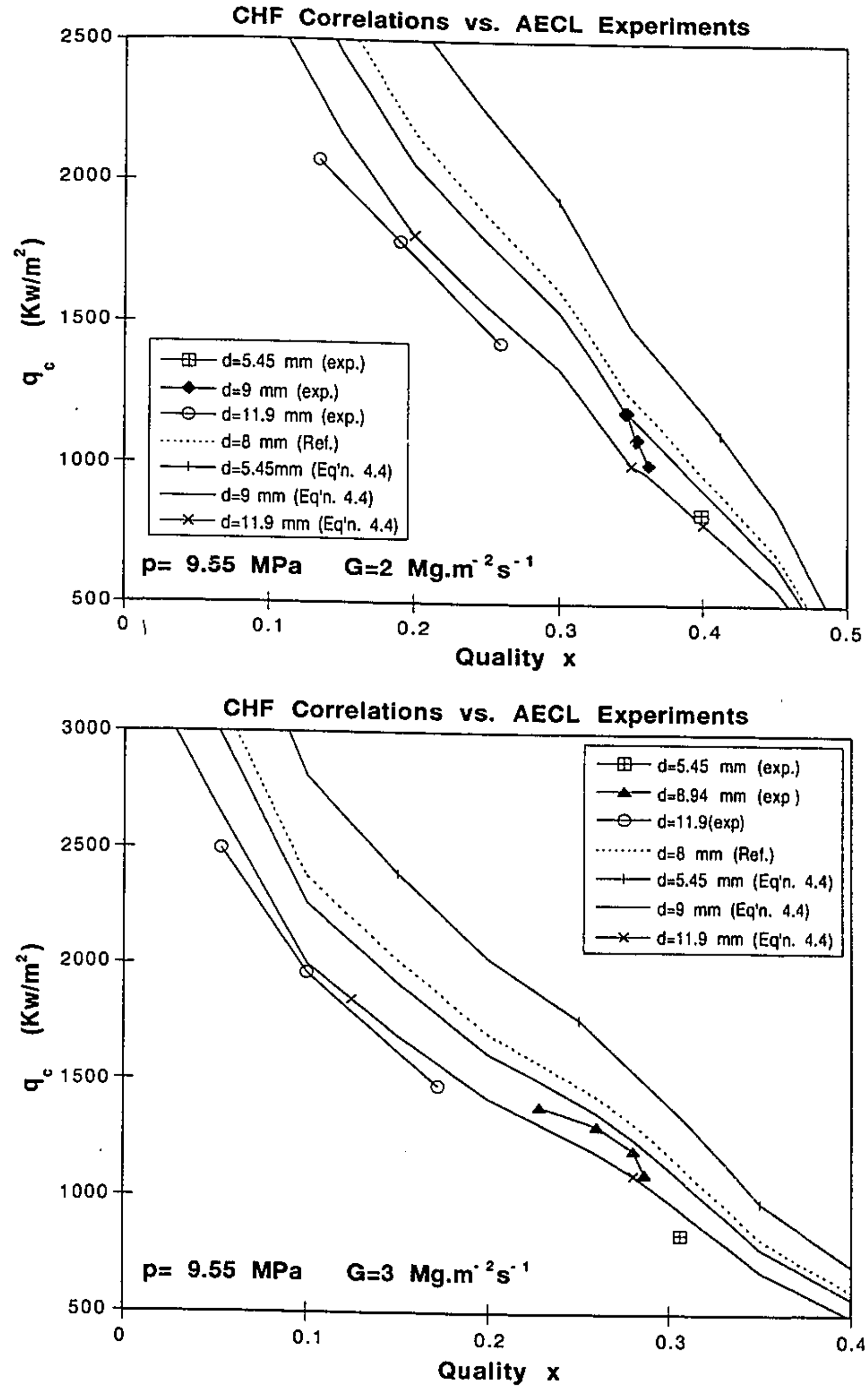

Figure 6.7: Correlation Equation (4.4) CHF Predictions vs. AECL Experiment (Pressure= 9.55 MPa, Mass Flux=2 and 3 $Mg.m^{-2}.s^{-1}$, Diameter=5.45, 8.94, 11.9 mm)

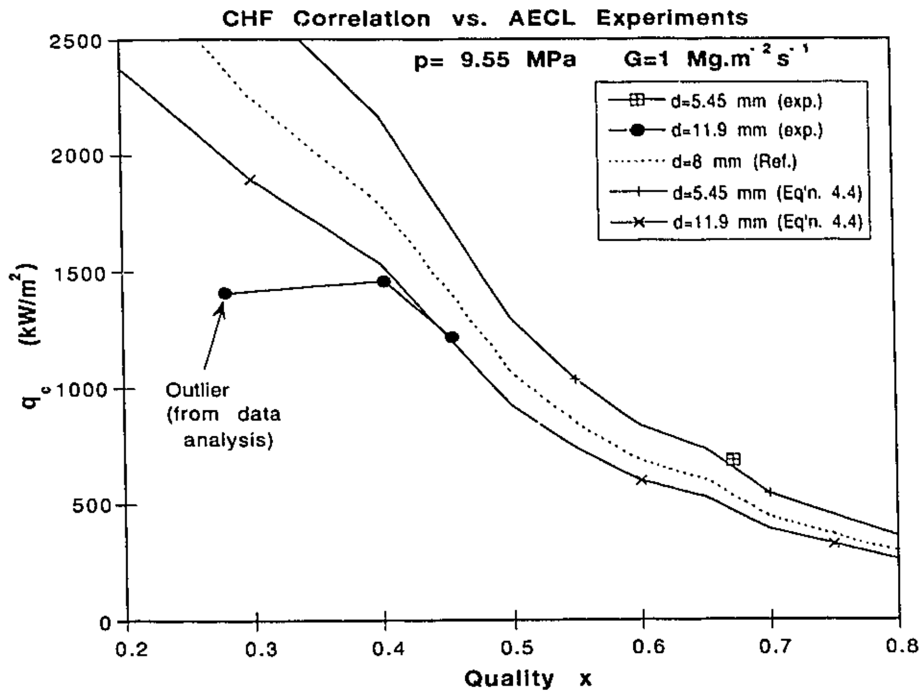

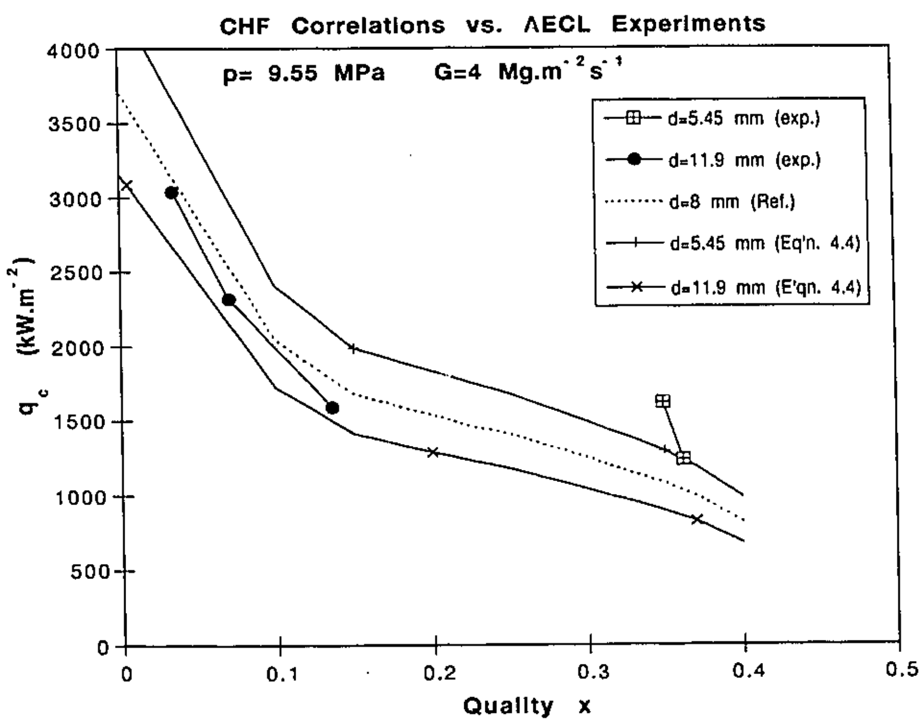

Figure 6.8: Correlation Equation (4.4) CHF Predictions vs. AECL Experiment (Pressure=9.55 MPa, Mass Flux=1 and 4 $Mg.m^{-2}.s^{-1}$ Diameter=5.45 and 11.9 mm)

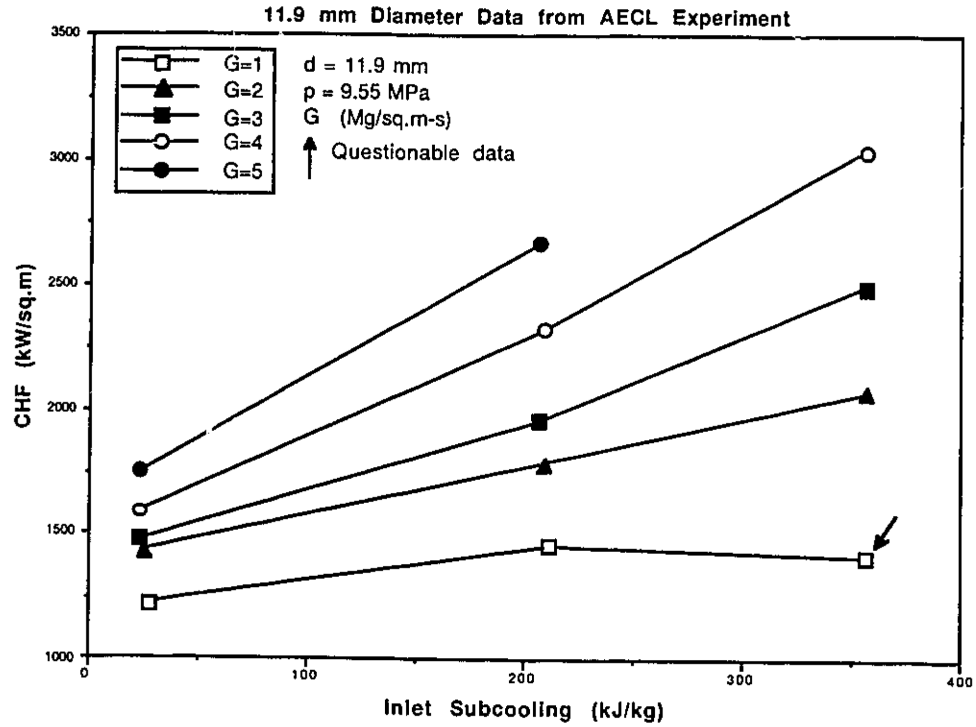

Figure 6.9: CHF vs. Inlet Subcooling for Various Mass Fluxes at Pressure 9.55 MPa (AECL Experiment for 11.9 mm Diameter Tube)

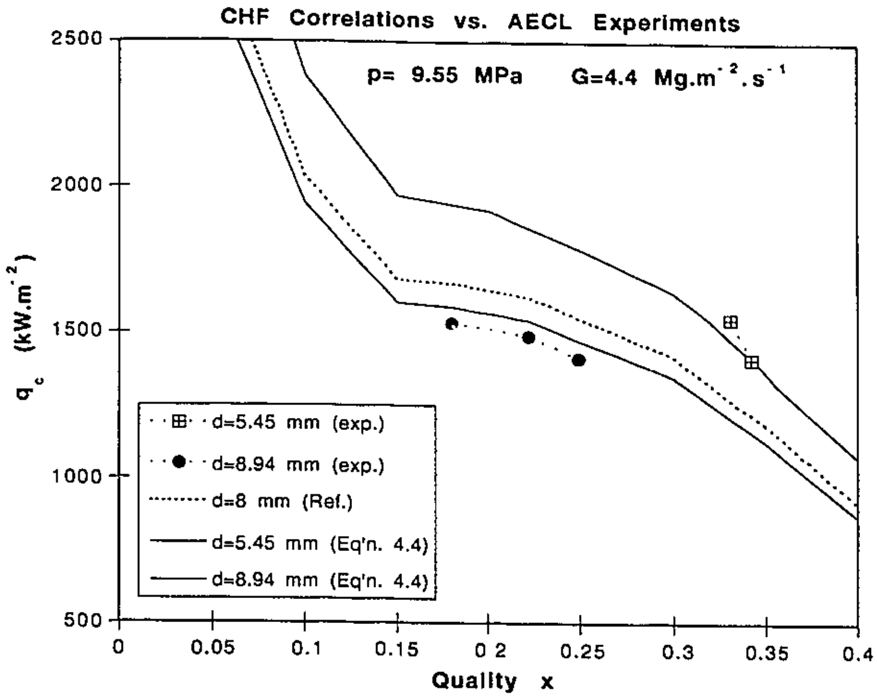

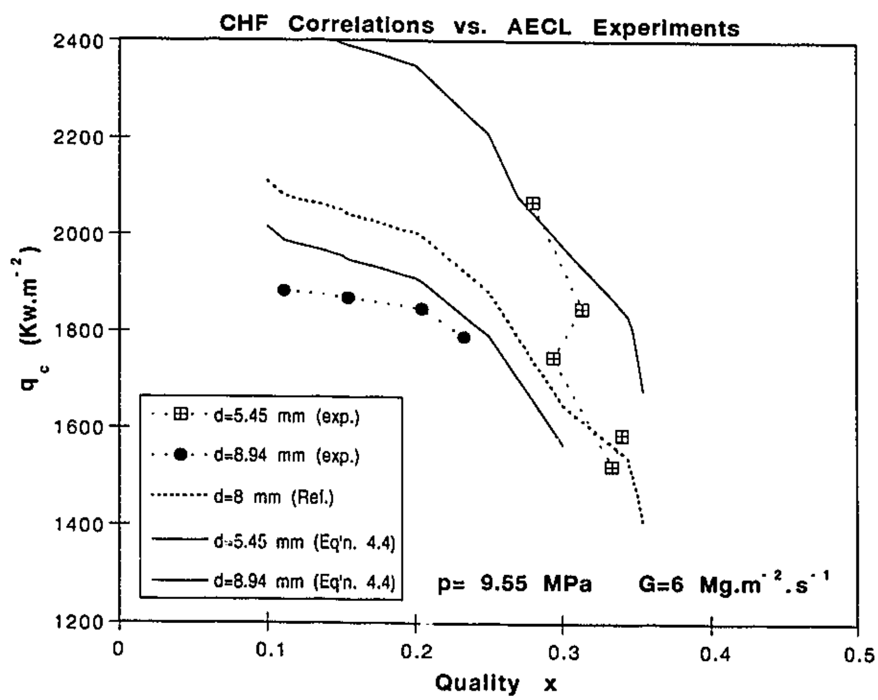

Figure 6.10: Correlation Equation (4.4) CHF Predictions vs. AECL Experiment (Pressure= 9.55 MPa, Mass Flux=4.4 and 6 $Mg.m^{-2}.s^{-1}$ Diameter=5.45 and 8.94 mm)

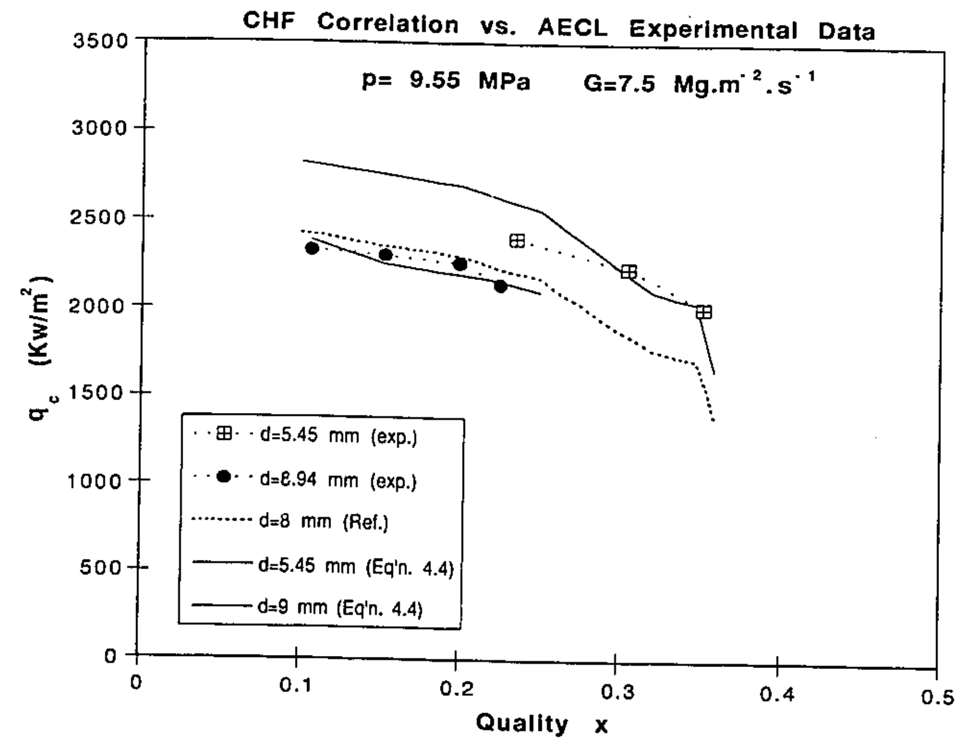

Figure 6.11: Correlation Equation (4.4) CHF Predictions vs. AECL Experiment (Pressure=9.55 MPa, Mass Flux=7.5 $Mg.m^{-2}.s^{-1}$ Diameter=5.45 and 8.94 mm)

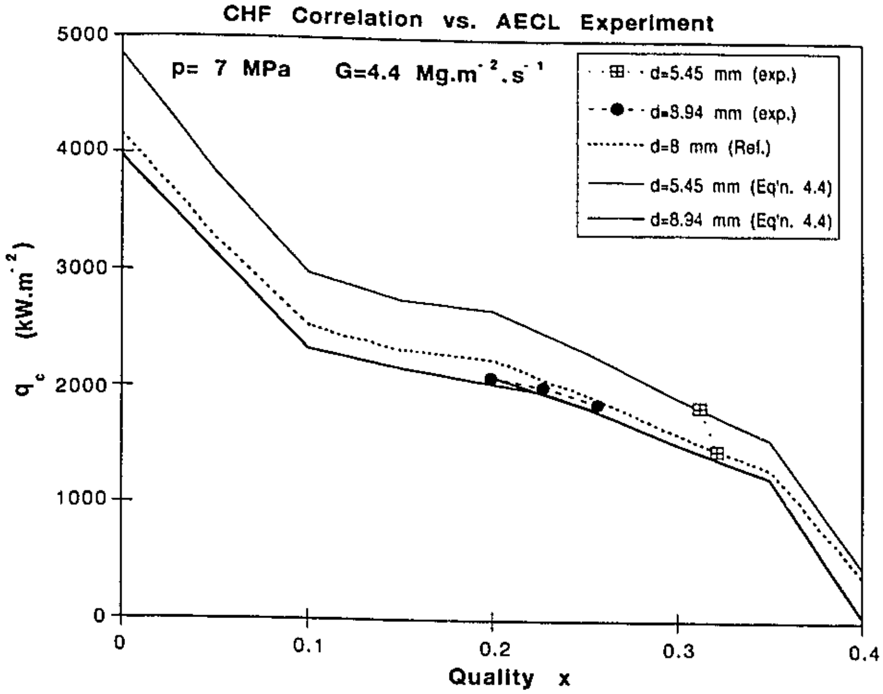

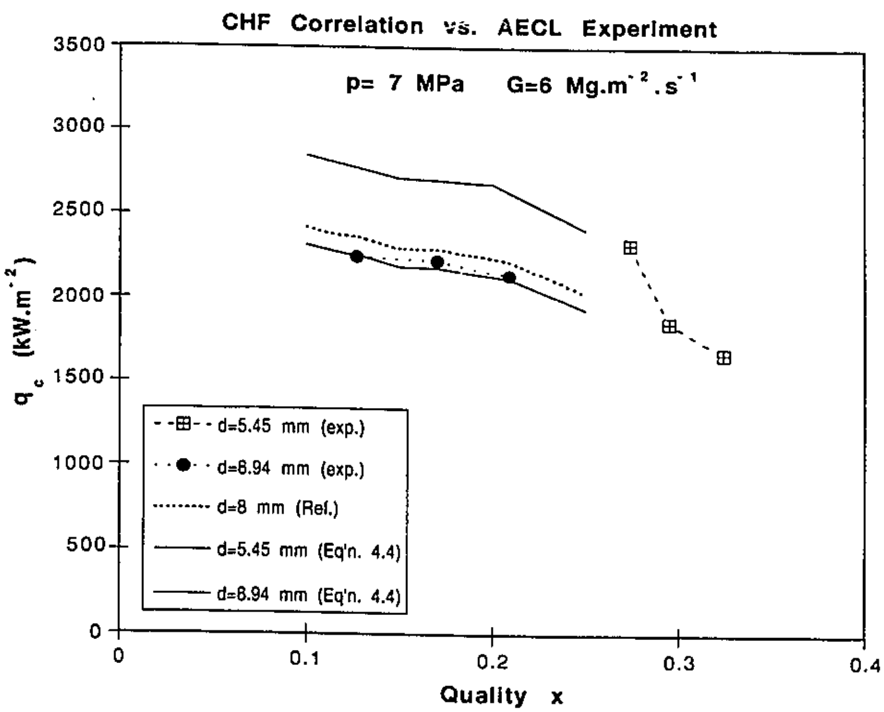

Figure 6.12: Correlation Equation (4.4) CHF Predictions vs. AECL Experiment (Pressure=7 MPa, Mass Flux=4.4 and 6 $Mg.m^{-2}.s^{-1}$ Diameter= 5.45 and 8.94 mm)

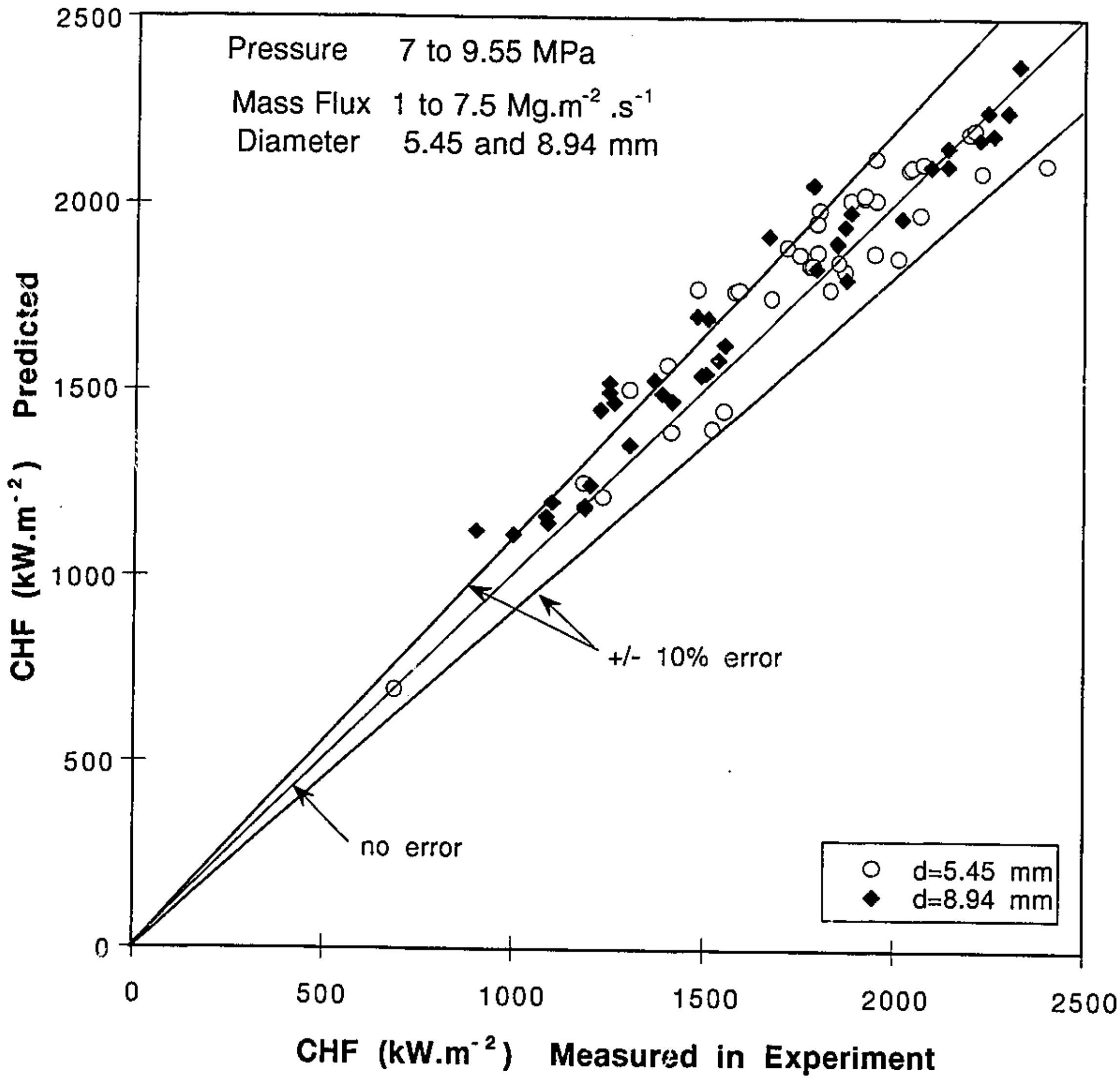

Figure 6.13: Predicted CHF vs. Measured CHF from AECL Experiment (Pressure=7 to 9.55 MPa, Mass Flux=1 to 7.5 $Mg.m^{-2}.s^{-1}$; Diameter=5.45 and 8.94 mm)

Table 6.1: AECL CHF Experimental Data and CHF Predicted by Equations (4.4)
(Tube diameter=8.94 mm, Heated length=2.49 m)

Experiment						Eq'n. (4.4) Prediction	
Run No.	p (MPa)	G ($kg.m^{-2}.s^{-1}$)	x	Subcooling ($kJ.kg^{-1}$)	CHF ($kW.m^{-2}$)	CHF ($kW.m^{-2}$)	Error
92318	9560	1956.3	0.353	145	1086.2	1162.6	0.0703
92418	9520	1979.7	0.347	201	1186.1	1185.9	-0.0001
92215	9500	1981.3	0.362	75	1000.2	1112.5	0.1123
92316	9510	1983.5	0.354	137	1091.6	1144.8	0.0487
92418	9510	1984.8	0.346	201	1186.1	1190.8	0.0039
92113	9570	1985.1	0.354	33	904.2	1124.1	0.2432
93117	9570	2972.1	0.236	29	1100.8	1199.8	0.0900
93218	9520	2974.0	0.280	73	1200.7	1246.9	0.0385
93320	9510	2998.1	0.260	134	1303.5	1355.2	0.0397
93422	9550	3035.8	0.228	203	1388.6	1494.4	0.0762
94424	9560	4339.4	0.147	201	1553.0	1625.2	0.0465
94323	9570	4500.3	0.180	139	1535.4	1586.2	0.0331
94223	9500	4506.9	0.222	70	1491.4	1542.7	0.0344
94121	9560	4512.5	0.249	16	1415.0	1473.6	0.0414
96428	9560	5928.2	0.111	205	1881.8	1981.2	0.0528
96228	9500	6011.7	0.204	67	1847.0	1896.6	0.0269
96328	9570	6019.5	0.154	140	1867.9	1943.4	0.0404
96228	9510	6021.0	0.204	68	1846.5	1898.9	0.0284
96127	9580	6041.0	0.233	18	1789.4	1830.0	0.0227
97132	9510	7529.7	0.225	13	2140.1	2153.7	0.0064
97234	9500	7442.3	0.199	70	2260.5	2188.2	-0.0320
97335	9500	7466.3	0.152	139	2299.0	2250.9	-0.0209
97435	9500	7611.9	0.106	198	2328.0	2376.1	0.0207
72422	7030	2006.8	0.403	229	1503.9	1547.1	0.0288
72219	7030	2009.1	0.414	79	1263.2	1468.9	0.1629
72320	7030	2016.6	0.405	146	1368.0	1528.6	0.1174
72219	7030	2026.2	0.409	73	1250.6	1496.1	0.1963
72219	7030	2030.3	0.405	77	1250.6	1522.3	0.2173
72118	7030	2051.2	0.414	44	1227.1	1449.2	0.1810
73122	7030	2994.4	0.325	61	1479.2	1701.7	0.1504
73223	7030	3001.1	0.325	71	1508.1	1696.2	0.1247
73325	7030	3017.7	0.306	155	1664.9	1916.3	0.1510
73426	7030	3025.2	0.292	216	1780.7	2053.4	0.1532
74330	7030	4494.4	0.227	160	2019.7	1965.8	-0.0267
74228	7030	4505.5	0.257	76	1872.9	1801.0	-0.0384
74431	7030	4531.3	0.199	215	2095.7	2103.0	0.0035
76232	7040	5935.0	0.209	88	2139.7	2106.4	-0.0156
76334	7040	6006.4	0.170	158	2225.2	2177.1	-0.0216
76434	7040	6033.3	0.127	224	2245.7	2251.6	0.0026
Total number of points: 39						Mean Error	0.0618
						RMS Error	0.0957

Table 6.2: AECL CHF Experimental Data and CHF Predicted by Equation (4.4)
(Tube diameter=5.45 mm, Heated length=2.51 m)

Experiment						Eq'n. (4.4) Prediction	
Run No.	p (MPa)	G ($kg.m^{-2}.s^{-1}$)	x	Subcooling ($kj.kg^{-1}$)	CHF ($kW.m^{-2}$)	CHF ($kW.m^{-2}$)	Error
91506	9550	1091.0	0.672	656	688.5	654.1	-0.0500
94211	9620	4100.6	0.362	71	1234.3	1229.9	-0.0036
94513	9590	4246.9	0.276	290	1519.6	1493.2	-0.0173
94412	9550	4245.6	0.297	210	1402.8	1599.1	0.1399
94110	9600	4223.7	0.361	33	1183.4	1269.3	0.0726
94311	9560	4291.9	0.317	134	1303.9	1528.8	0.1725
94313	9650	4368.7	0.342	141	1412.8	1416.0	0.0023
94414	9710	4430.9	0.331	205	1551.0	1477.1	-0.0476
96315	9550	5792.7	0.297	146	1712.2	1955.8	0.1423
96213	9580	5813.7	0.315	78	1578.7	1832.8	0.1609
96415	9580	5901.2	0.284	202	1867.2	1893.3	0.0140
96417	9640	5917.5	0.303	201	1945.4	1943.6	-0.0009
96214	9640	5933	0.334	73	1672.0	1814.8	0.0854
96517	9600	5936.4	0.245	276	1946.8	2214.1	0.1373
96113	9570	5993.5	0.340	34	1587.3	1837.9	0.1579
96518	9630	6013.6	0.280	259	2067.7	2057.2	-0.0051
96315	9550	6056.5	0.294	137	1746.4	1941.9	0.1119
97216	9570	6873.2	0.318	78	1882.3	2108.7	0.1203
97115	9570	6895.5	0.343	19	1792.3	1960.1	0.0936
97317	9570	6917.5	0.302	138	2036.3	2198.7	0.0798
97116	9550	6941.4	0.332	32	1796.9	2080.8	0.1580
97116	9550	6972.3	0.339	18	1790.9	2045.2	0.1420
97318	9510	6985.8	0.300	137	2044.5	2204.9	0.0785
97217	9560	7001.9	0.318	76	1919.9	2117.4	0.1029
97216	9570	7002.7	0.321	82	1948.2	2111.2	0.0837
97217	9560	7037.1	0.317	76	1919.1	2126.0	0.1078
97419	9560	7040.5	0.278	202	2197.1	2304.3	0.0488
97318	9550	7043.1	0.297	144	2073.1	2216.6	0.0692
97419	9530	7052.1	0.276	207	2210.4	2314.0	0.0469
97319	9580	7421.4	0.305	145	2229.9	2198.8	-0.0140
97521	9580	7461.3	0.235	278	2399.8	2229.9	-0.0708
97117	9580	7517.0	0.352	20	2008.2	1957.1	-0.0254
74515	7030	4212.5	0.314	305	1773.1	1826.1	0.0299
74515	7030	4227.1	0.314	305	1779.9	1826.0	0.0259
74515	7030	4226.6	0.323	304	1826.5	1761.7	-0.0355
74312	7050	4267.4	0.321	157	1478.9	1763.2	0.1922
74515	7030	4352.4	0.312	315	1849.5	1839.5	-0.0054
Total number of points: 37						Mean Error	0.0622
						RMS Error	0.0939

7. CONCLUSIONS AND FINAL REMARKS

(1) An in-depth analysis of the effect of tube diameter on CHF has been performed with the AECL CHF data bank. This has never been carried out before, since most data sets covered only a narrow range of flow conditions, or for one tube diameter.

(2) Available correlations and semi-analytical models have been systematically reviewed for their prediction of the tube-diameter effect on CHF. Most correlations account for the effect by expressing CHF in terms of the diameter to a power 'n' (i.e., CHF $\propto d^n$), which ranges from -0.6 to 0.2. Pressure- and quality-dependent coefficients of n have also been suggested. The methodology to account for the tube-diameter effect is not explicit in semi-analytical models. It is introduced through the closure relationships, which are often empirically based. In general, the tube-diameter effect on CHF can also be expressed in a form similar to the correlation (i.e., CHF $\propto d^n$); the values of 'n' are between -0.7 to -0.5.

(3) Based on the recommended form of the diameter correction factor, the coefficient 'n' has been modified to improve the prediction accuracy. Based on an optimization with a large amount of CHF data, pressure, mass flux, and quality effects have been included in this factor. The prediction accuracy has been improved with the updated expression of 'n', as compared to those of other correction factors previously suggested to account for the diameter effect. Furthermore, more data have been predicted with the updated expression within the ±10% error range than with the others.

(4) The prediction of the tube diameter effect on CHF has been examined in detail for two semi-analytical models: one for the subcooled boiling (near-wall bubbly flow), and the other for the saturated boiling (annular-film dryout). Based on the Reynolds analogy, the subcooled-boiling CHF model shows its characteristics with respect to the tube-diameter effect being similar to those of the updated correction factor. The annular-film dryout model exhibits a similar trend. However, its CHF predictions differ considerably from

the experimental data at most conditions. Contrary to the observations made from the examination of the AECL data base, the tube-diameter effect exhibited in this model appears to be less dependent on pressure, mass flux and quality.

(5) The updated correction factor for the tube-diameter effect has been validated using experimental data obtained in the high-pressure steam-water loop at Chalk River Laboratories. These data cover a wide range of flow conditions in tubes of two different inside diameters (5.45 mm and 8.94 mm). The overall average prediction error is 6.2% and the rms error is 9.54% for 76 data points.

(6) The updated correction factor can be further improved by introducing non-dimensional parameters. This has not been incorporated in the present study, which focused mainly on the high-pressure steam-water flow (for nuclear-reactor applications). By non-dimensionalizing the correction factor, the tube-diameter effect in tubes cooled by non-aqueous fluids (such as Freons) can also be accounted for.

(7) The complexity of the tube-diameter effect on CHF has been clearly demonstrated in this study, through its analysis of experimental data obtained in various test facilities and its review of correlations and semi-analytical models. While an empirical approach is taken into account for the diameter effect in this study, it is believed that a well-validated analytical model is the ideal tool by which to reflect the diameter effect as well as other separate effects on CHF. The validity of existing models is limited by the lack of relevant data with which to derive solid closure relationships. Further studies and research are needed to provide various closure equations (e.g., near-wall void fraction in subcooled boiling, entrainment rate, deposition rate) from future experimental data.

8. REFERENCES

Alekseev, G.V., Zenkevich, B.A., Peskov, O.L., Sergeev, N.D. and Subbotin, V.I., (1964), "Burn-Out Heat Fluxes Under Forced Water Flow", Third United Nations International Conference on the Peaceful Uses of Atomic Energy, paper 327a.

Barnett, P.G., (1983), "An Investigation into the Validity of Certain Hypothesis Implied by Various Burnout Correlations", AEEW-R 214.

Beattie, D.R.H., (1975), "Friction Factors and Regime Transitions in High Pressure Steam-water Flows", ASME 75-WA/HT-4.

Becker, K.M. and Soderquist, B., (1992), "Assessment of Round Tube CHF Tables", Paper Presented at the European Two-Phase Flow Group Meeting, Stockholm, June 1-3 (also KTH-NEL-55).

Becker, K.M., Strand, G., Djursing, D., Eklind, O., Lindberg, K. and Osterdahl, C., (1971), "Round Tube Burnout Data for Flow of Boiling Water at Pressures between 30 and 200 bar", KTH-NEL-14.

Becker, K.M. and Ling, C.H., (1970), "Burnout Measurements in a Round Tube of 7100 mm Heated Length", KTH-NEL-13.

Becker, K.M., (1965), "An Analytical and Experimental Study of Burnout Conditions in Vertical Round Ducts", AE-178.

Becker, K.M., Hernborg, G., Bode, M. and Eriksson, O., (1965), "Burnout Data for Flow of Boiling Water in Vertical Round Ducts, Annuli and Rod Clusters", AE-177.

Becker, K.M. and Persson, P., (1963), "Measurements of Burnout Conditions for Flow of Boiling Water in Vertical Round Ducts - Part 2", AE-114.

Becker, K.M. and Persson, P., (1963), "An Analysis of Burnout Conditions for Flow of Boiling Water in Vertical Round Ducts", ASME Publication 63-WA-51.

Becker, K.M., (1962), "Measurements of Burnout Conditions for Flow of Boiling Water in Vertical Round Ducts - Part 1", AE-87.

Bennett, A.W., Hewitt, G.F., Kearsey, H.A. and Keeys, R.K.F., (1965), "Measurements of Burnout Heat Flux in Uniformly Heated Round Tubes at 1000 p.s.i.a.", AERE-R 5055.

Bennett, A.W., Collier, J.G. and Lacey, P.M.C., (1963), "Heat Transfer to Mixtures of High Pressure Steam and Water in an Annulus, Part III: ", AERE-R 3934.

Bergel'son, B.R., (1980), "Burnout for Boiling With Preheating and Forced Convection", Teploenergetika, Vol. 58, No. 1 (from Kirillov, P.L., 1992).

Bergles, A.E., (1977), "Burnout in Boiling Heat Transfer. Part II: Subcooled and Low Quality Forced Convection Systems", Nuclear Safety, Vol. 18, No. 2.

Bergles, A.E., (1963), "Subcooled Burnout in Tubes of Small Diameter", ASME 63-WA-182.

Bergles, A.E., Lopina, R.F. and Fiori, M.P., (1967), "CHF and Flow Pattern Observations for Low Pressure Water Flowing in Tubes", Journal of Heat Transfer.

Bertoletti, S., Gaspari, G.P., Lombardi, C., Soldaini, G. and Zavattarelli, R., (1964), "Heat-Transfer Crisis in Steam-Water Mixtures - Experimental Data in Round Tubes and Vertical Upflow Obtained During the CAN-2 Program", CISE R-90.

Biasi, L., Clerici, G.C., Garribba, S., Sala, R. and Tozzi, A., (1967), "Studies on Burnout. Part 3: A New Correlation for Round Ducts and Uniform Heating and Its Comparison with World Data", Energia Nucleare, Vol. 14, pp. 530-536.

Boltenko, E.A., Katan, I.B. and Zyatnina, O.A., (1990), "Calculation of Heat Transfer Burnout in Channels with Different Flow Regimes", Proc. of Conference Thermophysics-90, Obninsk, Russia (in Russian).

Boltenko, E.A., Pomietko, R.S., Katan, I.B. and Ziatnina, O.A., (1989), "Effect of Diameter on CHF", (in Russian) (Translated by Doerffer, S.S., 1991).

Boltenko, E.A., Vinogradov, W.N., Katan, I.B. and Pomietko, R.S., (1988), "Effect of Tube Diameter on CHF at Various Two-Phase Flow Regimes", Report IPE-1889 (in Russian), Obninsk (Translated by Doerffer, S.S., 1991).

Borodin, A.S. and Macdonald, I.P.L., (1983), "Separate Measurements of Light Water (H_2O) and Heavy Water (D_2O) Flow Boiling Critical Heat Flux in a Vertical Cylindrical Tube Geometry", AECL report CRNL-2538.

Borodin, A.S. and MacDonald, I.P.L., (1984), AECL Internal unpublished report.

Bowring, R.W., (1972), "A Simple but Accurate Round Tubes: Uniform Heat Flux Dryout Correlation over the Pressure Range 0.7-17.0 MN/m^2", AEEW-R-789.

Burck, E., (1968), "The Influence of Artificial Roughness on the Increase in CHF for Water under Forced Convection in Annuli", EUR 404d.

Celata, G.P., Cumo, M., Mariani, M., Simoncini, M. and Zummo, G., (1994), "Rationalization of Existing Mechanistic Models for the Prediction of Water Subcooled Flow Boiling CHF", Int. J. Heat Mass Transfer, Vol. 37, pp. 347.

Celata, G.P., Mariani, A., Nariai, H. and Inasaka, F., (1993), "Influence of Channel Diameter on Subcooled Flow Boiling Burnout at High Heat Fluxes", Technical Notes, Int. J. Heat Mass Transfer, Vol. 36, No. 13, pp. 3407.

Celata, G.P., Cumo, M. and Mariani, A., (1993), "Burnout in Highly Subcooled Water Flow Boiling in Small Diameter Tubes", Int. Journal of Heat & Mass Transfer, Vol. 36. No. 5.

Celata, G.P., (1990), "Preliminary Remarks on High Heat Flux CHF in Subcooled Water Flow Boiling", Heat and Technology, Vol. 8, No. 1-2.

Chang, S.H., Baek, W.P. and Bae, T.M., (1991), "A Study of Critical Heat Flux for Low Flow of Water in Vertical Round Tubes Under Low Pressure", Nucl. Eng. Des., Vol. 132, No. 2, pp. 225-237.

Chang, Y.P., (1961), "An Analysis of the Critical Conditions and Burnout in Boiling Heat Transfer", USAEC Report TID-14004.

Cheng, S.C., Poon, K.T., Lau, P., Heng. K.T., Doan, T. and Chan, C.Y., (1983), "CHF Measurements and Construction of CHF Table", Final report submitted to AECL Research.

Cheng, X., Erbacher, F.J., Staron, E. and Zeggel, W., (1992), "Critical Heat Flux in Circular Tubes at High Pressures and High Mass Fluxes", Paper presented at the 5th International Topical Meeting on Nuclear Reactor Thermalhydraulics, Salt Lake City, Utah, USA.

Chin, L., (1984), "Annular Film Dryout Model", M.A.Sc. Thesis, University of Ottawa.

Collier, J.G., (1972), "Convective Boiling and Condensation", McGraw-Hill Book Company, New York.

De Bortoli, R.A., Green, S.J., Letourneau, B.W., Troy, M. and Weiss, A., (1958), "Forced Convection Heat Transfer Burnout Studies for Water in Rectangular Channels and Round Tubes at Pressures Above 500 p.s.i.a.", WAPD-188.

Dell, F.R., Hewitt, G.F., Keeys, R.K.F. and Stinchcombe, R.A., (1969), "Burnout Heat Flux Measurements in a Long Tube", AERE-M 2216.

Doroshchuk, V.E., Levitan, L.L. and Lanstman, F.P., (1980), "Boiling Crisis in Evaporator Tubes", Heat Transfer, Soviet Research, Vol. 12, No. 6.

Doroshchuk, V.E., Levitan, L.L. and Lantzman, F.P., (1975a), "Investigation into Burnout in Uniformly Heated Tubes", ASME Publication 75-WA/HT-22.

Doroshchuk, V.E., Levitan, L.L. and Lantzman, F.P., (1975b), "Recommendations for Calculating Burnout in a Round Tube with Uniform Heat Release", Teploenergetika, Vol. 22, No. 12, pp. 66-70.

Drobavicius, A.J. and Sinkunas, S.S., (1978), "Heat Transfer of a Turbulent Water Film at Different Initial Flow Conditions and High Temperature Gradients", 6th Int. Heat Transfer Conf., Toronto, August.

Era, A., Gaspari, G.P., Hassid, A., Milani, A. and Zavattarelli, R., (1967), "Heat Transfer Data in the Liquid Deficient Region for Steam-Water Mixtures at 70 kg/cm^2 flowing in Tubular and Annular Conduits", CISE R-184.

Govan, A.H., Owen, D.G. and Hewitt, G.F., (1988), "An improved CHF modeling Code", 2nd UK National Conference on Heat Transfer, Glasgow, September 14-16 (also IME Publications, Vol. 2, pp. 1746).

Griffel, J., (1965), "Forced Convection Boiling Burnout for Water in Uniformly Heated Tubular Test Sections", NYO-187-7.

Groeneveld, D.C., Leung, L.K.H., Kirillov, P.L., Bobkov, V.P., Smogalev, I.P., Vinogradov, V.N., Huang, X.C. and Royer, E., (1996), "The 1995 Look-up Table for Critical Heat Flux in Tubes", Nuc. Eng. Des. (in print).

Groeneveld, D.C. and Snoek, C.W., (1986), "A Comprehensive Examination of Heat Transfer Correlations Suitable for Reactor Safety Analysis", Multiphase Science and Technology, Vol. 2, pp. 181-274.

Groeneveld, D.C., Cheng, S.C. and Doan, T., (1986), "1986 AECL-UO Critical Heat Flux Look-up Table", Heat Transfer Engineering, Vol. 7, pp. 46-62.

Groeneveld, D.C., (1985), AECL undocumented data.

Groeneveld, D.C., (1982), "A General CHF Prediction Method for Water, Suitable for Reactor Accident Analysis", C.E.N.G. Report DRE/STT/SETRE/82-2-E/DG.

Haramura, Y. and Katto, Y., (1983), "A New Hydrodynamic Model of CHF, applicable widely to both Pool and Forced Convection Boiling on Submerged Bodies in Saturated Liquids", Int. J. Heat Mass Transfer, Vol. 26, pp. 389.

Hassid, A., Milani, A., Ravetta, R. and Rubiera, L., (1967), "Heat Transfer Crisis with Steam-Water Mixtures in Round Conduits: Reproducibility Tests with Different Experimental Facilities", CISE-R-236.

Hewitt, G.F. and Govan, A.H., (1990) "Phenomenological Modelling of Non-equilibrium Flows With Phase Change", Int. J. Heat Mass Transfer, Vol. 33, pp 229-242.

Hewitt, G.F., (1974), "Calculation of CHF in Forced Convective Boiling", Proc. of the 5th Int. Heat Transfer Conf., Tokyo, September 3-7, Vol. 4, pp. 290-294.

Hewitt, G.F. and Hall-Taylor N.S., (1970), "Annular Two Phase Flow", Pergamon Press.

Hewitt, G.F., Kearsey, H.A., Lacey, P.M.C. and Pulling, D.J., (1965), "Burnout and Film Flow in the Evaporation of Water in Tubes", AERE-R 4864.

Hewitt, G.F., (1964), "A Method of Representing Burnout Data in Two-phase Heat Transfer for Uniformly Heated Round Tubes", AERE-R 4613.

Inasaka, F. and Nariai, H., (1989), "Critical Heat Flux of Subcooled Flow Boiling With Water", Proc. of the 4th International Topical Meeting on Nuclear Reactor Thermalhydraulics, Vol. 1, pp. 111-120.

Jens, W.H. and Lottes, P.A., (1951), "Analysis of Heat Transfer, Burnout, Pressure Drop and Density Data for High Pressure Water", ANL-4627.

Jordan, D.P. and Leppert, G., (1962), "Pressure Drop and Vapor Volume With Subcooled Nucleate Boiling", Int. J. Heat Mass Transfer, Vol. 5, pp. 751-761.

Judd, D.F. and Wilson, R.H., (1967), "Non-Uniform Heat Generation Experimental Program", BAW-3238-13 (also EURAEC-1846).

Katto, Y., (1991), "A Prediction Model of Subcooled Water Flow Boiling CHF for Pressure in the Range 0.1-20 MPa", Int. J. Heat Mass Transfer, Vol. 35, No. 5, pp. 1115-1123.

Katto, Y., (1990a), "A Physical Approach to Critical Heat Flux of Subcooled Flow Boiling in Round Tubes", Int. J. Heat Mass Transfer, Vol. 33, No. 4, pp. 611-620.

Katto, Y., (1990b), "Prediction of Critical Heat Flux of Subcooled Flow Boiling in Round Tubes", Int. J. Heat Mass Transfer, Vol. 33, No. 9, pp. 1921-1928.

Katto, Y., (1978), "A Generalized Correlation of CHF for the Forced Convection Boiling in Vertical Uniformly Heated Round Tubes", Int. J. Heat Mass Transfer, Vol. 21, pp. 1527-1542.

Katto, Y., (1960), "An Analytical Investigation on CHF of Flow Boiling in Uniformly Heated Tubes with Special Reference to Governing Dimensionless Groups", Int. J. Heat Mass Transfer, Vol. 25, pp. 1353.

Kirillov, P.L., (1992), Private communication.

Kirillov, P.L., Bobkov, V.P., Boltenko, E.A., Vinogradov, V.N., Katan, I.B. and Smogalev, I.P., (1991a), "Lookup Tables of Critical Heat Fluxes", Atomnaya Energiya, Vol. 71, No. 1, pp. 18-28, July (in Russian).

Kirillov, P.L., Bobkov, V.P., Boltenko, E.A., Katan, I.B., Smogalev, I.P., Vinogradov, V.N., (1991b), "New CHF Table for Water in Round Tubes", Report IPPE-2225, Obninsk, Russia.

Kirillov, P.L., Bobkov, V.P., Vinogradov, V.N., Donisov, V.S., Ivashkevitch, A.A., Katan, I.B., Paniutchev, E.I., Smogalev, I.P. and Sal'nikova, O.B., (1989a), "On Standard Critical Heat Flux Data for Round Tubes", Proceedings of the 4th International Topical Meeting on Nuclear Reactor Thermalhydraulics, Karlsruhe, F.R.G., Vol. 1, pp. 103-108.

Kirillov, P.L., Bobkov, V.P., Boltenko, E.A., Vinogradov, V.N., Ivashkevitch, A.A., Katan, I.B. and Smogalev, I.P., (1989b), "A Method of the Development of Standard CHF Data for Tubes with Uniform Heat Flux", FEI-2030, Obninsk, USSR (in Russian).

Kirillov, P.L., Peskov, O.L. and Serdun', N.P., (1984), "Burnout Control Experiment for Water Flow in Tubes", Ser. 1, Vol. 54, IVTAN, Moscow, p. 423 (from Kirillov, P.L., 1992).

Kline, S.J. and McClintock, F.A., (1953), "Describing Uncertainties in Single-Sample Experiments", Mech. Eng., vol. 75, pp. 3-8.

Kutateladze, S.S., (1970), "Fundamentals of Heat Transfer Theory", Siberian Branch of the USSR Academy of Sciences, Nauka.

Kutateladze, S.S., (1966), "The Concept of a Fluid with Disappearing Viscosity & some Problems of the Phenomenological Theory of Turbulence Near the Wall", Invited Lecture, 3rd Int. Heat Transfer Conf., Chicago.

Kutateladze, S.S., Leont'ev, A.L., (1966), "Some Applications of the Asymptotic Theory of the Turbulent Boundary Layer", Proc. 3rd Int. Heat Transfer Conf., AIchE, Vol. III, New York, p. 1.

Landislau, L., (1978), "Effect of Pressure on Critical Thermal Fluxes of Medium Diameters (4 mm)", Proc. of the Thermophysical Investigations for Guaranteeing the Reliability and Safety of Water-Moderated Water-Cooled Nuclear Reactors CMEA, paper TF-78, Budapest (from Kirillov, P.L., 1992).

Lee, C.H. and Mudawwar, I., (1988), "A Mechanistic Critical Heat Flux Model for Subcooled Flow Boiling Based on Local Bulk Flow Conditions", Int. J. Multiphase Flow, Vol. 14, No. 6, pp. 711-728.

Lee, C.H., Mudawwar, I. and Sesonske, A., (1986), "A New CHF Model for Subcooled 2-phase Flow through a Vertical Tube", Proc. Int. Symposium on Multi-phase Transport, Paper 15-17, Florida, December.

Lee, D.H., (1966), "An Experimental Investigation of Forced Convection Burnout in High Pressure Water. Part IV, Large Diameter Tubes at about 1600 p.s.i.", AEEW-R 479.

Lee, D.H., (1965), "An Experimental Investigation of Forced Convection Burnout in High Pressure Water. Part III. Long Tubes with Uniform and Non-Uniform Axial Heating", AEEW-R-355.

Lee, D.H. and Obertelli, J.D., (1963), "An Experimental Investigation of Forced Convection Burnout in High Pressure Water. Part 1. Round Tubes with Uniform Flux Distribution", AEEW-R-213.

Lee Y.B., Baek, W.P. and Cheng, S.H., (1992), "Theoretical Investigation of Vapor Blanket Velocity Based on Mass, Energy, and Momentum Balance to Predict CHF at Low Quality Flow", Int. Comm. Heat Mass Transfer, Vol. 19, pp. 619-628.

Leung, L.K.H., (1996), Private communication.

Leung, L.K.H. (1994), "A Model for Predicting the Pressure Gradient Along a Heated Channel During Flow Boiling", Ph.D. thesis, University of Ottawa.

Leung, L.K.H. and Groeneveld, D.C., (1993), "1993 Update of The Critical Heat Flux Table for Upward Flow of Steam-water Mixture in Uniformly Heated Tubes", AECL Report ARD-TD-397.

Levitan, L.L., (1990), "Two-phase hydrodynamics and burnout", draft.

Levitan, L.L., Lantsman, F.P. and Dedneva, (1981), "Investigation of the Influence of Tube Diameter on Burnout of the Second Kind", Thermal Engineering, Vol. 28, No. 7.

Levitan, L.L. and Lantsman, F.P., (1975), "Investigating Burnout with Flow of a Steam-water Mixture in a Round Tube", Thermal Engineering, Vol. 22, No. 1, pp. 102-105.

Lowdermilk, W.H., Lanzo, C.D. and Siegel, B.L., (1958), "Investigation of Boiling Burnout and Flow Stability for Water Flowing in Tubes", NACA-TN 4382.

Levy, S., (1966), "Forced Convection Subcooled Boiling - Prediction of Vapour Volumetric Fraction", General Electric Report GEAP-5157.

Macbeth, R.V., (1963), "Burnout Analysis, Part 4: Application of Local Conditions Hypothesis to World Data for Uniformly Heated Round Tubes and Rectangular Channels", AEEW-R-267.

Matzner, B., Moeck, E.O., Casterline, J.E. and Wikhammer, G.A., (1965), "Critical Heat Flux in Long Tubes at 1000 psi With and Without Swirl Promoters", ASME 65-WA/HT-30.

Matzner, B., (1963), "Basic Experimental Studies of Boiling Fluid Flow and Heat Transfer at Elevated Pressures", TID-18978.

Mayinger, F., (1967), "Investigations into the Critical Heat Flux in Boiling Water", EUR-3347.

Megalla, K.F., (1990), "Prediction of CHF in Annular and Wispy Annular Flow Regimes for Uniformly Heated Vertical Tubes", Modeling, Simulation and Control, ASME Press, Vol. 28, No. 2, pp. 1-16.

Menegus, R.L., (1959), "Burnout of Heating Surfaces in Water", Dupont Rept. DP-363, pp. 24-33.

Nariai, H., Inasaka, F. and Shimura, T., (1987), "CHF of Subcooled Flow Boiling in narrow tube", Proc. of the 1987 ASME-JSME Thermal Engineering Conference, Hawaii, March.

Nguyen, D.M. and Yin, S.T., (1975), "An Experimental Investigation of Water Critical Heat Flux in a Tubular Channel in Both Horizontal and Vertical Attitudes", Canadian Westinghouse Technical Memorandum, CWTM-013-HT.

Ornatskiy, A.P., (1969), "The Effect of Basic Regime Parameters and Channel Geometry on Critical Heat Fluxes in Forced Convection of Subcooled Water", Heat Transfer - Soviet Research, Vol. 1, Nc. 3, pp. 17-22.

Rudzinski, K.F., (1992), Private communication.

Rybin, R.A., (1963), "Investigation of Tube Diameter Effect on CHF of Boiling Water", Inzhenerno-fizichesky Zural, No. 2.

Smolin, V.N. and Semenovker, I.E., (1981), "Regions of Existence of Two Forms of Dependencies of Critical Steam Content on Heat-flux Density with Burnout", Thermal Engineering, Vol. 28, No. 4.

Smolin, V.N., Shpanskii, V.S., Esikov, V.I. et al., (1979), "Experimental Data and Calculation Methodology for Boiling Water Circulating in Tubes with Uniform and Nonuniform Heating", Problems of Atomic Science and Technology, Ser. Physics and Technology of Nuclear Reactors, Vol. 9, No. 5 (from Kirillov, P.L., 1992).

Smolin, V.I., Polyakov, V.K. and Esikov, V.I., (1964), "Burnout in a Steam-Generating Tube", Atomnaya Energiya, Vol. 16, No. 5 (from Kirillov, P.L., 1992).

Smolin, V.I., Polyakov, V.K. and Esikov, V.I., (1962), "Burnout in a Steam-Generating Tube", Atomnaya Energiya, Vol. 13, No. 4 (from Kirillov, P.L., 1992).

Snoek, C.W., (1988), AECL internal unpublished report.

Sugawara, S., (1990), "Analytical Prediction of CHF by FIDAS Code Based on Three-fluid and Film-Dryout Model", J. of Nuclear Science & Technology, Vol. 27, No. 1, pp. 12-29.

Swenson, H.S., (1962), "Influence of Axial Heat Flux Distribution on Departure from Nucleate Boiling in Water Cooled Tubes", ASME 62-WA-297.

Teyssedou, A., Olekhnowitch, A., Tapucu, A., Champagne, P. and Groeneveld, D.C., (1995), "Critical Heat Flux Data in a Vertical Tube at Low and Medium Pressures", Nuclear Engineering Design.

Thompson, B., and Macbeth, R.V., (1964), "Boiling Water Heat Transfer in Uniformly Heated Round Tubes: A Compilation of World Data with Accurate Correlations", AEEW-R-356.

Thorgerson, E.J., Knoebel, D.H., Gibbons, J.H., (1974), "A Model to Predict Convective Subcooled CHF", Journal of Heat Transfer.

Tippets, F.E., (1964), "Analysis of the CHF Condition in High Pressure Boiling Water Flows", Transactions of ASME, Feb.

Tong, L.S., (1975), "A Phenomenological Study of Critical Heat Flux", ASME 75-HT-68.

Tong, L.S. and Hewitt, G.F., (1973), "Overall Viewpoint of Flow Boiling CHF Mechanisms", ASME-HT-54.

Tong, L.S., (1972), "Boiling Crisis & Critical Heat Flux", U.S.A.E.C. Critical Review Series, Report TID-25887.

Tong, L.S., (1968), "Boundary Layer Analysis of the Flow Boiling Crisis", Int. Journal of Heat Mass Transfer, Vol. 11, No. 7, pp. 1208-1211.

Tong, L.S., (1964), "DNB (Burnout) Studies on an Open Lattice Core", Westinghouse Rept. WCAP-3736.

Toping, J., (1966), "Errors of Observation and Their Treatment", The Institute of Physics and the Physical Society, Monographs for Students, 3rd Edition, Chapman and Hall Limited, London.

Turner, J.M. and Wallis, G.B., (1965), "An Analysis of the Liquid Film in Annular Flow", USAEC Report NYO-3114-13.

Ueda, T. and Kim, K., (1982), "Dryout Heat Flux and Size of Entrained Drops in a Flow Boiling System", JSME, Vol. 200, pp. 200-212.

Vaitekunas, D.A., Tain, R.M. and Cheng, S.C., (1995), "Assessment of CHF Models", Topical report submitted to AECL, University of Ottawa.

Vandervort, C.L., Bergles, A.E. and Jensen, M.K., (1990), "Ultimate Limits of Boiling Heat Fluxes", Proc. of the 8th Symposium on Energy Engineering Sciences, Studies of Multiphase Media, ANL, Argonne, pp. 95.

Wallis, G.B., (1970), "Annular Two-phase Flow", J. Basic Engineering, Vol. 92, No. 1, pp. 59.

Weisman, J. and Pei, B.S., (1983), "Prediction of Critical Heat Flux in Flow Boiling at Low Qualities", Int. J. Heat Mass Transfer, Vol. 26, pp. 1463-1477.

Whalley, P.B., Hutchinson, P. and James, P.W., (1978), "Calculation of CHF in Complex Situations Using an Annular Flow Model", Proc. of the 6th Int. Heat Transfer Conf., Toronto, August.

Whalley P.B. and Hewitt G.F., (1978), "The Correlation of Liquid Entrainment Fraction and Entrainment Rate in Annular Two-phase Flow", U.K.A.E.A. Harwell Report AERE-R 9187.

Wheatherhead, R.J., (1963), "Nucleate Boiling Characteristics and the CHF Occurrence in Subcooled Axial Flow Water System", Argonne Nat. Lab. Report, ANL-6675.

White, F.M., (1991), "Viscous Fluid Flow", 2nd edition, New York, McGraw-Hill.

Williams, C.L. and Beus, S.G., (1980), "Critical Heat Flux Experiments in a Circular Tube With Heavy Water and Light Water", Westinghouse Electric Co. Report WAPD-TM-1462, Pittsburgh, Pa.

Yin, S.T., Liu, T.J., Huang, Y.D. and Tain, R.M., (1988), "Measurements of Critical Heat Flux in Forced Flow at Pressures up to the Vicinity of the Critical Point of Water", Proc. of the 25th National Heat Transfer Conference, Houston, Texas, July 24-27.

Young, H.D., (1962), "Statistical Treatment of Experimental Data", McGraw-Hill, New York.

Zenkevich, B.A., (1974), "Analysis and Generalization of Experimental Data on Heat Transfer Crisis Associated with Forced Convection of Cooling Water in Tubes", AECL-tr-Misc.-304.

Zenkevich, B.A., Peskov, O.L. and rgeev, N.D., (1971), "Burnout for Internal Water Flow in Uniformly Heated Long Tubes", Report FEI-254, Obninsk, Russia (from Kirillov, P.L., 1992).

Zenkevich, B.A., Peskov, O.L., Petrishcheva, G.A. et al., (1969), "Analysis and Correlation of Experimental Burnout Data for Forced Flow of Boiling Water in Tubes", Atomizdat, Moscow (from Kirillov, P.L., 1992).

Zuber, N. and Staub, F.W., (1966), "Stability of Dry Patches Forming in Liquid Films Flowing Over Heated Surfaces", Int. J. Heat Mass Transfer, Vol. 9, pp. 897.

Zuber, N., (1959), "Hydrodynamic Aspects of Boiling Heat Transfer", USAEC Report AECU-4439.

APPENDIX I

Plots of Experimental Data vs. Fitted Function $q_c = f(x)\ d^n$
for Data Set From Same Sources

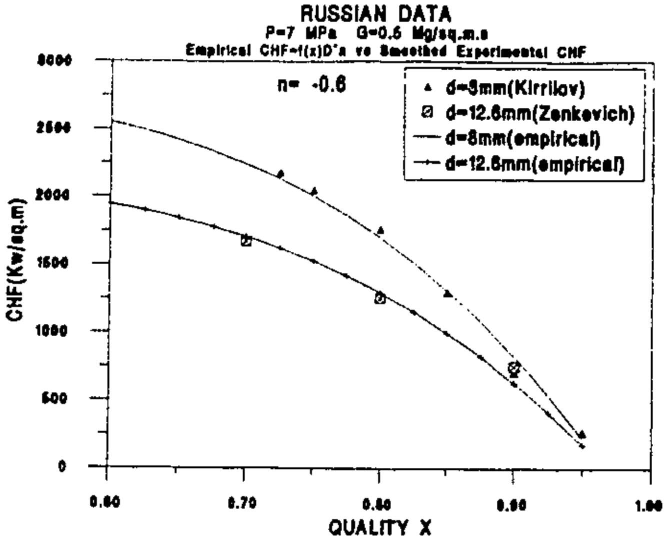
RUSSIAN DATA
P=7 MPa G=0.5 Mg/sq.m.s
Empirical CHF=f(x)D^n vs Smoothed Experimental CHF
n= -0.6
d=8mm(Kirrilov)
d=12.6mm(Zenkevich)
d=8mm(empirical)
d=12.6mm(empirical)
CHF(Kw/sq.m)
QUALITY X

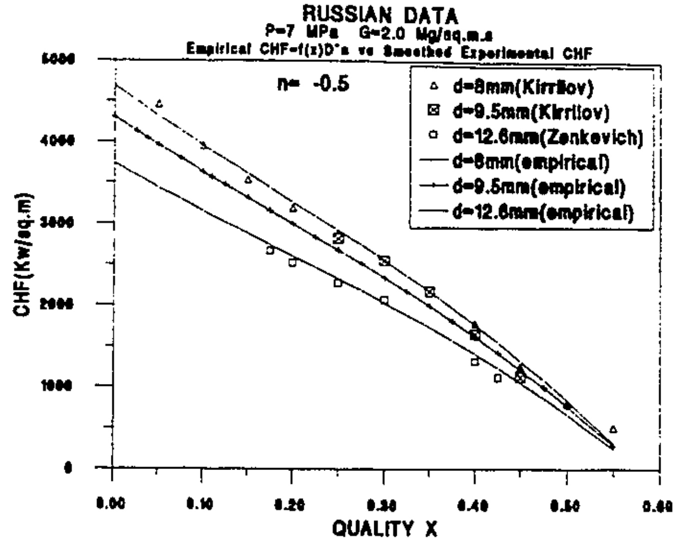
RUSSIAN DATA
P=7 MPa G=2.0 Mg/sq.m.s
Empirical CHF=f(x)D^n vs Smoothed Experimental CHF
n= -0.5
d=8mm(Kirrilov)
d=9.5mm(Kirrilov)
d=12.6mm(Zenkevich)
d=8mm(empirical)
d=9.5mm(empirical)
d=12.6mm(empirical)
CHF(Kw/sq.m)
QUALITY X

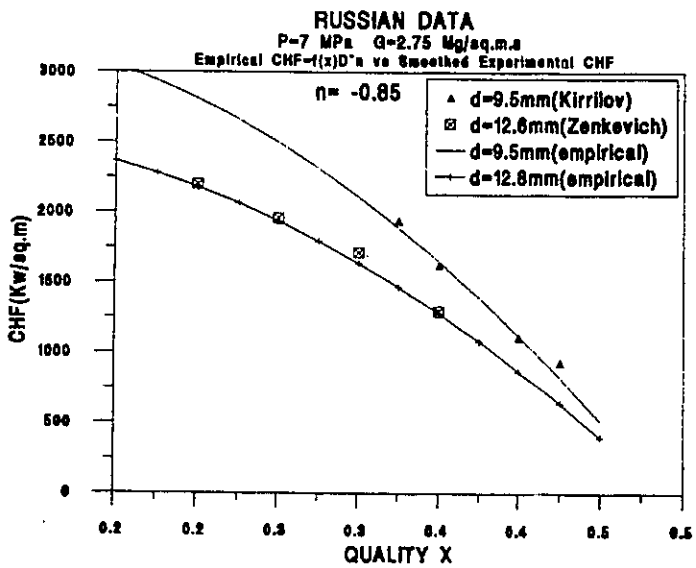
RUSSIAN DATA
P=7 MPa G=2.75 Mg/sq.m.s
Empirical CHF=f(x)D^n vs Smoothed Experimental CHF
n= -0.85
d=9.5mm(Kirrilov)
d=12.6mm(Zenkevich)
d=9.5mm(empirical)
d=12.6mm(empirical)
CHF(Kw/sq.m)
QUALITY X

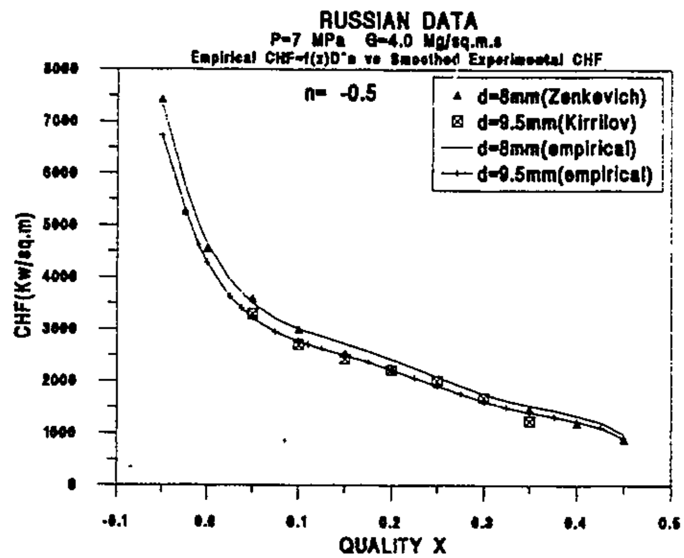
RUSSIAN DATA
P=7 MPa G=4.0 Mg/sq.m.s
Empirical CHF=f(x)D^n vs Smoothed Experimental CHF
n= -0.5
d=8mm(Zenkevich)
d=9.5mm(Kirrilov)
d=8mm(empirical)
d=9.5mm(empirical)
CHF(Kw/sq.m)
QUALITY X

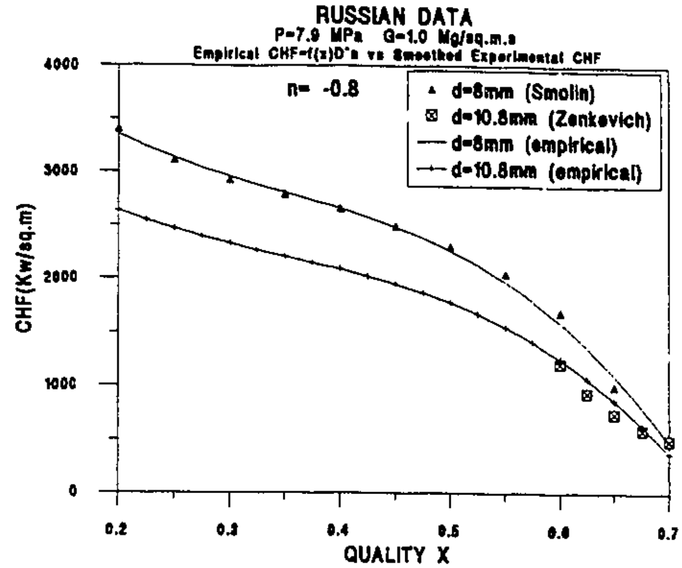
RUSSIAN DATA
P=7.9 MPa G=1.0 Mg/sq.m.s
Empirical CHF=f(x)D^n vs Smoothed Experimental CHF
n= -0.8
d=8mm (Smolin)
d=10.8mm (Zenkevich)
d=8mm (empirical)
d=10.8mm (empirical)
CHF(Kw/sq.m)
QUALITY X

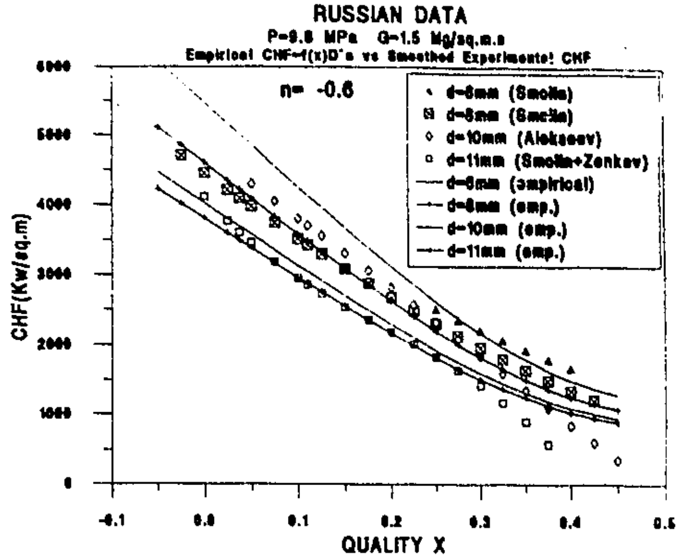
RUSSIAN DATA
P=9.8 MPa G=1.5 Mg/sq.m.s
Empirical CHF=f(x)D^n vs Smoothed Experimental CHF
n= -0.6
d=6mm (Smolin)
d=8mm (Smolin)
d=10mm (Alekseev)
d=11mm (Smolin+Zenkev)
d=6mm (empirical)
d=8mm (emp.)
d=10mm (emp.)
d=11mm (emp.)
CHF(Kw/sq.m)
QUALITY X

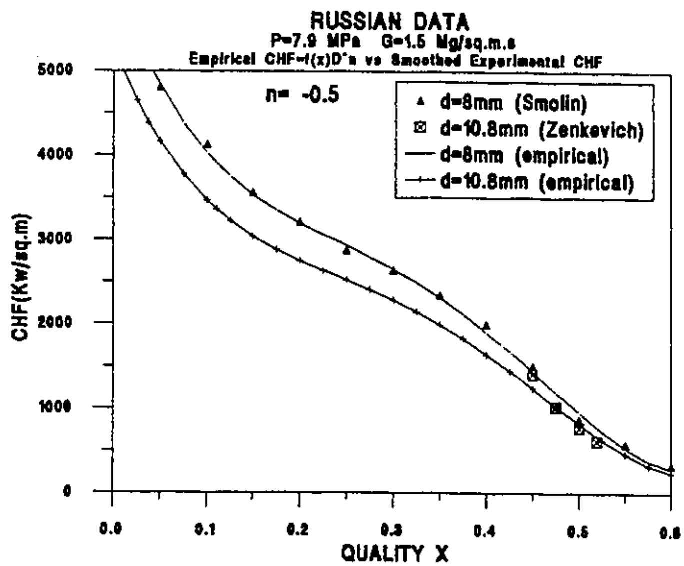
RUSSIAN DATA
P=7.9 MPa G=1.5 Mg/sq.m.s
Empirical CHF=f(x)D^n vs Smoothed Experimental CHF
n= -0.5
d=8mm (Smolin)
d=10.8mm (Zenkevich)
d=8mm (empirical)
d=10.8mm (empirical)
CHF(Kw/sq.m)
QUALITY X

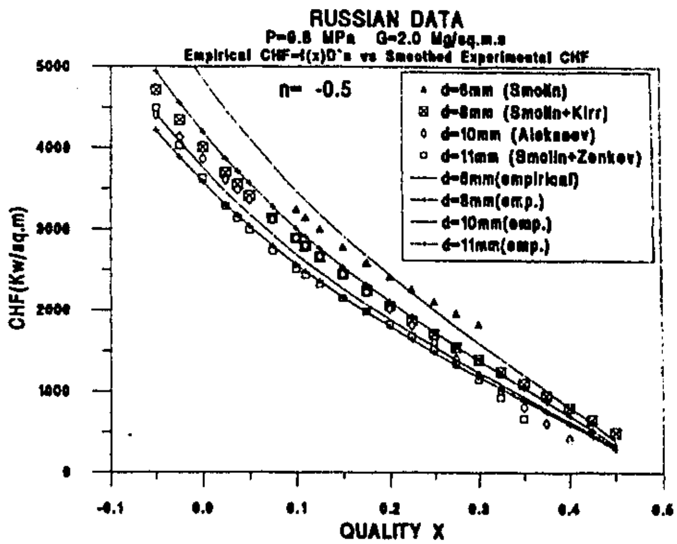
RUSSIAN DATA
P=9.8 MPa G=2.0 Mg/sq.m.s
Empirical CHF=f(x)D^n vs Smoothed Experimental CHF
n= -0.5
d=6mm (Smolin)
d=8mm (Smolin+Kirr)
d=10mm (Alekseev)
d=11mm (Smolin+Zenkev)
d=6mm(empirical)
d=8mm(emp.)
d=10mm(emp.)
d=11mm(emp.)
CHF(Kw/sq.m)
QUALITY X

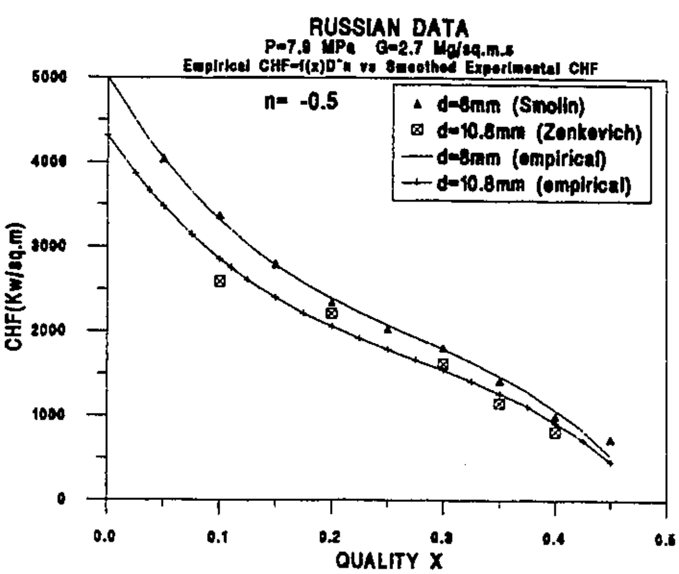
RUSSIAN DATA
P=7.9 MPa G=2.7 Mg/sq.m.s
Empirical CHF=f(x)D^n vs Smoothed Experimental CHF
n= -0.5
d=8mm (Smolin)
d=10.8mm (Zenkevich)
d=8mm (empirical)
d=10.8mm (empirical)
CHF(Kw/sq.m)
QUALITY X

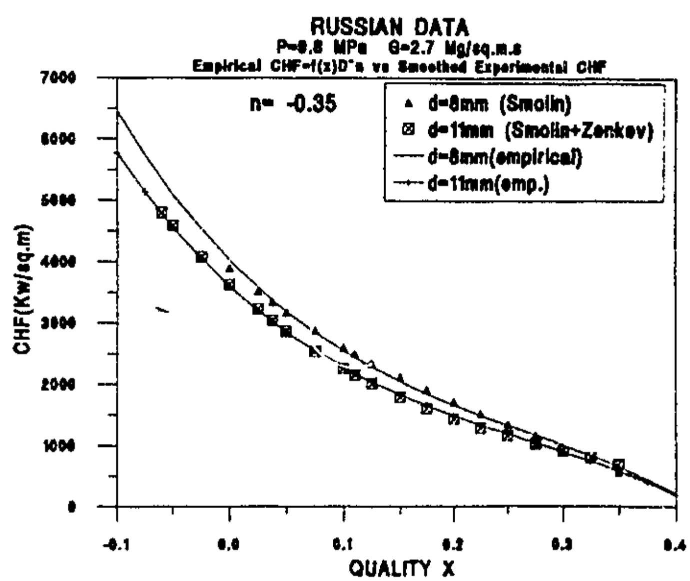
RUSSIAN DATA
P=9.8 MPa G=2.7 Mg/sq.m.s
Empirical CHF=f(x)D^n vs Smoothed Experimental CHF
n= -0.35
d=8mm (Smolin)
d=11mm (Smolin+Zenkev)
d=8mm(empirical)
d=11mm(emp.)
CHF(Kw/sq.m)
QUALITY X

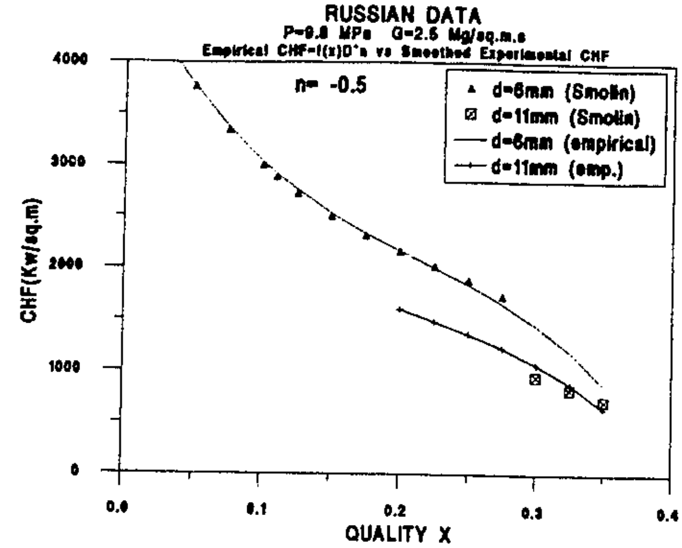
RUSSIAN DATA
P=9.8 MPa G=2.5 Mg/sq.m.s
Empirical CHF=f(x)D^n vs Smoothed Experimental CHF
n= -0.5
d=6mm (Smolin)
d=11mm (Smolin)
d=6mm (empirical)
d=11mm (emp.)
CHF(Kw/sq.m)
QUALITY X

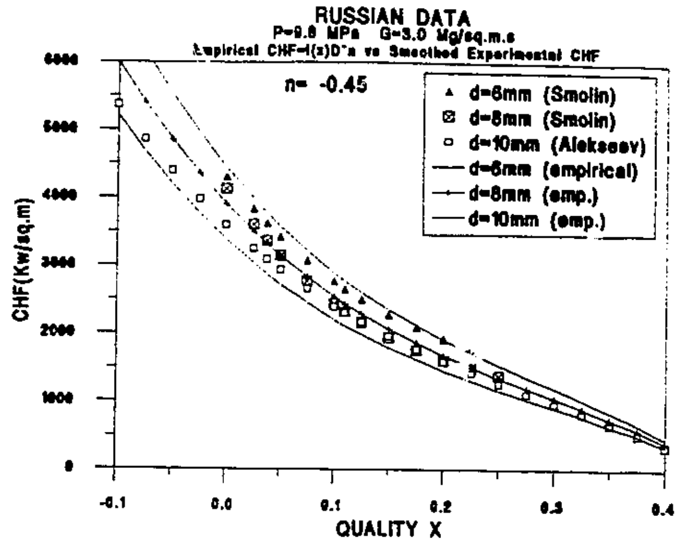
RUSSIAN DATA
P=9.8 MPa G=3.0 Mg/sq.m.s
Empirical CHF=f(x)D^n vs Smoothed Experimental CHF
n= -0.45
d=6mm (Smolin)
d=8mm (Smolin)
d=10mm (Alekseev)
d=6mm (empirical)
d=8mm (emp.)
d=10mm (emp.)
CHF(Kw/sq.m)
QUALITY X

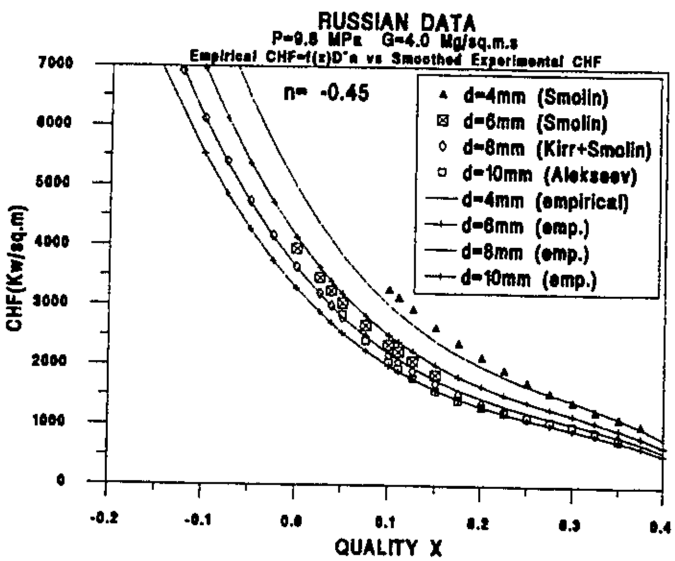
RUSSIAN DATA
P=9.8 MPa G=4.0 Mg/sq.m.s
Empirical CHF=f(x)D^n vs Smoothed Experimental CHF
n= -0.45
d=4mm (Smolin)
d=6mm (Smolin)
d=8mm (Kirr+Smolin)
d=10mm (Alekseev)
d=4mm (empirical)
d=6mm (emp.)
d=8mm (emp.)
d=10mm (emp.)
CHF(Kw/sq.m)
QUALITY X

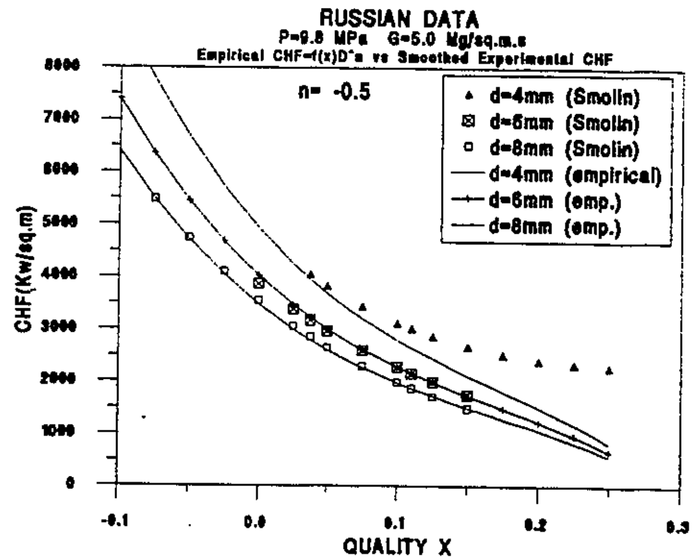
RUSSIAN DATA
P=9.8 MPa G=5.0 Mg/sq.m.s
Empirical CHF=f(x)D^n vs Smoothed Experimental CHF
n= -0.5
d=4mm (Smolin)
d=6mm (Smolin)
d=8mm (Smolin)
d=4mm (empirical)
d=6mm (emp.)
d=8mm (emp.)
CHF(Kw/sq.m)
QUALITY X

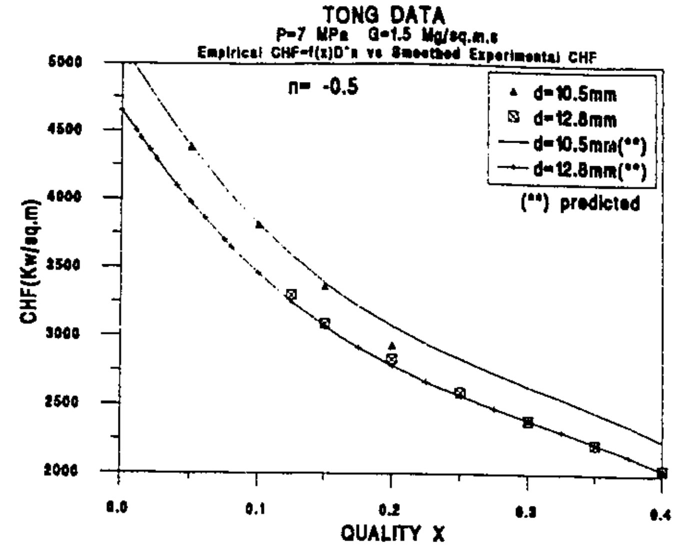
TONG DATA
P=7 MPa G=1.5 Mg/sq.m.s
Empirical CHF=f(x)D^n vs Smoothed Experimental CHF
n= -0.5
d=10.5mm
d=12.8mm
d=10.5mm(**)
d=12.8mm(**)
(**) predicted
CHF(Kw/sq.m)
QUALITY X

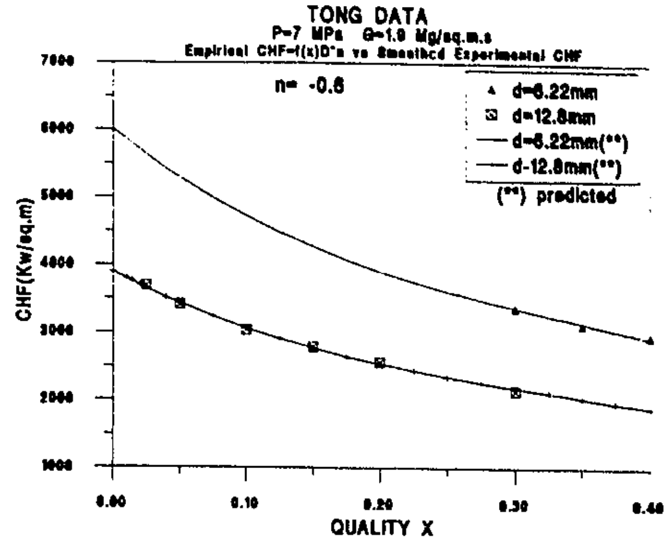
TONG DATA
P=7 MPa G=1.9 Mg/sq.m.s
Empirical CHF=f(x)D^n vs Smoothed Experimental CHF
n= -0.8
d=6.22mm
d=12.8mm
d=6.22mm(**)
d-12.8mm(**)
(**) predicted
CHF(Kw/sq.m)
QUALITY X

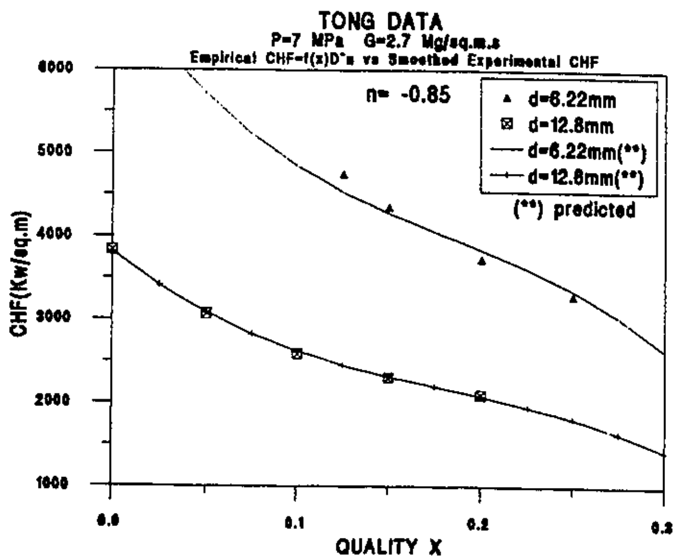
TONG DATA
P=7 MPa G=2.7 Mg/sq.m.s
Empirical CHF=f(x)D^n vs Smoothed Experimental CHF
n= -0.85
d=6.22mm
d=12.8mm
d=6.22mm(**)
d=12.8mm(**)
(**) predicted
CHF(Kw/sq.m)
QUALITY X

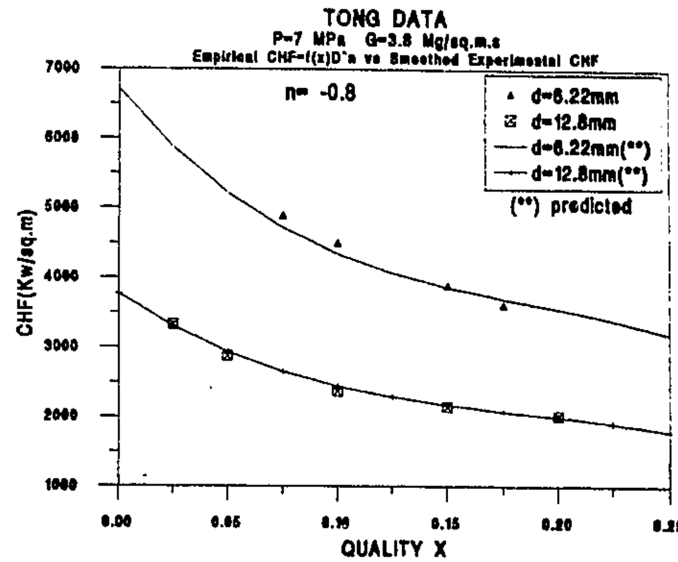
TONG DATA
P=7 MPa G=3.8 Mg/sq.m.s
Empirical CHF=f(x)D^n vs Smoothed Experimental CHF
n= -0.8
d=6.22mm
d=12.8mm
d=6.22mm(**)
d=12.8mm(**)
(**) predicted
CHF(Kw/sq.m)
QUALITY X

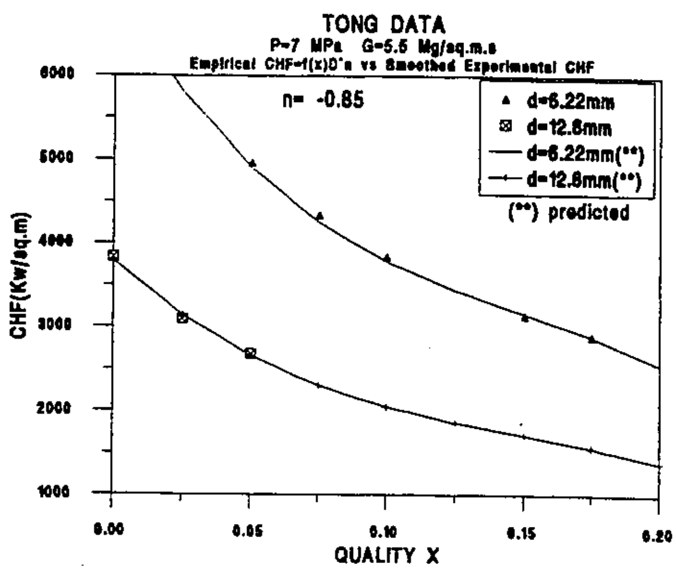
TONG DATA
P=7 MPa G=5.5 Mg/sq.m.s
Empirical CHF=f(x)D^n vs Smoothed Experimental CHF
n= -0.85
d=6.22mm
d=12.8mm
d=6.22mm(**)
d=12.8mm(**)
(**) predicted
CHF(Kw/sq.m)
QUALITY X

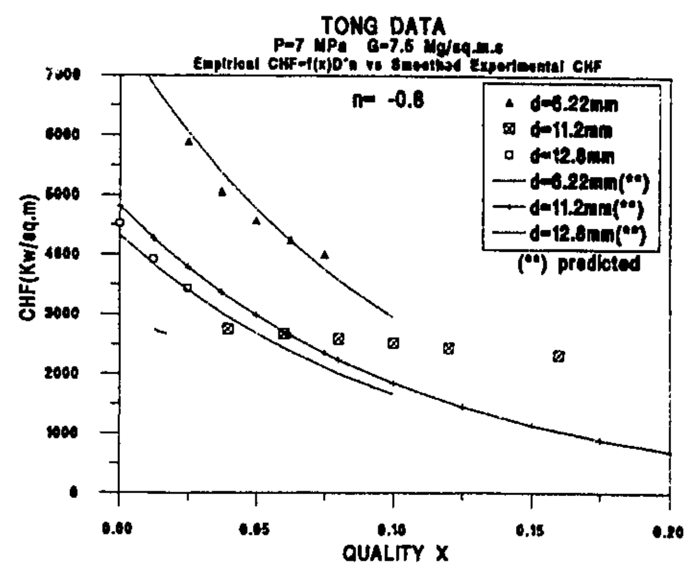
TONG DATA
P=7 MPa G=7.5 Mg/sq.m.s
Empirical CHF=f(x)D^n vs Smoothed Experimental CHF
n= -0.8
d=6.22mm
d=11.2mm
d=12.8mm
d=6.22mm(**)
d=11.2mm(**)
d=12.8mm(**)
(**) predicted
CHF(Kw/sq.m)
QUALITY X

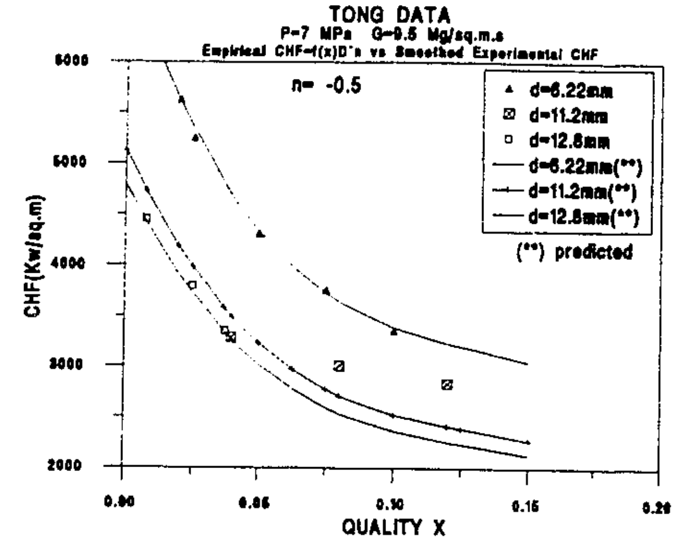
TONG DATA
P=7 MPa G=9.5 Mg/sq.m.s
Empirical CHF=f(x)D^n vs Smoothed Experimental CHF
n= -0.5
d=6.22mm
d=11.2mm
d=12.8mm
d=6.22mm(**)
d=11.2mm(**)
d=12.8mm(**)
(**) predicted
CHF(Kw/sq.m)
QUALITY X

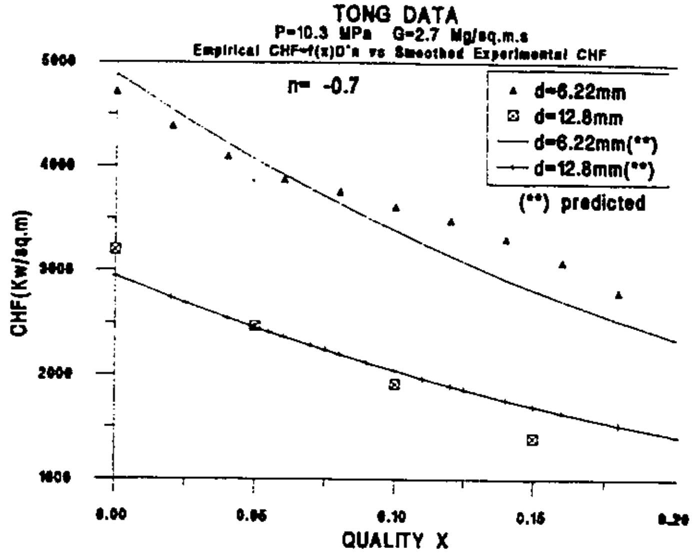
TONG DATA
P=10.3 MPa G=2.7 Mg/sq.m.s
Empirical CHF=f(x)D^n vs Smoothed Experimental CHF
n= -0.7
d=6.22mm
d=12.8mm
d=6.22mm(**)
d=12.8mm(**)
(**) predicted
CHF(Kw/sq.m)
QUALITY X

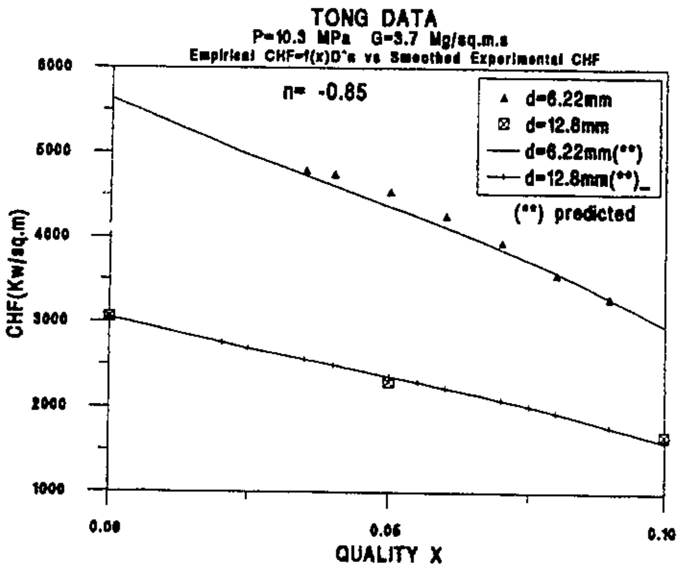
TONG DATA
P=10.3 MPa G=3.7 Mg/sq.m.s
Empirical CHF=f(x)D^n vs Smoothed Experimental CHF
n= -0.85
d=6.22mm
d=12.8mm
d=6.22mm(**)
d=12.8mm(**)
(**) predicted
CHF(Kw/sq.m)
QUALITY X

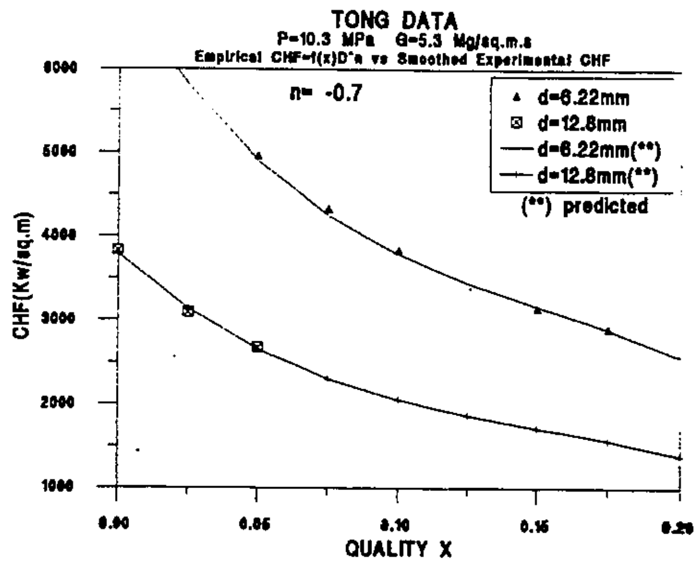
TONG DATA
P=10.3 MPa G=5.3 Mg/sq.m.s
Empirical CHF=f(x)D^n vs Smoothed Experimental CHF
n= -0.7
d=6.22mm
d=12.8mm
d=6.22mm(**)
d=12.8mm(**)
(**) predicted
CHF(Kw/sq.m)
QUALITY X

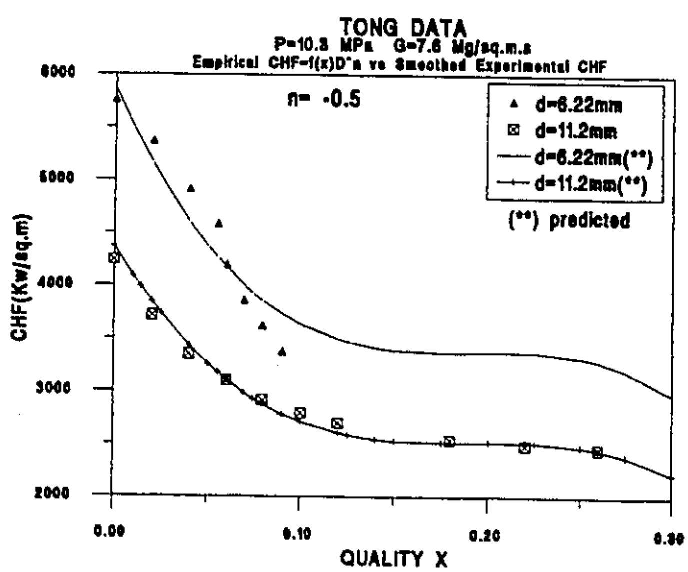
TONG DATA
P=10.3 MPa G=7.6 Mg/sq.m.s
Empirical CHF=f(x)D^n vs Smoothed Experimental CHF
n= -0.5
d=6.22mm
d=11.2mm
d=6.22mm(**)
d=11.2mm(**)
(**) predicted
CHF(Kw/sq.m)
QUALITY X

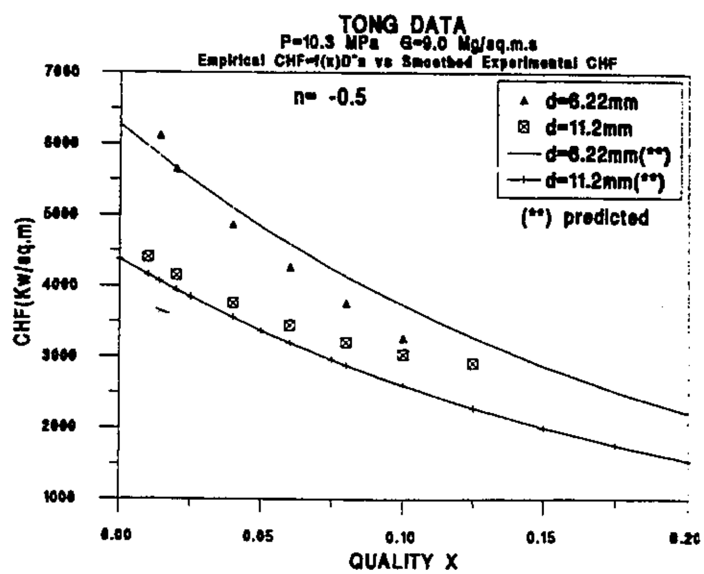
TONG DATA
P=10.3 MPa G=9.0 Mg/sq.m.s
Empirical CHF=f(x)D^n vs Smoothed Experimental CHF
n= -0.5
d=6.22mm
d=11.2mm
d=6.22mm(**)
d=11.2mm(**)
(**) predicted
CHF(Kw/sq.m)
QUALITY X

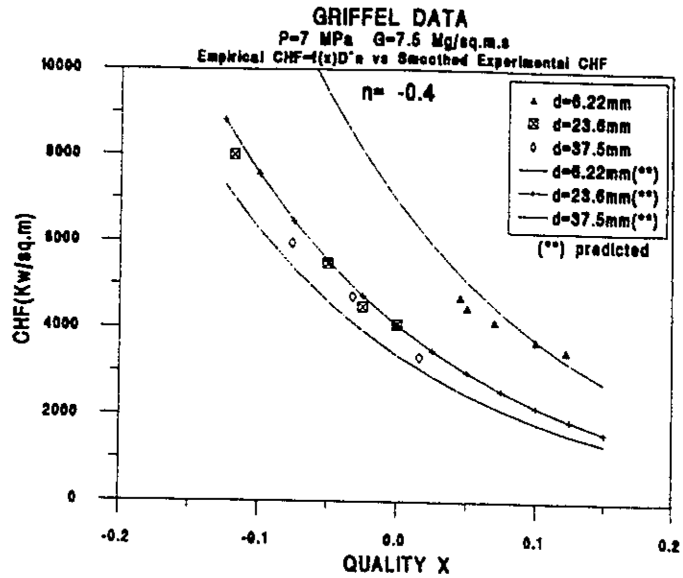
GRIFFEL DATA
P=7 MPa G=7.5 Mg/sq.m.s
Empirical CHF=f(x)D^n vs Smoothed Experimental CHF
n= -0.4
d=6.22mm
d=23.6mm
d=37.5mm
d=6.22mm(**)
d=23.6mm(**)
d=37.5mm(**)
(**) predicted
CHF(Kw/sq.m)
QUALITY X
10000
8000
6000
4000
2000
0
-0.2
-0.1
0.0
0.1
0.2

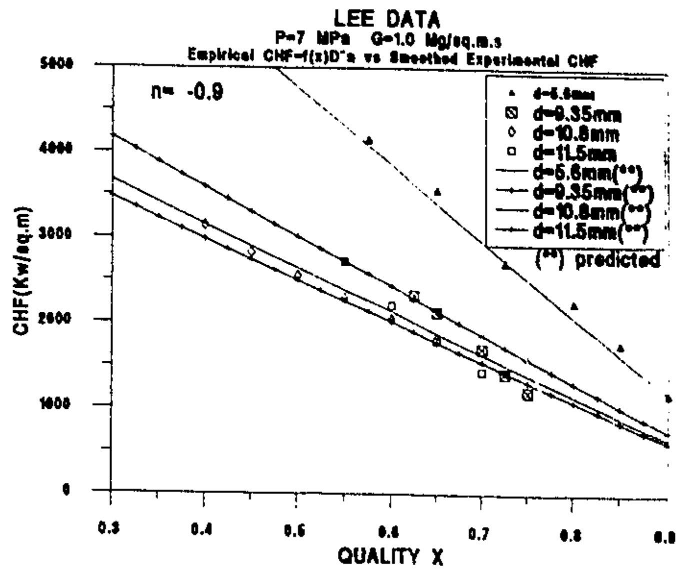
LEE DATA
P=7 MPa G=1.0 Mg/sq.m.s
Empirical CHF=f(x)D^n vs Smoothed Experimental CHF
n= -0.9
d=9.35mm
d=10.8mm
d=11.5mm
d=5.6mm(**)
d=9.35mm(**)
d=10.8mm(**)
d=11.5mm(**)
(**) predicted
CHF(Kw/sq.m)
QUALITY X

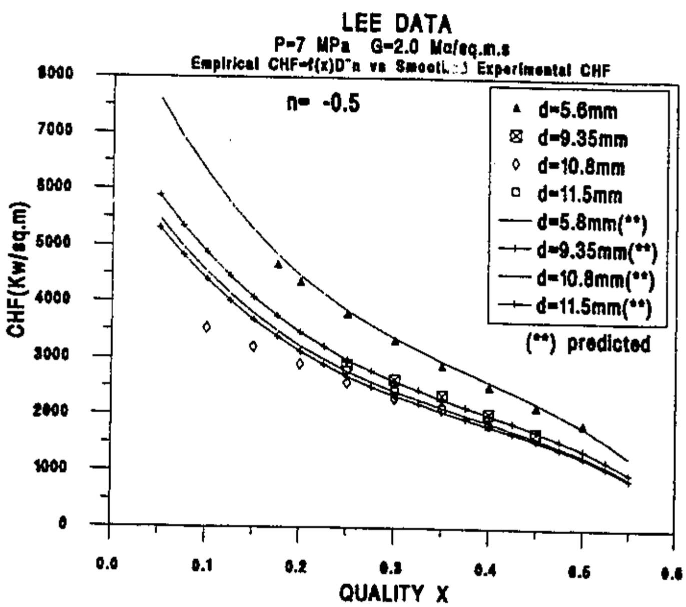
LEE DATA
P=7 MPa G=2.0 Mg/sq.m.s
n= -0.5
d=5.6mm
d=9.35mm
d=10.8mm
d=11.5mm
d=5.8mm(**)
d=9.35mm(**)
d=10.8mm(**)
d=11.5mm(**)
(**) predicted
CHF(Kw/sq.m)
QUALITY X
7000
5000
4000
3000
2000
1000
0
0.0
0.1
0.2
0.3
0.4
0.5

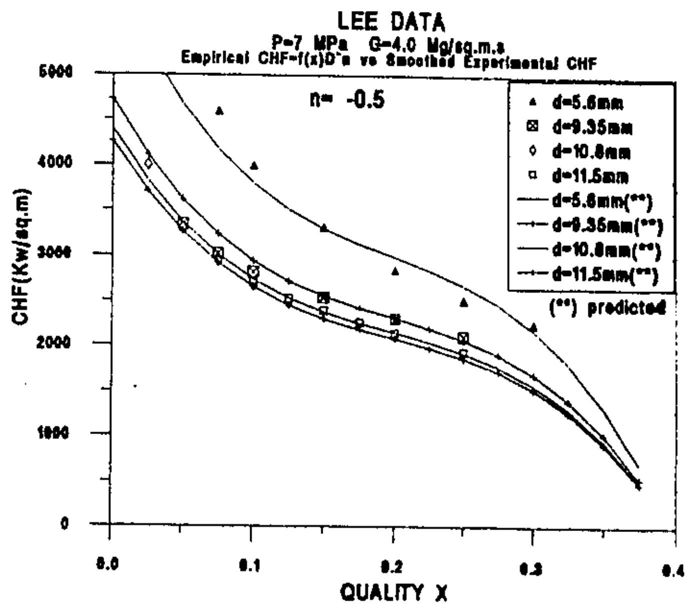
LEE DATA
P=7 MPa G=4.0 Mg/sq.m.s
Empirical CHF=f(x)D^n vs Smoothed Experimental CHF
n= -0.5
d=5.6mm
d=9.35mm
d=10.8mm
d=11.5mm
d=5.6mm(**)
d=9.35mm(**)
d=10.8mm(**)
d=11.5mm(**)
(**) predicted
CHF(Kw/sq.m)
QUALITY X
5000
4000
3000
2000
1000
0
0.1
0.2
0.3
0.4

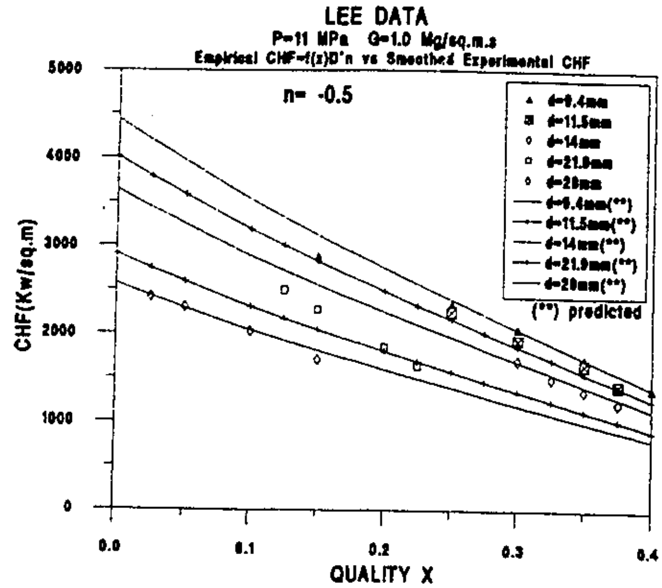
LEE DATA
P=11 MPa G=1.0 Mg/sq.m.s
Empirical CHF=f(x)D^n vs Smoothed Experimental CHF
n= -0.5
d=9.4mm
d=11.5mm
d=14mm
d=21.9mm
d=28mm
d=9.4mm(**)
d=11.5mm(**)
d=14mm(**)
d=21.9mm(**)
d=28mm(**)
(**) predicted
CHF(Kw/sq.m)
QUALITY X

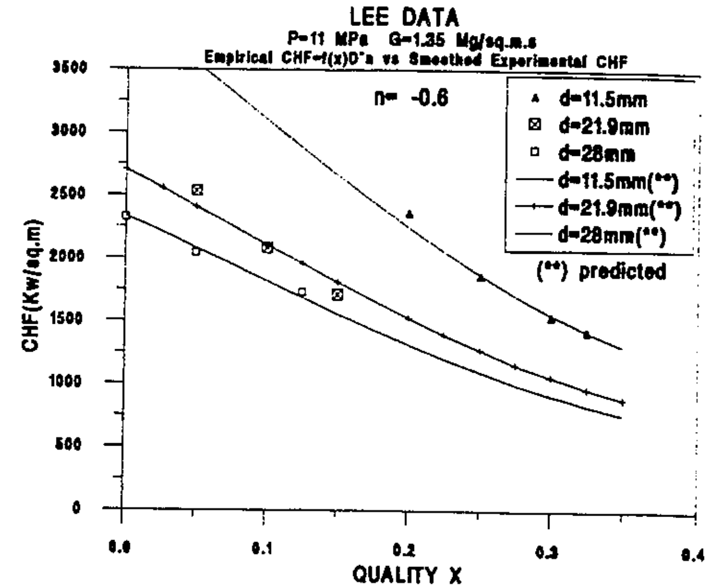
LEE DATA
P=11 MPa G=1.35 Mg/sq.m.s
Empirical CHF=f(x)D^n vs Smoothed Experimental CHF
n= -0.6
d=11.5mm
d=21.9mm
d=28mm
d=11.5mm(**)
d=21.9mm(**)
d=28mm(**)
(**) predicted
CHF(Kw/sq.m)
QUALITY X

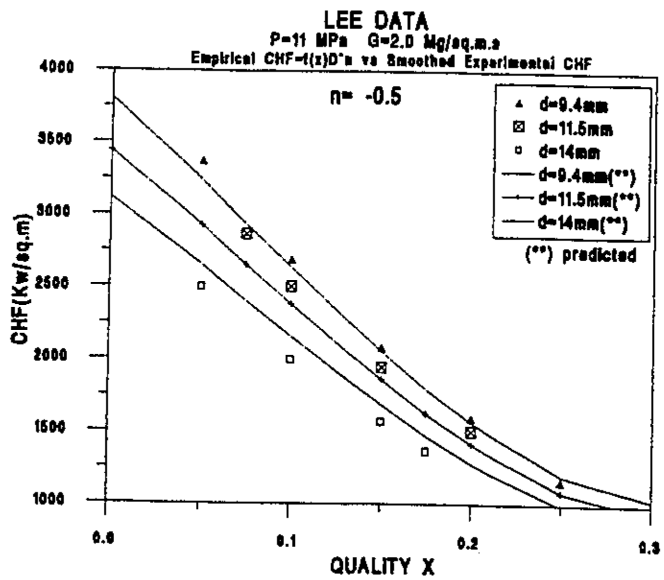
LEE DATA
P=11 MPa G=2.0 Mg/sq.m.s
Empirical CHF=f(x)D^n vs Smoothed Experimental CHF
n= -0.5
d=9.4mm
d=11.5mm
d=14mm
d=9.4mm(**)
d=11.5mm(**)
d=14mm(**)
(**) predicted
CHF(Kw/sq.m)
QUALITY X

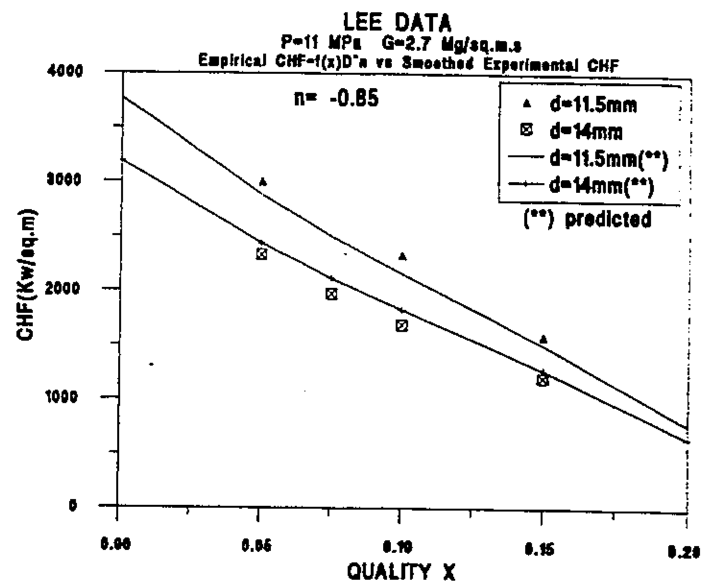
LEE DATA
P=11 MPa G=2.7 Mg/sq.m.s
Empirical CHF=f(x)D^n vs Smoothed Experimental CHF
n= -0.85
d=11.5mm
d=14mm
d=11.5mm(**)
d=14mm(**)
(**) predicted
CHF(Kw/sq.m)
QUALITY X

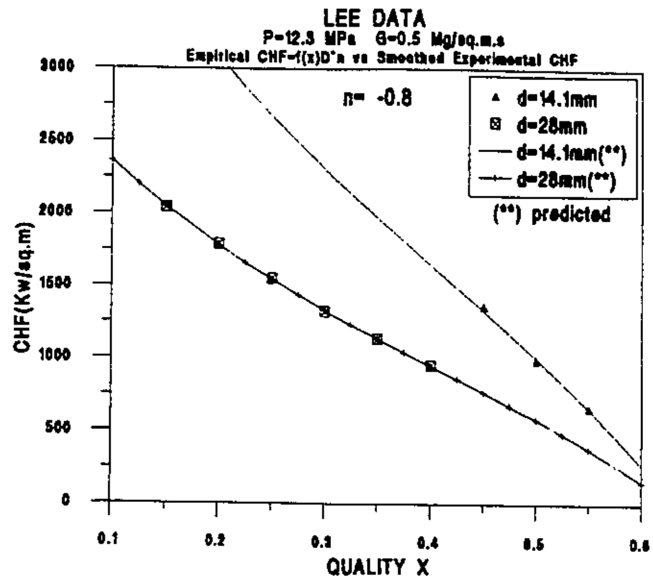

LEE DATA
P=12.3 MPa G=0.5 Mg/sq.m.s
Empirical CHF=f(x)D^n vs Smoothed Experimental CHF
n= -0.8
d=14.1mm
d=28mm
d=14.1mm(**)
d=28mm(**)
(**) predicted
CHF(Kw/sq.m)
QUALITY X

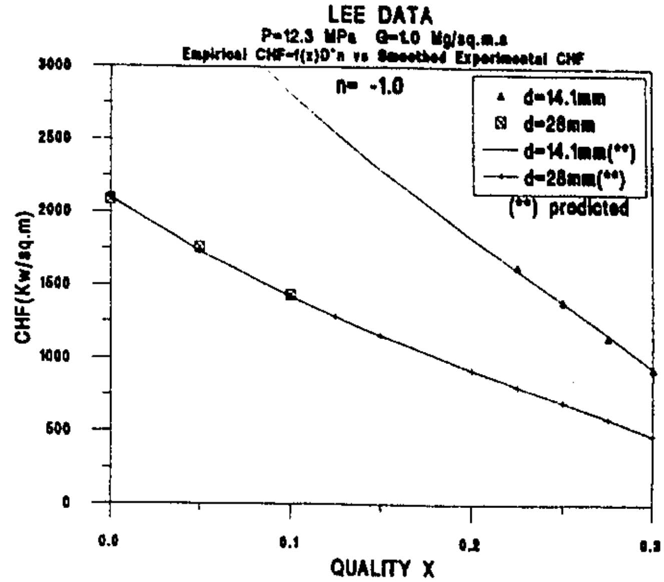

LEE DATA
P=12.3 MPa G=1.0 Mg/sq.m.s
Empirical CHF=f(x)D^n vs Smoothed Experimental CHF
n= -1.0
d=14.1mm
d=28mm
d=14.1mm(**)
d=28mm(**)
(**) predicted
CHF(Kw/sq.m)
QUALITY X

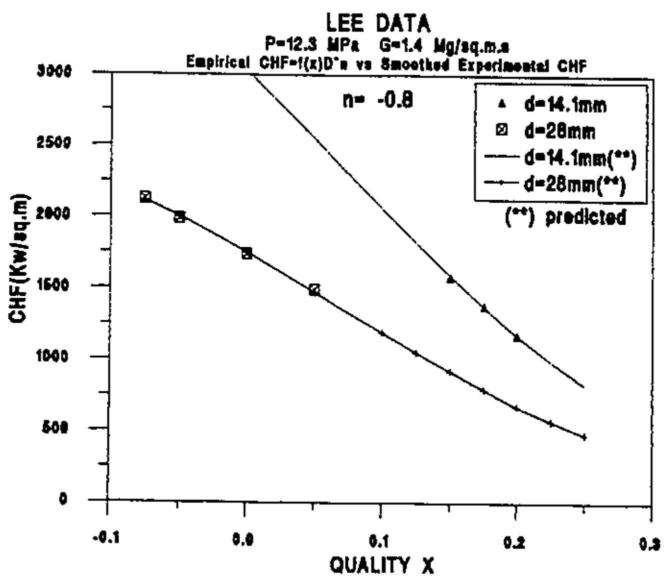

LEE DATA
P=12.3 MPa G=1.4 Mg/sq.m.s
Empirical CHF=f(x)D^n vs Smoothed Experimental CHF
n= -0.8
d=14.1mm
d=28mm
d=14.1mm(**)
d=28mm(**)
(**) predicted
CHF(Kw/sq.m)
QUALITY X

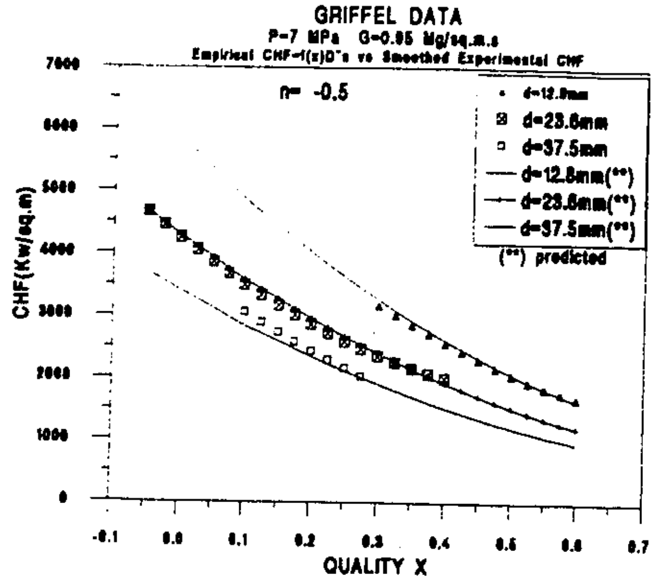
GRIFFEL DATA
P=7 MPa G=0.95 Mg/sq.m.s
Empirical CHF=f(x)D^n vs Smoothed Experimental CHF
n= -0.5
d=12.8mm
d=23.6mm
d=37.5mm
d=12.8mm(**)
d=23.6mm(**)
d=37.5mm(**)
(**) predicted
CHF(Kw/sq.m)
QUALITY X

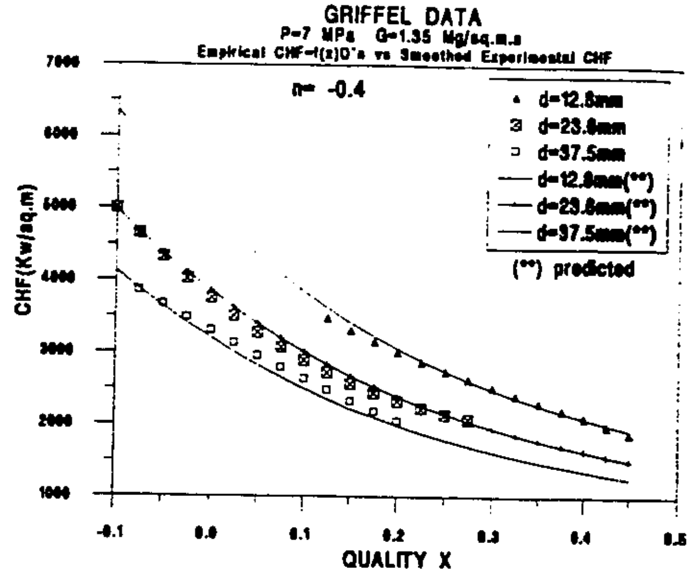
GRIFFEL DATA
P=7 MPa G=1.35 Mg/sq.m.s
Empirical CHF=f(x)D^n vs Smoothed Experimental CHF
n= -0.4
d=12.8mm
d=23.8mm
d=37.5mm
d=12.8mm(**)
d=23.8mm(**)
d=37.5mm(**)
(**) predicted
CHF(Kw/sq.m)
QUALITY X

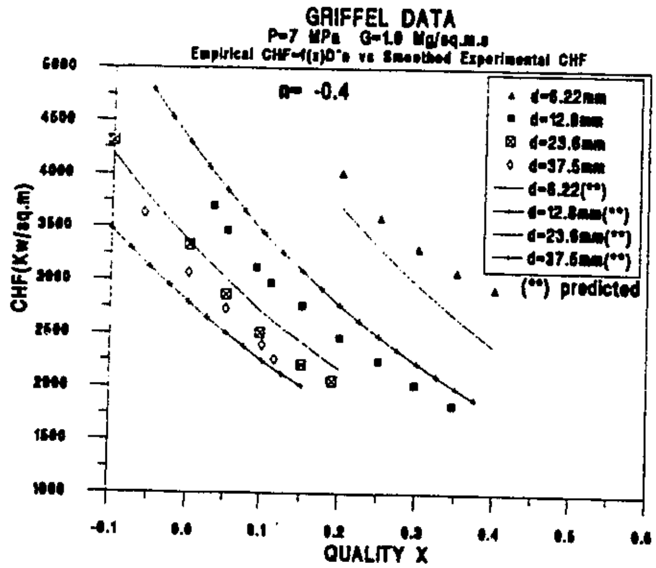
GRIFFEL DATA
P=7 MPa G=1.9 Mg/sq.m.s
Empirical CHF=f(x)D^n vs Smoothed Experimental CHF
n= -0.4
d=6.22mm
d=12.8mm
d=23.6mm
d=37.5mm
d=6.22(**)
d=12.8mm(**)
d=23.6mm(**)
d=37.5mm(**)
(**) predicted
CHF(Kw/sq.m)
QUALITY X

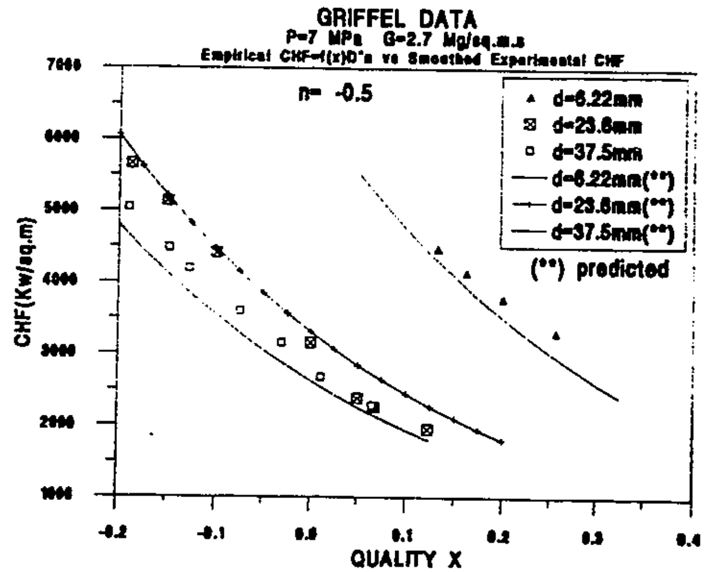
GRIFFEL DATA
P=7 MPa G=2.7 Mg/sq.m.s
Empirical CHF=f(x)D^n vs Smoothed Experimental CHF
n= -0.5
d=6.22mm
d=23.6mm
d=37.5mm
d=6.22mm(**)
d=23.6mm(**)
d=37.5mm(**)
(**) predicted
CHF(Kw/sq.m)
QUALITY X

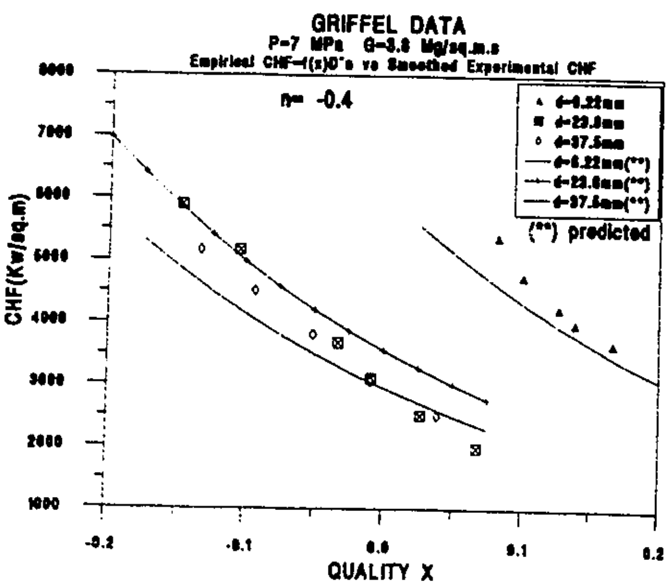
GRIFFEL DATA
P=7 MPa G=3.8 Mg/sq.m.s
Empirical CHF=f(x)D^n vs Smoothed Experimental CHF
n= -0.4
d=6.22mm
d=23.8mm
d=37.5mm
d=6.22mm(**)
d=23.6mm(**)
d=37.5mm(**)
(**) predicted
CHF(Kw/sq.m)
QUALITY X

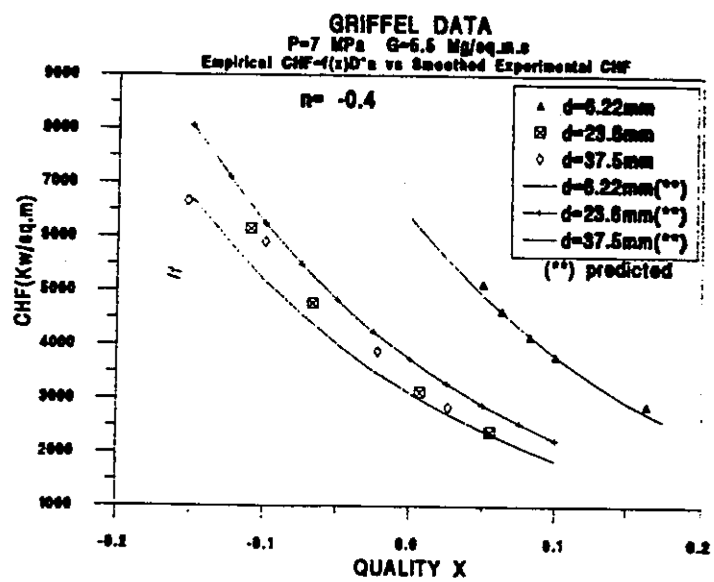
GRIFFEL DATA
P=7 MPa G=5.5 Mg/sq.m.s
Empirical CHF=f(x)D^n vs Smoothed Experimental CHF
n= -0.4
d=6.22mm
d=23.6mm
d=37.5mm
d=6.22mm(**)
d=23.6mm(**)
d=37.5mm(**)
(**) predicted
CHF(Kw/sq.m)
QUALITY X

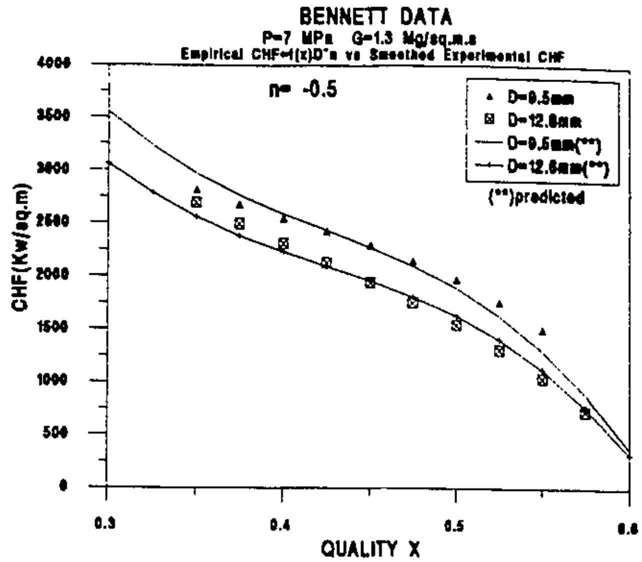
BENNETT DATA
P=7 MPa G=1.3 Mg/sq.m.s
Empirical CHF=f(x)D^n vs Smoothed Experimental CHF
n= -0.5
D=9.5mm
D=12.6mm
D=9.5mm(**)
D=12.6mm(**)
(**)predicted
CHF(Kw/sq.m)
QUALITY X

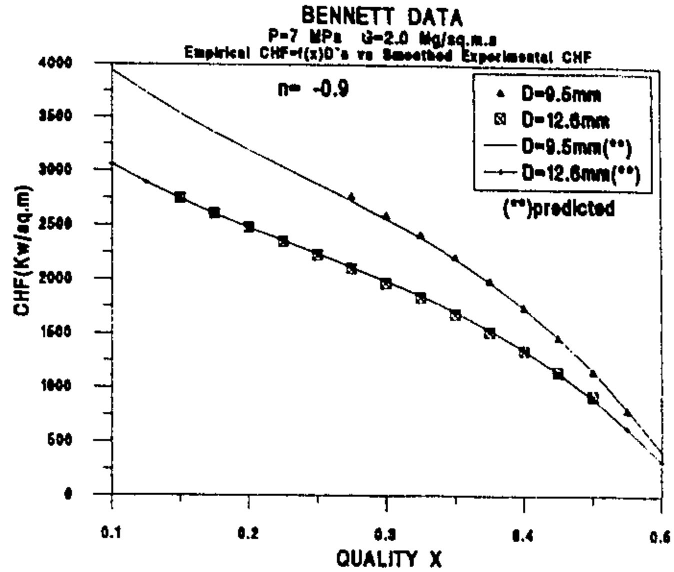
BENNETT DATA
P=7 MPa G=2.0 Mg/sq.m.s
Empirical CHF=f(x)D^n vs Smoothed Experimental CHF
n= -0.9
D=9.5mm
D=12.6mm
D=9.5mm(**)
D=12.6mm(**)
(**)predicted
CHF(Kw/sq.m)
QUALITY X

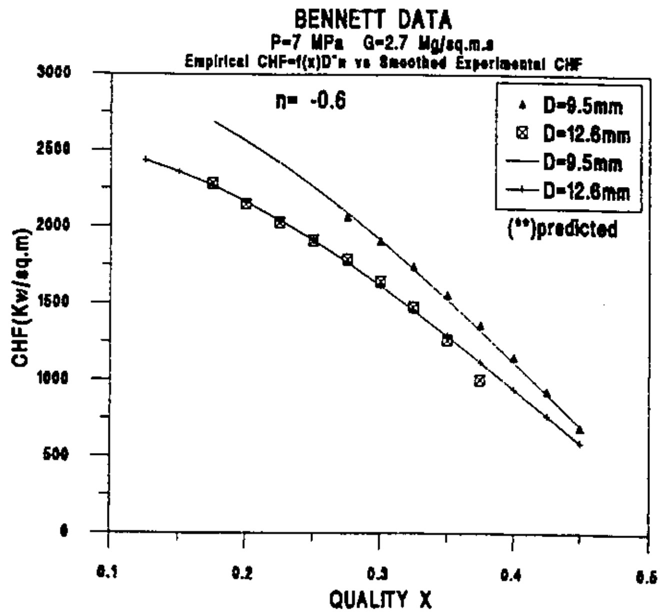
BENNETT DATA
P=7 MPa G=2.7 Mg/sq.m.s
Empirical CHF=f(x)D^n vs Smoothed Experimental CHF
n= -0.6
D=9.5mm
D=12.6mm
D=9.5mm
D=12.6mm
(**)predicted
CHF(Kw/sq.m)
QUALITY X

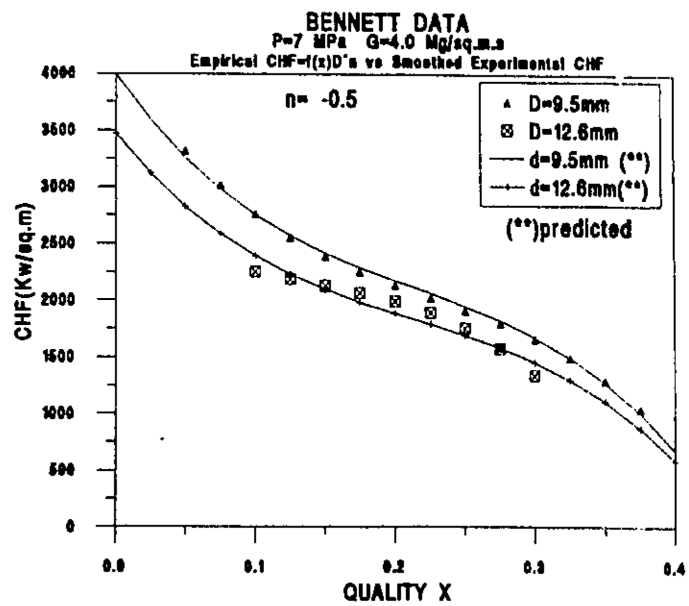
BENNETT DATA
P=7 MPa G=4.0 Mg/sq.m.s
Empirical CHF=f(x)D^n vs Smoothed Experimental CHF
n= -0.5
D=9.5mm
D=12.6mm
d=9.5mm (**)
d=12.6mm(**)
(**)predicted
CHF(Kw/sq.m)
QUALITY X

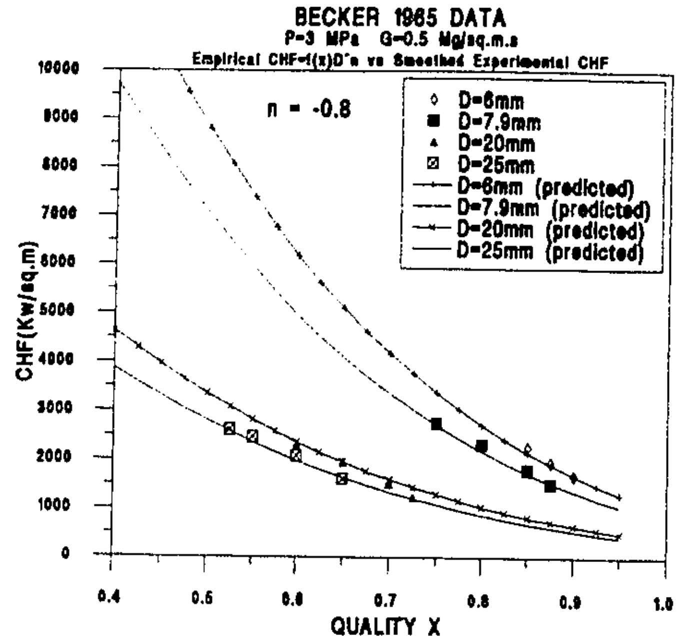
BECKER 1965 DATA
P=3 MPa G=0.5 Mg/sq.m.s
Empirical CHF=f(x)D^n vs Smoothed Experimental CHF
n = -0.8
D=6mm
D=7.9mm
D=20mm
D=25mm
D=6mm (predicted)
D=7.9mm (predicted)
D=20mm (predicted)
D=25mm (predicted)
CHF(Kw/sq.m)
QUALITY X

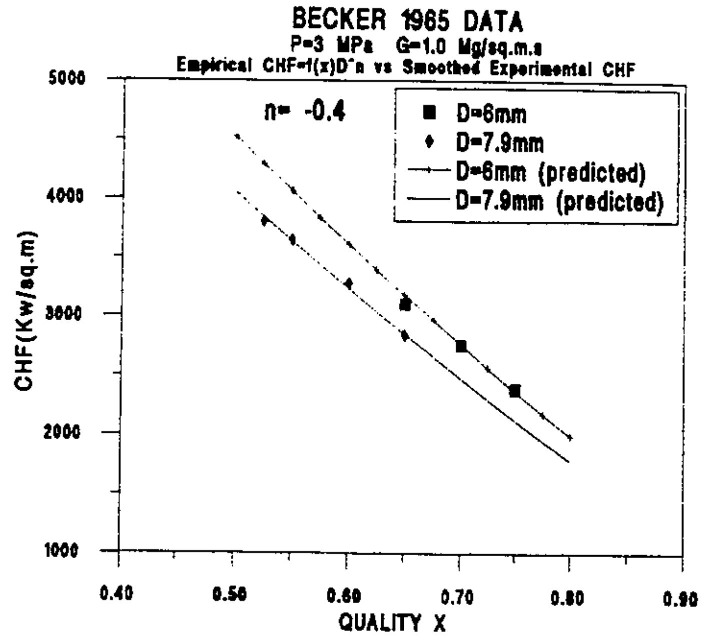
BECKER 1965 DATA
P=3 MPa G=1.0 Mg/sq.m.s
Empirical CHF=f(x)D^n vs Smoothed Experimental CHF
n= -0.4
D=6mm
D=7.9mm
D=6mm (predicted)
D=7.9mm (predicted)
CHF(Kw/sq.m)
QUALITY X

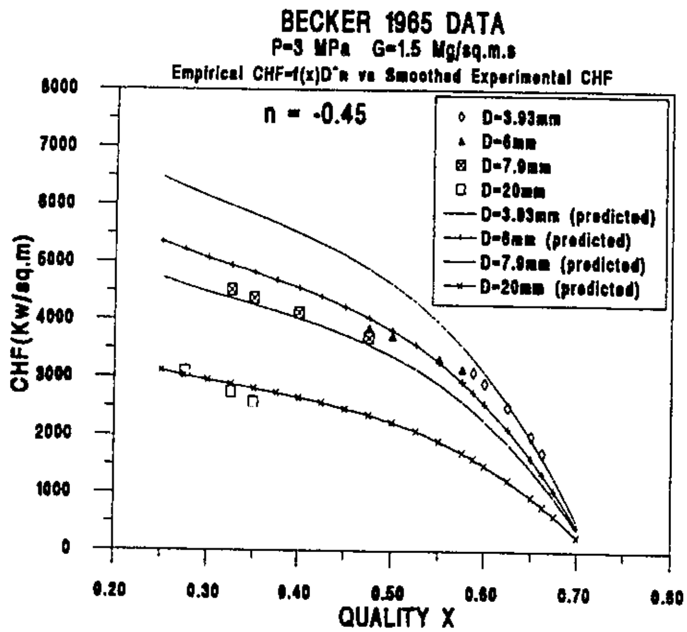
BECKER 1965 DATA
P=3 MPa G=1.5 Mg/sq.m.s
Empirical CHF=f(x)D^n vs Smoothed Experimental CHF
n = -0.45
D=3.93mm
D=6mm
D=7.9mm
D=20mm
D=3.93mm (predicted)
D=6mm (predicted)
D=7.9mm (predicted)
D=20mm (predicted)
CHF(Kw/sq.m)
QUALITY X

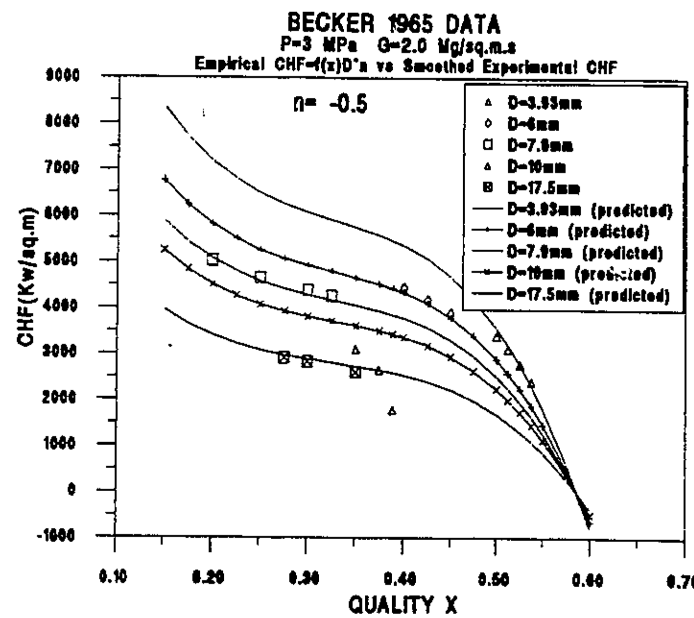
BECKER 1965 DATA
P=3 MPa G=2.0 Mg/sq.m.s
Empirical CHF=f(x)D^n vs Smoothed Experimental CHF
n= -0.5
D=3.93mm
D=6mm
D=7.9mm
D=10mm
D=17.5mm
D=3.93mm (predicted)
D=6mm (predicted)
D=7.9mm (predicted)
D=17.5mm (predicted)
CHF(Kw/sq.m)
QUALITY X

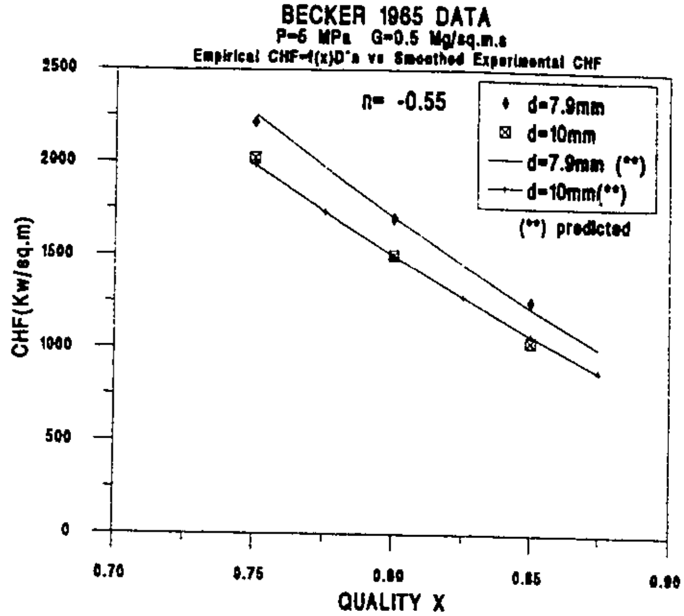
BECKER 1965 DATA
P=5 MPa G=0.5 Mg/sq.m.s
Empirical CHF=f(x)D^n vs Smoothed Experimental CHF
n= -0.55
d=7.9mm
d=10mm
d=7.9mm (**)
d=10mm(**)
(**) predicted
CHF(Kw/sq.m)
2500
2000
1500
1000
500
0
0.70
0.75
0.80
0.85
0.90
QUALITY X

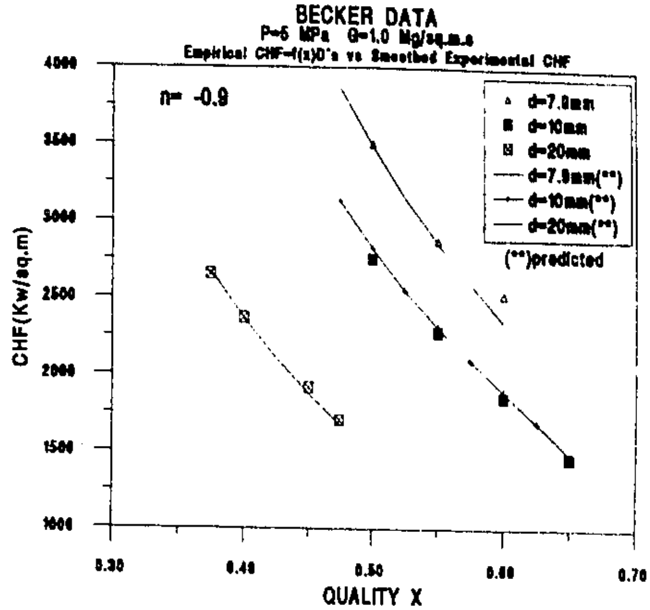
BECKER DATA
P=5 MPa G=1.0 Mg/sq.m.s
Empirical CHF=f(x)D^n vs Smoothed Experimental CHF
n= -0.9
d=7.9mm
d=10mm
d=20mm
d=7.9mm(**)
d=10mm(**)
d=20mm(**)
(**)predicted
CHF(Kw/sq.m)
4000
3500
3000
2500
2000
1500
1000
0.30
0.40
0.50
0.60
0.70
QUALITY X

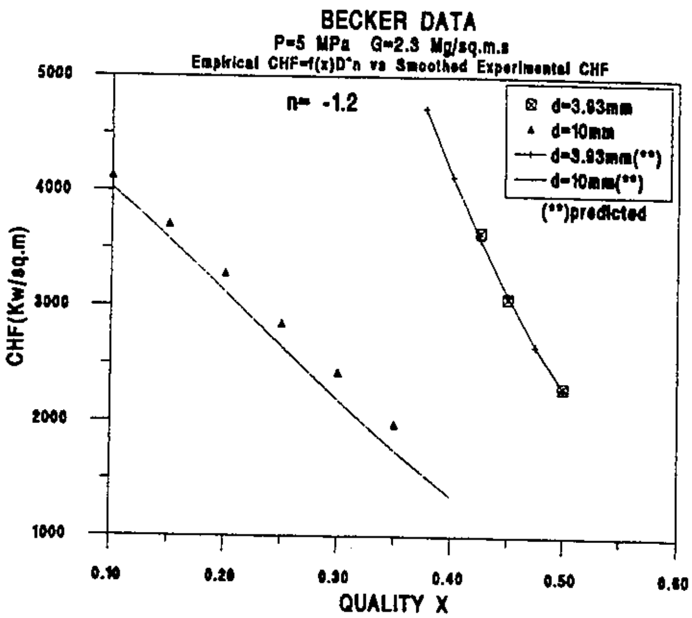
BECKER DATA
P=5 MPa G=2.3 Mg/sq.m.s
Empirical CHF=f(x)D^n vs Smoothed Experimental CHF
n= -1.2
d=3.93mm
d=10mm
d=3.93mm(**)
d=10mm(**)
(**)predicted
CHF(Kw/sq.m)
5000
4000
3000
2000
1000
0.10
0.20
0.30
0.40
0.50
0.60
QUALITY X

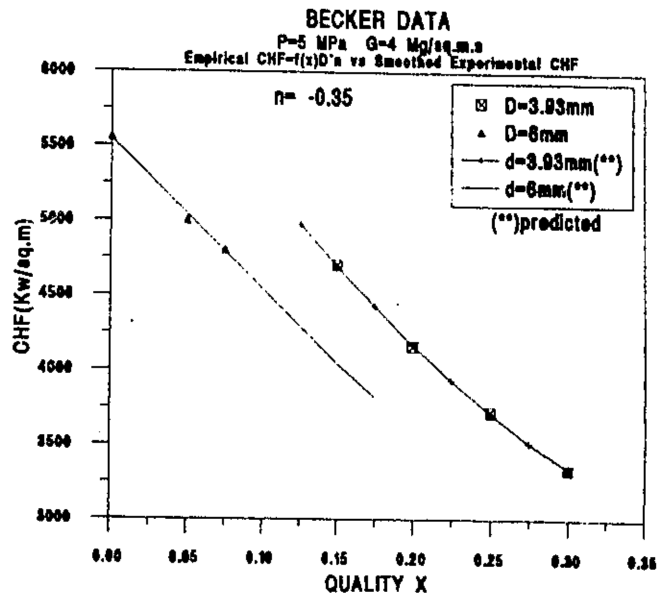
BECKER DATA
P=5 MPa G=4 Mg/sq.m.s
Empirical CHF=f(x)D^n vs Smoothed Experimental CHF
n= -0.35
D=3.93mm
D=6mm
d=3.93mm(**)
d=6mm(**)
(**)predicted
CHF(Kw/sq.m)
6000
5500
5000
4500
4000
3500
3000
0.00
0.05
0.10
0.15
0.20
0.25
0.30
0.35
QUALITY X

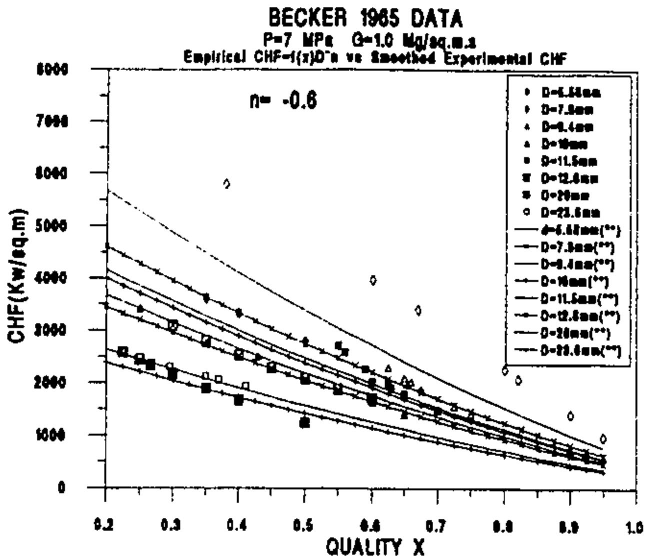
BECKER 1965 DATA
P=7 MPa G=1.0 Mg/sq.m.s
Empirical CHF=f(x)D^n vs Smoothed Experimental CHF
n= -0.6
CHF(Kw/sq.m)
QUALITY X

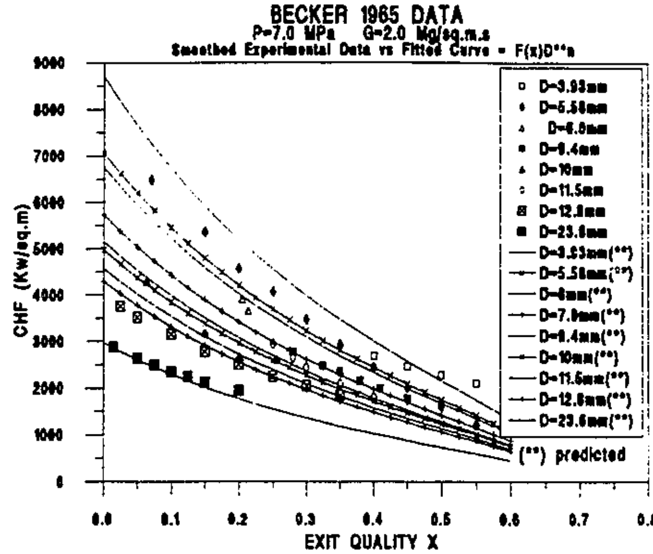
BECKER 1965 DATA
P=7.0 MPa G=2.0 Mg/sq.m.s
Smoothed Experimental Data vs Fitted Curve = F(x)D**n
CHF (Kw/sq.m)
EXIT QUALITY X
(**) predicted

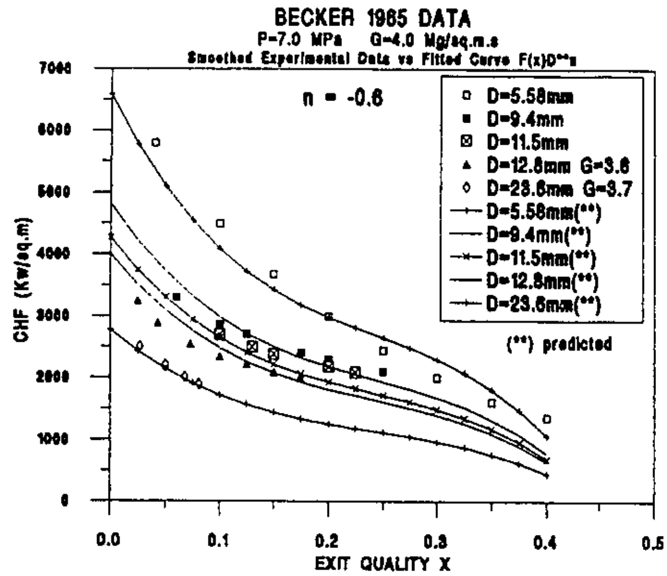
BECKER 1965 DATA
P=7.0 MPa G=4.0 Mg/sq.m.s
Smoothed Experimental Data vs Fitted Curve F(x)D**n
n = -0.6
D=5.58mm
D=9.4mm
D=11.5mm
D=12.8mm G=3.6
D=23.6mm G=3.7
D=5.58mm(**)
D=9.4mm(**)
D=11.5mm(**)
D=12.8mm(**)
D=23.6mm(**)
(**) predicted
CHF (Kw/sq.m)
EXIT QUALITY X

APPENDIX II

Measurements From AECL CHF Experiment

For 5.45 mm and 8.94 mm Diameter Tubes

Measured Data from Experiment of the 8.94 mm Diameter Tube

RUN NAME	PT-108 PRESS. OUT MPa	TE-103 TEMP. IN °C				TE-133 TEMP AMB. °C	FT-1/2 FLOW g/s	JS-100 POWER T/S kW	PDT-01 PRESS. DIFF. kPa	PDT-02 PRESS. DIFF. kPa	PDT-03 PRESS. DIFF. kPa	PDT-04 PRESS. DIFF. kPa	PDT-05 PRESS. DIFF. kPa	PDT-06 PRESS. DIFF. kPa
92318	9.56	281.8	283.3	309.6	307.9	29.5	122.82	80.94	16.53	19.39	14.89	12.02	9.65	71.09
92215	9.50	294.2	295.7	309.0	307.5	28.6	124.39	74.53	15.72	19.55	16.05	12.77	9.94	73.98
92316	9.51	282.9	284.3	309.1	307.5	27.9	124.53	81.34	16.76	19.93	15.43	12.38	8.20	73.11
92418	9.51	270.5	271.9	309.0	307.5	28.6	124.61	88.38	17.74	19.97	14.89	11.47	7.11	71.09
92113	9.57	302.4	303.8	309.6	307.9	15.2	124.63	67.38	15.60	18.74	15.81	12.64	13.63	73.98
93117	9.57	303.1	304.4	309.3	307.8	28.9	185.60	82.03	24.84	28.40	24.39	20.17	20.87	116.68
93218	9.52	294.7	295.7	308.9	307.5	28.7	186.72	89.47	25.24	28.63	23.97	20.38	14.38	113.51
93320	9.51	283.3	284.3	308.9	307.4	28.3	188.23	97.13	25.76	28.13	23.20	18.56	11.29	107.45
93422	9.55	270.3	271.4	309.4	307.8	28.5	190.60	103.47	25.53	26.74	22.16	14.02	11.81	99.37
94424	9.56	270.9	271.9	309.3	307.6	29.3	272.44	115.72	34.36	38.48	28.63	17.32	16.66	134.58
94323	9.57	282.9	283.8	309.2	307.5	31.0	282.54	114.41	39.73	40.29	37.75	24.25	19.44	160.55
94223	9.50	295.1	296.1	308.4	307.0	28.9	282.96	111.13	43.48	45.33	39.52	35.47	22.77	187.67
94121	9.56	305.3	306.5	308.9	307.4	28.7	283.31	105.44	44.35	48.48	41.98	37.23	37.65	207.87
96428	9.56	270.0	271.0	308.9	307.3	28.7	372.19	140.22	56.52	59.21	35.90	24.90	25.03	200.37
96228	9.50	295.7	296.6	307.9	306.6	28.8	377.43	137.63	71.53	70.57	61.56	54.30	33.44	294.73
96328	9.57	282.8	283.8	308.7	307.2	30.1	377.92	139.19	64.14	64.18	55.87	32.64	28.38	244.81
96127	9.58	305.0	306.1	308.5	306.9	28.6	379.27	133.34	75.57	79.88	65.80	60.22	54.74	335.42
97234	9.50	295.1	296.1	307.5	305.9	27.7	467.25	168.44	111.23	108.04	93.84	74.42	45.39	484.89
97335	9.50	282.3	283.2	307.5	305.9	27.0	468.76	171.31	101.02	98.77	80.03	44.61	37.52	358.21
97132	9.51	305.3	306.5	307.5	305.6	28.2	472.74	159.47	115.91	124.85	103.89	91.05	69.78	518.37
97435	9.50	271.0	271.9	307.9	306.3	27.0	477.90	173.47	94.32	90.23	51.75	37.11	34.64	303.96
72422	7.03	240.3	240.8	288.2	286.6	28.2	125.99	112.06	30.61	31.17	22.32	14.46	8.36	108.04
72219	7.03	271.0	272.4	288.1	286.7	28.2	126.14	94.13	28.11	30.72	24.50	17.74	12.91	114.27
72320	7.03	257.4	258.5	288.2	286.6	27.5	126.61	101.94	29.06	30.95	23.53	16.20	10.46	111.32
72219	7.03	272.0	273.1	288.2	286.7	28.1	127.21	93.19	28.40	30.72	24.50	17.85	13.11	114.85
72219	7.03	271.2	272.4	288.1	286.6	28.1	127.47	93.19	28.69	30.84	24.46	17.74	13.01	115.42
72118	7.03	277.6	279.0	288.1	286.6	27.6	128.78	91.44	27.76	30.99	25.50	18.88	14.70	119.18
73122	7.03	274.3	275.3	288.1	286.3	27.6	188.00	110.22	42.65	45.30	37.66	27.87	20.83	176.60
73223	7.03	272.4	273.3	288.0	286.3	28.1	188.42	112.38	43.40	45.46	37.66	27.58	19.95	175.74
73325	7.03	255.7	256.6	288.0	286.3	27.4	189.46	124.06	44.86	44.78	35.27	24.23	13.29	165.12
73426	7.03	243.0	243.7	288.1	286.3	27.7	189.93	132.69	45.44	44.67	32.67	20.43	11.30	155.65
74330	7.03	254.7	255.6	287.5	285.9	27.6	282.17	150.50	69.86	63.44	52.36	34.37	18.51	241.40
74228	7.03	271.4	272.4	287.4	285.8	27.6	282.87	139.56	70.53	70.20	58.59	45.61	28.72	275.87
74431	7.03	243.2	243.9	287.6	285.9	27.6	284.49	156.16	66.74	60.49	47.13	24.02	17.06	218.27
76232	7.04	269.2	270.1	286.6	285.0	27.7	372.62	159.44	99.85	90.44	72.55	60.31	33.63	360.13
76334	7.04	255.2	255.7	286.7	285.2	27.5	377.10	165.81	95.09	76.85	69.55	38.68	25.85	308.70
76434	7.04	241.5	242.2	287.1	285.5	27.7	378.79	167.34	81.17	74.65	46.90	26.07	23.92	254.63

Measured Data From Experiment of the 5.45 mm Diameter Tube Experiment

RUN NAME	PT-108 PRESS. OUT MPa	TE-103 TEMP. IN °C				TE-133 TEMP AMB. °C	FT-1/2 FLOW g/s	JS-100 POWER T/S kW	PDT-01 PRESS. DIFF. kPa	PDT-02 PRESS. DIFF. kPa	PDT-03 PRESS. DIFF. kPa	PDT-04 PRESS. DIFF. kPa	PDT-05 PRESS. DIFF. kPa	PDT-06 PRESS. DIFF. kPa
91506	9.55	259.0	262.8	309.2	307.7	29.3	25.44	29.59	18.37	19.93	14.78	9.91	5.11	71.09
94211	9.62	296.3	300.0	310.5	308.8	32.0	95.60	53.05	91.73	94.88	87.53	67.39	39.13	388.51
94110	9.61	303.2	307.4	310.3	308.6	33.2	98.47	50.86	93.63	96.04	93.34	75.54	51.15	418.81
94513	9.59	253.3	254.8	309.8	308.1	33.0	99.01	65.31	79.03	68.49	50.87	27.16	24.66	258.66
94311	9.56	283.8	285.7	309.4	307.7	29.6	100.06	56.04	75.80	88.49	70.18	50.12	27.99	374.37
94311	9.56	283.5	285.6	309.4	307.7	29.6	100.87	55.08	78.51	89.15	69.72	48.95	27.88	354.75
94313	9.71	284.3	288.1	311.2	309.3	31.9	101.85	60.72	99.11	100.19	81.30	55.52	33.52	372.07
94414	9.71	271.9	275.7	311.2	309.3	31.5	103.30	66.66	100.51	92.30	74.68	41.80	32.01	342.57
96315	9.55	281.9	283.3	309.5	307.8	30.1	135.05	73.59	130.28	139.51	108.66	73.02	43.41	508.56
96213	9.58	294.7	296.3	309.9	308.1	31.3	135.54	67.85	131.20	142.01	122.12	94.32	51.57	539.72
96415	9.58	271.1	272.9	309.8	308.3	28.0	137.58	80.25	132.24	122.32	102.54	56.51	43.60	471.33
96417	9.64	271.8	275.2	310.8	308.8	30.9	137.96	83.61	156.19	142.05	113.27	60.35	49.31	532.22
96214	9.64	296.0	299.4	310.6	308.8	30.2	138.32	71.86	158.96	157.87	142.86	109.69	59.72	641.58
96517	9.58	256.1	257.6	309.8	308.1	26.8	138.40	83.67	125.78	111.31	80.34	45.78	42.82	417.95
96113	9.57	304.2	306.1	309.8	308.0	31.9	139.65	65.45	138.88	153.71	136.24	112.63	76.27	615.04
96113	9.63	303.2	307.0	310.7	308.9	30.2	139.73	68.22	161.10	159.17	152.09	123.20	76.53	685.16
96518	9.63	259.9	262.8	310.6	308.8	31.5	140.20	88.87	150.65	129.63	94.04	53.78	49.93	489.80
96315	9.52	283.3	286.5	309.3	307.5	32.8	141.20	75.06	141.24	146.48	119.24	80.32	46.77	542.89
97216	9.57	294.7	296.6	309.8	308.1	30.4	160.24	80.90	184.70	190.95	163.94	126.34	67.18	733.92
97115	9.57	305.3	307.1	309.8	308.1	31.2	160.76	77.03	190.42	197.38	178.10	148.86	99.10	810.68
97317	9.57	283.2	284.8	309.9	308.1	30.9	161.27	87.52	182.97	197.57	149.48	98.42	59.00	683.14
97116	9.55	302.6	306.1	310.0	308.1	27.7	161.83	77.23	204.04	196.88	185.84	150.15	88.37	839.25
97116	9.52	305.0	308.4	309.4	307.8	32.3	162.55	76.97	190.94	184.88	182.30	151.84	101.17	821.36
97318	9.51	283.3	286.2	309.4	307.6	29.7	162.86	87.87	188.97	188.41	155.86	102.29	60.50	706.51
97217	9.56	294.7	298.0	309.9	308.1	26.9	163.24	82.17	205.54	200.03	177.91	133.12	71.20	801.45
97216	9.56	293.8	295.7	309.8	308.1	31.7	163.26	83.73	192.20	196.92	169.79	130.31	69.41	760.18
97519	9.58	258.0	259.4	309.8	308.1	30.4	163.79	96.70	171.14	148.44	105.08	61.05	57.18	558.19
97217	9.52	294.7	298.0	309.3	307.8	31.5	164.06	82.48	192.61	192.07	175.30	134.47	71.28	776.92
97419	9.53	271.0	273.3	309.4	307.7	31.0	164.14	94.43	187.70	177.37	140.98	75.05	57.52	645.05
97318	9.55	282.3	285.5	309.8	308.1	26.8	164.20	89.10	205.31	197.38	159.67	95.54	64.19	735.08
97519	9.52	252.7	255.2	309.3	307.5	29.9	164.30	97.85	168.48	152.94	95.88	60.53	55.78	538.57
97419	9.56	269.5	271.0	309.8	308.1	32.1	164.41	95.00	182.57	159.98	135.24	70.30	58.71	621.38
97319	9.58	282.4	283.8	310.3	308.5	29.0	173.02	95.84	213.56	0.00	0.00	0.00	0.00	0.00
97521	9.58	255.7	257.1	310.0	308.4	29.1	173.95	103.14	190.59	0.00	0.00	0.00	0.00	0.00
97117	9.59	305.1	306.9	310.3	308.6	28.4	175.25	86.31	226.77	0.00	0.00	0.00	0.00	0.00
74515	7.03	224.2	226.3	288.2	286.6	25.2	98.21	76.23	125.61	112.08	70.03	28.90	23.11	371.49
74515	7.03	224.2	226.2	288.2	286.7	25.1	98.55	76.50	124.74	111.89	70.49	28.98	23.00	367.45
74515	7.03	224.4	226.4	288.3	286.8	25.3	99.47	78.50	128.08	116.20	74.01	30.38	23.65	403.71
74312	7.05	255.6	258.1	288.6	286.9	23.3	99.49	63.56	117.76	116.66	94.53	53.13	25.75	406.11
74515	7.04	221.9	223.4	288.6	287.0	28.5	101.47	79.49	130.74	113.70	70.95	29.31	24.77	372.07
76316	7.05	258.1	260.4	288.6	287.1	24.4	135.64	79.73	185.74	187.68	142.09	81.13	41.52	631.48
76114	7.01	281.2	282.9	288.4	286.9	29.8	139.84	71.80	198.09	189.30	178.14	137.09	75.26	793.08
76520	7.00	224.8	225.8	288.2	286.8	30.1	140.26	99.92	199.53	164.48	105.12	46.51	42.14	570.02
77115	7.04	283.3	285.2	288.6	287.2	31.1	159.15	78.50	246.98	236.01	219.35	167.61	92.47	972.57
77521	7.04	224.4	225.8	288.6	287.1	30.5	162.70	108.55	235.95	192.30	111.08	57.54	54.17	649.66
77319	7.03	255.7	257.6	288.6	287.1	25.8	164.22	96.15	256.27	243.78	175.26	97.30	57.10	811.26

APPENDIX III

Uncertainty analysis of AECL CHF Experiment
for 5.45 mm and 8.94 mm Diameter Tubes

NOMENCLATURE

Symbol	Definition	Unit
A	area	m^2
a	constant in orifice coefficient	
b	constant in orifice coefficient	
C	constant in flow evaluation	m^2
d	inside diameter	m
F	flow orifice thermal expansion factor	
f	fractional uncertainty	
G	mass flux	$Mg.m^{-2}.s^{-1}$
h	enthalpy	$J.kg^{-1}$
K	flow orifice coefficient	
L	length	m
N	dimensionless number	
P	electric power	W
p	pressure	Pa
q	heat flux	$W.m^{-2}$
W	mass flow	$kg.s^{-1}$
x	vapour quality	

Greek

Δ	difference in inlet subcooling or pressure drop	
μ	viscosity	$kg.m^{-1}.s^{-1}$
ρ	density	$kg.m^{-3}$

Subscript

a	accurate
F	cross-sectional flow
f	saturated liquid state
fg	state change from saturated liquid to saturated vapour
g	saturated vapour
H	heated
in	inlet
l	subcooled liquid state
m	measured
o	outlet or local when used with vapour quality
op	flow orifice pipe

or	flow orifice
Po	power number

ANALYSIS OF UNCERTAINTY OF CRL CHF EXPERIMENT

III.1 Description of Analysis

This appendix presents a specific application using statistical concepts to estimate the possible values of errors in the measured and derived quantities for the CRL experiment on CHF as presented in Chapter 6. The statistical concepts employed are well established and may be explained in references by Borodin, A.S. and Macdonold, I.P.L. (1983), Toping, J. (1966), Young, H.D. (1962) and Kline, S.J. (1962).

The *error of measurement* is defined as the difference between the observed value of a quantity and the "actual" value. There are three classifications of error: (1) *accidental error* is random in frequency and magnitude which may be assessed statistically to repeated measurements, (2) *systematic error* arises from "improperly" calibrated instruments which is difficult to assess, (3) personal error is from the experiment operator which may be assessed by comparing measurements by others.

The uncertainty of measurement is the possible error thought or expected to have. It is assumed that the "actual" values exist and lie between the limits of uncertainty. If an uncertainty cannot be precisely evaluated, a reasonable degree of uncertainty is then assumed based on experience and partially on relevent information available.

The present analysis is limited to determining the *most probable* values of uncertainty. Assuming that the systematic errors have been eliminated through appropriate corrections, the most probable uncertainty for a quantity of several components is defined as the square root of the sum of the squares of the individual uncertainties. For a similarly corrected quantity of a single term, the uncertainty is defined as the square root of the mean of the sum of the squares of the repeated determinations. This method assumes that the most probable uncertainties are estimates for standard deviations, and various confidence intervals may then be established by assuming that the Gaussian normal distribution of errors applies. The present analysis considers that an estimate is sufficient for one standard deviation that corresponds to a confidence level of 68.3%.

The assessment of the uncertainties on the results of the AECL experiment reported in this thesis is presented in the following sections. Since detailed calibrations of the measuring means and evaluation of the uncertainties were performed and reported by Borodin, A.S. and Macdonold, I.P.L. (1983), on the same loop (the MR-1 Loop), and on a similar experiment, the present assessment adapts the evaluation methods and includes some valid data from this report. The present assessment is primarily on the 8.94 inside diameter tube.

III.2 Measured Quantities

The measured quantities are loosely defined as those of a fundamental nature. For the experiment, these quantities include geometric dimensions, temperatures, pressures, flows and the electrical power for the heating of the tubes. The calculated or estimated uncertainty is expressed as fraction ($f_{subscript}$) of each quantity.

III.2.1 Geometric Dimensions

For the tube of nominal inside diameter 8.94 mm:

	quantity	variation	uncertainty
outside tube diameter	11.440 mm (nominal)	+/- 0.005 mm	
inside tube diameter	8.940 mm (calculated)	+/- 0.015 mm	$f_d = 0.028$*
wall thickness	1.250 mm (nominal)	+/- 0.010 mm	
heated length	2.50 m (nominal)	+/- 0.018 m	$f_L = 0.0072$*
cross-sectional flow area	6.277×10^{-5} m^2 (calculated)		$f_{A_F} = 0.056$
inside heated area	0.007021 m^2 (calculated)		$f_{A_H} = 0.029$

* estimated value

The values of uncertainty for the inside diameter and heated length are adapted from the estimation of the Borodin report mentioned above which was based on repeated measurements of the diameter with a similar tube during a previous experiment at AECL similar to the one presented in this thesis.

The uncertainty of the cross-sectional flow area:

$$f_{A_F} = \frac{2\Delta d}{d} = 2f_d \qquad \text{(III.1)}$$

The uncertainty of the inside heated area:

$$f_{A_H}{}^2 = f_d{}^2 + f_L{}^2 \qquad \text{(III.2)}$$

III.2.2 Temperatures

The uncertainty of temperature measurements is also taken from the Borodin report which recorded a maximum systematic discrepancy of 1.4°C from a static calibration between 23 to 307°C and then confirmed by measurements during actual loop operating conditions.

The estimated fractional uncertainty in temperature measurements:

$$f_T = 0.004$$

III.2.3 Pressures

The uncertainty of outlet pressure measurement is also considered valid from the Borodin report based on the calibration under actual loop operating conditions. This uncertainty was reported as ten times the values compared to a static pressure calibration between pressures of 0 to 9.7 MPa. The reported uncertainty in the test section pressire drop was determined from calibration over a pressure range from 0 to 1.7 MPa.

The uncertainty of the outlet pressure (under actual loop operating condition):

$$f_p = 0.004$$

The uncertainty in the test section pressire drop:

$$f_{-\Delta p} = \frac{986}{-\Delta p} \text{ (where p is in Pa)} \qquad \text{(III.3)}$$

Within the range of the CHF experiment reported in this thesis, the uncertainties of pressure drop ranged from 0.001 to 0.01.

III.2.4 Flows

Flow measurements of the test section in the MR-1 Loop, over three flow ranges, were obtained from pressure drop signals across the orifice-plate meters. Flows were calculated iteratively from the following equations:

$$W = C_{or} K F \left[\rho_f \left(-\Delta p_{or}\right)\right]^{\frac{1}{2}} \tag{III.4}$$

$$K = a + b\left[\frac{4}{\pi}\right]\left[\frac{W}{d_{op}\mu_f}\right]^{\frac{1}{2}} \tag{III.5}$$

The flow coefficient of the orifice, K, was evaluated with a reference flow; and the constants a and b were determined from a weighing tank calibration procedure.

The uncertainty in the flow:

$$f_w^{\,2} = f_K^{\,2} + f_F^{\,2} + \frac{1}{4} f_{\rho_f}^{\,2} + \frac{1}{4} f_{-\Delta p_{or}}^{\,2} \tag{III.6}$$

The uncertainties of the flows were evaluated in the Borodin report, as listed below:

	Mass Flow (kg.s^{-1})		
	low	medium	high
	0.03 to 0.18	0.09 to 0.45	0.35 to 1.76
f_K	0.04	0.003	0.003
f_F	0.0002	0.0002	0.0002
$f_{\rho f}$	0.0084	0.0084	0.0084
$f_{-\Delta p_{or}}$	0.0011	0.005	0.005
f_W	**0.04**	**0.01**	**0.01**

III.2.5 Electric Power

The systematic discrepancies of the measurements of the electric power supplied to the test section were assessed in the Borodin report, and this assessment is still considered valid to the recent experiment reported in this thesis. The electric energy measured was compared to heat balances performed for single-phase liquid diabatic flow of light water. An equation was derived from the heat balance data to obtain the accurate power value, P_a, from measured power value, P_m.

$$P_a = 820.77 P_m + 1.34 P_m^2 - 0.00261 P_m^3 \quad \text{(III.7)}$$

The uncertainty in the measured power, in the range encountered during experiment, was estimated:

$$f_P = 0.032$$

III.3 Referenced Quantities

Referenced quantities are defined as values taken from other sources such as a reference. The quantities here referred to are the thermodynamic properties of water.

III.3.1 Thermodynamic Properties

The thermodynamic properties include density and enthalpy of water. The effect of uncertainties to these properties is considered primarily due to the uncertainties in the measurements of pressure and temperature, especially because of pressure fluctuation under actual loop operating conditions. The estimated uncertainties of these properties are as the following.

$$f_{\rho_l} = 0.0084$$

$$f_{\rho_f} = 0.0084$$

$$f_{\rho_g} = 0.0084$$

$$f_{h_l} = 0.003$$

$$f_{h_f} = 0.002$$

$$f_{h_{fg}} = 0.002$$

III.4 Derived Quantities

The derived quantities are defined as those obtained from a combination of the measured and the referenced quantities.

III.4.1 Mass Flux

The uncertainty in the mass flux was evaluated by the following equations.

$$G = \frac{W}{A_F} \tag{III.8}$$

$$f_G{}^2 = f_W{}^2 + f_{A_f}{}^2 \tag{III.9}$$

The uncertainties were evaluated from tests in Borodin's report and taken as the following for the three ranges of mass flux.

	Mass Flux ($Mg.m^{-2}.s^{-1}$)		
	low	medium	high
	0.48 to 2.87	1.43 to 7.2	5.6 to 28
f_W	0.04	0.010	0.010
f_{A_F}	0.056	0.056	0.056
f_G	**0.069**	**0.057**	**0.057**

III.4.2 Heat Flux

The uncertainty in heat flux was calculated from the following.

$$q = \frac{P}{A_H} \tag{III.10}$$

$$f_q^2 = f_P{}^2 + f_{A_F}{}^2 \tag{III.11}$$

Here, $f_q = 0.043$

III.4.3 Inlet Subcooling

The inlet subcooling:

$$\Delta h_{in} = h_f - h_l \qquad \text{(III.12)}$$

The fractional uncertainty:

$$f_{\Delta h_{in}} = \left[\frac{(f_{h_l} h_l)^2 + (f_{h_f} h_f)^2}{(h_f - h_l)^2} \right]^{\frac{1}{2}} \qquad \text{(III.13)}$$

The uncertainty $f_{\Delta h_{in}}$ depends on the inlet condition, for the experiment the range was typically from 0.002 up to 0.3.

III.4.4 Inlet Thermodynamic Equilibrium Quality

$$x_{e,in} = \frac{-\Delta h_{in}}{h_{fg}} \qquad \text{(III.14)}$$

The fractional uncertainty:

$$f_{x_e,in}^{\ 2} = f_{\Delta h_{in}}^{\ 2} + f_{h_{fg}}^{\ 2} \qquad \text{(III.15)}$$

The value of this uncertainty depends on the inlet condition and is almost the same magnitude as $f_{\Delta h_{in}}$.

III.4.5 Local Thermodynamic Equilibrium Quality

The local thermodynamic quality at the outlet:

$$x_{e,o} = N_{po} + x_{e,in} \qquad \text{(III.16)}$$

its fractional uncertainty:

$$f_{x_{e,o}} = \left[\frac{(f_{N_{po}} N_{po})^2 + (f_{x_{e,in}} x_{e,in})^2}{x_{e,o}^{\ 2}} \right]^{\frac{1}{2}} \qquad \text{(III.17)}$$

where the power number:

$$N_{po} = \frac{\pi q_c L d}{h_{fg} W} \tag{III.18}$$

and its uncertainty :

$$f_{N_{po}}{}^2 = f_q{}^2 + f_L{}^2 + f_d{}^2 + f_W{}^2 + f_{H_{fg}}{}^2 \tag{III.19}$$

Over the range of experimental conditions of interest, the range of $f_{N_{po}}$ was between 0.05 to 0.065; while $f_{x_{e,o}}$ was typically between 0.08 to 0.09.

III.5 The Uncertainties of the Quantities for the Tube of Smaller Diameter

The uncertainties evaluated above are primarily for the tube of 8.94 mm inside diameter. However, for the tube with the inside diameter of 5.45 mm, the magnitudes of the uncertainties for the corresponding quantities were estimated to be quite similar to the 8.94 mm diameter tube. Hence, the analysis was not repeated here for this smaller diameter tube, and the uncertainties are assumed to be the same values as determined in the above sections.